# Neurometric Encoding and Decoding: Using Multivariate Functional Connectivity Methods to Describe Cognitive States, Traits and Clinical Endophenotypes

A DISSERTATION SUBMITTED TO THE FACULTY OF THE UNIVERSITY OF MINNESOTA
BY

Craig A. Moodie

IN PARTIAL FULFILLMENT OF THE REQUIERMENTS
FOR THE DEGREE OF DOCTOR OF PHILOSOPHY

Advisors: Angus W. MacDonald III, PhD; Kelvin O. Lim, MD

Graduate Program in Neuroscience,
University of Minnesota Medical School.

October, 2014

# Copyright Page

# Acknowledgements

I would like to acknowledge all of the persons that assisted with the data collection and analyses performed for my doctoral dissertation. Dr. Bryon Mueller, Dr. James Porter, Dr. Laura Hemmy, and Christopher Bell helped with the data collection for these analyses and I am grateful to them for their contributions. Edward Patzelt, Andrew Poppe, Krista Wisner, Samantha Abram, Ian Ramsay and Dr. Gowtham Alturi all helped me to learn the statistical package R™ and to develop many aspects of the functions that served as the foundation of my analysis pipelines. Dr. Stephen Malone and Dr. Ruskin Hunt were instrumental in the conceptualization and implementation of the analyses of the Pirate task data included in chapter three. Dr. Paul Tuite and Dr. Michael Howell assisted with the interpretation of findings and text editing done for the study of Parkinson's disease and REM sleep disorder in chapter five. I would like to specially thank Andrew Poppe and Krista Wisner for all their help, advice and support. Andrew was indispensable, as he developed several programs that made the preprocessing and initial analysis of the network task data more streamlined. I definitely could not have gotten this far without Krista, who was my editor, sounding board, co-conspirator, and friend. I would also like to thank my committee chair Dr. Matthew Chaffee for his guidance through this process, as well as my non-departmental committee member Dr. Scott Sponheim, for his excellent comments and contributions. Finally, my advisors, Dr. Angus MacDonald III and Dr. Kelvin Lim have supported me in every way, including academically, financially and personally, through both trials and triumphs. My advisors nurtured my scientific curiosity throughout my doctoral work and have constantly encouraged my development as a scientist. They gave me a lot of intellectual freedom,

while also ensuring that all the work I produced was reasonable and intelligible. I will forever be in their debt.

# Dedication

I would like to dedicate this dissertation to my mother, Carolyn R. Moodie, who is an amazing woman and my unfaltering cheerleader. She has encouraged me from birth to realize my maximum potential and has made me the person that I am. Without her, none of this would have been possible.

# Abstract

This research was undertaken for the purpose of demonstrating the neurometric utility of functional connectivity methods by combining metrics that utilize information derived from independent component analyses (ICAs) with traditional fMRI and graph theory analyses. The combination of these methodologies was used to establish traits and evaluate cognitive states from a behavioral genetics perspective, as well as to posit connectivity endophenotypes related to psychiatric and neurological diseases. The studies described below demonstrate that the metrics used to study intrinsic connectivity networks (ICNs) are useful tools for studying the in vivo brain in states of normalcy and disease. For instance, by examining ICNs across tasks and monozygotic twins, it was possible to establish these brain networks as traits. The ICNs were stable across cognitive states, while still exhibiting sensitivity to specific demands. In addition, the state-dependent modulation of these ICNs, as well as their other characteristics, was shown to be influenced by genetic factors in two separate twin samples. In the second twin sample, and a study of connectivity phenotypes related to schizophrenia, ICNs were useful for establishing the relationships between ICNs and tasks in both cases. The task-related characteristics and resting state profiles of ICNs were also useful for establishing novel endophenotypes of the disease states of schizophrenia and Parkinson's disease. Overall, this research serves to establish the study of the brain's intrinsic connectivity across the domains of both cognitive and clinical neuroscience and this work serves a contribution to the understanding of the dimensions along which normal and abnormal neurobiological functioning lie, and how intrinsic connectivity networks can be examined in both spheres.

# Table of Contents

# List of Tables

# List of Figures

**Chapter Two**



**Chapter Three**

**Chapter Four**

**Chapter Five**

# Introduction

One of the overarching goals of the field of neuroscience is to provide neurobiological explanations for the complex cognitive, behavioral and psychosocial phenomena that constitute the many facets of the normal human experience, as well as the abnormal states that underlie psychiatric and neurological illnesses (Barch et al., 2013). In response to this directive, modern neurometric techniques are being developed to provide optimized quantitative axes along which any set of observations –whether they be psychological, social, behavioral, genetic, or neuroscientific –can be distributed and understood (Zagha & McCormick, 2014). This is being done to learn more about the normative range of functioning and, by doing so, to facilitate the anchoring of psychiatric and neurological symptoms along dimensions that include categorical descriptions of both normal and abnormal behavior. This is of particular importance at this point in mental health research, as there has been a big push to provide brain-based mechanisms to complement and augment traditional diagnostic and treatment methodologies (Krueger, Hopwood, Wright, & Markon, 2014). However, before incremental increases in knowledge based on neuroscientific findings translate to proportional increases in diagnostic or prognostic power and treatment efficacy, it is necessary to fully explore and concretize the aforementioned dimensions of functioning.

While there has been an increase in research dedicated to this endeavor, much of this domain is still unexplored. This body of work will describe two sets of experiments that explore traits in the normative range using behavioral genetics, and two sets of experiments which assess potential endophenotypes related to disease states. The neurometric tools being employed in these studies primarily are concerned with the

encoding of functional magnetic resonance imaging (fMRI) data. These encoding methods are all employed to provide explicit, quantitative descriptions of the information represented in the activity of voxels (three-dimensional volumes in which fMRI data is recorded), and at a higher level, derived brain networks (Naselaris, Kay, Nishimoto, & Gallant, 2011). The fundamental property of encoding, in this context, is that information about brain activity in the input space, which is relevant to stimuli or brain states, is encoded into feature spaces. These feature spaces in fMRI encoding include either the complement of voxels or brain networks, and their activity is then used to determine patterns or provide inferences related to how the information regarding states in the brain is related to activity in the voxels or networks. Hence, these encoding methods can be thought of being synonymous to the descriptive and inferential statistical methods that are employed in fMRI analyses (Naselaris et al., 2011). On the other hand, decoding refers to the utilization of the encoded voxel or network activity to predict the presentation of stimuli or differentiate between brain states using classification algorithms (Tong & Pratte, 2012). Consequently, it can be determined how well the encoding methods provide an accurate description of the underlying properties of the brain. Hence, the combination of traditional encoding methods such as general linear models (GLMs) and model-free methods like independent component analyses (ICAs), which will both be described later, affords a more complete description of brain functioning. Moreover, the addition of the decoding methods provides a means for increasing the utility of these methods for classification and prediction, which translates into a direct impact on the validity of the descriptions of brain function, as well as an increase in the predictive power of diagnostic and prognostic models. Taken together, these studies are a foray into

using intrinsic connectivity phenotypes to establish a neurometric foundation for the interpretation of brain activity.

The primary methodology applied in this neurometric research is the application of functional connectivity methods that describe the brain's intrinsic connectivity as measured in fMRI (Arbabshirani, Havlicek, Kiehl, Pearlson, & Calhoun, 2012; Behrens & Sporns, 2011; Hagmann et al., 2010). However, this type of methodology is not limited to fMRI and is applicable to other domains of functional imaging, such as electroencephalography (EEG), magnetoencephalography (MEG), electrocorticography (ECoG), event-related optical signaling (EROS), and any other methods that record activity timecourses, for instance multielectrode electrophysiology (Smith, 2012). Functional connectivity, in the most basic sense, refers to the relationship between two separate fluctuating signals and, in the context of fMRI, refers to relationships between voxel signals (Li, Guo, Nie, Li, & Liu, 2009). In contrast, fMRI data is traditionally analyzed using general linear models (GLMs). The general linear model employs a regression based technique in which a model is utilized to determine the extent to which the activity of the brain corresponds with the presentation a stimulus or the timeline of a particular task or event (Beckmann, Jenkinson, & Smith, 2003). Hence, these GLMs are applied in stimulus-driven task paradigms in order to derive activation maps showing the regions of the brain that have a significant suprathreshold relationship to the task. These activation maps are produced by comparing the hemodynamic response function (HRF), which is the timecourse of the blood-oxygen dependent (BOLD) signal, at times when the stimulus or task is present with the periods in which it is absent, otherwise know as the baseline (Smith, 2004). Hence, instead of comparing the timecourses of two or more

separate hemodynamic signals, as in the case of functional connectivity, a GLM compares the timeline of a task predictor to the timecourses of BOLD signals in all voxels in the brain.

The first study that employed a functional connectivity technique to fMRI data was done by Biswal and colleagues (Biswal, Yetkin, Haughton & Hyde, 1995), and they assessed the connectivity between regions during a finger-tapping exercise. These researchers first determined which area had the highest activity related to the finger-tapping task using a GLM. The activation map produced indicated that the hand area of the primary motor cortex was most relevant to the task and, consequently, they compared the activity of voxels in this region with activity in voxels across the remainder of the brain in a task-free, resting state scan. This was done to determine which other regions had a significant relationship to activity in the motor region of interest (ROI), as a proof of principle of the existence of functional connectivity, and was the first demonstration of the seed-based method of function connectivity. As the name suggests, seed-based connectivity uses the activity of a particular area as the source to which the activity of the remainder of the brain is contrasted (Beckmann, 2012). This technique is quite powerful for identifying regions of the brain that have meaningful relationships to the ROI, but it is biased to only show the connectivity related to that particular region, but not connectivity that is otherwise present and unrelated.

In the studies included in this thesis, functional connectivity first refers to the connectivity between voxels that together comprise functionally-derived brain networks, otherwise known as intrinsic connectivity networks (ICNs). These ICNs are derived using the aforementioned ICA techniques. The application of ICA to questions regarding the

exploration of the dimensions of brain functioning is seen as preferable to seed-based techniques, as the ICA is unbiased (Calhoun & Adali, 2001). Seed-based techniques could also be used to answer these questions, but seeds would have to be set in whatever number of regions, dictated by the seed size, that cover the entire brain to ensure that the results generated from these analyses were not providing an unbiased picture. On the other hand, the information about brain networks derived from ICA analyses of fMRI data yields relatively unbiased estimates which are more ubiquitous representations of the underlying brain regions (Xu, Potenza, & Calhoun, 2013). As a result, the properties of these ICNs can be examined to determine how these networks behave both in the absence of any external influence, which is commonly referred to as the resting state, as well as to contrast how these networks respond to particular demands in task paradigms (Arbabshirani et al., 2012; Calhoun, Kiehl, & Pearlson, 2008). The probabilistic ICA algorithms used in these analyses derive the functional networks (ICNs) based on the principle that the voxels contained in each network will have a pattern of covariance that is distinguishable from the covariance of the voxels within another network (Guo & Pagnoni, 2008). Consequently, the global signal across all brain voxels can be parsed into the constitutive ICNs based on this principle.

The use of ICA as a blind source separation tool for deriving functional networks was first described by McKeown and colleagues (McKeown et al., 1998) and has since been used in over 1000 articles. In 2009, Smith and colleagues showed that the functional networks that are derived from resting state scans using ICA show a high degree of similarity to the activation networks derived from a ICA of thousands of maps generated from traditional GLM analyses of a wide variety of task scans (Smith et al., 2009). This

study was a seminal contribution to the validation of the networks generated using ICA, as it showed that there was a strong correspondence between the ICA networks and the regions that are typically associated with particular tasks. The activation maps derived from task data were then examined within a meta-analysis framework by Laird and colleagues in order to quantify the task-association of the activation networks, and the resting-state ICNs that they exhibited homology to (Laird et al., 2011). These functional, or intrinsic, connectivity networks have also been shown to have a strong relationship to the underlying structural architecture of the brain (Honey & Sporns, 2010; van den Heuvel, Mandl, Kahn & Pol, 2009). These ICNs have also been shown to be moderately reliable (Wisner et al., 2013) and it is arguable that the upper bound on the observed reliability is impacted by limitations in the acquisition and pre-processing of the data. Furthermore, not only are these ICNs valid, reliable and physiologically relevant, they provide a novel domain in which to assess brain activity in a manner that is distinct from traditional GLM activation analyses. In the case of the GLM, the results only show which region(s) are most relevant to the task but do not include any information about the other regions that have not passed the statistical threshold. Hence, it remains an open question whether these other brain regions are truly task-irrelevant, or simply have a weaker, sub-threshold association with the task events. ICA analyses provide an ideal means of answering this question as all brain networks can be described, regardless of task relevance (Deco & Corbetta, 2012). Moreover, while the ICA itself is agnostic to the task, the dynamics of the networks derived from the ICA preserve the level of task engagement for each of the ICNs (Calhoun, Kiehl, & Pearlson, 2008). Hence, the full set of networks can be queried to determine the varying degrees of task associations, whether they are

positive or negative, as well as true task irrelevance (Calhoun, Adali, Stevens, Kiehl, & Pekar, 2005). For this reason, the ICA-derived ICNs constitute the primary building blocks for all subsequent neurometric analyses included in this work.

Metrics of functional connectivity that assess the fluctuations of voxels within an ICN are based on intra-connectivity or network coherence. However, functional connectivity is also described in terms of the relationships between disparate groups of voxels either in nodes or, as in this case, networks (Bullmore & Sporns, 2009). The fluctuation in voxels that are considered to be distinct from each other is termed interconnectivity and this phenomenon is studied using a variety of techniques. One of the most popular techniques that is used to study interconnectivity is graph theory, and this domain also encompasses the interconnectivity methodology utilized in this work (Bullmore & Sporns, 2009). Graph theory has been adopted from the work of Euler and other mathematicians who were studying physical graphs in order to study the characteristic of the interactions of brain regions (Biggs, Lloyd, & Wilson, 1986). Typical graph theory analyses examine the interactions of a set of pre-defined nodes, which are groups of voxels delineated using atlases like the Freesurfer or AAL atlases (Behrens & Sporns, 2011). Using this methodology, the BOLD signal in the voxels within a certain node is averaged and then these average BOLD timecourses are correlated with each other to create connectivity matrices and, subsequently, adjacency matrices from which the graph metrics are computed. There is one major departure from the typical graph theory analyses in this work, in that the timecourses are not averages taken from pre-defined nodes, but instead are the timecourses of the data-derived ICNs themselves. This is significant as it means that the timecourses are derived from networks that have not

been assumed to have a particular spatial location or time signature. One of the possible confounds of using pre-defined regions is that the voxels in that area could be spanning more that one distinct brain regions (Duff, E. P., et al., 2012). Hence, there will be a mixture of signals being captured in that area. Moreover, while the ICA separates out noise variance, these pre-defined ROIs might also contain noise unrelated to brain activity. In addition, these methods are more susceptible to spatial distortions and there is no reason to expect the morphology of any pre-defined node to be optimized for a particular data set (Duff, E. P., et al., 2012). Hence, it is more principled to utilize the ICN timecourses from an ICA as they reflect the dynamics of networks derived from the data itself. Additionally, this allows for the application of both intraconnectivity and interconnectivity metrics within a single pipeline. Hence, the properties of ICNs themselves and their relationships to each other can be assessed directly in the same data.

Given this context, these functional connectivity methods offer a new lens on the relationship between brain regions and the scientific questions that are being asked in fMRI studies. These data-driven function connectivity methods have the potential of providing a more complete and consistent depiction of these relationships, which in turn makes them quite useful for the aforementioned effort to anchor these relationships along quantitative dimensions. The first study engages this assertion in a proof-of-principle approach in which traits are examined across varying behavioral and cognitive states. In this study, ICNs are derived separately from imaging data from two disparate functional localizer tasks. These tasks were designed to drive brain activity in a localized fashion in distinct brain regions and, therefore, the consistency of these ICNs across the tasks speaks to their stability in varying brain states, which is consequently an indication of

their canonical nature. Moreover, this study is a behavioral genetics studying utilizing monozygotic twins and, hence, it is possible to measure the genetic contribution to the observed trait-line nature of the ICNs (Glahn et al., 2010; Mueller et al., 2013). This trait familiality is a domain in which the characteristics like stability and differential responsivity to external demands can be evaluated with respect to how ICN dynamics are influenced across states, but also how this differential responsivity is influenced by genes. The second study also continues in the vein of behavioral genetics, but goes a step further to attempt to directly compare and contrast the information yielded by ICA and GLM analyses to reveal the extent to which this information is complementary as well as familial. This study uses a reward paradigm in an sample of adolescent twins, which means that the ICN analyses can also address the trait dimensions of functioning and reward responsivity from a developmental perspective (Casey, Giedd, & Thomas, 2000). The third study then takes this methodology and applies it to the realm of psychopathology. In this case, both activation and functional connectivity tools are used to explore cognitive deficits in schizophrenia. The aim of this investigation is to determine whether this combination of methodologies provides information over and above the information yielded by either technique alone, and whether these findings are relevant to understanding schizophrenia as a disease state. Another goal is to show that ICN characteristics can provide novel targets for the exploration of endophenotypes, which are more stable, tractable, disease-relevant phenotypes that subsume diseases like schizophrenia (Gottesman & Gould, 2003; Miller & Rockstroh, 2013; Smit et al., 2010; White & Gottesman, 2012). Finally, the fourth study is a graph theory exploration of the relationship between rapid eye movement sleep behavior disorder (RBD) and Parkinson's

disease (PD), which explores whether there is functional connectivity evidence that supports the notion that RBD is an intermediate, pre-clinical phenotype of PD (Postuma, et al., 2012). In this analysis, graph theory timecourses are derived from the ICNs themselves and it is queried whether the RBD cases can be used to blindly identify Parkinson's disease based on the similarities of their interconnectivity profiles. As a whole, these analyses aim to provide a proof of concept that the brain's intrinsic connectivity is relevant to investigations in all spheres of functioning. Hence, network characteristics will be used as the means of exploring what types of brain dynamics we would expect in different situations in a normal context based on trait familiality, as well as how they elucidate changes in disease states. Consequently, this work has obvious utility for understanding brain function and dysfunction in a unified context and should provide a framework for future neurometric functional connectivity research.

# Chapter Two

Characteristics of Canonical Intrinsic Connectivity Networks
Across Tasks and Monozygotic Twin Pairs

Summary

Intrinsic connectivity networks (ICNs) are becoming more prominent in analyses of in-vivo brain activity as the field of neurometrics has revealed their importance for augmenting traditional cognitive neuroscience approaches. Consequently, tools that assess the coherence, or connectivity, and morphology of ICNs are being developed to support inferences and assumptions about the dynamics of the brain. Recently, we reported trait-like profiles of ICNs showing reliability over time and reproducibility across different contexts. The current study further examined the trait-like and familial nature of ICNs by utilizing two divergent task paradigms in twins. The study aimed to identify stable network phenotypes that exhibited sensitivity to individual differences and external perturbations in task demands. Analogous ICNs were detected in each task and these ICNs showed consistency in morphology and intra-network coherence across tasks, while the ICN timecourse dynamics showed sensitivity to task demands.

Specifically, the timecourse of an arm/hand sensorimotor network showed the strongest correlation with the timeline of a hand imitation task, and the timecourse of a language-processing network showed the strongest temporal association with a verb generation task. The area V1/simple visual stimuli network exhibited the most consistency in morphology, coherence and timecourse dynamics within and across tasks. Likewise, this network exhibited familiality in all three domains as well. Hence, this experiment is a proof of principle that the morphology and coherence of ICNs can be consistent both within and across tasks, that ICN timecourses can be differentially and meaningfully modulated by a task, and that these domains can exhibit familiality.

## Introduction

The burgeoning field of functional connectivity magnetic resonance imaging (fcMRI) has shown marked interest in developing our understanding of brain activity from the perspectives of both functional specialization and integration (Behrens & Sporns, 2011; Smith, 2012). Several methods have been developed for assembling the voxel-wise fcMRI signals across the brain to form networks based on their functional covariation, that is, their intrinsic connectivity or coherence (Beckmann & Smith, 2004; Calhoun & Adali, 2001; Fox & Raichle, 2007; Mckeown et al., 1998), and the existence of these networks has been corroborated using other techniques such as MEG and EEG (Calhoun, Liu, & Adali, 2009; Pasquale et al., 2012). These findings show that intrinsic connectivity networks, or ICNs, observed using fcMRI techniques, can be moderately reliable non-artifactual networks that correspond in their location and behavioral significance to well established areas and canonical brain processes such as vision, motor control and executive function (Behrens & Sporns, 2011; Deco, Jirsa, Mcintosh, Sporns, & Ko, 2009; Lahaye, Poline, & Flandin, 2003; Meier, Wildenberg, Liu, & Chen, 2012; Repovš & Barch, 2012; Smith, 2012; Snyder & Raichle, 2012). For instance, an independent components analysis (ICA) of activation maps from the numerous behavioral paradigms in the BrainMap database generated activation networks that were morphologically similar to the ICNs extracted from resting state scans (Smith et al., 2009). Furthermore, functional associations were derived for the BrainMap networks as a guide for tests of the reverse inference of data-driven ICNs, such as this study (Laird et al., 2011).

Other groups have been interested in how ICNs may be useful for studying individual differences and/or the biological basis of psychopathology (Fornito &

Bullmore, 2012; C. C. Guo et al., 2012; Van Dijk et al., 2010). However, it is important to first consider whether ICNs possess a neurometric profile necessary for these purposes. Some findings suggest ICNs are not only reproducible and replicable at a group level, but that their test-retest reliability is also strong at the individual level (Anderson, Ferguson, Lopez-Larson, & Yurgelun-Todd, 2011; Chou, Panych, Dickey, Petrella, & Chen, 2012; Shehzad et al., 2009; Thomason, Dennis, & Joshi, 2011; Zuo et al., 2010). Hence, with some caveats, the network profiles appear to be reliable individual difference traits (Poppe et al., 2013; Wisner, Atluri, Lim, & MacDonald, 2013). These findings are consistent with studies showing ICNs appear to be present irrespective of task demands or cognitive states, including rest and sedation (Arbabshirani, Havlicek, Kiehl, Pearlson, & Calhoun, 2012; Biswal, Eldreth, Motes, & Rypma, 2010; Calhoun et al., 2001; Calhoun & Adali, 2001; Calhoun, Kiehl, & Pearlson, 2008; Deco, Jirsa, & McIntosh, 2011; Greicius et al., 2008; Li, Wang, Yao, Hu, & Friston, 2012; Poppe et al., 2013; Sämann et al., 2011; Smith et al., 2009). To further examine the trait-like nature of ICNs, the current study builds on these previous neurometric findings by examining 1) whether individual differences in canonical ICNs are consistent within tasks, 2) across tasks within participants, 3) the manner in which network consistency may vary with task demands and engagement, and 4) to what extent these individual differences might be similar across monozygotic twin pairs.

The question of the consistency of ICNs, both within task and across different tasks, has both theoretic and practical significance. Two fundamental questions about the nature of ICNs that remain are whether they are stable over time and whether they reflect structural-functional “priors” or, in effect, networks in a reserve state, waiting to be

activated by appropriate cognitive demands (Deco et al., 2011). A great deal of work has preceded under the unexamined assumption that individual differences in the profiles of "reserve" ICNs anticipates individual differences in ICNs when they are relevant to brain functioning. There is indirect evidence that resting state (reserve) ICNs have a similar structure to task-related networks (Calhoun et al., 2008; Kristo et al., 2012; Smith et al., 2009), thus supporting this hypothesis and the potential for predictive capacity across task demands. However, there is no direct evidence, to date, that the characteristics of a complement of data-driven ICNs can describe traits across the brain and across circumstances.

One approach to this question is to examine whether phenotypes exhibited by ICNs during one task are predictive of phenotypes in a different task. It should then be possible to determine the degree to which each ICN, observed in each behavioral assay, is involved with that task and how its characteristics change with respect to changing task demands. By doing so, this approach can also be used to validate the functional associations of canonical networks recently described in a meta-analysis of activation studies (Laird et al., 2011). Additionally, by using functional localizer tasks, which are paradigms that were designed to drive activation reflecting specific cognitive processes, the present study also examined whether ICNs were detected equally well across paradigms, enabling a test of convergence and divergence of ICNs across cognitively driven brain states.

Another consideration when establishing new metrics is the extent to which they are influenced by familial versus non-shared environmental factors. Familiality, which includes both heritable and shared environment influences, can be examined using twin

study designs. Heritable influences have been reported on cognitive-behavioral assessments as diverse as intelligence, memory, personality, as well as psychiatric syndromes such as schizophrenia, depression and autism (Blokland et al., 2011; Hallmayer et al., 2011; Jang et al., 2011; Molloy et al., 2001; Tost, Bilek, & Meyer-Lindenberg, 2011). It is therefore not surprising then that twin studies have also found that the development, structural architecture, cortical profile, and functional activity of the brain also show large heritable components (Ambrosius et al., 2008; Belmonte & Carper, 2006; Blokland et al., 2008; Borgwardt et al., 2010; Brun et al., 2009; Chen et al., 2012; Chiang et al., 2011; Deco et al., 2011; Duarte-Carvajalino et al., 2012; Glahn et al., 2010; Hagmann et al., 2010; Honey, Thivierge, & Sporns, 2010; Jahanshad et al., 2010; Matthews et al., 2007; Meyer-Lindenberg, 2009; Munn et al., 2007; Rimol et al., 2010; Tarokh et al., 2011; Yang et al., 2012).

These findings support the investigation of the heritability of ICNs and, hence, population variance in ICNs should be related to population variance in genes. Monozygotic twin designs provide a division between non-shared environmental influences and familial influences, which include shared environmental and additive genetic factors, of which the primary source of familial variance is genetic (Belmonte & Carper, 2006; Blokland et al., 2011; Matthews et al., 2007). As a result, in this study we assessed the familial, and therefore primarily genetic, contribution to the characteristics of ICA-derived ICNs by using a monozygotic twin sample to examine the consistency of ICN measurements in two paradigms. Hence, this proof of principle approach allowed us to investigate the extent to which ICNs could be viewed as traits, and whether ICNs that were trait-like were also familial in this sample.

## Methods

### *Participants*

Twenty-six pairs of right-handed monozygotic twins (13 female pairs, 13 male pairs, mean age 25.02 ± 5.36 SD, range 19-34) were recruited for this study from a larger sample of 1388 twin pairs from the Minnesota Twin Registry. All twins were pre-screened for pre-existing medical, neurological or psychiatric conditions and personality characteristics relevant to a decision-making task not further reported here. All participants were given written, informed consent before participating in the study, and the Institutional Review Board of the University of Minnesota approved all experiments. Five twin pairs were excluded from the analysis due to one member not having the entire complement of scans, or technical problems during the scanning session.

### *Hand Imitation & Verb Generation Tasks*

Each participant was trained prior to the start of the experiment and all participants performed two behavioral tasks, *Hand Imitation* (HI) & *Verb Generation* (VG), that were designed to drive brain activity in a specific way (functional localizers). The tasks included a six minute run each of HI and VG, from the International Consortium on Brain Mapping (ICBM) test battery, within a single scanning session (Mazziotta et al., 2009; Mazziotta et al., 2001). HI and VG had an identical block design and subtraction condition: six 30'' experimental blocks were interspersed with 30'' control blocks, in which participants performed an arrow monitoring activity. The two tasks had the same Nyquist frequency (0.17 Hz), as well as the same trial frequency (0.5 Hz) and the total experimental time for each task was six minutes. Within the experimental blocks for both tasks, there were 15 analogous two-second trial periods. For

HI, participants imitated a novel hand position during the two-second trial period. For VG, a drawing of a familiar object was flashed on-screen for a 500 millisecond presentation period, followed by a 1.5 second response window for participants to silently generate a verb associated with the picture without actually moving their lips. The control task involved fixating on a central cross, after which an arrow would appear on the screen pointing in one of four directions. Participants pressed a button with their left thumb when the arrow was pointing left.

***MR Acquisition and Preprocessing***

All data were collected on a 3T Siemens Trio MRI scanner using a 6 channel transmit, 12-channel receive head coil. One identical whole-brain functional scan each was collected for the hand imitation and verb generation tasks (EPI; TR=2000ms, TE = 28ms; FA = 90°; voxel size = 3.5x3.5x3.5mm; matrix size = 64 x 64, axial orientation; number of slices = 34, slice thickness = 3.5mm, spacing between slices = 3.5mm, interleaved slice acquisition). In addition, a high-definition structural T1-weighted image (MPRAGE) was also collected per participant.

All MRI data were preprocessed and analyzed using the FMRIB FSL 4.1.8 software package (http://www.fmrib.ox.ac.uk/fsl). Pre-statistical processing steps included high-pass temporal filtering (70s = .014 Hz), motion correction via the MCFLIRT linear registration algorithm (Jenkinson, Bannister, Brady, & Smith, 2002), BET brain extraction, interleaved slice-timing correction, and spatial smoothing with a 5-mm full-width half-maximum Gaussian kernel. For each participant, the functional scans were registered to their high-resolution T1 images and then to the 2mm standard-space

MNI brain using nonlinear algorithms (FNIRT) with a 2mm resampling resolution and 10mm warp kernel (Andersson, Jenkinson, & Smith, 2007).

### *FMRI Data Analysis*

#### *Intrinsic Connectivity Network Generation*

In order to generate reliable data-driven networks that reflected functional regions in the brain, the EPI scans for both tasks were processed via temporal concatenation group independent component analyses (TC-GICAs) using FSL's MELODIC ICA toolkit (Beckmann & Smith, 2004). The algorithms were constrained using a dimensionality of thirty (30) components and all components that clearly did not reflect physiologically relevant BOLD-dependent signal were excluded from subsequent analyses. The remaining non-artifactual components were subsequently identified as ICNs (Beckmann, 2012; Calhoun et al., 2009; Zuo et al., 2010). Given that roughly one third of components tended to be artifactual, thirty components was the optimal dimensionality to match the non-artifactual components with the twenty BrainMap networks derived by Laird et al. (2011) and utilize said networks for reverse inference (Bhaganagarapu, Jackson, & Abbott, 2013; Ray et al., 2013).

Additionally, to avoid artificially inflating correlations between tasks and twins, and to allow for cross-validation analyses, group-level ICNs were generated separately for each task (HI, then VG) and, within each task, for two sub-groups containing one member of each twin pair (all twin 1's and then all twin 2's). Due to possible participant scan concatenation and initial random value effects, a participant-order permutation and combination procedure was performed, which involved running multiple MELODICs and

deriving a set of meta-level ICNs reflecting consistent components across the permutations (see Wisner et al., 2013). Once the meta-level ICNs were obtained, the FSL spatio-temporal regression algorithm was used to generate participant-level network spatial maps and timecourses for the ICNs derived from each task (http://www.fmrib.ox.ac.uk/analysis/dualreg).

*ICN Morphology Analyses*

When assessing ICN morphology, all 3D spatial maps were thresholded using a conservative threshold (z=6) to limit the maps to only voxels that were highly significant and contributed most to the ICN morphology (K. M. Wisner et al., 2013). Spearman rank correlations and Dice similarity indices were then calculated in each set of comparisons. Given the relationship between the Dice similarity index and Cohen's kappa, a Dice of s $\geq$ 0.4 (max=1.0) represented fair to good overlap (Agresti, 2013; Banerjee, Capozzoli, Mcsweeney, & Sinha, 2012). These metrics were first computed between thresholded group-level ICNs (z = 6) from the HI and VG tasks and the ICNs were then displayed at higher thresholds during 3D rendering in order to simplify the maps for viewing. Second, these metrics were computed between group-level ICNs and the canonical BrainMap networks (Laird et al., 2011) at the standard threshold (z = 6) for reverse inference testing. ICNs with good Dice similarity (s >0.4) for these comparisons were considered to have a reasonable amount of overlap with the BrainMap networks. Hence, this test functioned as one external validation for the ICNs generated from the two distinct functional scans.

Next, similar procedures were completed at the participant level. Participant-specific spatial maps of the ICNs were thresholded as above (z=6) and spatial correlations were performed between each twin and his or her co-twin, as well as every

other participant in the study for each ICN. Heatmap matrices were generated per ICN to visualize these spatial correlations and to determine if twin pair correlation scores were distinguishable from the correlation scores for the entire sample. All ICN correlation matrices were averaged to produce a final heatmap with a value for the average spatial correlation across all ICNs for all twins. A t-test contrasting the mean ICN correlation scores for twin pairs versus scores for pairs of unrelated participants was performed. Subsequently, a non-parametric permutation test (Hothorn & Hornik, 2011), employing random reassignment of twin pair membership, was completed to validate the results of the t-test using a method in which no assumptions would be violated by genetic covariance.

Finally, spatial correlation analyses that included Spearman and Dice coefficient tests were performed between the participant-level ICN spatial maps and the spatial maps of the group level ICNs. This was done to determine the extent to which each individual's spatial maps conformed to the group ICN spatial maps. For the spatial familiality metric, an ICC of the Dice similarity coefficients within twin pairs was calculated per ICN to ascertain which ICNs exhibited familiality.

*ICN Coherence Analyses*

The intra-network coherence of an ICN is an estimate of how well the timecourses of voxels in a participant-level ICN fit the group-level timecourse vector and, hence, is a measure of the intrinsic connectivity strength of that network. To obtain an estimate of the familiality of intra-network coherence, both voxelwise and network-level mean intraclass correlations (ICC's) were computed using an image data (nifti file)

algorithm and the ICC package in R™ from CRAN (http://cran.r-project.org/), respectively (Revelle, 2011). First, the participant-level network spatial maps were masked using a binarized image of a task-specific group-level ICN map that had been pre-thresholded (z = 6). Voxelwise ICC's were then calculated across twins using the FMRIB fslmaths algorithm, and the mean of the ICC values across the voxels within the mask was recorded per ICN, per participant (see supplementary methods). Second, the network-level mean coherence score for each thresholded ICN spatial map was calculated per participant using the fslstats tool (see supplementary methods). R™ was then used to calculate ICC's of the resulting average network coherence coefficients across twins for all ICNs, within each task separately, and this was used as the basis of the coherence familiality metric.

*ICN Timecourse Analyses*

To examine the relationship between the ICNs and the respective task designs, Pearson correlations were performed between the timecourse of each participant-level ICN and the convolved task hemodynamic response function (HRF) design matrix for that individual. Hence, the relationship between the timecourse of each ICN and the HRF associated with task demands could be computed per individual. This consequently revealed the extent to which each network was engaged by the task, for both the HI and VG paradigms. For each task, these correlations (after z-transformation) were averaged across all participants per ICN and the mean correlations were used as the basis for determining the degree to which each ICN was involved with the task in the "relationship

to task" metric. Additionally, z-transformed correlation scores were correlated within twin pairs for the task HRF familiality metric (Revelle, 2011).

*Participant-level ICN Consistency within Task (Split-Half Analysis)*

To address the question of ICN consistency within task, each scan was divided into equal halves and the group-level ICNs from the meta-ICAs of each task were used as the templates in separate dual regressions performed on the corresponding halved data sets (for HI and VG, respectively). The meta-ICA maps were used for these analyses to allow for interpretability of subsequent comparisons of these split-half data to other metrics. The resulting participant-level spatial maps and timecourses from the subsequent dual regressions were used for a split-half analysis of the consistency within task of the following three metrics previously described above: i) spatial overlap, ii) mean coherence, iii) and the relationship to task during each scan.

To assess how much the participant-level spatial maps changed during the scan, a Dice's similarity calculation was performed between ICN spatial maps generated from the two respective halves of each task. These coefficients were averaged across individuals per ICN and described as the *Spatial Overlap Consistency* within each task (HI and VG). For the *Mean Coherence Consistency*, mean intra-network coherence was calculated for the participant-level spatial maps generated for the two halves of data, for each task respectively, as described above (and in the supplementary methods) and the reliability within each task was calculated using ICC's. The task EV vectors were also halved and each half was correlated with the ICN timecourses generated from the corresponding half of the scan data using the calculation described in the network

timecourse analyses section. These task-relevance scores were then z-transformed and submitted to an ICC in the *ICN Relationship to Task Consistency* metric.

*Participant-level ICN Consistency across tasks (Cross-Task Network Correspondence)*

Additional metrics were computed to assess the extent to which network characteristics were stable from one task condition to the other at the participant-level. At the group level, 15 networks were matched across the two tasks based on at least a modest level of Dice similarity (Dice threshold of $s \geq 0.4$). First, ICN consistency was assessed by performing 3D spatial correlations of the amount of overlap between matched participant-level ICN maps (HI vs VG). Second, the consistency of the ICN coherence across tasks was assessed by calculating ICC's of the mean intra-network coherence scores generated for the matched task ICNs across all individuals. Third, the set of z-transformed correlations between the task timeline and participant-level ICN timecourses, for each task, were then submitted to an ICC calculation to assess the stability of ICN task-relevance across tasks in an individual.

## Results

*Relationship to Canonical Brain Networks*

Non-artifactual group-level networks generated from the separate ICAs of the first twin group and second twin group exhibited a high degree of similarity (Supplementary Figure 1). As a result, the group components from the HI and VG tasks that were produced from the meta-ICA of the first twin group were selected for use in all subsequent analyses. These two sets of group-level maps were consequently back

transformed into participant-level component maps and time courses for all participants and, hence, full twin pairs. By using maps derived from only the first twin group the analyses were not artificially inflated by genetic covariance.

In both the HI and VG data, 17 of the 30 components generated by the meta-ICA procedure were non-artifactual (Figure 1a). Dice similarity coefficients calculated between these two sets of group-level ICN spatial maps highlighted a one-to-one or a one-to-two correspondence between the ICNs derived from the two tasks (Figure 1b). The canonical networks from the BrainMap database (Laird et al., 2011) were subsequently correlated with each set of ICNs for comparison and reverse inference of function. This showed that there was modest or good correspondence between each BrainMap network and an ICA derived-ICN (Figure 2). To determine whether the ICNs derived from the different tasks were related to the BrainMap networks in a similar way, we tested the relationship between the group-level inference correlation scores from Table 1 (data columns 1 and 2). These were correlated at $r = 0.50$ ($p = 0.057$), indicating that the ICNs that were the best matches to the BrainMap networks could be consistent across the two tasks.

*Relationship to Task*

Time course analyses showed both strongly positive and strongly negative correlations between the ICN timecourses and the convolved HRF design matrix vectors for both tasks (Table 1, columns 3 and 4). In all tests, significance testing with the effective sample size and Bonferroni correction were applied. For the HI task, the networks that had significant positive relationships to the task were the arm/hand

sensorimotor network (r = 0.82), MT + MST / association visual network (r = 0.81), area V1 / simple visual stimuli network (r = 0.61), and the visuospatial reasoning network (r = 0.56). Additionally, the subgenual cingulate cortex & orbitofrontal cortex network had a significant anticorrelation with the task timeline (r = -0.56). For the VG task, the networks that had significant positive relationships to the task were the area V1 / simple visual stimuli network (r = 0.70) and left executive and language processing network (r = 0.66); no networks showed a significant anticorrelation with the task timeline. Taken together, these results show that the networks that were most engaged by each task were networks with functions relevant to the particular task demands, including visual processing of stimuli, sensorimotor processing for HI, and language processing for VG.

*Participant-level Network Consistency Within Task (Split-Half)*

In the split-half analysis of ICN spatial overlap consistency, average Dice overlap scores ranged from s = 0.64 to s = 0.90 for the HI task, and from s = 0.64 to s = 0.91 for the VG task. For HI, the highest spatial consistency within-task was observed in the midbrain/interoception network (s = 0.90), followed by the default mode network (s = 0.86), and the area V1 / simple visual stimuli network (s = 0.85). For VG, the highest spatial overlap was observed in the area V1 / simple visual stimuli network (s = 0.91), followed by the hand-eye coordination network (s = 0.87) and the default mode network (s = 0.86). The overall consistency of the morphology of the ICNs during the task was excellent and comparable in both tasks (s = 0.76 for HI; s = 0.74 for VG) (Table 2, data columns 1 & 2).

The ICC's from the split-half analysis of mean coherence consistency ranged from 0.19 to 0.75 for HI, and from 0.18 to 0.79 for VG. For HI, mean network coherence was most consistent within-task in the fronto-parietal network (ICC = 0.75), followed by the area V1 / simple visual stimuli network (ICC = 0.64). For VG, mean network coherence was most consistent in the visuospatial reasoning network (ICC = 0.79), followed by the fronto-parietal network (ICC = 0.76). The overall consistency of mean network coherence during the task was good for both tasks (ICC = 0.51 for HI; ICC = 0.64 for VG)(Table 2, data columns 4 & 5).

The ICC's from the split-half analysis of z-transformed scores for the ICNs' relationship to task had a range of 0.01 to 0.88 for HI and 0.21 to 0.70 for VG. The task-relevance of the ICNs was most consistent during the task for the arm/hand sensorimotor network (ICC = 0.88) for HI and the basal ganglia network for VG (ICC = 0.70). The overall consistency of the task-relevance of the ICNs was found to be good and comparable in both tasks (ICC = 0.56 for HI; ICC = 0.47 for VG) (Table 2, data columns 7 & 8).

*Participant-level Network Consistency Across Different Tasks (Cross-Task)*

For the analysis of the correspondence of individual level spatial maps across tasks, it was found that the midbrain / interoception network had the highest participant-level spatial consistency (s= 0.82), followed by the default mode network (s = 0.81) (Table 2). Overall, the task-to-task spatial consistency across all individuals and matched networks was found to be 0.51 (Table 2, data column 3). The fronto-parietal / right executive network showed the highest consistency for mean coherence scores across the

two tasks (ICC = 0.77), and the overall consistency of ICN coherence across tasks was 0.46 (Table 2, data column 6). When looking at the consistency of each network's response to differential task demands (task-relevance), ICN timecourses were most similar across tasks for the area V1 / simple visual stimuli network (ICC = 0.61). However, due to the fact that the ICNs showed differential task-relevant changes in their timecourses during each task, there was low overall consistency of ICN timecourses across tasks (ICC = 0.14) (Table 2, data column 9), suggesting many of the ICNs were sensitive to specific aspects of task demands.

*Task Familiality*

Using the task HRF familiality metric, which assessed the degree to which twins showed similar relationships between ICN time courses and the task timeline, four ICNs showed significant correspondence within twin pairs after Bonferroni correction in the HI task (Table 3, data column 1). These ICNs were the area V1 / simple visual stimuli network (ICC = 0.63), the hand-eye coordination network (ICC = 0.59), the basal ganglia network (ICC = 0.49), and the emotion & executive network (ICC = 0.49). In the VG task, the networks that showed significant task HRF familiality after Bonferroni correction were the left executive / language processing network (ICC = 0.57), the visuomotor timing and movement preparation network (ICC = 0.57), the default mode network (ICC = 0.48) and the arm/hand sensorimotor network (ICC = 0.48) (Table 3, data column 2). Given that the levels of ICN task HRF familiality did not simply map onto the magnitude of task-relevance in either task, this suggests the familiality metric measured covariance in twins' brains over-and-above task-relevance.

*Spatial Familiality*

The spatial overlap familiality metric was used to indicate the correspondence of twin scores for the extent of spatial overlap of individual level ICN spatial maps with the group maps in each task. Of the networks that passed multivariate significance thresholds in the HI task, it was found that the basal ganglia reward network exhibited the highest familiality (ICC = 0.65), followed by the fronto-parietal / right executive network (ICC = 0.61) and the midbrain interoception network (r = 0.49) (Table 3, data column 3). In the VG analysis, significant familiality was observed in the arm/hand sensorimotor network 1b (ICC = 0.66), the emotion & executive network (ICC = 0.51), the midbrain/interoception network (ICC = 0.48), the area V1 / simple visual stimuli network (ICC = 0.48), and the arm/hand sensorimotor network (ICC = 0.48) (Table 3, data column 4).

*Intra-network Coherence Familiality*

In order to assess coherence familiality, mean network coherence score ICC's and voxelwise ICC's were calculated. There were several networks that were found to exhibit significant familiality for the mean network coherence analysis after corrections for multiple comparisons. For ICNs from the HI task, the ICN with significance that survived Bonferroni correction was the MT + MST / association visual network (ICC = 0.63) (Table 3, data column 5). For ICNs from the VG task, the area V1 / simple visual stimuli network exhibited the highest familiality (ICC = 0.68), followed by the fronto-parietal / right executive network (ICC = 0.65), and the arm/hand sensorimotor network (ICC =

0.62) (Table 3, data column 6). There was only a modest, non-significant correlation between the coherence familiality observed in each task (r = 0.30)

The magnitudes of the mean network coherence ICC's were two to three times the magnitude of the same metric when calculated voxel-by-voxel. For example, for HI task, the three highest voxelwise ICC scores were for the midbrain interoceptive network (ICC = 0.33), basal ganglia / reward network (ICC = 0.27), and area V1 / simple visual stimuli network (ICC = 0.21), but none of these reached the level of significance (Supplementary Figure 2a). Similarly, for the VG task, the highest voxelwise ICC's were for the area V1 / simple visual stimuli network (ICC = 0.31), midbrain interoceptive network (ICC = 0.28), and cerebellar network associated with autonomic and naming tasks (ICC = 0.26), which were also non-significant (Supplementary Figure 2b). Interestingly, the area V1 / simple visual stimuli network was found to be one of the networks with the highest familiality using both the mean network coherence and voxelwise coherence metrics, which suggests that this network exhibits robust coherence familiality; however, it appeared that the network-level analyses amalgamate the signal more efficiently than voxelwise analyses.

*Permutation Testing*

After selecting the group components from the ICA, the back transformed participant-level spatial maps were used to generate heatmaps showing spatial correlations across all participants (Figure 3). This analysis provided a different way of looking at familiality since in this case, all study participants were compared to each other and, consequently, the twin scores could be compared within this larger sample to see if there are group mean differences between twins and unrelated individuals. In the

resulting heatmap, the diagonal showed that twins tend to have scores that are higher with their co-twin, i.e. for the twin pair than for unrelated individuals. This observation was then validated by performing a t-test of the group of twin pairs scores versus scores for unrelated participants and it was found that the correlations were significantly higher within the twin pair (diagonal elements) than for unrelated individuals (off-diagonal elements) ($t = 6.6856$, $df = 21.455$, $p = 5.765e\text{-}07$). In addition, this finding was confirmed by a non-parametric permutation test, in which twin pair membership was randomly reassigned ($t = 19.5595$, $p = 3.373e\text{-}13$). Overall these tests recapitulated that the ICNs exhibited a significant degree of familiality.

## Discussion

To examine the consistency and familiality of intrinsic connectivity networks, we examined the cross-twin correlations of ICN phenotypes during two functional localizer tasks performed by 21 twin pairs. These analyses revealed (1) common ICN characteristics that (2) showed a great degree of participant-level reproducibility within and across tasks, but were nevertheless (3) modulated to some degree by changes in task demands. (4) Several features showed significant familiality, including the extent to which brain networks were modulated by task demands, intra-network coherence and network morphology.

### *Relationship to Canonical Brain Networks & Tasks*

There was at least a modest Dice correlation, with strong one-to-one mappings, between the data-driven, group-level ICNs from the analyses of the HI and VG tasks, as well as between the ICNs from each task and the BrainMap networks. As such, the present study is a validation of the functional associations from the BrainMap meta-analyses using raw data from task scans (Laird et al., 2011; for replication see Wisner, et al., 2013) and shows that the meta-ICA algorithm was robust and captured generally the same networks from two highly dissimilar tasks. Furthermore, since a congruent set of networks was present in very different ICBM tasks, the findings of the present study are evidence that a large proportion of the ICNs were not specific to a particular task. These results are consistent with previous studies that have shown that ICNs are not stimulus dependent, since similar networks have been derived during task and rest (Arbabshirani et al., 2012; Calhoun et al., 2008), as well as from an extensive task activation meta-analysis and resting state scans (Laird et al., 2011; Smith et al., 2009). However, given that the ICNs from each task in the present study were not identical, with some showing greater disparity compared to others, it remains to be determined how much of this results from systematic task-dependent variation versus instabilities in measurement and processing. Nonetheless, this study serves as a proof of principle that complements of brain networks can be captured under different circumstances, and that the same general network can be examined across varying contexts to examine how it changes.

Another goal of these analyses was to show that not only could canonical ICNs be derived from various behavioral paradigms, but that the ICA algorithms would be sensitive to task manipulations in a manner that is complementary to traditional fMRI activation studies. In doing so, this study provides a separate, additional validation of the

BrainMap functional associations by not only using the spatial correspondence of activation networks and ICNs, but also employing direct analysis of raw fMRI data and the resulting ICN timecourses. Consequently, task-relevance was established for networks with meta-analytical functional associations to hand motions in the hand imitation task, including a network with premotor areas that are putative mirror neuron regions, as well as for language related networks in the verb generation task. These functionally relevant ICNs were not only selectively and significantly related to separate tasks using timecourse analyses, but they also contained regions that had been previously reported to be related to these tasks in traditional GLM paradigms. Within the HI task, this is true for the visuospatial reasoning ICN, which contained the superior parietal lobe and ventral premotor cortex, as well the association visual ICN, which contained the extrastriate visual cortex, and lastly the network which encapsulated the primary visual cortex (area V1). The arm/hand sensorimotor ICN contained the hand regions of the pre- and post-central gyri, and all of these areas contained within the ICNs have previously been found to be related to hand imitation (Grafton & Hamilton, 2007; Iacoboni, 2005; Jackson, Meltzoff, & Decety, 2006; Koski, Iacoboni, Dubeau, Woods, & John, 2003). The same was true for the left executive and language processing ICN that was significantly related to the verb generation task timeline, since it contained both Broca's and Wernice's area, which have been heavily associated with verb generation (Crivello et al., 1995; Edwards, Nagarajan, & Dalal, 2010; Indefrey & Levelt, 2004; Indefrey, 2011).

These findings lend credence to the assertion that the data is not overfit, and that this ICA method can be used to examine task manipulations (Calhoun et al., 2001). These ICNs reflect the activity of real, relevant brain regions and the ICA method used to

produce them can provide information about which networks receive even subtle perturbations from the task presentation, which might not be captured by a typical GLM subtraction paradigm. Hence, it is apparent that this new approach can provide information that is complementary to activation paradigms (Smith, 2012). However, any claims can only be made about the relevance of ICN modulation by these two tasks. Hence, future studies will directly relate the results of a traditional GLM to an ICA in the same task data set in order to determine the extent to which this is a general principle.

The arm/hand sensorimotor and visuospatial reasoning networks were strongly related to the task timeline of the hand imitation (HI) task, but the hand-eye coordination network was not related at all. There are several explanations for this curious finding, including that the participants were lying supine in the scanner and, as such, were not looking at their hands and not making parabolic, grasping or other complex actions that might have engaged the hand-eye coordination network. A similar finding is that in the analysis of the verb generation task, the left executive and language processing network, which includes both Broca's and Wernicke's areas, was significantly related to the task, but the speech sensorimotor network and the composite network associated with emotion and executive functioning, language and the primary auditory cortices did not exhibit strong task-relevance. In the case of the verb generation task, the participants were instructed to look at a picture and generate a verb or action without actually speaking it out loud. Hence, it is possible that the task engaged the left executive and language processing network as well as visuomotor timing and movement preparation network, but not the speech sensorimotor network since there was no verbal output and associated activity in that part of the motor cortex. Similarly, since the participants were producing

no sounds, it is reasonable that the auditory network was also not engaged by the task in a significant manner.

Another observation is that both the default mode network (DMN) and the executive networks were anticorrelated with the task. This at first seemed counterintuitive, since executive networks are typically described as being antagonistic to the DMN (Fox & Raichle, 2007; Raichle et al., 2001). However, the control condition is a passive monitoring task, which the DMN has been shown to be involved in (Greicius & Krasnow, 2003; Li et al., 2012). Additionally, this monitoring task probably recruited the executive networks more than the task condition due to the need for sustained vigilance for the particular arrow that required a button press response, in contrast to the hand imitation and verb generation tasks that elicited more stereotyped responses.

*Within Task Split-Half and Cross-Task Consistency*

In general it was found that ICNs have good to excellent consistency within tasks, regardless of the metric used. For the spatial overlap split-half consistency, the midbrain and default mode networks consistently had some of the highest scores in both the HI and VG tasks. Hence, it is not surprising that this results in these two networks having the highest scores for the cross-task reproducibility of the spatial maps. This observation also holds for the area V1/simple visual stimuli network, as it also had one of the highest levels of spatial reproducibility and mean coherence for the split-half analyses and, subsequently, the cross task analysis. While there are other networks that had high scores in those morphology and coherence analyses as well, when considering the relationship to task, area V1 had good reliability in both tasks for the split-half analyses and a

comparable score for the cross-task analysis, which was almost twice the magnitude as the next highest ICNs, making this a unique finding.

Previous studies, such as Zuo et al. (2010) have employed test-retest reliability measures to ICA data and they found that the networks with the highest within-participant reproducibility were their medial visual network, fronto-parietal networks, DMN, and executive control network. In a later study, Wisner et al. (2013) found that group-level reproducibility was highest for the V1 / simple visual stimuli network, followed by the DMN. In addition, when comparing the ICN group maps from their test-retest and cross-validation samples with BrainMap networks, the simple visual stimuli network showed the highest level of consistent spatial overlap (K. M. Wisner et al., 2013). These findings are supported by those of the present study which show that the area V1 / simple visual stimuli network emerges as the ICN with the best consistency. Hence, V1 had the highest average rank (and group of averages) for the consistency metrics, both within the each task and across tasks. This is likely due to the fact that V1 is a unimodal input area that has a stereotyped response, and this will be discussed further below.

In general, the three methods of assessing the consistency of ICNs provided evidence that the morphology and coherence of the ICNs showed good overall consistency, both within and across tasks. However, while the relationship to task was stable within each task, this metric exhibited low consistency across tasks, which implies that the dynamics of a functional network when engaged in different tasks are stable but divergent and the ICA therefore captures context-dependent variability in ICN timecourses. Moreover, the characteristics of these ICNs being relatively stable within and across tasks, with the exception of divergent task relevance, is supported by findings

that show that there is a correspondence between network states during a task and at rest (Calhoun et al., 2008; Hampson & Driesen, 2006; Hermundstad et al., 2013; Li et al., 2013). Hence, our findings are in line with the assertion that the brain is typically in a multistable state that is optimized and primed for different forms of either endogenous or exogenous activity (Deco & Corbetta, 2012). Given that stable functional connectivity architecture has been reported across many studies, which include task paradigms, these results support the notion that the introduction of a task doesn't override the baseline state in the brain (Arfanakis et al., 2000; Biswal, Mennes, & et, 2010; Fox & Raichle, 2007).

*Familiality*

Given that there are several networks that are significantly related to task but that don't show task HRF timecourse familiality and vice versa, the results of the present study suggest that the familiality of network timecourses is not solely dependent on how those network timecourses are being modulated or driven by the task timeline. Similarly, familiality does not appear to be a function of split-half or cross-task consistency. This is significant since it shows that the observed familiality is not simply a reflection of how well captured or stable the network is, nor is it based on how regularized the signal is because it is being driven by task presentation. However, future work is needed to determine the upper and lower bounds of reliability and task influence on heritability estimates. Hence, the same methods need to be applied to data from a great variety of paradigms to determine if there are networks that are both strongly heritable and consistently impervious to task modulation.

Nevertheless, the present findings support a notable level of familiality worth investigating further. The heatmaps of ICN correlations show a clear diagonal, which indicates that the highest (hottest) scores were those between co-twins and the t-test and permutation test validated the significance of this finding. In particular, the area V1 / simple visual stimuli network was not only familial, but was significantly related to task in both the HI and VG paradigms, and showed strong consistency within and across tasks in all three domains (V1 was prominent in almost all analyses). Hence, it is possible that the primary visual cortex is the most robust marker of functional connectivity, since it was well captured by the ICA, could be modulated by exogenous activity, but also preserved a level of consistency as well as genetic covariance in its morphology, timecourse and coherence.

It is interesting that area V1 was one of the networks that exhibited the most robust network consistency and heritability estimates given the recent observation that interparticipant variability in inter-network coherence is lowest in visual areas and highest in fronto-parietal networks (Mueller et al., 2013). These authors argue that individual differences in inter-network connectivity are related to the phylogenetic development of brain structures, which makes variability highest in multimodal association cortex areas, but lowest in unimodal sensory regions. One way to contextualize these findings is to note that while it is true that having zero variability precludes the observation of any familiality, high interparticipant variability does not automatically imply familiality since other studies have found that there is an increase in discordance in certain brain regions and functions in twins over time and experience (Lessov-Schlaggar et al., 2012; Wallace et al., 2006). In addition, it has been shown that

brain activity in visual areas is heritable, which implies that if the reduction of variability in sensorimotor regions means that they are less sensitive to non-genetic influences, instead of driving down familiality this would actually boost familiality (Park, Shedden, & Polk, 2012).

*Limitations*

One relevant aspect of this discussion that these results could not directly assess is the proportion of covariance in twins that might be attributable to shared environment since the participants were all monozygotic twins and no dizygotic twins were recruited for this study. In addition, even though the sample size is comparable to other fMRI twin studies, this study is underpowered when compared to larger behavioral genetics heritability models. Lastly, we only administered two tasks and this limits the generalizability of the results. In the hand imitation and verb generation paradigms the participants could not be rated on how well they were performing the tasks and, as a result, we cannot infer how ICN consistency or familiality was reflected in behavior. Hence, future work will need to be done to include tasks in many more domains, including tasks that have measurable behavioral output.

*Conclusions*

The present study advances the current understanding of the trait-like nature of ICN based metrics pertaining to task-relevance, consistency and familiality. In the current study monozygotic twins completed two dissimilar and stereotypical tasks that were designed for use within the ICBM battery to produce activation in discrete brain regions

by using stimuli that would drive activity in specific brain networks. Hence, these tasks have an identical design and periodicity and share an identical button press 'off' state, but they are quite different in their cognitive demands. As a result, they have provided a useful means for exploring and contrasting the ways in which exogenous demands can affect the characteristics of ICNs. We found that the ICA-derived ICNs detected across two dissimilar task states were stable across time within each task, highly similar in their morphology and coherence across tasks, and their timecourses reflected task-dependent modulation selectivity in networks with functional relevance to each task. Based on the present analyses, it appears that the extent to which an ICN is driven by the task does not determine it's familiality, but rather this familiality seems to be selectively expressed and its detection may be somewhat limited by the network's consistency. Taken together, these results suggest that it is possible that the familiality of ICNs is related to the variability or complexity of the underlying neuronal architecture, but more work needs to be done to further establish and explore this principle.

Tables

**Table 1. Summary Statistics for Reverse Inference and the ICN Relationships to the Tasks**

| Network | Reverse Inference Component | Inference Correlation | | Relationship to Task | |
|---|---|---|---|---|---|
| | | HI (90% CI) | VG (90% CI) | HI (95% CI) | VG (95% CI) |
| 1 | Medial temporal / Emotion & Limbic Network 1 | **0.45** (0.10 0.70) | 0.43 (0.00 0.73) | -0.24 (-0.32 -0.15) | 0.24 (0.17 0.31) |
| 2 | Subgenual ACC & OFC / Reward 1a | **0.52** (0.19 0.75) | **0.46** (0.04 0.74) | **-0.56 *** (-0.63 -0.50) | -0.36 (-0.41 -0.30) |
| 3 | Basal Ganglia / Reward Network 2 | **0.43** (0.07 0.69) | 0.27 (-0.18 0.63) | 0.03 (-0.07 0.13) | -0.10 (-0.15 -0.04) |
| 4 | Emotion & Executive / Language & Auditory Cortices | 0.20 (-0.18 0.53) | 0.36 (-0.08 0.69) | 0.00 (-0.09 0.08) | -0.17 (-0.24 -0.11) |
| 5 | Midbrain / Interoception Network | **0.56** (0.24 0.77) | **0.53** (0.13 0.78) | 0.05 (-0.05 0.15) | -0.05 (-0.10 0.00) |
| 6 | Visuospatial Reasoning Network | 0.39 (0.02 0.66) | 0.42 (-0.01 0.72) | **0.56 *** (0.49 0.61) | 0.05 (-0.04 0.13) |
| 7 | Arm/Hand Sensorimotor Network | 0.32 (-0.06 0.62) | 0.31 (-0.14 0.65) | **0.82 *** (0.78 0.86) | -0.21 (-0.29 -0.13) |
| 8 | Hand-eye Coordination Network | **0.44** (0.08 0.70) | **0.51** (0.10 0.77) | 0.00 (-0.09 0.08) | -0.17 (-0.24 -0.10) |
| 9 | MT + MST / Areas V2 & V3 / Covert reading | 0.38 (0.01 0.66) | 0.36 (-0.08 0.69) | **0.81 *** (0.78 - 0.84) | -0.18 (-0.27 -0.09) |
| 10 | Area V1 / Simple Visual Stimuli Network | **0.49** (0.15 0.73) | **0.59 *** (0.21 0.81) | **0.61 *** (0.54 - 0.70) | **0.70 *** (0.65 0.74) |
| 11 | Social Cognition / Default Mode Network | **0.58 *** (0.27 0.78) | **0.55** (0.16 0.79) | **-0.39** (-0.47 -0.31) | -0.35 (-0.44 -0.26) |
| 12 | Cerebellum / Autonomic / Naming Network | **0.46 (0.11 0.71)** | **0.63 *** (0.27 0.83) | -0.20 (-0.31 -0.07) | 0.21 (0.14 0.28) |
| 13 | Fronto-parietal / Right Executive Network | **0.45** (0.10 0.70) | **0.44** (0.01 0.73) | **-0.34** (-0.42 -0.26) | -0.15 (-0.23 -0.06) |
| 14 | Speech Sensorimotor Network | 0.38 (0.01 0.66) | **0.51** (0.10 0.77) | -0.14 (-0.20 -0.08) | 0.04 (-0.05 0.12) |
| 15 | Left Executive / Language Processing | 0.22 (-0.16 0.55) | **0.47** (0.05 0.75) | **-0.39** (-0.47 -0.31) | **0.66 *** (0.59 0.71) |
| 16 | Medial temporal / Emotion 2 | 0.39 (0.02 0.66) | | 0.00 (-0.11 0.10) | |
| 17 | Subgenual ACC & OFC / Reward 1b | 0.29 (-0.09 0.60) | | -0.15 (-0.23 -0.06) | |
| 18 | Visuomotor Timing & Movement Preparation | | 0.35 (-0.10 0.68) | | **0.44** (0.40 0.49) |
| 19 | Arm/Hand Sensorimotor Network 1b | | 0.16 (-0.29 0.55) | | **-0.32** (-0.38 -0.27) |

**Note:** *Reverse inference component* and *Inference Correlation:* Reverse Inference Component labels derived from Laird, et al., 2011 (http://fsl.fmrib.ox.ac.uk/analysis/brainmap+rsns/). *Relationship to Task*: mean correlations of the participant-level design matrix hemodynamic response function (HRF) with ICN timecourses. Network correlation scores were bolded at significance threshold of $p < 0.05$. Significant correlations that survived Bonferroni correction were starred ($p < 0.0029$). Some confidence intervals do not include zero, but the values were not found to

be significant after adjustments with the effective sample size (see Methods). HI = hand imitation, VG = Verb Generation, CI = Confidence Interval.

**Table 2. Participant-level ICN Consistency within and across Tasks**

| Matched Network # | Reverse Inference Component | Spatial Overlap (Split Half - HI) (95% CI) | Spatial Overlap (Split Half - VG) (95% CI) | Spatial Overlap HI vs VG (95% CI) | Mean Coherence (Split Half - HI) (95% CI) | Mean Coherence (Split Half - VG) (95% CI) | Mean Coherence HI vs VG (95% CI) | Relationship to Task (Split Half - HI) (95% CI) | Relationship to Task (Split Half - VG) (95% CI) | Relationship to Task HI vs VG (95% CI) |
|---|---|---|---|---|---|---|---|---|---|---|
| 1 | Medial temporal / Emotion & Limbic Network 1 | 0.65 (0.63 0.67) | 0.64 (0.61 0.66) | 0.49 (0.48 0.49) | 0.31 (0.03 0.55) | 0.66 (0.45 0.80) | 0.47 (0.21 0.68) | 0.69 (0.49 0.82) | 0.40 (0.12 0.62) | 0.08 (-0.07 0.29) |
| 2 | Subgenual ACC & OFC / Reward 1a | 0.76 (0.73 0.80) | 0.68 (0.64 0.72) | 0.76 (0.75 0.77) | 0.63 (0.41 0.78) | 0.69 (0.48 0.82) | 0.59 (0.36 0.76) | 0.47 (0.19 0.67) | 0.21 (-0.10 0.48) | 0.25 (-0.06 0.52) |
| 3 | Basal Ganglia / Reward Network 2 | 0.83 (0.80 0.85) | 0.68 (0.66 0.71) | 0.26 (0.25 0.27) | 0.54 (0.29 0.72) | 0.55 (0.30 0.73) | 0.33 (-0.10 0.64) | 0.69 (0.48 0.82) | 0.70 (0.50 0.82) | -0.08 (-0.34 0.21) |
| 4 | Emotion & Executive / Language & Auditory Cortices | 0.69 (0.67 0.71) | 0.72 (0.70 0.73) | 0.55 (0.54 0.56) | 0.51 (0.25 0.71) | 0.53 (0.28 0.71) | 0.57 (0.33 0.74) | 0.61 (0.35 0.78) | 0.50 (0.24 0.70) | -0.04 (-0.27 0.23) |
| 5 | Midbrain / Interoception Network | 0.90 (0.89 0.92) | 0.81 (0.79 0.83) | 0.82 (0.82 0.83) | 0.52 (0.26 0.71) | 0.73 (0.55 0.84) | 0.18 (-0.08 0.44) | 0.64 (0.43 0.79) | 0.48 (0.21 0.68) | 0.10 (-0.18 0.38) |
| 6 | Visuospatial Reasoning Network | 0.75 (0.74 0.77) | 0.79 (0.77 0.81) | 0.51 (0.50 0.51) | 0.45 (0.18 0.66) | 0.79 (0.64 0.88) | 0.47 (0.21 0.68) | 0.56 (0.31 0.74) | 0.46 (0.18 0.67) | 0.09 (-0.07 0.30) |
| 7 | Arm/Hand Sensorimotor Network | 0.68 (0.67 0.70) | 0.64 (0.61 0.66) | 0.37 (0.36 0.37) | 0.57 (0.25 0.77) | 0.76 (0.58 0.86) | 0.15 (-0.08 0.42) | 0.88 (0.80 0.94) | 0.37 (0.09 0.60) | 0.01 (-0.02 0.06) |
| 8 | Hand-eye Coordination Network | 0.83 (0.81 0.85) | 0.87 (0.85 0.89) | 0.49 (0.49 0.50) | 0.47 (0.20 0.68) | 0.64 (0.42 0.79) | 0.50 (-0.02 0.76) | 0.59 (0.35 0.75) | 0.42 (0.14 0.63) | 0.11 (-0.14 0.36) |
| 9 | MT + MST / Areas V2 & V3 / Covert reading | 0.82 (0.80 0.83) | 0.49 (0.46 0.52) | 0.29 (0.28 0.29) | 0.56 (0.31 0.74) | 0.18 (-0.11 0.45) | 0.10 (-0.05 0.34) | 0.41 (0.13 0.63) | 0.52 (0.23 0.71) | -0.03 (-0.06 0.08) |
| 10 | Area V1 / Simple Visual Stimuli Network | 0.85 (0.84 0.87) | 0.91 (0.90 0.92) | 0.65 (0.64 0.65) | 0.64 (0.41 0.79) | 0.68 (0.48 0.81) | 0.57 (0.23 0.77) | 0.59 (0.34 0.76) | 0.68 (0.48 0.82) | 0.61 (0.31 0.79) |
| 11 | Social Cognition / Default Mode Network | 0.86 (0.84 0.87) | 0.86 (0.85 0.88) | 0.81 (0.80 0.81) | 0.44 (0.15 0.65) | 0.70 (0.48 0.83) | 0.60 (0.36 0.76) | 0.52 (0.27 0.71) | 0.62 (0.37 0.78) | 0.37 (0.07 0.60) |
| 12 | Cerebellum / Autonomic / Naming Network | 0.64 (0.61 0.67) | 0.78 (0.75 0.82) | 0.39 (0.38 0.39) | 0.51 (0.26 0.70) | 0.70 (0.51 0.83) | 0.56 (0.32 0.74) | 0.72 (0.54 0.84) | 0.58 (0.34 0.75) | 0.08 (-0.10 0.29) |
| 13 | Fronto-parietal / Right Executive Network | 0.73 (0.71 0.75) | 0.75 (0.73 0.77) | 0.65 (0.64 0.66) | 0.75 (0.58 0.86) | 0.76 (0.59 0.86) | 0.77 (0.61 0.87) | 0.40 (0.11 0.62) | 0.31 (0.00 0.56) | 0.25 (-0.03 0.50) |
| 14 | Speech Sensorimotor Network | 0.65 (0.63 0.67) | 0.76 (0.74 0.78) | 0.31 (0.26 0.36) | 0.19 (-0.11 0.46) | 0.75 (0.59 0.86) | 0.55 (0.30 0.73) | 0.01 (-0.29 0.31) | 0.36 (0.07 0.60) | 0.33 (0.02 0.58) |
| 15 | Left Executive / Language Processing | 0.75 (0.73 0.77) | 0.73 (0.71 0.74) | 0.27 (0.26 0.27) | 0.53 (0.28 0.72) | 0.55 (0.29 0.73) | 0.50 (0.16 0.71) | 0.60 (0.37 0.76) | 0.51 (0.25 0.70) | -0.03 (-0.07 0.07) |
| | **Average Across Networks** | 0.76 | 0.74 | 0.51 | 0.51 | 0.64 | 0.46 | 0.56 | 0.47 | 0.14 |

**Note.** *Spatial Overlap Consistency:* (a) for the split-half spatial overlap calculation, the participant-level ICN spatial maps generated from the two respective halves of each task were compared using Dice's similarity index and the similarity coefficients were averaged across individuals per ICN. (b) To assess the cross-task ICN spatial overlap (HI vs VG), spatial maps of matched ICNs from the ICAs of the HI and VG tasks underwent a Dice similarity calculation at individual level and these similarity coefficients were averaged per ICN. *Mean Coherence Consistency:* (c) for the split-half coherence consistency, the mean coherence was calculated for the participant-level ICNs generated from each half (see methods) and the reliability within task was calculated using ICC's. (d) For the cross-task coherence consistency, ICC's were calculated using the two sets of participant-level mean coherence values for matched ICNs (HI vs VG). *ICN Relationship to Task Consistency:* (e) in the split-half consistency calculation, the ICNs' relationships to the respective portions of the task was first established using a Pearson correlation and an ICC was then calculated of the z-transformed correlations scores for each half of the task. (f) In the cross-task "relationship to task" consistency metric (HI vs VG), the two sets of participant-level correlations of the ICN timecourse and the task timeline in each task were z-transformed and these z-transformed values were correlated across matched ICNs. *Average Across Networks:* Overall score within each modality (column averages). HI = hand imitation, VG = Verb Generation, CI = Confidence Interval.

## Table 3. Summary Statistics for ICN Familiality

| Network | Reverse Inference Component | Task HRF Familiality HI (95% CI) | Task HRF Familiality VG (95% CI) | Spatial Familiality HI (95% CI) | Spatial Familiality VG (95% CI) | Coherence Familiality HI (95% CI) | Coherence Familiality VG (95% CI) |
|---|---|---|---|---|---|---|---|
| 1 | Medial temporal / Emotion & Limbic Network 1 | 0.01 (-0.44 0.45) | 0.24 (-0.21 0.61) | 0.37 (-0.07 0.68) | 0.31 (-0.13 0.65) | 0.37 (-0.07 0.69) | **0.44** (0.01 0.73) |
| 2 | Subgenual ACC & OFC / Reward 1a | 0.20 (-0.25 0.58) | **0.38** (-0.03 0.69) | 0.25 (-0.17 0.60) | **0.46 *** (0.05 0.73) | 0.20 (-0.27 0.58) | 0.40 (-0.04 0.71) |
| 3 | Basal Ganglia / Reward Network 2 | **0.49 *** (0.07 0.76) | 0.14 (-0.27 0.53) | **0.65 *** (0.30 0.85) | 0.38 (-0.04 0.69) | **0.50** (0.08 0.76) | **0.51** (0.11 0.77) |
| 4 | Emotion & Executive / Language & Auditory Cortices | **0.49 *** (0.10 0.75) | **0.46** (0.04 0.74) | 0.17 (-0.29 0.56) | **0.51 *** (0.10 0.77) | 0.28 (-0.17 0.63) | 0.43 (0.01 0.72) |
| 5 | Midbrain / Interoception Network | **0.39** (-0.04 0.69) | 0.12 (-0.31 0.52) | **0.49 *** (0.02 0.77) | **0.48 *** (0.06 0.75) | **0.51** (0.10 0.80) | **0.57** (0.18 0.80) |
| 6 | Visuospatial Reasoning Network | 0.00 (-0.42 0.42) | **0.43** (0.00 0.72) | 0.14 (-0.26 0.51) | **0.43** (0.02 0.72) | 0.19 (-0.28 0.57) | **0.55** (0.17 0.79) |
| 7 | Arm/Hand Sensorimotor Network | -0.11 (-0.53 0.34) | **0.48 *** (0.08 0.75) | **0.41** (-0.01 0.71) | **0.48 *** (0.05 0.76) | **0.48** (0.06 0.75) | **0.62 *** (0.27 0.83) |
| 8 | Hand-eye Coordination Network | **0.59 *** (0.27 0.83) | 0.14 (-0.21 0.49) | 0.06 (-0.40 0.48) | 0.35 (-0.09 0.67) | -0.04 (-0.48 0.40) | **0.47** (0.04 0.74) |
| 9 | MT + MST / Areas V2 & V3 / Covert reading | -0.10 (0.07 0.76) | 0.02 (-0.44 0.45) | 0.29 (-0.11 0.63) | 0.08 (-0.38 0.49) | **0.63 *** (0.29 0.83) | **0.54** (0.17 0.78) |
| 10 | Area V1 / Simple Visual Stimuli Network | **0.63 *** (0.27 0.83) | **0.40** (-0.02 0.70) | 0.17 (-0.22 0.54) | **0.48 *** (0.08 0.75) | **0.54** (0.14 0.78) | **0.68 *** (0.37 0.86) |
| 11 | Social Cognition / Default Mode Network | **0.43** (0.00 0.72) | **0.48 *** (0.07 0.76) | 0.16 (-0.28 0.55) | 0.30 (-0.10 0.63) | **0.50** (0.09 0.76) | 0.40 (-0.03 0.70) |
| 12 | Cerebellum / Autonomic / Naming Network | **0.42** (-0.01 0.72) | 0.34 (-0.10 0.67) | 0.18 (-0.21 0.54) | 0.08 (-0.31 0.46) | 0.07 (-0.35 0.47) | **0.53** (0.13 0.78) |
| 13 | Fronto-parietal / Right Executive Network | 0.16 (-0.31 0.55) | **0.45** (0.04 0.73) | **0.61 *** (0.24 0.82) | 0.26 (-0.16 0.61) | 0.39 (-0.05 0.70) | **0.65 *** (0.31 0.84) |
| 14 | Speech Sensorimotor Network | -0.07 (-0.44 0.34) | 0.28 (-0.17 0.63) | **0.38** (-0.01 0.68) | -0.06 (-0.49 0.38) | 0.36 (-0.08 0.68) | 0.34 (-0.11 0.67) |
| 15 | Left Executive / Language Processing | 0.12 (-0.35 0.52) | **0.57 *** (0.21 0.80) | -0.01 (-0.46 0.43) | 0.21 (-0.20 0.57) | 0.27 (-0.18 0.63) | 0.15 (-0.32 0.55) |
| 16 | Medial temporal / Emotion 2 | 0.11 (-0.34 0.51) | | **0.40** (0.00 0.70) | | 0.13 (-0.31 0.53) | |
| 17 | Subgenual ACC & OFC / Reward 1b | 0.19 (-0.28 0.57) | | **0.45** (0.04 0.73) | | 0.17 (-0.28 0.55) | |
| 18 | Visuomotor Timing & Movement Preparation | | **0.57 *** (0.21 0.80) | | 0.19 (-0.28 0.57) | | 0.22 (-0.22 0.59) |
| 19 | Arm/Hand Sensorimotor Network 1b | | 0.07 (-0.32 0.46) | | **0.66 *** (0.32 0.85) | | 0.40 (-0.04 0.71) |

**Note.** *Task HRF Familiality*: cross-twin correlation of z-transformed scores of task correlation coefficients; *Spatial Familiality*: cross-twin correlation of z-transformed scores of correspondence between individual and group level maps; *Coherence Familiality*: cross-twin ICC of individuals' average coherence scores. Network correlation scores were bolded at an uncorrected significance threshold of $p < 0.05$. Significant correlations that survived Bonferroni correction were starred ($p < 0.0029$).

## Figures

**Figure 1**. **Three Dimensional Spatial Overlays and Cross-Task Correlations between the Spatial Maps of Networks from the Hand Imitation and Verb Generation Tasks**

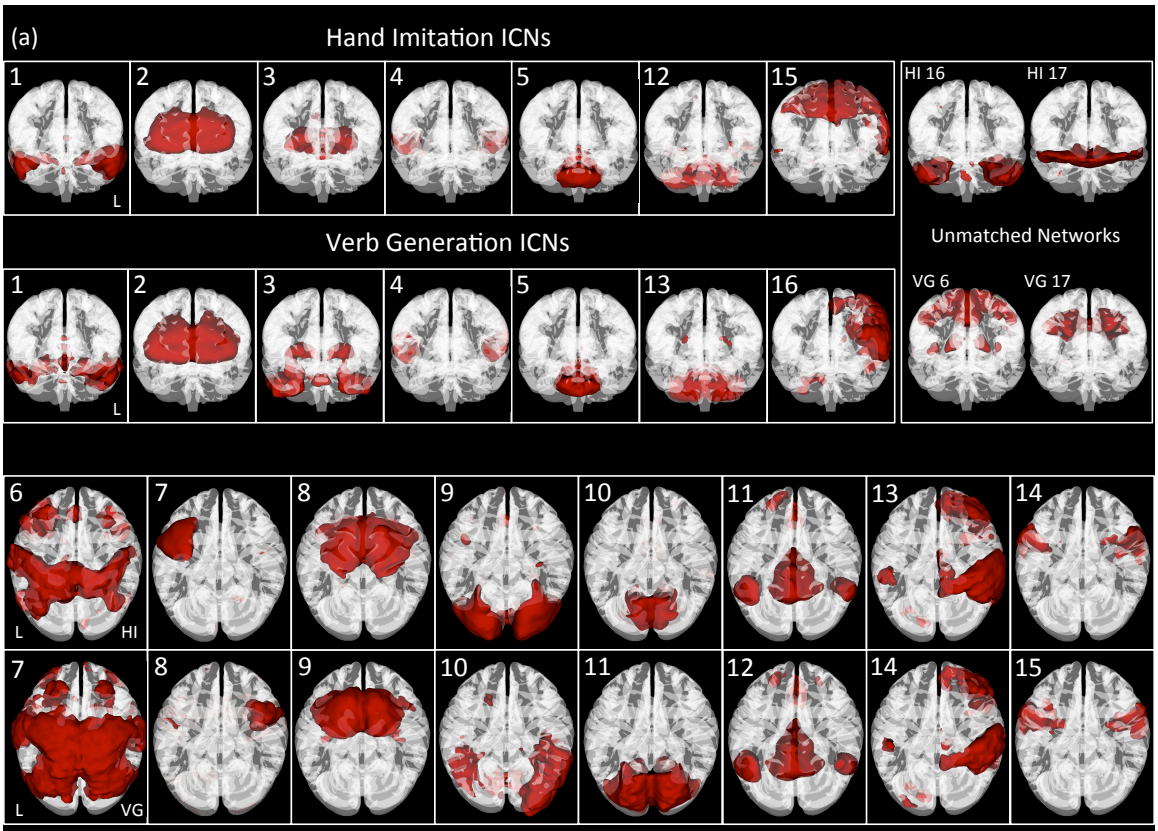


(b)

Networks generated from the Verb Generation Task

| | HI 10 | HI 9 | HI 11 | HI 2 | HI 13 | HI 12 | HI 4 | HI 3 | HI 6 | HI 15 | HI 8 | HI 14 | HI 7 | HI 17 | HI 5 | HI 1 | HI 16 | Dice |
|---|---|---|---|---|---|---|---|---|---|---|---|---|---|---|---|---|---|---|
| VG 11 | .53 | .45 | .01 | -.12 | -.14 | .13 | .00 | -.05 | -.02 | -.10 | -.05 | -.08 | .05 | -.08 | -.08 | -.08 | -.10 | .54 |
| VG 12 | .14 | .02 | .76 | .04 | .09 | -.10 | -.03 | .02 | .09 | .03 | -.05 | -.05 | -.12 | .01 | -.07 | .00 | -.09 | .75 |
| VG 2 | -.02 | .10 | -.02 | .76 | -.01 | -.10 | .07 | .13 | .04 | .12 | -.14 | .00 | -.13 | .04 | -.10 | -.05 | -.12 | .73 |
| VG 14 | .02 | .11 | .04 | .01 | .67 | -.01 | -.07 | -.03 | .16 | .07 | -.08 | -.10 | .01 | -.02 | -.08 | -.07 | -.12 | .66 |
| VG 16 | -.15 | .01 | .15 | .02 | -.05 | .09 | .02 | -.04 | .46 | .25 | -.06 | -.02 | .00 | -.02 | -.09 | .08 | -.08 | .53 |
| VG 13 | -.02 | -.07 | -.11 | -.09 | -.09 | .56 | -.14 | -.05 | -.14 | -.11 | -.10 | -.10 | -.07 | -.02 | .36 | -.08 | .03 | .50 |
| VG 4 | .18 | -.10 | -.03 | .09 | .04 | -.11 | .58 | .15 | .04 | -.09 | -.05 | .19 | .00 | -.04 | -.09 | .08 | -.12 | .59 |
| VG 6 | .20 | -.10 | -.09 | .08 | .09 | -.14 | -.05 | .37 | .18 | .31 | .15 | -.01 | .01 | -.10 | -.10 | .02 | -.09 | .46 |
| VG 17 | .05 | -.09 | .04 | .01 | -.06 | -.15 | -.12 | .03 | .01 | .13 | .17 | .12 | -.04 | -.08 | -.09 | -.04 | -.04 | .27 |
| VG 7 | .13 | .06 | .07 | -.07 | .07 | -.17 | -.12 | -.10 | .49 | -.14 | .17 | .03 | .17 | -.06 | -.12 | -.22 | -.07 | .54 |
| VG 9 | -.07 | -.08 | -.08 | -.09 | -.07 | -.01 | .02 | -.07 | -.10 | -.04 | .51 | .15 | .19 | -.05 | -.03 | -.09 | -.04 | .48 |
| VG 15 | -.05 | -.02 | -.08 | .01 | -.07 | -.12 | .11 | .16 | .02 | -.08 | -.02 | .50 | .05 | -.08 | -.07 | -.07 | -.08 | .48 |
| VG 8 | -.06 | .21 | -.08 | -.10 | -.11 | .05 | .03 | .04 | .02 | -.07 | .34 | .07 | .31 | -.01 | -.02 | -.16 | -.08 | .39 |
| VG 10 | .00 | .21 | .03 | -.10 | .10 | .32 | .11 | -.15 | .05 | -.11 | -.05 | -.02 | .13 | -.12 | .02 | .01 | .08 | .40 |
| VG 5 | -.06 | -.09 | -.07 | -.08 | -.09 | .11 | .00 | .05 | -.10 | -.06 | -.09 | -.06 | -.06 | -.06 | .71 | .06 | .10 | .72 |
| VG 1 | -.04 | .12 | -.02 | -.06 | -.12 | .01 | .05 | .01 | -.10 | -.11 | -.16 | -.13 | .01 | .02 | .03 | .47 | .27 | .53 |
| VG 3 | -.10 | -.08 | -.10 | -.05 | -.04 | -.05 | .07 | .29 | -.16 | -.05 | -.12 | -.01 | -.03 | .00 | .17 | .07 | .44 | .46 |

Networks generated via an ICA analysis of data from the Hand Imitation Task

**Note.** Networks generated from the hand imitation and verb generation tasks. (a) 3D overlays of ICNs were rendered in either coronal or axial orientations for the first two and last two rows respectively. For each orientation, the hand imitation ICNs are in the first row and the verb generation ICNs in the second (b) Spearman rank-order

correlations and Dice similarity correlations were calculated between ICN maps from the hand imitation and verb generation tasks. These two sets of ICA-derived ICNs underwent spatial correlations with a threshold for at least a modest score on the Dice similarity index ($s \geq 0.4$). In addition, the Spearman correlations were found to be significant above a threshold of ($r \geq 0.433$).

**Figure 2. Heatmaps of Reverse Inference Scores for the Two Paradigms**

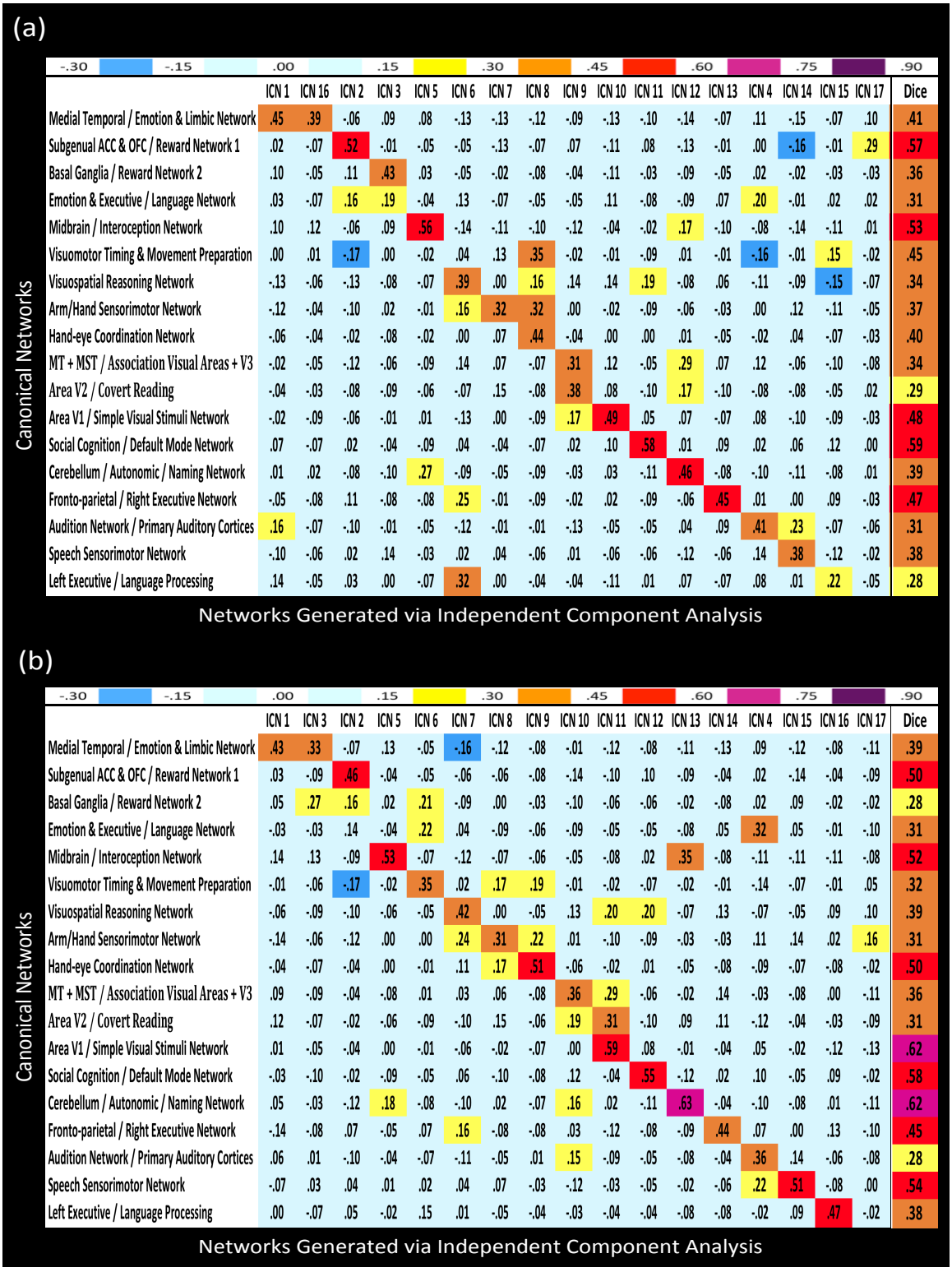

**Note.** Spearman rank-order correlations and Dice similarity correlations were calculated between the network masks from the BrainMap database and the ICN spatial maps generated from the ICA of functional data from (a) the hand imitation task and (b) the verb generation task. ICA networks were assessed for having at least a modest score on the Dice similarity index ($s \geq 0.4$) with a corresponding BrainMap network. In addition, the Spearman correlations were found to be significant above a threshold of ($r \geq 0.433$) at $\alpha < 0.05$.

**Figure 3a.**

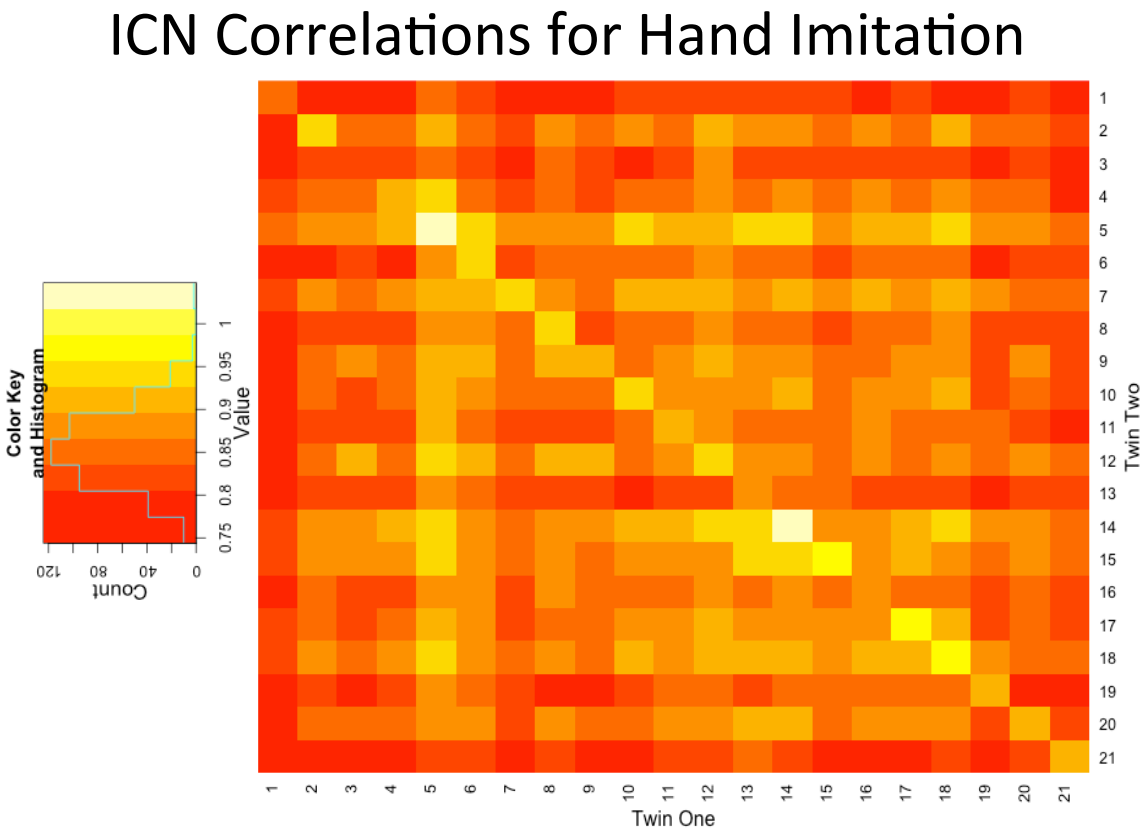
ICN Correlations for Hand Imitation
Color Key and Histogram
Count
0
40
80
120
Value
0.75
0.8
0.85
0.9
0.95
1
Twin One
1
2
3
4
5
6
7
8
9
10
11
12
13
14
15
16
17
18
19
20
21
Twin Two

**Figure 3b.**

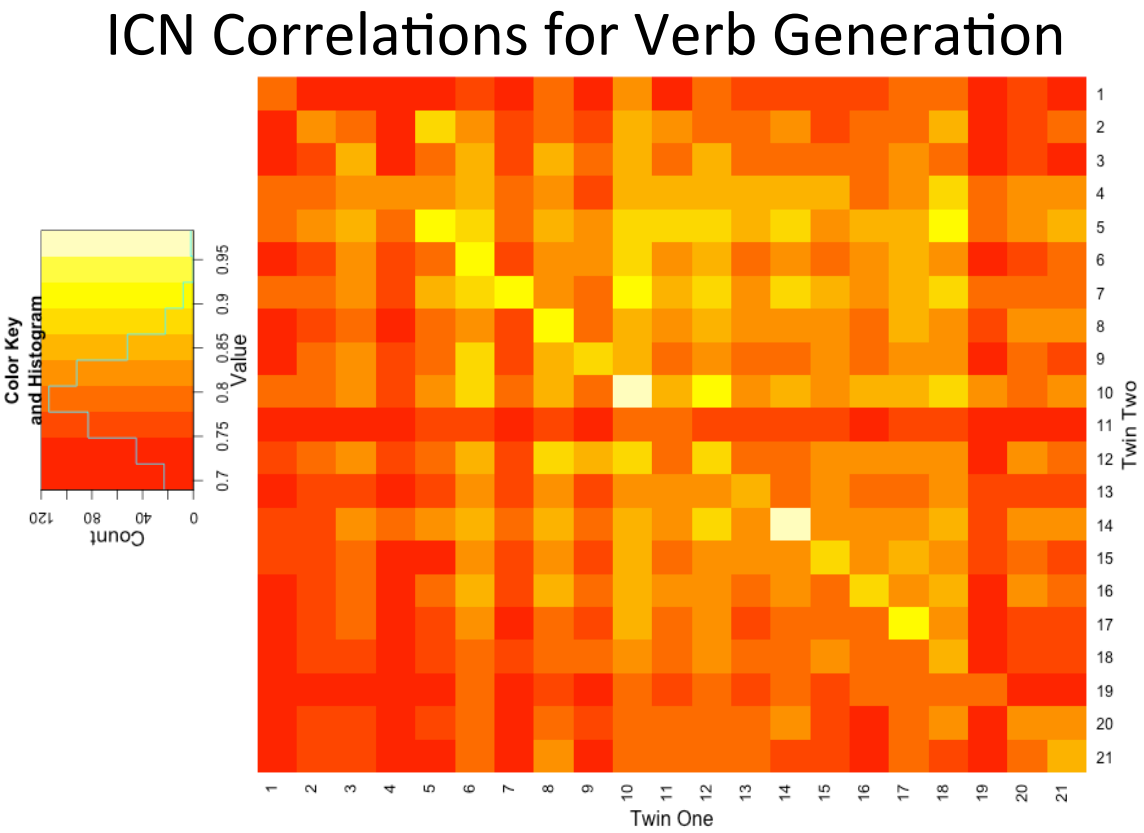


**Note.** Heatmaps showing spatial correlations across all participants. The correlations for each twin with their co-twin lie on the diagonal and the correlations with all other unrelated individuals can be found in the corresponding row or column. Correlation scores ranged from 0 – 1 and the scores for each task are represented in a 21 x 21 matrix.

## Supplementary Methods

### *Network Coherence Analyses*

#### *Mean Network Coherence Coefficient*

For each participant, the network coherence coefficient was calculated by taking the average regression coefficient across voxels for each back-transformed ICN map as follows. The participant-level maps were generated as the second stage of FSL's dual regression algorithm. First, the group-level component map was used as a spatial regressor in a general linear model (GLM) to determine participant-level component timecourses using each individual's preprocessed functional data. In the second stage, the values in the map resulted from using each participant's ICN timecourse as a temporal regressor for all brain voxels. Hence, these regression coefficient values represented how well each voxel cohered to that ICN's timecourse for that individual. Each participant-level map was then masked using the group-level map, which had been thresholded at z=6 and binarized, and the fslmaths tool was used to compute the average across voxels within the masked participant-level map. Hence, the resulting mean coherence value for that ICN map was a measure of intra-network coherence which could be used for individual difference measures, as well as cross-task consistency and familiality, as in this case.

#### *Voxel-wise Network Coherence Coefficient*

Similarly, the reliability of intra-network coherence between twins was assessed at the voxel-level using the intraclass correlation formula defined in Wisner et al. (2013). In this case, ICC's were calculated between twins per voxel (rather than for the average

across all voxels) within a given component. These voxel-level, twin-pair ICC's were then averaged per ICN to determine the voxel-wise familiality of each ICN.

### *Anatomical Similarity of Brains after Co-Registration*

*Spatial Overlap of High Resolution Structural Brain Scans*

In order to address the possible genetic contribution of anatomical similarity and structural covariance to the generation of the ICNs and the subsequent heritability estimates, Spearman correlations and Dice similarity calculations were performed on the T1 structural maps for all individuals after co-registration to the MNI 2mm brain using FSL's FLIRT algorithm. The subsets of scores for twin pairs and pairs of non-related individuals were then assessed for group differences using a non-parametric permutation test.

*Spatial Overlap of Functional Brain Scans*

It was pertinent to also assess the covariance of the spatial features of the actual functional data that was being input into the initial group ICA and dual regression algorithms to assess whether this covariance was higher for twins. Hence, an analogous Spearman correlation and permutation test procedure was performed on the functional scans after registration to the high-resolution scans and then the MNI 2mm brain.

### *Consistency of Head Movements*

Another analysis was done to address the potential confound of head motion being more similar between twins than among unrelated participants and this motion

correlation having an impact on networks generated via ICA in the two tasks. First, a root mean square displacement vector was calculated per individual from the six motion parameters measured using FSL's MCFLIRT algorithm which included estimates of translation in the three axes as well as roll, pitch and yaw rotations. Similar to the structural covariance metric, Spearman correlations were performed between the displacement vectors for all individuals and a permutation test was used to determine if there were group differences between twin scores and those of unrelated individuals.

Another concern was whether motion was influencing and/or inflating the ICN timecourses and the estimates of task-relatedness or timecourse familiality. Hence, an additional intraclass correlation calculation was performed between the motion displacement vector and ICN timecourses per individual. These ICC's were then averaged to determine the overall influence of motion on each of the ICNs.

***Significance Testing***

The significance thresholds for the inference correlations and the relationship to task correlations were established using t-tests of the transformed 'r' values with effective sample sizes. This is due to the fact that the monozygotic twins share an amount of genetic variance that could possible violate the assumption of independence in the t-test and, hence, this was addressed by adjusting the estimates using the effective sample size (Pedlow, Wang, & Muircheartaigh, 2005; Yang et al., 2011). Statistical significance for the spatial familiality metric, the coherence familiality metric, and the task HRF familiality metric were established using t-tests of the transformed values, which provided p-values and confidence intervals. For the spatial familiality metric, a t-

transform of the Spearman rho values was used for significance testing. For the coherence familiality metric, the ICC test that was performed provided p-values and confidence intervals (Revelle, 2011). For the task HRF familiality metric, the Pearson's 'r' correlation values were tested using a one-sample t-test of the transformed values. Finally, due to the fact that a t-test was performed per network, Bonferroni corrections for multiple comparisons were performed after significance testing in order to address the possibility of family-wise errors and to establish corrected significance thresholds.

### *3D Brain Figure Generation*

All brain images were generated using Mango (the Multi-image Analysis GUI) viewer from the Research Imaging Institute of University of Texas Health Science Center (http://ric.uthscsa.edu/mango/index.html). All ICN overlays from the group-level ICA output were rendered on a 3D surface build of the MNI 152 T1 1-mm brain template. This 3D rendering was then made to be translucent in order to reveal the subsurface structures contained in each ICN. This was particularly important for sub-cortical structures such as the basal ganglia network or subgenual OFC & ACC network.

## Supplementary Results

### *Anatomical Similarity of Brains after Co-Registration*

*Spatial Overlap of High Resolution Structural Brain Scans*

The non-parametric permutation test revealed no observable differences between twin scores and non-twin scores after registration to the MNI 2mm standard brain. Hence,

whatever genetic contribution there was to the anatomy of the twins' brains, that contribution was efficiently removed by the linear transformation into standard space and, consequently, the overlap of each brain with the standard MNI template was not heritable.

*Spatial Overlap of Functional Brain Scans*

After calculating the spatial Spearman correlation of transformed mean functional maps, these scores were not found to be familial using a permutation procedure. Hence, the process of co-registration of the functional data to the high resolution anatomical scans and then the standard brain template eliminated any possible contribution of structural similarities (Supplementary Figure 3a).

***Consistency of Head Movements***

No differences in movement were found between twins versus non-twins and, hence, motion was not heritable. In addition, the intraclass correlations between motion displacement and ICN timecourses were essentially zero across the board and this implies that motion did not influence the ICN timecourses in any way (Supplementary Figure 3b). These results are not surprising since temporal filtering is one of the preprocessing steps and artifactual ICA components related to respiration and other movements were previously identified and removed.

Supplementary Figures

**Supplementary Figure 1. Heatmap of Spatial Correlations between the Group-Level ICNs from Twin1 and Twin2 ICAs the Two Tasks**

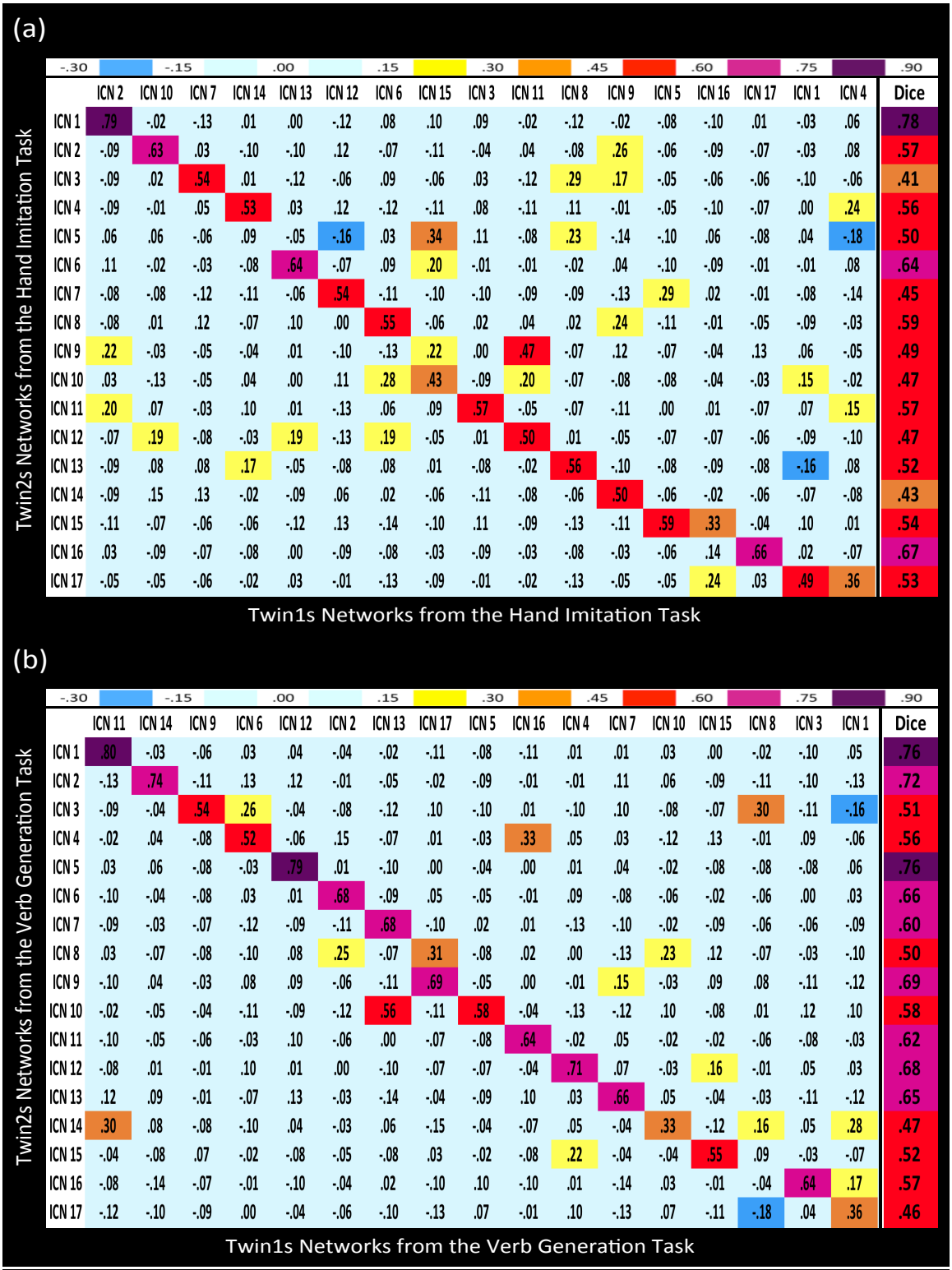

**Note.** Spearman rank-order correlations and Dice similarity correlations were calculated between ICN maps from an ICA of data from the first twin from each twin pair (Twin 1s) and the ICN maps from an ICA of data from the second twin from each twin pair (Twin 2s). These correlations were performed for data from both (a) the hand imitation task and (b) the verb generation task. The two sets of ICA-derived ICNs were assessed for having at least a modest score on the Dice similarity index ($s \geq 0.4$). In addition, the Spearman correlations were found to be significant above a threshold of ($r \geq 0.433$).

**Supplementary Figure 2.**

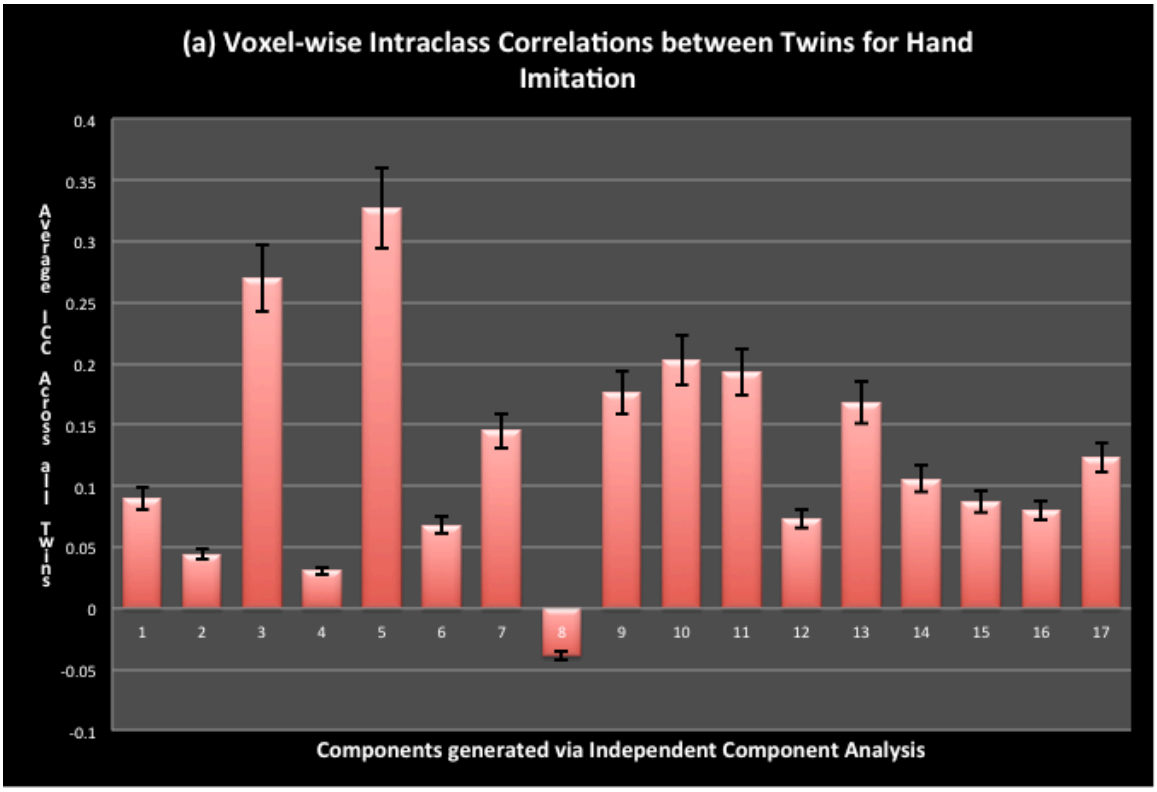

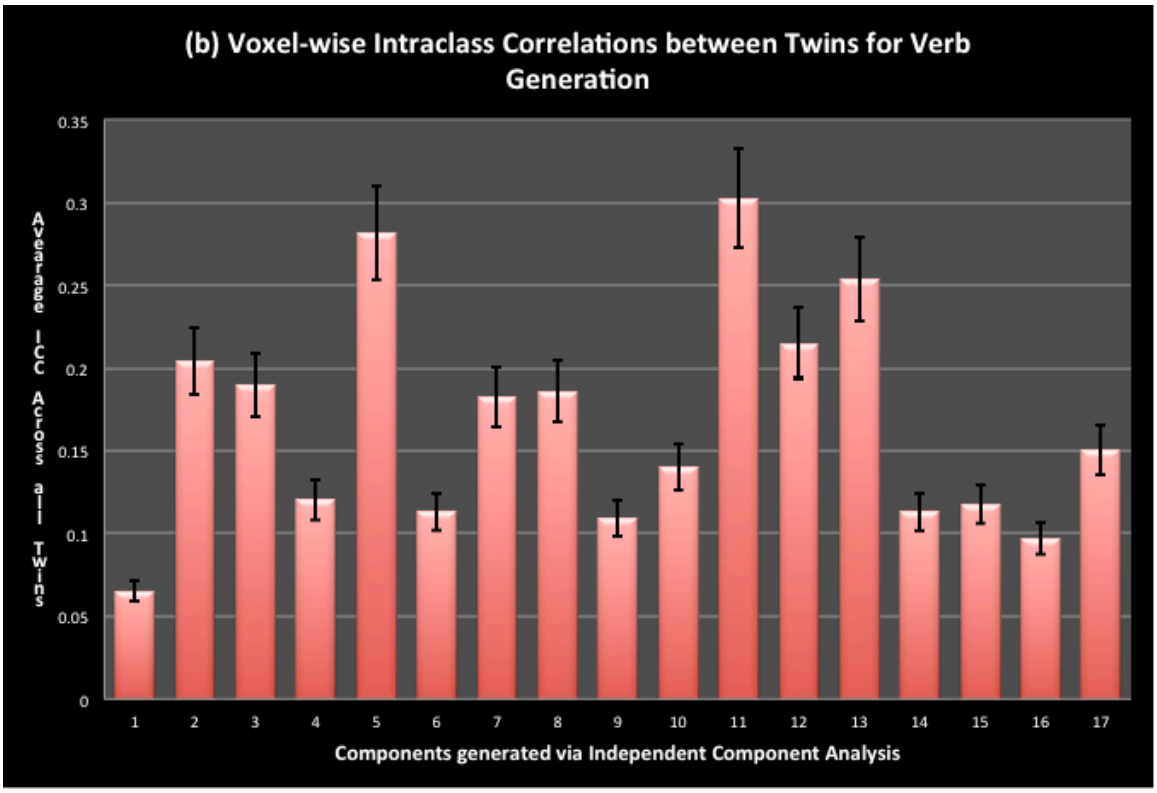


**Note.** Participant-level ICN spatial maps were first masked using a binarized image of the corresponding group-level map that had been pre-thresholded at z = 6. All of the voxelwise ICC computations for (a) hand imitation and (b) verb generation were performed using algorithms constructed with the fslmaths tool. (http://www.fmrib.ox.ac.uk/fslcourse/lectures/practicals/intro/index.htm)

**Supplementary Figure 3a. Spearman correlation of participant functional scans after co-registration**

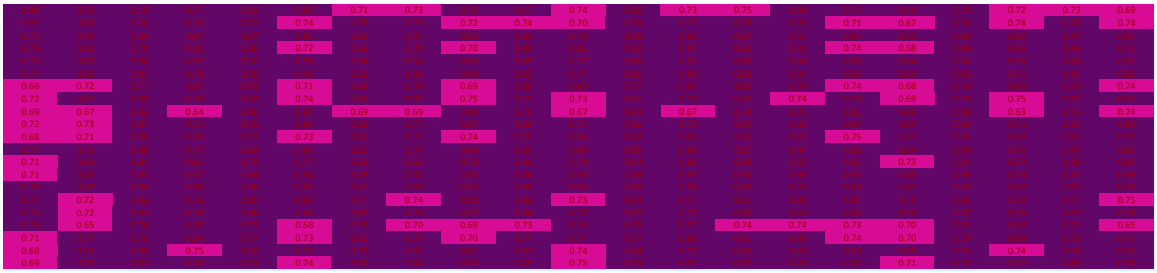

**Note.** As this functional data was derived from scans of monozygotic twins, this analysis was undertaken to verify that there was no longer a genetic (familial) influence embedded in the functional data after co-registration. Spatial correlations were completed using a Spearman's rho correlation algorithm.

## Supplementary Figure 3b. Intraclass correlations of movement and ICN timecourses

### (i) Hand Imitation

| Participant | ICN1 | ICN2 | ICN3 | ICN4 | ICN5 | ICN6 | ICN7 | ICN8 | ICN9 | ICN10 | ICN11 | ICN12 | ICN13 | ICN14 | ICN15 | ICN16 | ICN17 | Avg per person |
|---|---|---|---|---|---|---|---|---|---|---|---|---|---|---|---|---|---|---|
| 1 | 1.11E-07 | -1.51E-07 | -1.69E-07 | -1.91E-07 | -2.12E-08 | -4.24E-07 | -9.74E-07 | -1.02E-07 | -1.25E-06 | -5.66E-07 | 3.51E-07 | -4.58E-08 | -1.21E-06 | -3.85E-07 | -3.43E-07 | 2.79E-06 | -1.10E-05 | **-7.97E-07** |
| 2 | -2.88E-05 | -1.25E-06 | 2.04E-07 | -1.22E-06 | 3.65E-07 | -8.76E-07 | -1.49E-06 | -6.46E-08 | -2.44E-06 | -1.97E-06 | -5.80E-06 | -4.28E-06 | -3.64E-06 | -2.72E-06 | -2.82E-06 | 4.71E-05 | -3.68E-05 | **-2.73E-06** |
| 3 | -4.52E-05 | -9.30E-07 | 7.77E-07 | 2.00E-08 | -2.08E-06 | -9.78E-07 | -9.69E-07 | -6.11E-09 | -1.78E-06 | -7.80E-08 | -2.01E-06 | -1.62E-06 | -1.89E-06 | -2.90E-06 | -1.70E-06 | -2.38E-05 | 6.08E-06 | **-4.65E-06** |
| 4 | -5.62E-05 | -2.02E-05 | -7.51E-05 | -1.33E-05 | -1.19E-04 | -1.05E-05 | -1.63E-05 | 7.15E-07 | -2.21E-05 | -9.86E-06 | -1.54E-05 | -2.53E-05 | -1.43E-05 | -3.15E-05 | 5.66E-07 | -4.28E-04 | -1.51E-03 | **-1.39E-04** |
| 5 | -2.03E-05 | -1.82E-06 | 5.11E-07 | -2.23E-06 | -2.22E-06 | -7.94E-06 | -2.19E-05 | -1.20E-06 | -1.45E-05 | -4.46E-06 | -2.20E-06 | -2.69E-06 | -6.53E-06 | -5.98E-06 | 2.09E-06 | 3.72E-03 | -2.50E-05 | **2.12E-04** |
| 6 | 7.24E-07 | 5.57E-07 | 3.57E-07 | -3.62E-08 | -6.13E-07 | -3.36E-06 | -1.43E-05 | -5.18E-07 | -3.22E-06 | -9.00E-07 | -1.19E-07 | -5.43E-08 | -2.08E-06 | -2.32E-06 | 6.66E-07 | 6.90E-06 | -3.20E-06 | **-1.26E-06** |
| 7 | -1.22E-06 | -1.55E-08 | -2.43E-07 | -4.38E-07 | -8.11E-07 | 1.54E-07 | 4.43E-07 | -1.15E-08 | 3.89E-07 | 8.35E-08 | -3.70E-07 | -8.75E-07 | -1.96E-07 | -2.88E-07 | -2.09E-07 | -6.76E-06 | -1.28E-06 | **-6.85E-07** |
| 8 | -4.39E-07 | 2.81E-07 | -1.04E-07 | 8.23E-07 | -1.12E-06 | -4.89E-07 | -2.75E-06 | 1.98E-08 | -1.36E-06 | -4.64E-07 | 1.15E-07 | -2.02E-07 | -4.22E-08 | -5.26E-07 | -2.98E-07 | -4.19E-06 | 8.08E-07 | **-5.85E-07** |
| 9 | -2.57E-03 | -3.95E-06 | -1.39E-06 | -4.52E-06 | -1.02E-05 | -6.59E-06 | -3.21E-05 | -2.08E-06 | -1.24E-05 | -1.36E-06 | -2.70E-06 | -1.75E-05 | -1.58E-05 | -9.88E-06 | -2.90E-05 | -1.34E-05 | -3.35E-04 | **-1.81E-04** |
| 10 | -5.03E-06 | -3.67E-07 | -3.98E-07 | 2.30E-08 | -3.99E-07 | -7.60E-07 | -2.60E-06 | -2.70E-07 | -3.12E-07 | -1.18E-07 | -8.03E-07 | -6.09E-07 | -1.22E-06 | -1.97E-06 | -1.80E-06 | -5.00E-05 | 2.19E-05 | **-2.63E-06** |
| 11 | -9.10E-06 | -1.69E-06 | 8.31E-06 | -2.99E-06 | -2.81E-06 | -4.99E-06 | -1.76E-05 | -1.32E-06 | -1.24E-05 | -2.21E-06 | -2.77E-06 | -2.66E-06 | -4.34E-06 | 1.00E-06 | 8.71E-06 | -5.02E-04 | 7.27E-03 | **3.95E-04** |
| 12 | 7.93E-05 | -5.81E-06 | 6.11E-07 | -3.39E-06 | -1.03E-05 | -3.27E-06 | -5.25E-05 | 1.42E-06 | -2.88E-05 | -5.65E-06 | -4.90E-06 | -5.74E-05 | -1.20E-05 | -1.02E-05 | -3.76E-06 | 3.00E-03 | -6.25E-03 | **-1.98E-04** |
| 13 | -2.55E-05 | -6.93E-07 | 1.46E-05 | -2.75E-06 | 1.80E-04 | -2.44E-05 | -8.44E-05 | -3.38E-06 | -1.33E-05 | -1.05E-05 | -4.22E-06 | 2.00E-05 | -1.04E-05 | -2.33E-05 | -1.05E-05 | -2.61E-03 | -3.00E-04 | **-1.71E-04** |
| 14 | -1.20E-08 | 6.13E-07 | 1.64E-06 | 1.70E-07 | -6.18E-06 | -1.58E-06 | -3.10E-06 | 1.91E-07 | -1.23E-06 | -1.71E-07 | -3.77E-07 | -1.19E-07 | -1.53E-06 | -1.70E-06 | -5.77E-07 | -1.30E-02 | -1.13E-06 | **-7.65E-04** |
| 15 | -4.61E-06 | -2.26E-07 | -3.65E-07 | -7.15E-07 | -5.47E-07 | -6.84E-07 | -1.99E-06 | -1.60E-07 | -9.58E-07 | -4.52E-07 | -7.11E-08 | -7.68E-08 | -1.08E-06 | -9.20E-07 | -1.82E-08 | -1.07E-04 | 1.80E-05 | **-6.02E-06** |
| 16 | -6.16E-05 | -5.13E-06 | 6.84E-06 | 1.28E-05 | -9.50E-06 | -1.29E-05 | -5.98E-05 | -4.18E-06 | -1.88E-05 | -2.71E-06 | -6.60E-06 | 1.18E-05 | -4.27E-05 | -2.25E-05 | -2.49E-06 | -1.61E-04 | 6.15E-04 | **1.39E-05** |
| 17 | -2.00E-05 | -8.80E-07 | 4.09E-06 | 1.96E-06 | 1.19E-06 | -1.53E-06 | -3.75E-06 | -7.81E-07 | 1.04E-09 | 5.10E-07 | 1.12E-08 | 2.38E-07 | -8.38E-06 | -2.57E-06 | -3.07E-06 | 3.91E-05 | -1.56E-05 | **-5.53E-07** |
| 18 | -1.01E-04 | -8.24E-06 | -1.94E-05 | -6.48E-05 | -1.46E-04 | -2.12E-05 | -1.18E-04 | 8.62E-06 | -8.32E-05 | -1.69E-05 | 5.97E-06 | -1.29E-04 | -3.84E-05 | 1.50E-05 | 9.50E-06 | -1.62E-03 | 2.56E-04 | **-1.22E-04** |
| 19 | -3.93E-06 | -1.63E-07 | -7.57E-07 | -5.17E-07 | -1.32E-06 | 2.36E-07 | 1.20E-06 | 2.97E-08 | 7.77E-07 | 7.97E-08 | -7.91E-07 | -3.08E-07 | -4.57E-07 | -3.62E-07 | -2.10E-07 | -7.14E-06 | -1.42E-06 | **-8.86E-07** |
| 20 | -3.10E-04 | -4.14E-08 | 2.42E-08 | -3.17E-07 | 3.04E-07 | 6.36E-08 | -6.66E-07 | 7.46E-08 | -5.99E-08 | 1.85E-07 | 1.83E-08 | -4.01E-07 | 1.57E-07 | -3.21E-07 | -5.92E-07 | -4.53E-06 | -1.42E-04 | **-2.69E-05** |
| 21 | -9.30E-04 | -4.01E-07 | -1.60E-06 | -9.90E-07 | 5.26E-05 | -1.47E-06 | -4.99E-06 | -1.24E-07 | -2.17E-06 | -7.00E-07 | 5.52E-09 | -1.65E-07 | -2.53E-06 | -2.09E-06 | -6.19E-07 | -1.40E-07 | -9.73E-06 | **-5.33E-05** |
| 22 | -2.54E-06 | -2.08E-07 | -2.15E-07 | -1.67E-07 | -2.57E-06 | 2.03E-07 | 3.77E-07 | -7.24E-09 | 2.47E-08 | 3.54E-07 | -3.57E-07 | -5.93E-07 | 6.36E-09 | -1.23E-07 | -3.35E-07 | -6.71E-05 | -3.06E-05 | **-6.11E-06** |
| 23 | -1.69E-04 | 1.13E-05 | -6.51E-06 | -3.09E-05 | -6.32E-05 | -9.83E-06 | -1.79E-05 | 9.44E-06 | -1.34E-05 | -5.02E-06 | -1.24E-05 | -3.39E-05 | -8.59E-06 | -3.91E-05 | 1.40E-05 | -2.08E-03 | -2.80E-03 | **-3.09E-04** |
| 24 | -4.37E-05 | -1.04E-06 | -4.01E-07 | -1.24E-06 | -6.60E-06 | -2.85E-07 | 1.89E-06 | -1.54E-07 | -6.15E-07 | 4.24E-07 | -1.93E-06 | -3.90E-06 | -4.96E-06 | -3.36E-06 | -4.79E-06 | -2.83E-05 | -2.60E-04 | **-2.11E-05** |
| 25 | -2.68E-05 | -1.84E-06 | -2.61E-06 | -4.35E-06 | -5.66E-06 | -1.67E-06 | -6.99E-06 | 7.10E-07 | 8.76E-06 | 3.52E-07 | -1.33E-06 | -6.16E-06 | -4.21E-08 | -6.46E-06 | -5.76E-06 | -3.38E-04 | -2.33E-05 | **-2.48E-05** |
| 26 | -9.12E-05 | -1.77E-05 | -3.12E-05 | -4.35E-05 | -4.29E-05 | -2.95E-05 | -9.83E-05 | -6.33E-06 | 2.35E-05 | -1.41E-05 | -2.61E-05 | -9.12E-05 | -4.30E-05 | -4.16E-05 | -5.31E-05 | -9.74E-03 | -1.54E-03 | **-6.99E-04** |
| 27 | 4.52E-06 | 2.20E-07 | 1.08E-07 | 3.08E-07 | -2.83E-07 | -4.72E-07 | -1.31E-06 | 1.70E-08 | -1.13E-06 | -1.20E-07 | 2.79E-07 | -3.64E-08 | 5.42E-08 | -1.14E-09 | 2.26E-07 | -2.55E-06 | -3.62E-04 | **-2.13E-05** |
| 28 | -3.86E-06 | 1.74E-07 | 4.88E-07 | -8.22E-07 | -6.78E-07 | -6.35E-07 | -3.51E-06 | -3.41E-08 | -2.49E-06 | -8.49E-07 | -2.19E-07 | 8.04E-07 | -4.28E-07 | -4.87E-07 | 1.01E-06 | -3.03E-05 | -2.38E-07 | **-2.47E-06** |
| 29 | 4.71E-07 | -3.35E-08 | 6.22E-08 | 1.46E-07 | -1.82E-06 | -1.29E-07 | -2.62E-07 | 8.59E-09 | 2.19E-08 | -2.67E-08 | -8.88E-08 | -2.24E-07 | 1.31E-07 | 1.21E-07 | 9.81E-08 | -7.64E-06 | 7.56E-06 | **-9.42E-08** |
| 30 | 4.75E-05 | -2.76E-07 | 8.22E-07 | 8.93E-07 | 2.51E-06 | -4.12E-07 | -1.89E-06 | 2.78E-08 | -1.26E-06 | -9.93E-08 | 2.32E-07 | 8.73E-07 | -1.94E-07 | -4.50E-07 | -9.61E-07 | -1.21E-06 | -3.55E-05 | **6.24E-07** |
| 31 | -1.16E-05 | -2.68E-06 | 1.87E-06 | 3.16E-07 | 4.26E-06 | -2.10E-06 | -1.45E-05 | -6.60E-07 | -3.00E-06 | -4.03E-07 | -2.10E-06 | -5.58E-07 | -3.78E-06 | -6.34E-06 | -4.23E-06 | -2.91E-05 | -1.02E-04 | **-1.04E-05** |
| 32 | -2.02E-05 | -1.53E-06 | -1.65E-06 | -2.67E-06 | 1.70E-05 | -6.89E-07 | -6.12E-06 | -3.70E-08 | -2.71E-06 | -6.51E-07 | -1.92E-06 | -7.54E-06 | -1.13E-06 | -3.27E-06 | -4.70E-06 | -6.80E-05 | -9.64E-05 | **-1.19E-05** |
| 33 | 1.67E-05 | 2.13E-07 | 1.34E-07 | 5.73E-07 | 7.47E-07 | -3.41E-07 | -2.82E-06 | -5.62E-08 | -1.15E-06 | -2.76E-08 | 2.24E-07 | -2.90E-07 | 2.38E-07 | -6.67E-09 | 2.36E-07 | -1.11E-05 | -1.87E-04 | **-1.08E-05** |
| 34 | 2.88E-06 | 2.26E-07 | -3.25E-07 | 2.68E-07 | -1.37E-05 | 1.44E-07 | -8.82E-07 | 2.31E-07 | -1.29E-06 | 1.33E-07 | 3.20E-07 | -4.17E-07 | 3.95E-08 | -7.96E-09 | -2.30E-07 | -2.03E-06 | -3.44E-06 | **-1.06E-06** |
| 35 | -1.63E-04 | -3.76E-06 | -2.40E-06 | -1.43E-05 | 3.89E-06 | -3.89E-06 | -1.32E-05 | 1.64E-06 | -1.19E-06 | 1.26E-06 | -5.16E-07 | -1.79E-05 | -2.48E-06 | -5.97E-06 | -1.16E-05 | -1.97E-03 | -1.03E-04 | **-1.35E-04** |
| 36 | 2.15E-06 | -6.56E-08 | 8.87E-07 | 2.02E-07 | -1.63E-07 | -5.23E-07 | 4.89E-07 | -2.54E-07 | -5.08E-07 | 1.31E-07 | -1.27E-07 | 1.31E-06 | -3.11E-06 | -1.07E-06 | -8.98E-08 | -4.92E-06 | 2.95E-03 | **1.73E-04** |
| 37 | -1.05E-05 | -1.47E-07 | -1.00E-06 | -3.75E-07 | -1.69E-06 | -1.69E-06 | -5.74E-06 | -2.93E-07 | -2.16E-06 | -7.31E-07 | -2.35E-07 | -3.99E-07 | -1.38E-06 | -5.40E-07 | -6.87E-07 | -2.70E-05 | -9.39E-06 | **-3.77E-06** |
| 38 | -3.75E-06 | -9.32E-07 | -2.94E-08 | -1.02E-06 | -1.59E-06 | -1.61E-06 | -2.99E-06 | -1.07E-06 | -3.98E-06 | -1.15E-06 | -1.26E-06 | -1.22E-06 | -8.81E-06 | -1.32E-06 | -4.01E-06 | -7.00E-05 | 8.86E-07 | **-6.11E-06** |
| 39 | 4.88E-05 | 6.15E-07 | 2.25E-06 | -9.69E-07 | 1.06E-06 | -1.29E-06 | -1.29E-05 | -5.53E-08 | -1.55E-06 | 7.61E-07 | 7.09E-07 | -3.42E-06 | -1.28E-06 | -2.06E-06 | -5.03E-07 | -4.18E-04 | 5.56E-04 | **9.85E-06** |
| 40 | -5.24E-06 | 4.88E-09 | 2.22E-07 | 5.68E-07 | -1.65E-06 | -2.98E-07 | -3.98E-07 | -6.84E-08 | -9.51E-07 | 1.24E-07 | -1.65E-07 | -2.54E-08 | -8.16E-07 | -3.73E-07 | 1.53E-07 | -1.29E-04 | 3.10E-06 | **-7.92E-06** |
| 41 | -5.24E-05 | -1.08E-06 | 5.46E-06 | -1.15E-05 | 1.11E-05 | -6.12E-06 | -2.33E-05 | 2.92E-06 | -1.60E-06 | -6.42E-08 | -1.67E-06 | -1.33E-05 | -5.53E-06 | -1.15E-05 | -1.85E-05 | -6.45E-05 | -1.12E-04 | **-1.79E-05** |
| 42 | -4.30E-05 | 5.45E-08 | 2.80E-07 | -5.52E-07 | 1.48E-05 | -5.86E-07 | -2.11E-06 | 1.04E-07 | -7.33E-07 | -2.33E-07 | -3.95E-08 | -6.04E-07 | -2.59E-07 | -8.15E-07 | -6.43E-07 | -8.58E-07 | -3.56E-06 | **-2.28E-06** |
| Avg per ICN | **-1.12E-04** | **-1.68E-06** | **-2.33E-06** | **-4.66E-06** | **-4.42E-06** | **-4.01E-06** | **-1.58E-05** | **6.96E-08** | **-5.50E-06** | **-1.90E-06** | **-2.23E-06** | **-9.50E-06** | **-6.19E-06** | **-5.62E-06** | **-3.18E-06** | **-6.54E-04** | **-6.34E-05** | **-5.27E-05** |

### (ii) Verb Generation

| Participant | ICN1 | ICN2 | ICN3 | ICN4 | ICN5 | ICN6 | ICN7 | ICN8 | ICN9 | ICN10 | ICN11 | ICN12 | ICN13 | ICN14 | ICN15 | ICN16 | ICN17 | ICN18 | Avg per person |
|---|---|---|---|---|---|---|---|---|---|---|---|---|---|---|---|---|---|---|---|
| 1 | -1.05E-06 | 3.95E-07 | -1.89E-07 | -1.31E-06 | -3.90E-09 | -6.44E-07 | -1.43E-06 | -3.91E-07 | -6.35E-07 | 5.01E-08 | -8.78E-07 | -3.35E-07 | 2.32E-08 | -5.58E-07 | 7.81E-07 | -3.50E-07 | -6.52E-07 | -9.57E-07 | **-4.52E-07** |
| 2 | -1.27E-06 | -3.73E-06 | -9.45E-07 | -2.56E-06 | 4.53E-06 | -2.52E-06 | -2.44E-06 | -6.62E-07 | 1.90E-06 | -1.39E-06 | -1.05E-06 | -2.95E-07 | 1.77E-07 | -2.04E-06 | -1.93E-06 | -6.80E-06 | -2.86E-06 | -1.67E-02 | **-9.31E-04** |
| 3 | 5.71E-07 | -1.89E-07 | -1.04E-07 | -1.59E-06 | 2.59E-06 | 1.10E-06 | -2.30E-07 | -4.42E-07 | 1.29E-08 | -1.13E-07 | -5.28E-07 | -4.86E-07 | -3.43E-07 | -1.46E-07 | -8.08E-07 | 4.98E-08 | 6.81E-07 | -1.49E-05 | **-8.27E-07** |
| 4 | -4.29E-07 | -1.77E-06 | -7.89E-06 | -3.34E-06 | -3.77E-06 | -1.79E-05 | 1.75E-06 | 4.46E-06 | 2.62E-06 | -3.72E-06 | 6.82E-07 | 1.82E-06 | -1.60E-06 | -1.69E-06 | 4.52E-06 | 7.14E-06 | -8.08E-06 | 6.71E-05 | **2.22E-06** |
| 5 | -5.82E-06 | -5.49E-07 | 3.88E-06 | 2.78E-06 | -7.74E-07 | 4.11E-06 | 3.22E-06 | 7.72E-06 | 1.54E-06 | 3.98E-06 | -7.30E-06 | -2.40E-06 | 1.50E-06 | 2.37E-06 | -6.19E-07 | 6.31E-06 | -1.80E-06 | 1.43E-04 | **8.96E-06** |
| 6 | -1.92E-06 | 1.36E-06 | 8.81E-07 | -2.21E-06 | -1.04E-05 | -3.71E-07 | 2.90E-08 | 2.27E-06 | -1.75E-06 | 8.19E-07 | -2.30E-06 | -1.57E-06 | 1.51E-07 | -4.71E-07 | 8.73E-07 | -8.58E-07 | -3.25E-06 | 3.25E-05 | **7.64E-07** |
| 7 | 1.00E-07 | -1.97E-07 | 7.51E-08 | -2.85E-07 | 4.93E-07 | -5.10E-07 | -3.61E-09 | 2.63E-07 | 1.11E-07 | -1.32E-07 | -1.36E-07 | -3.61E-08 | 5.28E-08 | -1.68E-08 | -8.55E-08 | 2.66E-07 | -2.34E-07 | 6.48E-06 | **3.44E-07** |
| 8 | -1.73E-07 | 1.58E-07 | 7.99E-07 | 1.37E-07 | -3.41E-06 | -6.59E-07 | -2.21E-07 | 4.74E-07 | -6.23E-07 | 1.53E-06 | -2.54E-08 | -9.68E-08 | 3.15E-07 | -6.99E-08 | 2.97E-06 | 4.48E-07 | -6.03E-07 | 3.87E-05 | **2.20E-06** |
| 9 | -4.70E-07 | 1.42E-06 | 7.82E-07 | 3.05E-06 | 2.88E-06 | -2.64E-06 | -1.13E-06 | 4.63E-06 | -1.07E-05 | -5.22E-07 | 5.28E-07 | 1.19E-06 | -1.98E-07 | -1.46E-06 | -1.50E-06 | 8.71E-07 | -1.23E-05 | -7.44E-06 | **-1.28E-06** |
| 10 | -1.66E-07 | -1.21E-07 | 6.09E-08 | -3.18E-07 | -2.04E-06 | -6.96E-08 | -1.41E-07 | 6.98E-07 | -5.44E-07 | -1.61E-08 | -1.81E-07 | -5.59E-09 | 7.13E-08 | 2.47E-07 | -1.61E-07 | 9.28E-07 | -1.80E-06 | 6.73E-05 | **3.54E-06** |
| 11 | -2.38E-06 | 9.24E-08 | 2.21E-06 | -2.31E-07 | -1.23E-05 | -1.52E-06 | 2.16E-06 | 2.54E-06 | -2.82E-06 | 4.41E-06 | 6.69E-08 | -1.84E-06 | -3.44E-07 | 7.84E-07 | 8.80E-07 | 5.41E-07 | -7.80E-06 | 2.38E-03 | **1.31E-04** |
| 12 | -3.44E-06 | 4.85E-07 | -3.70E-06 | -5.80E-07 | -8.53E-06 | -3.30E-06 | -6.51E-07 | 3.87E-06 | -3.05E-06 | 2.27E-07 | -1.17E-06 | -3.61E-06 | -1.20E-06 | -8.79E-07 | -1.63E-06 | -8.08E-07 | -1.09E-05 | -2.90E-05 | **-3.77E-06** |
| 13 | -1.14E-05 | 8.45E-06 | 1.00E-06 | 7.99E-06 | -1.73E-05 | 5.70E-07 | -4.56E-06 | 2.03E-05 | -5.58E-06 | -5.11E-06 | 4.45E-07 | 2.12E-06 | 2.69E-07 | 6.44E-07 | 7.81E-06 | -5.56E-05 | -2.29E-05 | -4.96E-05 | **-6.81E-06** |
| 14 | 6.82E-07 | 9.81E-07 | 4.66E-07 | 2.25E-06 | 7.28E-06 | 1.33E-06 | 9.82E-07 | 5.08E-06 | 2.42E-06 | -1.02E-06 | 1.89E-06 | 1.12E-06 | 1.25E-06 | 9.11E-07 | -2.79E-06 | -1.86E-06 | 9.49E-06 | 2.08E-03 | **1.17E-04** |
| 15 | -3.86E-07 | 4.14E-07 | -2.37E-07 | -3.33E-07 | -1.51E-06 | -1.64E-07 | 2.72E-09 | -3.81E-07 | -5.74E-07 | -2.24E-07 | -2.85E-08 | -6.40E-08 | -2.07E-08 | -1.26E-07 | -7.11E-07 | 2.67E-07 | -1.46E-06 | 1.04E-03 | **5.74E-05** |
| 16 | -4.09E-06 | -4.88E-07 | -2.11E-06 | 5.73E-06 | -4.13E-06 | -3.62E-06 | -8.42E-06 | -2.22E-06 | -3.51E-06 | -1.22E-06 | 4.85E-07 | -3.01E-06 | 8.01E-07 | -1.46E-06 | 6.48E-06 | -3.17E-06 | -5.98E-06 | -1.47E-04 | **-9.85E-06** |
| 17 | -5.37E-07 | -4.18E-07 | -2.12E-07 | 2.11E-06 | 2.34E-06 | 3.32E-09 | -1.04E-06 | -8.75E-07 | -3.23E-07 | -8.45E-08 | -5.22E-07 | -7.42E-07 | -9.79E-07 | -4.02E-08 | -2.22E-07 | -1.99E-07 | -3.16E-07 | 1.69E-05 | **8.26E-07** |
| 18 | -1.45E-05 | -2.44E-06 | 3.43E-06 | -8.16E-06 | -2.03E-05 | -1.88E-06 | 1.50E-05 | 6.57E-06 | -1.28E-05 | 9.65E-06 | -5.54E-06 | -1.11E-05 | -8.34E-06 | 1.26E-06 | -1.12E-05 | -1.42E-06 | 5.42E-06 | 2.92E-05 | **-1.50E-06** |
| 19 | 2.55E-07 | -1.38E-07 | -1.55E-07 | -2.08E-07 | 6.67E-07 | -7.16E-08 | -2.38E-07 | 7.21E-08 | 2.18E-07 | -2.08E-07 | 4.07E-08 | 6.16E-08 | -1.37E-07 | -1.17E-07 | -5.49E-07 | -2.15E-07 | 1.45E-07 | 2.21E-05 | **1.20E-06** |
| 20 | -2.15E-07 | 4.44E-08 | -5.58E-08 | 6.94E-08 | 3.14E-07 | 2.78E-08 | -1.37E-07 | -1.44E-06 | -3.61E-08 | -1.06E-07 | 2.42E-08 | -4.52E-07 | -1.92E-07 | -1.78E-07 | -3.57E-07 | 9.10E-07 | -1.53E-06 | 6.38E-07 | **-1.48E-07** |
| 21 | -1.99E-07 | 6.01E-07 | 3.80E-07 | 5.86E-07 | 2.02E-07 | 1.13E-06 | -5.43E-07 | -1.21E-07 | 6.75E-07 | -2.13E-07 | 4.89E-07 | 5.53E-07 | 1.17E-07 | -9.11E-09 | 4.81E-06 | -8.64E-05 | -1.18E-05 | -8.01E-06 | **-5.43E-06** |
| 22 | -8.51E-09 | -5.99E-08 | -9.93E-08 | 2.11E-07 | 2.75E-07 | 3.62E-10 | -3.51E-08 | 1.28E-07 | 1.34E-07 | -1.12E-08 | 1.52E-07 | 4.64E-08 | -1.72E-07 | -2.80E-08 | -3.93E-07 | -6.72E-07 | 2.09E-07 | -3.27E-06 | **-2.00E-07** |
| 23 | -5.57E-05 | -3.57E-05 | -6.23E-07 | -4.30E-06 | -1.24E-04 | -6.48E-05 | -4.61E-05 | -6.80E-05 | 3.86E-06 | -2.68E-05 | -1.24E-05 | 4.71E-06 | -3.11E-05 | -3.73E-05 | -2.88E-05 | -5.48E-05 | -1.89E-05 | 2.00E-05 | **-3.23E-05** |
| 24 | 1.06E-06 | -1.60E-06 | -9.78E-08 | 4.97E-07 | 2.71E-06 | 8.10E-07 | -6.61E-07 | 5.43E-07 | 1.24E-06 | 3.62E-07 | -6.80E-07 | -1.01E-06 | 8.79E-07 | -3.97E-07 | 1.97E-06 | -3.77E-07 | -1.25E-06 | -1.96E-05 | **-8.69E-07** |
| 25 | 1.36E-06 | 4.01E-07 | -1.22E-06 | -1.33E-06 | 4.39E-06 | 7.48E-07 | -1.75E-06 | -2.89E-06 | 1.81E-06 | -2.41E-06 | -4.89E-07 | -4.14E-07 | -1.07E-06 | -1.35E-06 | -2.10E-06 | -7.35E-07 | -2.61E-06 | -4.38E-04 | **-2.49E-05** |
| 26 | -5.19E-06 | -6.76E-06 | -2.11E-06 | 2.99E-06 | -2.07E-06 | -1.92E-05 | -1.14E-05 | -1.41E-05 | -5.84E-06 | -7.44E-07 | -8.76E-06 | -5.73E-06 | -2.67E-06 | -3.42E-06 | 3.50E-06 | -1.50E-05 | -4.73E-05 | -2.03E-04 | **-1.93E-05** |
| 27 | -1.57E-07 | 2.33E-07 | 1.14E-07 | 1.02E-07 | -1.59E-06 | -3.50E-07 | 1.84E-08 | 5.71E-07 | 4.48E-09 | 1.07E-07 | -6.53E-08 | 2.66E-08 | 7.45E-08 | 8.99E-08 | 3.45E-07 | 2.74E-07 | -3.65E-07 | 1.03E-03 | **5.73E-05** |
| 28 | -7.17E-07 | 6.31E-08 | 2.19E-07 | 6.80E-07 | -4.18E-06 | -6.23E-08 | -3.52E-07 | 1.35E-07 | -6.83E-07 | 3.29E-07 | -7.99E-08 | -2.81E-08 | -6.43E-08 | 2.39E-07 | 1.80E-06 | -1.65E-07 | -5.78E-07 | -9.56E-06 | **-7.23E-07** |
| 29 | 8.49E-08 | 1.45E-07 | 7.30E-08 | 1.50E-07 | 5.11E-07 | -5.10E-07 | -3.72E-07 | 1.37E-07 | 4.58E-08 | 2.40E-07 | -4.58E-08 | -2.59E-08 | 4.77E-08 | -6.40E-09 | 4.61E-07 | 4.75E-08 | -3.65E-07 | 9.40E-06 | **5.57E-07** |
| 30 | -4.29E-07 | 5.04E-08 | -3.26E-07 | -1.41E-07 | -1.40E-06 | 1.38E-07 | 1.33E-07 | 4.72E-07 | -6.32E-07 | 2.63E-08 | -3.23E-07 | -5.95E-07 | -1.30E-07 | -2.74E-07 | 1.39E-07 | -4.67E-07 | -2.25E-06 | 1.32E-05 | **4.00E-07** |
| 31 | 1.03E-06 | 6.02E-08 | -1.65E-06 | 1.03E-06 | 2.04E-06 | 1.63E-07 | -1.28E-06 | -1.19E-06 | 1.66E-06 | -1.18E-06 | 3.46E-07 | -2.70E-07 | 1.42E-06 | 2.31E-09 | -7.96E-07 | 7.25E-07 | 1.14E-06 | -1.54E-05 | **-6.76E-07** |
| 32 | 7.24E-07 | -1.05E-06 | -7.83E-07 | 2.12E-06 | -5.04E-07 | 3.60E-06 | -4.05E-07 | -9.47E-07 | 2.33E-06 | -2.35E-06 | 6.35E-07 | 1.43E-06 | 4.75E-07 | 9.88E-07 | 4.66E-06 | 5.61E-06 | 9.84E-07 | -4.54E-06 | **7.21E-07** |
| 33 | -5.13E-07 | 3.90E-08 | 3.20E-08 | -2.33E-07 | -2.02E-06 | -8.43E-07 | 2.37E-07 | -3.65E-07 | -5.99E-07 | 4.05E-07 | -1.38E-07 | -4.73E-08 | -2.54E-07 | 1.61E-08 | -1.74E-08 | -1.02E-06 | -1.09E-06 | 1.85E-03 | **1.02E-04** |
| 34 | -5.31E-07 | -2.20E-07 | 6.70E-07 | -2.20E-08 | -1.11E-06 | -2.05E-06 | 3.23E-07 | 1.26E-06 | -4.67E-07 | 1.64E-06 | -1.63E-07 | 1.18E-07 | -2.52E-07 | 1.04E-07 | -2.60E-07 | 6.38E-06 | -5.27E-06 | 1.39E-05 | **7.79E-07** |
| 35 | 3.15E-07 | 4.66E-07 | -3.03E-06 | -1.28E-06 | 2.76E-06 | 2.20E-06 | -7.55E-07 | -6.77E-08 | 9.68E-07 | -6.47E-07 | -3.08E-07 | 5.35E-08 | 2.28E-07 | -2.52E-07 | 4.22E-07 | -2.88E-06 | -1.12E-06 | -1.00E-04 | **-5.73E-06** |
| 36 | 7.18E-07 | -1.11E-07 | -1.43E-07 | -4.67E-07 | 5.05E-07 | -4.50E-07 | 3.96E-07 | -2.12E-07 | 2.71E-07 | 5.16E-08 | -9.76E-08 | -7.54E-08 | 2.56E-08 | -2.52E-07 | -3.11E-07 | 1.12E-07 | 8.58E-08 | 8.40E-06 | **4.69E-07** |
| 37 | -9.82E-07 | -2.28E-10 | 1.01E-06 | 2.02E-07 | -3.52E-06 | -5.16E-07 | -3.39E-07 | 5.07E-06 | -1.08E-06 | 6.62E-07 | -5.36E-07 | -3.09E-07 | 2.78E-07 | -6.18E-08 | 8.50E-07 | 7.03E-07 | -3.42E-06 | 2.88E-05 | **1.49E-06** |
| 38 | -1.15E-06 | 2.10E-07 | 3.39E-07 | -6.43E-07 | -4.31E-06 | -1.22E-06 | -3.17E-07 | -1.52E-06 | -1.84E-06 | 8.15E-08 | -3.87E-07 | -2.21E-07 | -6.56E-07 | -6.29E-07 | 3.32E-07 | 2.25E-06 | -1.31E-06 | 5.16E-05 | **2.25E-06** |
| 39 | -3.36E-07 | 6.03E-07 | -1.31E-07 | -3.91E-07 | -6.37E-07 | 7.82E-07 | -7.19E-07 | 3.17E-06 | -9.93E-07 | -5.91E-07 | -6.42E-07 | -8.22E-07 | -8.39E-08 | -7.32E-07 | -9.51E-07 | -1.19E-06 | 5.21E-08 | -1.04E-04 | **-5.98E-06** |
| 40 | 1.65E-07 | -2.60E-07 | -1.27E-07 | -4.91E-07 | 3.87E-07 | -4.45E-07 | -9.24E-07 | 1.64E-06 | 9.62E-08 | -4.51E-07 | -4.03E-07 | -2.91E-07 | 5.65E-08 | -3.84E-07 | -1.40E-07 | -5.66E-07 | -1.66E-06 | -2.08E-03 | **-1.16E-04** |
| 41 | 2.36E-06 | 4.50E-07 | -2.68E-06 | 2.39E-06 | 1.20E-06 | 4.04E-06 | -1.55E-06 | 1.03E-05 | 7.98E-06 | -2.34E-06 | 5.35E-07 | 2.95E-07 | 1.34E-06 | 4.95E-07 | -2.41E-06 | 9.42E-06 | 1.44E-05 | -6.12E-06 | **2.23E-06** |
| 42 | -3.46E-08 | -2.04E-08 | 6.20E-07 | 3.57E-07 | -6.22E-07 | -1.95E-07 | 1.06E-07 | 3.07E-06 | 9.66E-07 | 4.15E-07 | -1.44E-08 | 3.79E-08 | 3.17E-07 | 1.29E-07 | 2.07E-07 | 4.57E-06 | 4.82E-07 | 3.20E-05 | **2.35E-06** |
| Avg per ICN | **-2.56E-06** | **-9.43E-07** | **-2.98E-07** | **1.13E-07** | **-4.73E-06** | **-2.57E-06** | **-1.56E-06** | **-3.29E-07** | **-6.13E-07** | **-6.60E-07** | **-9.47E-07** | **-5.44E-07** | **-9.83E-07** | **-1.13E-06** | **-3.69E-07** | **-4.69E-06** | **-3.64E-06** | **-2.69E-04** | **-1.64E-05** |

**Note.** As in the previous analysis of the functional data, this analysis assessed whether there were any confounding genetic (familial) similarities in movement that inadvertently biased the network timecourse analyses to exhibit inflated estimates of familiality. Here, intraclass correlations (ICCs) were performed between the root mean square vectors describing movement throughout the scan and the ICN timecourses.

# Chapter Three

Reward Representation in Adolescent Twins:
An Investigation of Intrinsic Connectivity Networks As Familial Traits

## Summary

Impulsivity and reward responsivity are constructs that are quite salient when considering adolescence, and recent neurometric developments allow for the deconstruction of the brain mechanisms underlying these phenomena. With that in mind, this study explored the intrinsic network connectivity of adolescent twins' brains and how these characteristics are captured in the context of reward. To achieve this, concurrent GLMs and independent component analyses (ICAs) were completed. The GLMs were used to show that regions of the visual cortex and basal ganglia were activated by the task and responded to rewards, which recapitulated previous findings using this task. On the other hand, the ICAs were able to show that the entire complement of brain networks (ICNs) was present during the task but specific ICNs, e.g. the primary and association visual ICNs, were related to task components such as anticipation. In addition, the assessment of the relationship between the activation beta weights and ICN task relevance showed that the ICNs were engaged in a manner that matched increases in the underlying brain activity. However, while this positive association was observed in an omnibus assessment of all task components, it was driven primarily by the activity to connectivity correspondence seen in the anticipation phase of the task. Familiality was assessed for ICNs in the domains of timecourse dynamics, task relevance, spatial overlap and intranetwork coherence. It was observed that familiality was highest for a visual network (V2), which corroborates our previous findings using separate tasks in a different sample of monozygotic twins.

## Introduction

There is a general consensus that the brains of adolescents are rapidly changing as they transition into adults (Casey et al., 2010). By adolescence, most of the infrastructure of the human brain has reached its mature state, but there is evidence that the synaptic architecture of the frontal lobe continues to be refined (Casey et al., 2000). These seemingly subtle changes on the neuron level correspond to significant changes in behavior over the period between adolescence and early adulthood (Crews, He, & Hodge, 2007). For example, some of the most pertinent differences that have been observed relate to executive control, decision making and reward responsivity before and after this maturational transition (Steinberg, 2005). Several studies have observed that there are substantive differences between the reactions and choices of adolescents in tasks that have reward components when compared to those of adults (Galvan, Hare, Voss, Glover, & Casey, 2007; Gullo & Dawe, 2008; Spear, 2000). These differences have not only been observed in the adolescent behavior, but also the activity of adolescent brains as well (Ernst & Mueller, 2008; Luna, Padmanabhan, & O'Hearn, 2010). While it has been shown that adolescents are both behaviorally and neurobiologically hypersensitive to reward, little has been done to establish this developmental difference as a brain network trait.

If reward sensitivity is characteristic of development, then that raises the question of what is the extent of genetic control of this complex trait? To that end, we have been exploring the stability and trait-like nature of the brain within the relatively new framework of the brain's intrinsic connectivity. We recently demonstrated that not only are intrinsic connectivity networks moderately reliable and can be trait-like, but they can

also be specifically engaged by particular tasks (Moodie et al, 2014; Poppe et al, 2013, Wisner et al., 2013). However, the relationship between task-relevant activation and intrinsic network characteristics is a domain that has remained relatively unexplored. Moreover, little, if anything, is known about the intrinsic connectivity of the adolescent brain. Hence, it is important to explore this domain in teenagers and it is useful to examine intrinsic network connectivity in the context of reward processing. Finally, by studying twins in this age range, this allows us to not only explore the adolescent brain in new ways, but also to determine if the observed network characteristics are trait-like at this developmental stage.

Further, determining the extent to which suprathreshold brain activity in a model compares to new model-free, data-driven methods of parsing global brain signal is important since this will serve to complement traditional fMRI analyses in answering these developmentally-relevant questions. Several studies have shown that intrinsic connectivity networks (ICNs) derived from fMRI data capture signal from all brain regions independently and simultaneously (Beckmann & Smith, 2004; Calhoun & Adali, 2001). These ICNs are stable across time at rest and during task, and the same ICNs are not only present during a task, but are also sensitive to task dynamics (Arbabshirani et al., 2012; Brown et al., 2009; Calhoun et al., 2001). Moreover, identical ICNs can be detected in distinct task presentations and, while ICN morphology and connectivity are consistent across tasks, the ICN time courses show sensitivity to task demands (Korgaonkar, Ram, Williams, Gatt, & Grieve, 2014). Using a previous twin sample, we were able to show that the ICN characteristics of morphology, connectivity and time course dynamics also exhibit familiality and, taken together, these results support the

notion that ICNs are trait-like (Moodie, Wisner, & MacDonald III, 2014). Given that we had detected ICN across behavioral states using functional connectivity methods, the next logical step for this study was to investigate traits in an earlier developmental stage, in the contexts of both activation and functional connectivity. Hence, in this analysis, typical general linear models (GLMs) were combined with ICA to see if these methods provide complementary assessments of neurobiological traits related to reward states in adolescents.

Activity in the brain is typically described using functional magnetic resonance imaging (fMRI) platforms in terms of activation that is modeled in a general linear model (GLM) (Beckmann et al., 2003). These activation paradigms employ a subtraction procedure in which some task or stimulus-relevant epoch is contrasted against a baseline. However, these models cannot speak to what may be occurring in the brain outside the bounds of the task parameters, and also could be potentially throwing away a lot of signal by assuming an arbitrary level of baseline activity (Calhoun & Adali, 2001). To address this caveat, other methods like independent component analyses (ICAs) can be utilized to derive model-free representations of brain dynamics and can provide information germane to traditional general linear models.

To address these questions about activity and connectivity traits related to reward, GLMs and independent component analyses (ICAs) of data from a delayed response two-choice reward task were completed using a larger sample of twins in this current study. These monozygotic twins performed a delayed response two-choice reward task known as the Pirate task, in which the subjects were required to specify on which side of the screen a particular cue had appeared. The cues were pictures of three distinguishable

pirates and each pirate was associated with a particular reward magnitude (small, medium and large). This task presented an opportunity to employ a slow-event related design for the analyses, which can be used to contrast with the block design used in our previous analyses (Moodie et al. 2014).

Moreover, the assessment of phenotypes related to this reward design will also include an exploration of the familiality of the reward-related phenotypes generated from both the GLM and ICA. To achieve this, familiality will be assessed for spatial overlap, intranetwork connectivity, or coherence, as well as ICN timecourse dynamics, and task relevance. Hence, as a whole, this research will afford the opportunity to extend our understanding of the relationship between activation and connectivity even further in the context of the genetic effects on adolescent brain networks.

## Methods

### *Participants*

Seventy-five participants, 31 pairs of monozygotic twins, 13 singletons (35 females, 40 males, mean age = 15.5, ranging from 14.0 to 16.8) were included in this analysis from a larger sample recruited for the AdBrain study of the Minnesota Center for Twin and Family Research. AdBrain is a population-representative sample of 48 pairs of adolescent twins and their mothers who lived in the Twin Cities metropolitan area (i.e., within an hour and a half drive of the university). Subjects completed a comprehensive battery of clinical, personality, neuropsychological, electrophysiological, and MRI measures twice in a one-year span. However, only the task scans from the year one visits

were included in this analysis. Additional sample details are available elsewhere (Malone et al., 2014).

For inclusion in the analysis, participants were required to meet the following criteria. Data from all five runs of the task were required, with a maximum of two errors of any type within a given run. In addition, to help reduce the effects of motion artifact, an absolute linear root mean square (rms) motion threshold of one voxel (3.125 mm) was required within each run. Of the original ninety-eight potential participants, the following were excluded from analysis: MRI contraindication (N=1); computer or other hardware malfunction (N=5); incomplete data set (fewer than five runs; N=14); incorrect finger-to-button mapping (N=2); and motion (N=1).

All participant information was de-identified at the beginning of the study and the Institutional Review Board of the University of Minnesota approved all protocols. Adolescent participants gave written, informed assent before participating in the study, while mothers gave written informed consent for their children's participation.

***Experimental Design***

This study is based on the MR imaging battery conducted at the initial visit of the AdBrain study, which included a functional scan in which participants performed a version of the a delayed response two-choice task known as the Pirate Reward task (Galvan et al., 2006). High resolution anatomical T1- weighted images (MPRAGE) were also acquired. The Pirate task acquisition utilized a slow event-related design for a 6-minute scan in which the participants were asked to respond to the presentation of one of three pirates, which were cues related to increasing reward amounts, represented as treasure chests (Figure 1). The participants had to indicate which side of the screen the

pirate had appeared on and they were rewarded for accurate responses. All cue presentations were counterbalanced and presented on either side in a pseudorandom order. There were a total of 18 trials per run, with six of each reward type being presented per run.

***MR Acquisition and Imaging Parameters***

All functional data were collected on a 3T Siemens Trio MRI scanner using a whole-body transmit, 12-channel receive head coil. Vacuum pillows were used to reduce head motion. One identical whole-brain functional scan was collected per participant (EPI; TR = 2000 ms, TE = 28 ms; FA = 90°; in-plane voxel size = 3.125 x 3.125 mm; FOV = 200 mm, matrix size = 64 x 64, axial orientation; number of slices = 34, slice thickness = 4 mm, spacing between slices = 0 mm, interleaved slice acquisition, 182 volumes). A matching fieldmap was obtained immediately prior to the functional data acquisition for later use in unwarping the task data. Additionally, a structural T1-weighted image (MPRAGE) was collected per participant and used for the anatomical registration of the functional scans (TE = 3.65 ms, TR = 2530 ms, flip angle = 7**°,** FOV = 256 mm, matrix = 256 x 256, slice thickness = 1 mm, 240 sagittal slices).

***Image Data Preprocessing***

All data were preprocessed and analyzed with FMRIB's FSL 4.1.9 toolbox (http://www.fmrib.ox.ac.uk/fsl). Preprocessing steps included motion correction using a linear registration algorithm (Jenkinson et al., 2002); interleaved slice-timing correction, BET brain extraction, fieldmap-based unwarping, high-pass temporal filtering, and a 6-mm full-width half-maximum Gaussian spatial smoothing kernel. Subsequently, the

images were registered to high-resolution T1 anatomical images and the MNI152 2mm brain image.

### *FMRI Image Data Analysis*

#### *Intrinsic Connectivity Network (ICN) Generation*

Data-driven functional networks, which will henceforth be referred to as ICNs, were generated from the functional EPI scans using FSL's temporal concatenation independent component analysis (TICA) software in the MELODIC ICA toolkit (Beckmann & Smith, 2004). The ICA algorithm was used to generate thirty (30) group-level spatial maps and time courses, in order to standardize the number of group and participant level components (Moodie et al., 2013), and the resulting group-level components were permuted using the meta-melodic procedure to account for initial random value and input-order effects (Wisner, Atluri, Lim, & MacDonald III, 2013).

All noise and artifactual components were removed from the final set of group-level components (Beckmann, 2012), and the remaining components comprised the set of non-artifactual, referred to as ICNs, that were included in subsequent analyses. These ICNs were then used as group-level templates for the back-transformation of spatial maps and timeseries per participant using FSL's dual spatio-temporal regression software.

#### *Reverse Inference Testing*

The BrainMap networks used for reverse inference in this analysis is a set of canonical networks that had been previously described using meta-analytical tools and which have established functional associations across a wide range of functional

paradigms (Laird et al., 2011). Consequently, we employed these network maps from the BrainMap database in order to validate the identity of the networks generated using ICA, as well as any significant task associations with these networks. Reverse inference tests were performed by calculating Spearman's rho correlations between group-level network maps and the BrainMap networks.

*General Linear Models (GLMs)*

The predictors used for the network task relevance metrics are the explanatory variables (EVs) that were taken from the general linear models set up using the FSL Feat GUI (http://fsl.fmrib.ox.ac.uk/fsl/fslwiki/FEAT). Three main EVs and several confound EVs were included in the regression models pertaining to this data. The first of the three main EVs corresponds to the EV in the omnibus GLM applied in the Galvan study (2006) and, hence, models all events during the trial against a baseline of fixation in the inter-stimulus interval between trials (Figure 1). An EV for the anticipation of reward was also included, which encapsulated the first fixation and the cue, as well as an EV for the receipt of reward, which included the time points (TRs) covering when the reward is presented and the first portion of the inter-stimulus interval, respectively (Figure 1).

*Network Time Course Analyses*

To determine whether the time courses of the ICNs reflected dynamics related to task demands, participant-level Pearson correlations were performed between ICN time course vectors and the convolved hemodynamic response function (HRF) design vectors for each of the three EVs. Hence, this metric assessed how engaged each network was by the task in all three models (omnibus/Galvan, anticipation, and reward). These ICN-EV

correlation scores were averaged across all participants per ICN and these averaged correlation sores were reported in "relationship to task" metric for each EV. Additionally, participant-level ICN-EV correlations were z-transformed and correlated within twin pairs per ICN in the task HRF familiality metric (Revelle, 2011). Since there were no magnitude effects on familiality, the timecourse familiality scores were averaged across magnitude for each EV. A separate timecourse familiality calculation was performed, in which the values indicating the coherence of the BOLD signal in the voxels *over time* within each ICN in the participant level timecourses were correlated within twin pairs to determine the extent of familiality of the raw ICN timecourses.

*Spatial Overlap Familiality*

This metric measured the amount of overlap between the participant-level ICN spatial maps of the twin pairs to determine whether ICN morphology was familial. Hence, after being generated via dual regression, the whole-brain, participant-level ICN maps were masked with group-level maps that had been thresholded (z =6) and binarized. Within the set of maps for each ICN, these masked participant ICN maps were then aggregated into twin vectors (i.e. twin 1 vs. twin 2) and overlap calculated using Spearman's rank-order correlation and the Dice similarity metric. Similar to the calculations for timecourse familiality, there were no magnitude effects for spatial familiality. Hence, the familiality scores for spatial overlap were also averaged across magnitude for each EV.

*Intranetwork Coherence Familiality*

This metric was developed to determine the extent to which the average of connectivity values *within each participant's ICN map* varied according to familiality. As in the spatial overlap familiality metric, the masked participant ICN maps were used in this analysis. The mean value of all the voxels within these masked participant ICN maps was then calculated and correlated within twin pairs per ICN. As in the above cases, there were no magnitude effects for coherence familiality and all scores were averaged across magnitude for each EV.

*ICA vs. GLM Comparisons*

These analysis was undertaken in order to explore the relationship between connectivity dynamics and activation and to contextualize the magnitude of the correlation seen between the ICN time courses and the three EVs. Hence, the comparison of parameter estimate (COPE) maps from the first-level GLMs that were run for each participant were masked iteratively by each ICN. Within each ICN-masked COPE (comparison of parameter estimate) map, the voxel beta values were standardized by employing a formula that utilized the standard deviation of the response variable (beta) and the design (predictor timecourse). This was done for maps from GLMs for each of the three predictors and the resulting standardized beta coefficients were converted to correlation scores and these transformed values were then plotted against the task-relevance values from the "relationship to task" metric. Finally, regression lines were fit to the scatterplots of the transformed betas versus ICN task relevance scores. This yielded the slope and intercept for the association between these two metrics, as well as the variance explained ($R^2$). This analysis was, thus, able to provide an "apples-to-apples"

comparison of the two techniques, and had the added advantage of not only being able to contrast the magnitude of the values, but also was also useful for the directionality of the effects.

## Results

*Generation of Group-Level Components*

Based on previous findings, the group-level networks for this dataset were generated using a subset of participants, which included only one member of any twin pair included in the analysis. This was done in order to avoid the possibility of inflating the twin familiality scores (Moodie et al., 2014). The MELODIC ICA algorithm was run using this sample at a dimensionality of 30, which yielded a set of 20 non-artifactual group-level components (Figure 2). These non-artifactual components are henceforth referred to as ICNs (Laird et al., 2011). These group-level networks were then back-transformed into individual-level space to produce participant-specific spatial maps and timecourses for each component. This back-transformation was done for all participants, which included all twin pairs.

Reverse inference tests were performed on the set of group-level networks to facilitate naming of the networks and the interpretability of the ICN task relevance results. Spearman's rho correlations between the maps of the group-level networks and the BrainMap networks were used as the metric for reverse inference. It was found that there was a good mapping of ICA-derived ICNs onto the BrainMap meta-analytically generated networks (Table 1). For the Spearman correlations, rho ranged up to 0.67 and

there was mostly a one-to-one mapping of task networks to BrainMap networks (Supplementary Figure 1).

*Task Relevance of Network Timecourses*

Each of the ICN timecourses were correlated with the convolved design matrix vectors for the omnibus Galvan EV, anticipation EV, and reward EV respectively and these task relevance scores were averaged within ICN, as well as within and across magnitude (Table 1). For the Galvan omnibus EV, no networks had significant associations with the timeline of that predictor (Figure 3a). However, for the anticipation predictor, the area V2 network exhibited significant task relevance in all reward magnitudes (Figure 3b). On the other hand, for the reward predictor, there were again no significant task associations between ICNs and this predictor in any magnitude (Figure 3c).

*GLM Activation versus Network Task-Relevance*

The Galvan omnibus predictor elicited activation and ICN coherence responses of corresponding magnitude and direction ($R^2 = 0.79$), but the scores themselves were of lower magnitude for both activation and ICN task relevance for this EV compared to the activation EV (described below). After plotting the transformed activation beta weights against the ICN correlation scores, it was found that there was a strong positive relationship between the transformed beta correlations and the network task relevance correlation scores for the activation EV ($R^2 = 0.85$). However, this was not the case for the comparison of the transformed activation scores and task relevance scores for the reward predictor; in this case there seemed to be no relationship between the activation

scores for voxels within a network and the corresponding network task relevance ($R^2$ = 0.00043).

*Familiality Metrics*

For the spatial overlap familiality, the average ICN familiality score was r = 0.27, and ranged from no familiality for some ICNs to r = 0.58 (Table 2, Column 2). A relatively higher level of familiality was observed for the mean coherence / intranetwork connectivity scores of the ICNs. However, this observed familiality was lower than the familiality of the timecourses, and had a wider range. Hence, the twin correlations for network coherence ranged from r = 0.01 to r = 0.88, with an overall ICN coherence familiality of r = 0.55 (Table 2, Column 3). The highest level of familiality was observed for the ICN timecourses generated from the Pirate task. The twin correlations for timecourse dynamics ranged from r = 0.31 to r = 0.99, with an overall timecourse familiality of r = 0.74 (Table 2, Column 4). The overall familiality for these ICN characteristics was 0.52 across the three metrics (Table 2, Column 5).

The task relevance scores for each of the predictors were also correlated within twins to see if the ICNs were engaged by the task in a familial manner. These scores ranged from r = -0.1 to r = 0.12 across the three predictors and, hence, there was very little task relevance familiality (Table 3).

## Discussion

*Task Relevance of Network Timecourses*

The ICA of the data from the Pirate task produced a set of networks with a range of functional associations that were both task relevant and task independent, and, consequently all canonical processes and networks were represented in the data. The participant-level timecourses from this set of networks were correlated with the three task predictors (anticipation, reward, and omnibus) in order to determine the extent of engagement of the networks by each of these task components. It was observed that the anticipatory portion of the task had a significant positive relationship with the association visual network. The portion of the task related to the receipt of reward had lower, non-significant associations with the task ICNs, with the strongest positive association with the right executive network, and negative associations with the visuomotor timing network and the arm/hand sensorimotor network. The ICNs showed the lowest associations with omnibus predictor that included all task elements and this is likely due to the fact that the timecourse of this predictor is too general to show any meaningful associations with the ICNs as they are being engaged by particular task elements.

It is unclear why only the association visual network exhibited significant task relevance, and only in the anticipation phase of the task. This could be due to the task being very easy and, as a result, not being engaging enough for the adolescents but, as exit questionnaires were not administered, this postulation cannot be confirmed. However, in the first study in chapter two, the visual networks were the most robust ICN markers and, hence, it is likely that even in the presence of subthreshold engagement, the visual

networks in this task still were able to show significant task relevance. Hence, it is likely that more significant task relevance could be revealed in a more engaging task.

*GLM Activation versus Network Task-Relevance*

For the activation and omnibus predictors it appears that the BOLD signal in voxels contained within the boundaries of a particular ICN fluctuates in a manner that is positively related to changes in network coherence for the same ICN during that time period. Hence, this implies that as a network is recruited by a particular event or task element, the coherence within the network also increases, ostensibly because the task is streamlining the activity of the neurons in that region and, hence, this regularizes the signal. However, the lack of this phenomenon in the case of the reward predictor shows that this is not always the case, and it is likely that there are also tasks or events that will drive down coherence in networks while increasing the task-related BOLD signal. For instance, if a network contains sub-regions that can be differentially recruited by different types of stimuli or neuronal processes, then this network might not show any change in overall coherence when recruited by one particular type of task. The network could also even show a decrease in coherence if differentially recruited by various task demands, but future studies are necessary to test this hypothesis.

On the other hand, the omnibus EV activation vs. ICN task-relevance plot shows that, in the case of the Galvan predictor, the structure of the dependency between the anticipation-related activation and network timecourses is preserved. However, in the omnibus task relevance plot, the effect is harder to detect since all task components have been included and this is likely swamping the signal (i.e. driving down the correlations).

Hence, in general, the task engages endogenous brain networks in a manner that can be detected using both traditional GLMs and ICN task relevance calculations. The information provided by each method is complementary and the distinction between the positive versus neutral associations between the betas and ICN correlations seen for the anticipation and reward predictors hint toward differential effects of task engagement on brain networks. This could be quite useful for elucidating the dynamics of multimodal brain networks and more work needs to be done in this area.

*Familiality*

Four familiality metrics were computed in this analysis, namely for spatial overlap, intranetwork connectivity / coherence, timecourse dynamics and task relevance. The raw network timecourses were highly heritable, which means on average twins timecourses tend to follow the same central tendency. However, the task relevance twin correlations were very weak and this is likely due to the fact that the level of task engagement, as assessed with each predictor, was very low for most of the networks. Hence, this indicates that there is too much noise, or unrelated variance, in the other portions of the network timecourses when they are not engaged, and this masks any familiality in manner in which the networks were engaged by the task.

Nevertheless, the heritability of the raw ICN timecourses implies that the manner in which the networks are engaged by the task elements should also be familial and, in fact, our previous work does show this familiality in selected networks (Moodie, Wisner, & MacDonald III, 2014). However, that previous study employed two stereotypical functional localizer block designs, while this study employed a slow event related design.

The block design task relevance scores for hand imitation and verb generation (Moodie, Wisner, & MacDonald III, 2014) were higher than those of other event-related designs that had been previously examined (Poppe et al., 2013), as is the case for the ICN task relevance scores in this event-related design. Taken together, this evidence suggests that it is not that the way in which networks are engaged by tasks cannot be familial but, rather, that the familiality signal is being swamped by the larger unrelated ICN dynamics. Consequently, this type of design might not be ideal for investigating the familiality of ICN task relevance.

Both the domains of morphology (spatial overlap) and network coherence within ICN maps exhibited familiality at lower, but comparable, level as the network timecourses, and both had higher magnitudes than the network task relevance. Across the domains of familiality of ICN morphology, coherence and timecourse dynamics, the area V2 network showed the highest familiality. This was also the network that showed the highest, and only significant, task relevance to a task predictor, which was the anticipation of reward across magnitudes. This finding is corroborated by the previous findings in chapter 2, in which a visual network, V1 showed the highest level of consistency, task relevance and familiality. Hence, the visual input areas appear to be the most robust marker of relevant ICN properties such as trait expression, task engagement and familiality. However, more work needs to be done to understand the genetic and environmental influences that drive the differential expression of familiality across these domains.

*Limitations*

This study employed a forced-choice reward task with an implicit learning component that should have shown behavioral effects of both learning and reward magnitude. The theorized behavioral effects were not observed and, hence, the network analyses were not evaluated in the context of behavior. It will be necessary to employ similar techniques to an analysis of data from a task with behavioral effects that have been pre-established in pilot data.

*Conclusions*

The ICN profiles observed in this study were shown to have selective relationships to particular elements of rewarding circumstances in adolescence. Specifically, the network timecourses were modulated differentially by the three task elements, and this modulation occurred in networks with pre-existing relationships to these cognitive features. The ICN timecourses exhibited a positive relationship to the task as a whole, as evidenced by the relationship to the omnibus predictor. This relationship held true for the anticipation of reward within the task, but was not present for the receipt of reward. This is possibly an indication of the prefrontal cognitive control deficit that is thought to be characteristic of adolescence, but more work needs to be done to concretize this assertion. The ICN characteristics were also familial, which means that genetic influences also play a role in the expression of ICNs and their role in development. Hence, this work provides a framework in which future studies can track the changes in ICN profiles over the course of development.

## Tables

**Table 1. Reverse Inference of ICN Functional Associations and Task Relevance Across Magnitudes of Reward Contingencies.**

| ICN Number | Reverse Inference Component | Inference Correlation | Average Task Relevance (S,M,L) | | |
|---|---|---|---|---|---|
| | | | Omnibus | Anticipation | Reward |
| 1 | Fronto-parietal / Right Executive Network | 0.43 | 0.03 | -0.01 | 0.07 |
| 2 | Subgenual ACC & OFC / Language & Auditory Cortices | 0.26 | 0.01 | 0.00 | 0.00 |
| 3 | Arm + Hand Sensorimotor / Insula / Emotion & Executive | 0.34 | 0.00 | 0.06 | -0.03 |
| 4 | Visuomotor Timing & Movement Preparation | 0.40 | -0.05 | 0.06 | -0.13 |
| 5 | Social Cognition / Default Mode Network | 0.50 | -0.01 | -0.09 | 0.00 |
| 6 | Visuospatial Reasoning Network / Right Executive Network | 0.24 | -0.03 | 0.10 | -0.08 |
| 7 | Subgenual ACC & OFC / Reward | 0.57 | 0.00 | -0.06 | 0.01 |
| 8 | Left Executive / Language Processing | 0.49 | 0.01 | -0.04 | 0.03 |
| 9 | MT + MST / Visual Tracking | 0.49 | -0.02 | 0.12 | -0.02 |
| 10 | Language & Auditory Cortices | 0.44 | -0.03 | -0.04 | -0.03 |
| 11 | Medial temporal / Emotion & Limbic Network | 0.46 | 0.00 | -0.08 | 0.02 |
| 12 | Area V1 / Simple Visual Stimuli Network | 0.66 | -0.01 | 0.15 | 0.00 |
| 13 | Areas V2 & V3 / Covert reading | 0.62 | -0.01 | **0.37** | -0.05 |
| 14 | Arm/Hand Sensorimotor Network | 0.46 | -0.03 | 0.25 | -0.12 |
| 15 | Hand-eye Coordination Network | 0.61 | -0.02 | -0.04 | -0.04 |
| 16 | Default Mode Network / Basal Ganglia / Thalamus | 0.29 | 0.01 | -0.11 | 0.04 |
| 17 | Basal Ganglia / Reward Network 2 | 0.67 | -0.01 | 0.10 | -0.05 |
| 18 | Midbrain / Interoception Network | 0.38 | -0.01 | -0.08 | -0.01 |
| 19 | Cerebellum / Autonomic / Naming Network | 0.55 | 0.02 | -0.04 | 0.02 |
| 20 | Speech Sensorimotor Network | 0.46 | 0.00 | -0.07 | 0.00 |

**Note.** The 'inference correlation' column shows the reverse inference scores for the Spearman correlations of the group-level spatial maps from the ICA (the ICNs) and the BrainMap meta-data networks. The 'Reverse Inference Component' is the resulting name and functional association of each network. All ICNs are ordered using the same numbering as in the group-level ICN spatial map overlays in Figure 2. The ICN task relevance scores in Figure 3 were averaged across magnitude for the three types of predictors (omnibus, anticipation, and reward) and included in the 'Average Task Relevance' columns. 'S' refers to the small reward magnitude; 'M' refers to the medium

reward magnitude; 'L' refers to the large reward magnitude. Task relevance scores were bolded at the adjusted significance level ($r = 0.375$, $t = 3.265$, $p < 0.00083$, $df = 73$).

**Table 2. Familiality Scores across the three ICN Metrics**

| Intrinsic Connectivity Network # | Spatial Overlap Familiality | Mean Coherence Familiality | ICN Timecourse Familiality | Overall ICN Familiality |
|---|---|---|---|---|
| # | r | r | r | r |
| 1 | 0.31 | **0.72** | **0.82** | 0.62 |
| 2 | **0.57** | **0.71** | 0.31 | 0.53 |
| 3 | 0.35 | **0.72** | **0.63** | 0.57 |
| 4 | 0.38 | 0.24 | **0.85** | 0.49 |
| 5 | -0.09 | **0.77** | **0.78** | 0.49 |
| 6 | 0.13 | 0.01 | **0.81** | 0.32 |
| 7 | 0.39 | **0.68** | **0.60** | 0.56 |
| 8 | 0.26 | **0.74** | 0.48 | 0.49 |
| 9 | -0.01 | 0.03 | **0.91** | 0.31 |
| 10 | 0.11 | 0.46 | **0.79** | 0.45 |
| 11 | 0.35 | **0.74** | **0.67** | 0.59 |
| 12 | 0.29 | **0.75** | **0.91** | 0.65 |
| 13 | **0.58** | **0.50** | **0.99** | 0.69 |
| 14 | 0.31 | 0.36 | **0.97** | 0.55 |
| 15 | 0.42 | 0.33 | **0.76** | 0.50 |
| 16 | 0.34 | **0.62** | **0.74** | 0.57 |
| 17 | 0.21 | **0.51** | **0.81** | 0.51 |
| 18 | 0.10 | **0.88** | **0.79** | 0.59 |
| 19 | **0.57** | **0.69** | **0.53** | 0.60 |
| 20 | -0.15 | **0.64** | **0.73** | 0.41 |
| ICN Average | 0.27 | 0.55 | 0.74 | 0.52 |

**Note.** The correlations between twin pairs for the overlap of spatial maps, as well as correspondence of intranetwork coherence scores and ICN timecourse dynamics, were averaged per ICN. All scores that passed the adjusted significance threshold (# of pairs = 31, $r = 0.49$, $t = 3.038$, $df = 29$) were bolded. The scores from each familiality metric were then averaged per column (across metrics) and included in the 'Overall ICN Familiality' column.

**Table 3. Summary of Familiality of ICN Task Relevance for the three predictors**

| ICN | Omni (Sm) | Omni (Med) | Omni (Lg) | Ant (Sm) | Ant (Med) | Ant (Lg) | Rew (Sm) | Rew (Med) | Rew (Lg) | Omni (Avg) | Ant (Avg) | Rew (Avg) |
|---|---|---|---|---|---|---|---|---|---|---|---|---|
| 1 | 0.00 | 0.06 | -0.09 | -0.23 | -0.07 | -0.01 | 0.04 | 0.02 | 0.12 | -0.01 | -0.10 | 0.06 |
| 2 | -0.08 | 0.03 | 0.04 | -0.06 | 0.05 | 0.19 | 0.07 | -0.06 | 0.06 | -0.01 | 0.06 | 0.02 |
| 3 | 0.00 | -0.11 | 0.09 | -0.04 | 0.14 | -0.03 | -0.16 | -0.18 | 0.16 | -0.01 | 0.02 | -0.06 |
| 4 | -0.07 | 0.08 | 0.06 | -0.13 | -0.02 | -0.04 | 0.05 | -0.01 | 0.02 | 0.02 | -0.06 | 0.02 |
| 5 | -0.02 | -0.08 | 0.11 | -0.02 | 0.06 | -0.05 | 0.02 | 0.10 | -0.06 | 0.00 | 0.00 | 0.02 |
| 6 | -0.02 | -0.01 | 0.01 | 0.02 | 0.04 | -0.05 | 0.02 | -0.06 | -0.06 | -0.01 | 0.00 | -0.04 |
| 7 | 0.04 | -0.06 | 0.10 | -0.17 | -0.08 | -0.08 | -0.13 | -0.08 | -0.01 | 0.03 | -0.11 | -0.07 |
| 8 | 0.03 | 0.00 | -0.05 | -0.06 | 0.10 | -0.10 | -0.01 | 0.02 | 0.06 | -0.01 | -0.02 | 0.02 |
| 9 | 0.02 | -0.13 | 0.15 | 0.08 | 0.04 | -0.05 | -0.18 | 0.06 | 0.14 | 0.01 | 0.02 | 0.01 |
| 10 | 0.02 | 0.06 | -0.06 | 0.04 | 0.07 | -0.15 | -0.01 | 0.01 | 0.08 | 0.01 | -0.01 | 0.03 |
| 11 | -0.06 | 0.07 | -0.10 | -0.03 | 0.06 | 0.02 | -0.10 | -0.08 | -0.01 | -0.03 | 0.02 | -0.06 |
| 12 | -0.11 | -0.08 | 0.04 | -0.13 | -0.08 | -0.09 | -0.05 | 0.03 | 0.02 | -0.05 | -0.10 | 0.00 |
| 13 | -0.17 | -0.12 | -0.08 | -0.08 | -0.14 | -0.06 | -0.24 | 0.04 | 0.03 | -0.12 | -0.09 | -0.06 |
| 14 | 0.15 | 0.04 | -0.02 | -0.09 | -0.02 | -0.02 | -0.12 | 0.00 | -0.10 | 0.05 | -0.04 | -0.07 |
| 15 | 0.05 | -0.13 | -0.09 | 0.02 | 0.00 | -0.14 | -0.23 | 0.10 | -0.16 | -0.05 | -0.04 | -0.10 |
| 16 | -0.08 | -0.09 | 0.00 | 0.13 | 0.03 | 0.00 | -0.13 | -0.07 | 0.06 | -0.06 | 0.05 | -0.05 |
| 17 | 0.00 | 0.13 | -0.07 | -0.06 | 0.00 | 0.11 | 0.16 | -0.02 | 0.07 | 0.02 | 0.02 | 0.07 |
| 18 | -0.06 | -0.09 | -0.12 | 0.00 | 0.07 | -0.04 | 0.06 | -0.02 | 0.01 | -0.09 | 0.01 | 0.02 |
| 19 | 0.16 | 0.10 | 0.04 | -0.13 | -0.04 | -0.14 | -0.07 | -0.12 | 0.08 | 0.10 | -0.10 | -0.04 |
| 20 | 0.15 | -0.08 | 0.04 | 0.02 | 0.12 | -0.12 | -0.13 | -0.03 | 0.01 | 0.04 | 0.01 | -0.05 |

**Note.** The familiality scores for the ICN timecourse correlations with each of the task predictors were averaged within each magnitude. 'Omni' refers to the omnibus predictor; 'Ant' refers to the anticipation predictor; 'Rew' refers to the reward predictor. 'Sm' refers to the small reward magnitude; 'Med' refers to the medium reward magnitude; 'Lg' refers to the large reward magnitude. All scores were tested for significance (# of pairs = 31, $r = 0.49$, $t = 3.038$, $df = 29$), but none of these task relevance familiality scores passed the significance threshold.

Figures

**Figure 1.**

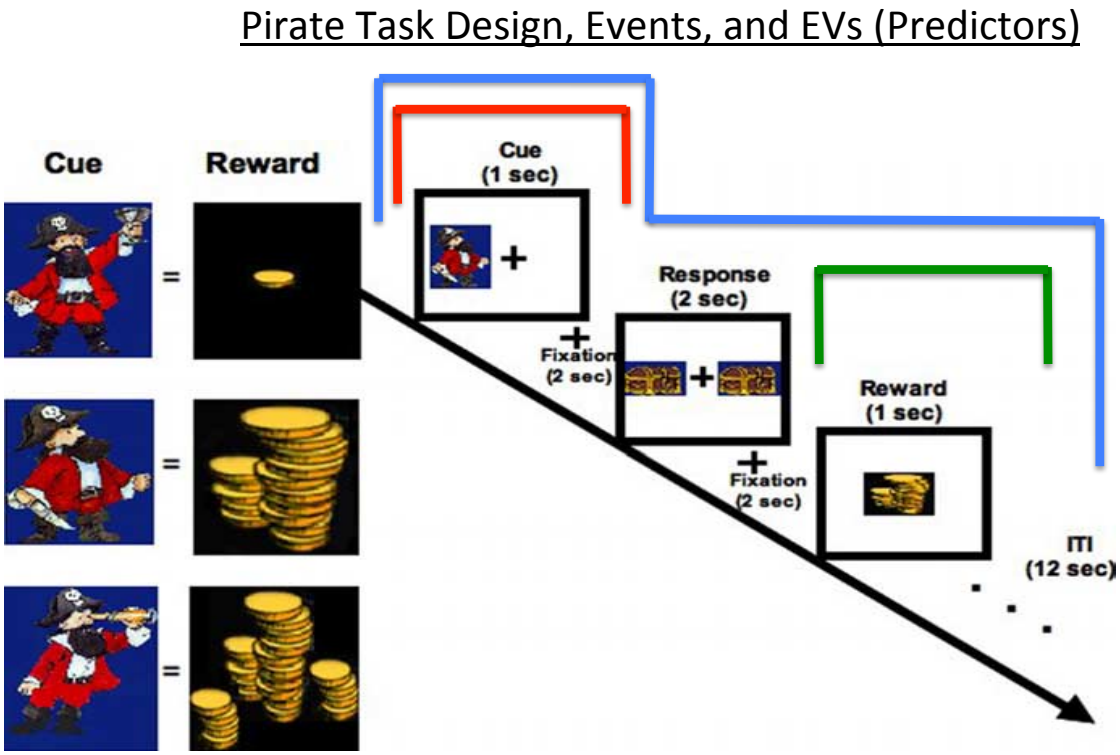


**Figure 1.** Behavioral paradigm. Left panel, Three cues were each paired with a distinct reward value (counterbalanced across subjects) that remained constant throughout the experiment. Right panel, The paradigm consisted of a cue, response, and reward that were temporally separated in time with 12 s ITI. Total trial length was 20 s.

Note: Color bars for predictors were added as a visual representation of the three GLM EVs. Figure adapted from Galvan, A., Hare, T. a, Parra, C. E., Penn, J., Voss, H., Glover, G., & Casey, B. J. (2006). Earlier development of the accumbens relative to orbitofrontal cortex might underlie risk-taking behavior in adolescents. The Journal of neuroscience, 26(25), 6885–92.

**Figure 2.**

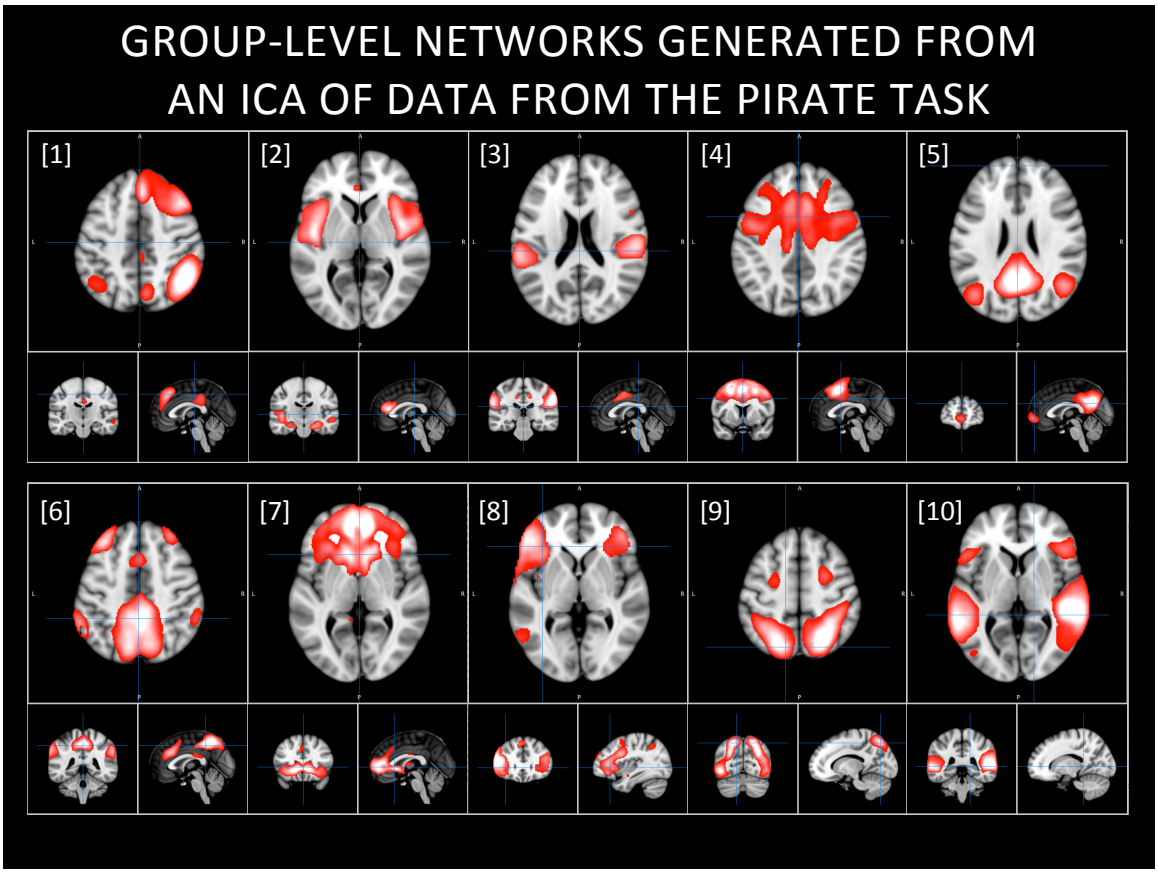
GROUP-LEVEL NETWORKS GENERATED FROM AN ICA OF DATA FROM THE PIRATE TASK
[1]
[2]
[3]
[4]
[5]
[6]
[7]
[8]
[9]
[10]

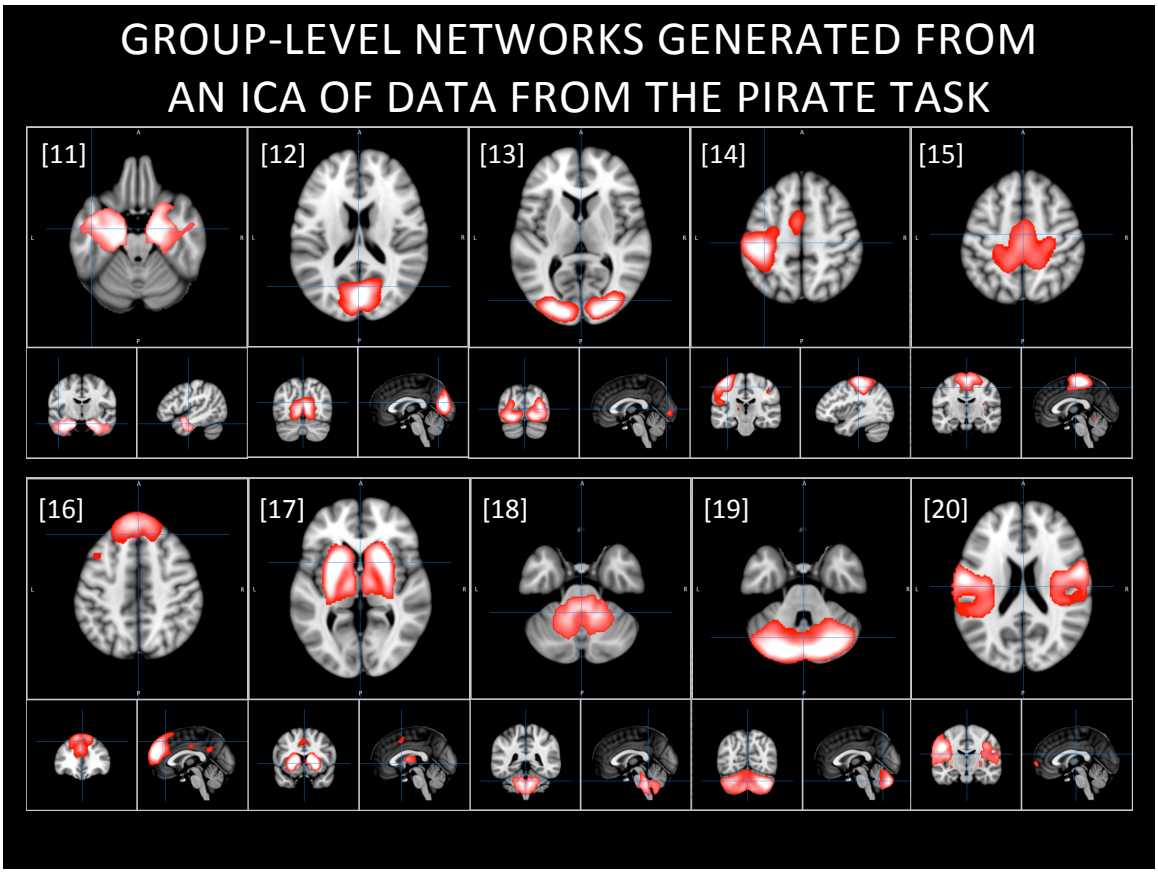


**Note.** The spatial maps of the ICNs that were output by the FSL MELODIC ICA algorithm were thresholded (z = 6) and overlaid on three slice views corresponding to axial, coronal and sagittal axes, respectively. The coordinates (depth) of the slices in each axis are not identical, but instead were selected to reveal the largest surface area of the ICN in that plane. 'ICA' refers to the Independent Component Analysis implemented using FSL MELODIC algorithm and the meta-ICA procedure.

**Figure 3a.**

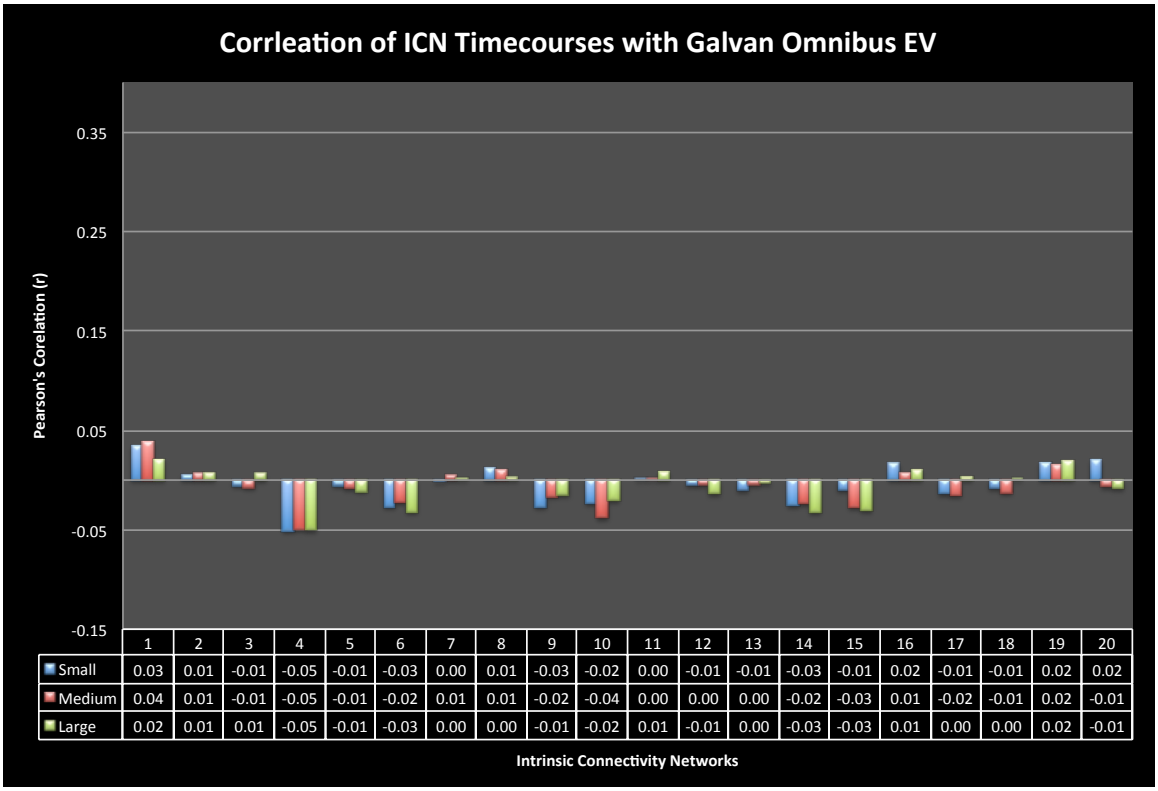


| | 1 | 2 | 3 | 4 | 5 | 6 | 7 | 8 | 9 | 10 | 11 | 12 | 13 | 14 | 15 | 16 | 17 | 18 | 19 | 20 |
|---|---|---|---|---|---|---|---|---|---|---|---|---|---|---|---|---|---|---|---|---|
| Small | 0.03 | 0.01 | -0.01 | -0.05 | -0.01 | -0.03 | 0.00 | 0.01 | -0.03 | -0.02 | 0.00 | -0.01 | -0.01 | -0.03 | -0.01 | 0.02 | -0.01 | -0.01 | 0.02 | 0.02 |
| Medium | 0.04 | 0.01 | -0.01 | -0.05 | -0.01 | -0.02 | 0.01 | 0.01 | -0.02 | -0.04 | 0.00 | 0.00 | 0.00 | -0.02 | -0.03 | 0.01 | -0.02 | -0.01 | 0.02 | -0.01 |
| Large | 0.02 | 0.01 | 0.01 | -0.05 | -0.01 | -0.03 | 0.00 | 0.00 | -0.01 | -0.02 | 0.01 | -0.01 | 0.00 | -0.03 | -0.03 | 0.01 | 0.00 | 0.00 | 0.02 | -0.01 |

**Note.** The participant-level ICN timecourses were correlated with the three omnibus predictors, which included all events in the small, medium and large reward trials, respectively. These correlation scores for task relevance were then averaged across all participants (twin pairs and singletons, n = 75) per ICN and plotted in a bar graph. The significance of the relationships between the ICNs and each task predictor were then tested and the significance level was adjusted for multiple comparisons across ICNs and reward magnitude ($r = 0.375$, $t = 3.265$, $p < 0.00083$, $df = 73$). For the omnibus predictors, none of the ICNs showed significant task relevance and, hence, no ICN bars were starred.

**Figure 3b.**

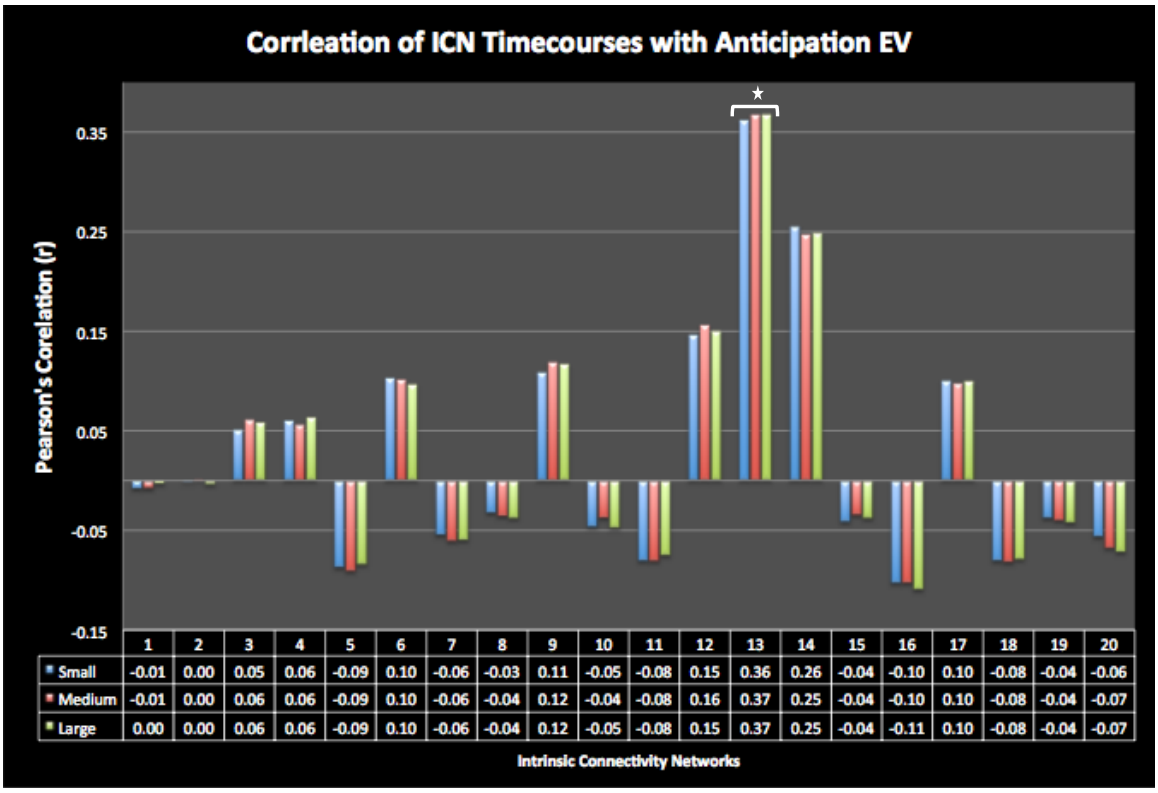


| | 1 | 2 | 3 | 4 | 5 | 6 | 7 | 8 | 9 | 10 | 11 | 12 | 13 | 14 | 15 | 16 | 17 | 18 | 19 | 20 |
|---|---|---|---|---|---|---|---|---|---|---|---|---|---|---|---|---|---|---|---|---|
| Small | -0.01 | 0.00 | 0.05 | 0.06 | -0.09 | 0.10 | -0.06 | -0.03 | 0.11 | -0.05 | -0.08 | 0.15 | 0.36 | 0.26 | -0.04 | -0.10 | 0.10 | -0.08 | -0.04 | -0.06 |
| Medium | -0.01 | 0.00 | 0.06 | 0.06 | -0.09 | 0.10 | -0.06 | -0.04 | 0.12 | -0.04 | -0.08 | 0.16 | 0.37 | 0.25 | -0.04 | -0.10 | 0.10 | -0.08 | -0.04 | -0.07 |
| Large | 0.00 | 0.00 | 0.06 | 0.06 | -0.09 | 0.10 | -0.06 | -0.04 | 0.12 | -0.05 | -0.08 | 0.15 | 0.37 | 0.25 | -0.04 | -0.11 | 0.10 | -0.08 | -0.04 | -0.07 |

**Note.** The participant-level ICN timecourses were correlated with the three anticipation predictors, which included the anticipation of small, medium and large rewards, respectively. These correlation scores for task relevance were then averaged across all participants (twin pairs and singletons, n = 75) per ICN and plotted in a bar graph. The significance of the relationships between the ICNs and each task predictor were then tested and the significance level was adjusted for multiple comparisons across ICNs and reward magnitude ($r = 0.375$, $t = 3.265$, $p < 0.00083$, $df = 73$). The bars representing ICNs showing significant task relevance were starred.

**Figure 3c.**

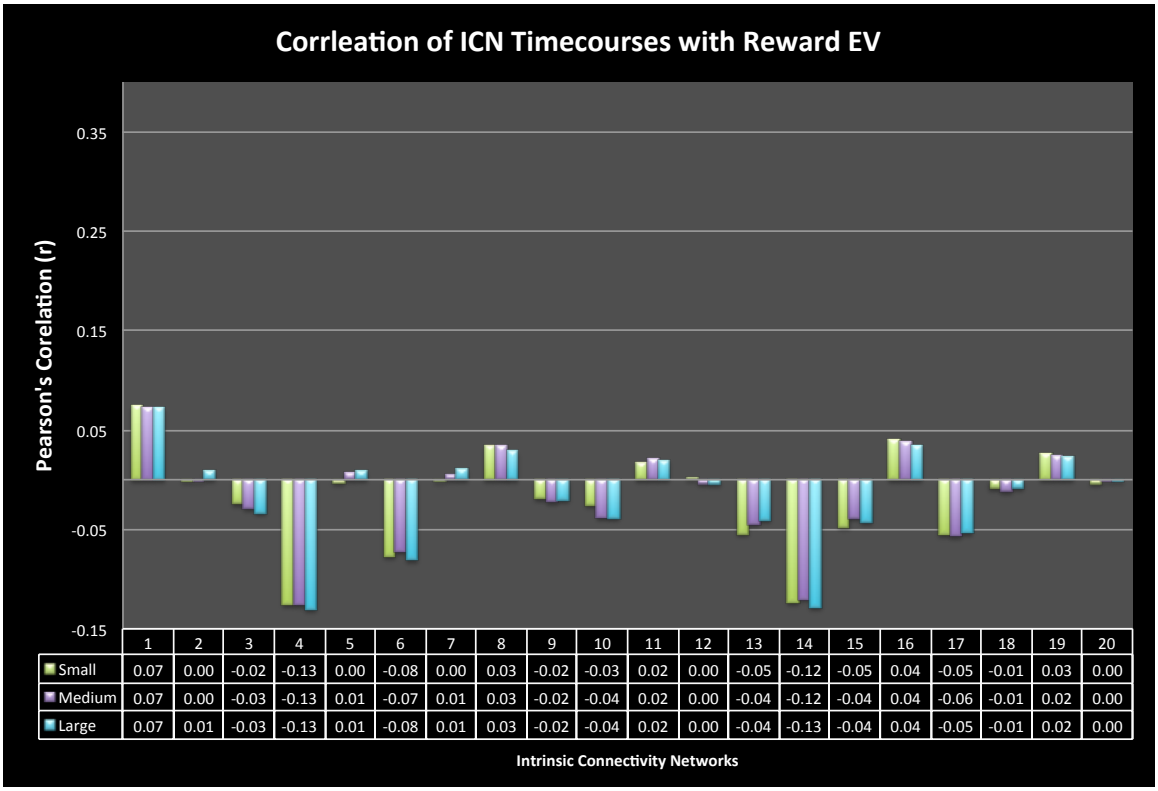


| | 1 | 2 | 3 | 4 | 5 | 6 | 7 | 8 | 9 | 10 | 11 | 12 | 13 | 14 | 15 | 16 | 17 | 18 | 19 | 20 |
|---|---|---|---|---|---|---|---|---|---|---|---|---|---|---|---|---|---|---|---|---|
| Small | 0.07 | 0.00 | -0.02 | -0.13 | 0.00 | -0.08 | 0.00 | 0.03 | -0.02 | -0.03 | 0.02 | 0.00 | -0.05 | -0.12 | -0.05 | 0.04 | -0.05 | -0.01 | 0.03 | 0.00 |
| Medium | 0.07 | 0.00 | -0.03 | -0.13 | 0.01 | -0.07 | 0.01 | 0.03 | -0.02 | -0.04 | 0.02 | 0.00 | -0.04 | -0.12 | -0.04 | 0.04 | -0.06 | -0.01 | 0.02 | 0.00 |
| Large | 0.07 | 0.01 | -0.03 | -0.13 | 0.01 | -0.08 | 0.01 | 0.03 | -0.02 | -0.04 | 0.02 | 0.00 | -0.04 | -0.13 | -0.04 | 0.04 | -0.05 | -0.01 | 0.02 | 0.00 |

**Note.** The participant-level ICN timecourses were correlated with the three reward predictors, which included the receipt of small, medium and large rewards, respectively. These correlation scores for task relevance were then averaged across all participants (twin pairs and singletons, n = 75) per ICN and plotted in a bar graph. The significance of the relationships between the ICNs and each task predictor were then tested and the significance level was adjusted for multiple comparisons across ICNs and reward magnitude ($r = 0.375$, $t = 3.265$, $p < 0.00083$, $df = 73$). The bar plots representing ICNs that showed significant task relevance were starred.

**Figure 4a.**

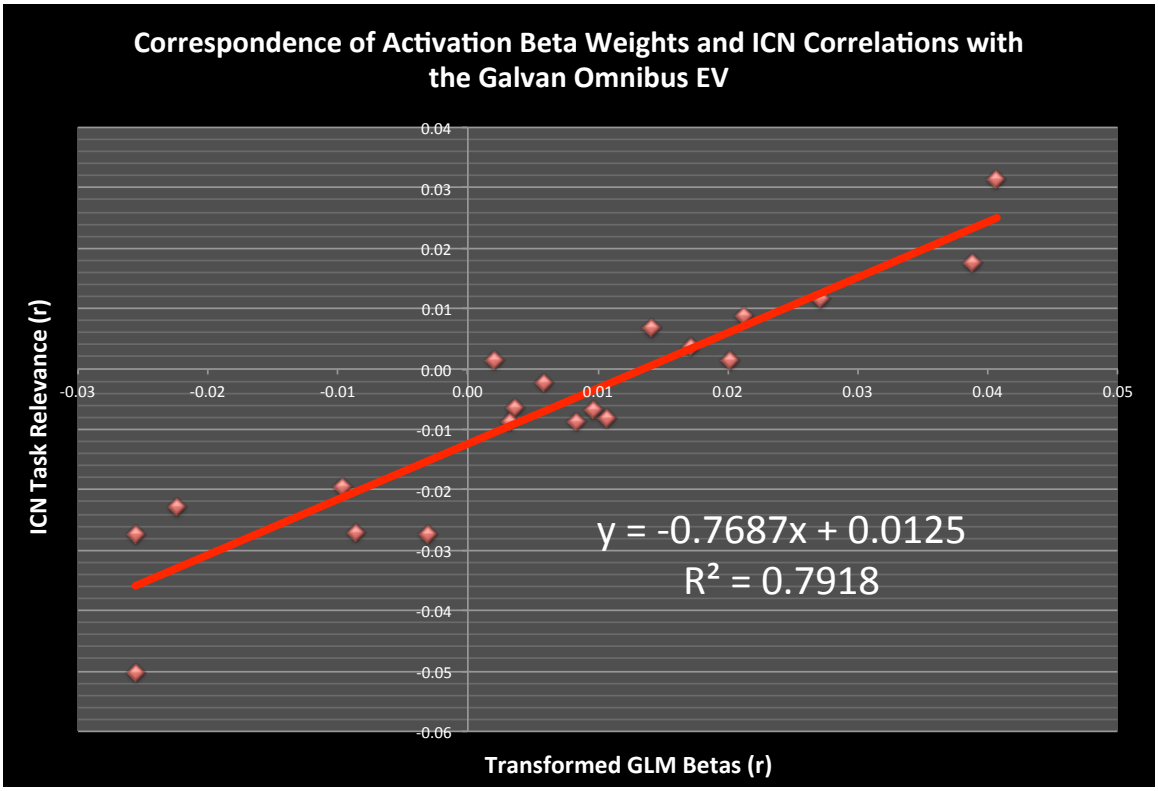


**Note.** The ICN task relevance scores for the ICN relationships to the events in the omnibus predictors were averaged across magnitude and plotted against the transformed beta weight correlation scores (which had also been averaged across magnitude). These two sets of correlation scores were then graphically depicted in a scatterplot and a trendline was added. A data point represents the coordinate of the matched task relevance score and beta weight for each of the 20 ICNs.

**Figure 4b.**

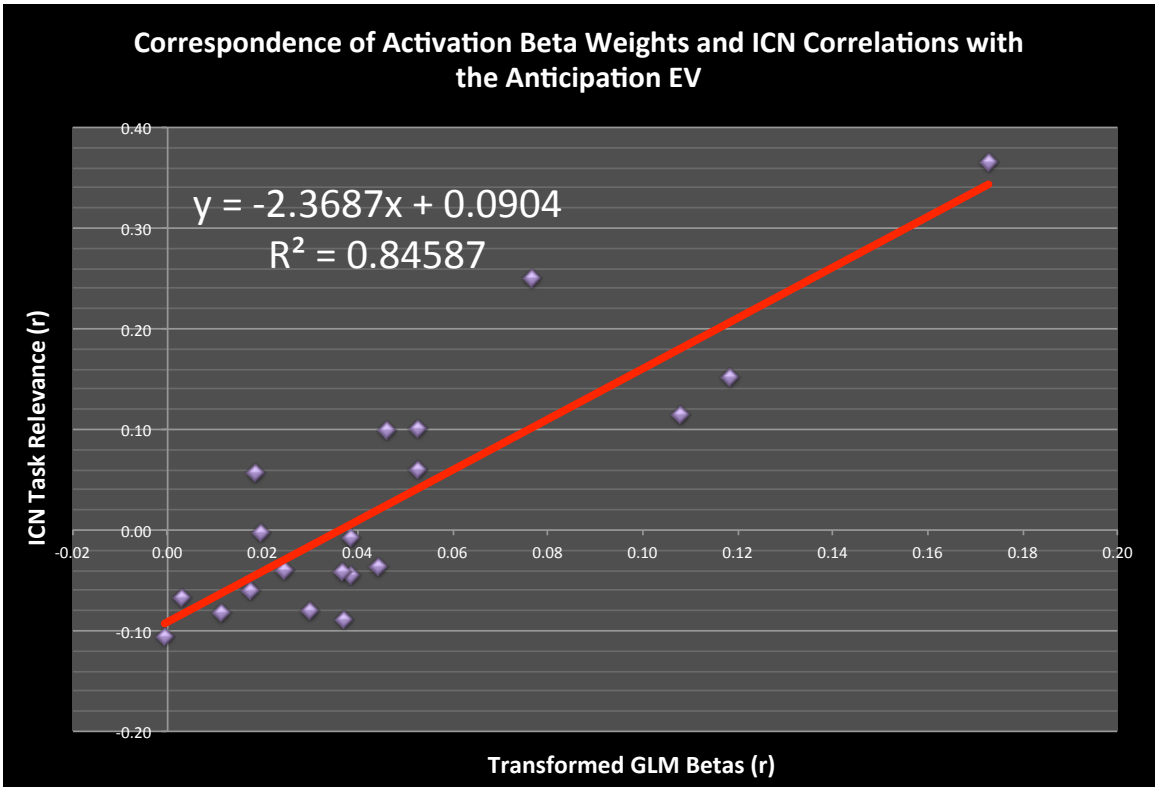


**Note.** The ICN task relevance scores for anticipation were averaged across magnitude and plotted against the transformed beta weight correlation scores (which had also been averaged across magnitude). These two sets of correlation scores were then graphically depicted in a scatterplot and a trendline was added. A data point represents the coordinate of the matched task relevance score and beta weight for each of the 20 ICNs.

**Figure 4c.**

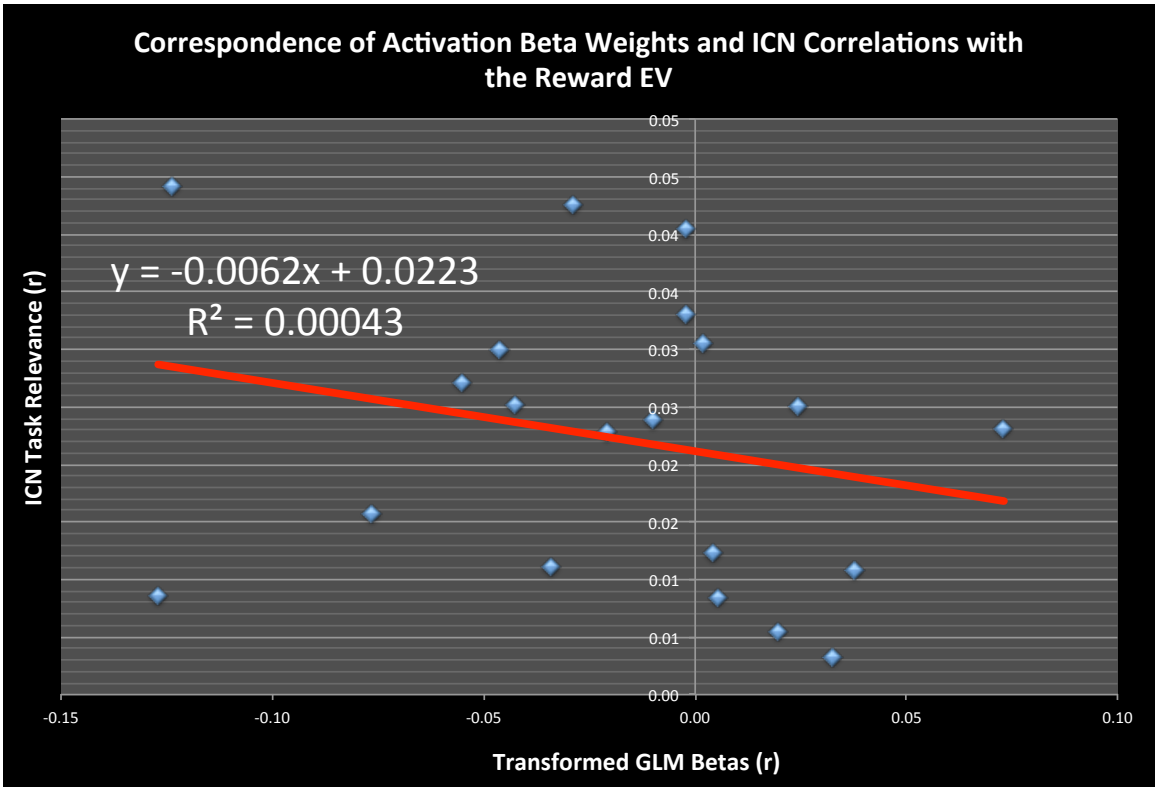


**Note.** The ICN task relevance scores for the ICN relationships to the receipt of rewards were averaged across magnitude and plotted against the transformed beta weight correlation scores (which had also been averaged across magnitude). These two sets of correlation scores were then graphically depicted in a scatterplot and a trendline was added. A data point represents the coordinate of the matched task relevance score and beta weight for each of the 20 ICNs.

**Supplementary Figure 1. Spearman Reverse Inference Correlation Scores**

| | -0.15 | | 0.00 | | 0.15 | | 0.30 | | 0.45 | | 0.60 | | 0.75 | | 0.90 | | | | | |
|---|---|---|---|---|---|---|---|---|---|---|---|---|---|---|---|---|---|---|---|---|
| | 1 ICN 13 | 2 ICN 8 | 3 ICN 24 | 4 ICN 26 | 5 ICN 5 | 6 ICN 20 | 7 ICN 4 | 8 ICN 21 | 9 ICN 11 | 10 ICN 16 | 11 ICN 14 | 12 ICN 6 | 13 ICN 28 | 14 ICN 1 | 15 ICN 12 | 16 ICN 29 | 17 ICN 10 | 18 ICN 22 | 19 ICN 3 | 20 ICN 7 |
| BM1 | 0.62 | 0.15 | 0.11 | -0.05 | -0.11 | -0.08 | -0.06 | -0.08 | -0.11 | -0.09 | -0.09 | -0.07 | -0.09 | -0.11 | 0.16 | -0.06 | 0.03 | 0.00 | 0.26 | -0.13 |
| BM2 | 0.02 | 0.72 | 0.09 | -0.03 | -0.11 | -0.07 | -0.10 | -0.07 | -0.09 | -0.07 | -0.07 | 0.02 | -0.04 | 0.01 | -0.12 | -0.06 | -0.01 | 0.15 | 0.01 | -0.05 |
| BM3 | -0.04 | 0.08 | 0.63 | -0.04 | -0.06 | -0.03 | -0.05 | -0.04 | -0.09 | -0.06 | -0.06 | -0.06 | -0.06 | -0.06 | -0.07 | -0.04 | -0.06 | -0.06 | -0.04 | -0.08 |
| BM4 | 0.00 | 0.18 | 0.05 | -0.02 | 0.07 | -0.03 | 0.19 | -0.03 | -0.07 | -0.03 | -0.04 | -0.04 | -0.03 | 0.05 | 0.13 | -0.01 | 0.19 | 0.03 | 0.16 | 0.16 |
| BM5 | 0.11 | -0.01 | -0.02 | 0.38 | -0.07 | -0.05 | -0.04 | -0.08 | -0.07 | -0.08 | -0.03 | 0.02 | 0.22 | -0.08 | -0.11 | -0.08 | -0.09 | -0.10 | 0.09 | -0.10 |
| BM6 | -0.01 | -0.12 | -0.01 | -0.03 | 0.40 | 0.13 | -0.10 | 0.17 | 0.05 | -0.02 | -0.04 | -0.05 | -0.01 | -0.06 | 0.00 | -0.01 | -0.02 | 0.00 | -0.05 | 0.00 |
| BM7 | -0.04 | -0.09 | -0.07 | -0.04 | 0.01 | 0.07 | -0.03 | -0.04 | 0.46 | 0.02 | 0.16 | 0.15 | -0.05 | 0.06 | -0.05 | -0.05 | 0.00 | -0.20 | -0.06 | 0.24 |
| BM8 | -0.06 | -0.09 | -0.06 | 0.03 | -0.03 | 0.45 | 0.34 | 0.19 | 0.12 | -0.08 | -0.07 | -0.09 | -0.03 | -0.03 | -0.02 | 0.06 | -0.04 | -0.05 | -0.04 | 0.04 |
| BM9 | -0.04 | 0.00 | -0.06 | -0.04 | -0.04 | 0.08 | 0.01 | 0.61 | 0.09 | -0.04 | -0.03 | 0.02 | -0.06 | -0.06 | -0.07 | -0.04 | -0.06 | -0.01 | -0.02 | 0.07 |
| BM10 | -0.05 | -0.10 | -0.07 | -0.06 | -0.01 | -0.06 | 0.00 | -0.07 | 0.45 | 0.33 | 0.05 | -0.02 | -0.06 | -0.03 | 0.17 | -0.03 | -0.01 | -0.07 | -0.06 | -0.07 |
| BM11 | -0.03 | -0.07 | -0.06 | -0.04 | -0.07 | -0.05 | -0.05 | -0.05 | 0.06 | 0.62 | 0.04 | -0.07 | 0.06 | -0.07 | -0.09 | -0.05 | -0.06 | -0.07 | -0.05 | -0.09 |
| BM12 | -0.03 | -0.05 | -0.05 | -0.04 | -0.07 | -0.04 | -0.04 | -0.07 | -0.03 | 0.28 | 0.62 | 0.08 | -0.01 | -0.06 | -0.07 | -0.05 | -0.06 | -0.05 | -0.04 | -0.03 |
| BM13 | -0.05 | 0.06 | -0.09 | -0.07 | -0.01 | -0.09 | 0.11 | -0.05 | -0.06 | -0.09 | 0.02 | 0.53 | -0.07 | 0.07 | 0.27 | -0.07 | -0.05 | 0.29 | -0.02 | 0.14 |
| BM14 | -0.04 | -0.05 | -0.07 | 0.17 | -0.09 | 0.00 | -0.06 | -0.06 | -0.01 | 0.05 | 0.03 | -0.08 | 0.65 | -0.05 | -0.03 | -0.06 | -0.01 | -0.04 | -0.04 | -0.08 |
| BM15 | -0.06 | 0.03 | -0.07 | -0.05 | 0.03 | -0.05 | 0.12 | -0.08 | 0.05 | -0.04 | -0.07 | -0.07 | -0.07 | 0.43 | 0.13 | -0.06 | 0.16 | -0.02 | -0.03 | 0.17 |
| BM16 | -0.03 | -0.05 | -0.05 | -0.05 | -0.07 | -0.03 | 0.08 | -0.03 | -0.08 | -0.06 | -0.07 | -0.07 | -0.05 | -0.04 | 0.44 | 0.31 | 0.00 | -0.05 | 0.22 | -0.05 |
| BM17 | -0.04 | -0.02 | 0.08 | -0.04 | -0.03 | 0.06 | 0.27 | -0.07 | -0.05 | -0.05 | -0.03 | -0.02 | -0.04 | -0.08 | -0.07 | 0.46 | 0.02 | -0.05 | 0.09 | -0.04 |
| BM18 | -0.04 | -0.01 | -0.04 | -0.05 | 0.12 | 0.02 | -0.05 | -0.06 | 0.05 | -0.06 | -0.07 | -0.03 | -0.06 | -0.06 | 0.06 | 0.00 | 0.49 | 0.02 | 0.00 | 0.01 |
| BM19 | 0.09 | -0.08 | -0.08 | 0.08 | -0.07 | -0.07 | -0.03 | -0.07 | -0.10 | -0.07 | -0.07 | -0.08 | 0.20 | -0.02 | 0.02 | -0.07 | -0.08 | -0.04 | -0.07 | -0.09 |
| BM20 | -0.02 | -0.05 | -0.07 | -0.04 | 0.27 | -0.01 | -0.05 | -0.07 | -0.01 | -0.04 | -0.04 | 0.02 | -0.05 | 0.19 | 0.00 | -0.02 | -0.03 | 0.28 | -0.04 | 0.08 |

**Note.** The Spearman's rho spatial similarity metric scores for the overlap between the group-level spatial maps of the ICNs and the Brain Map networks were calculated and

rearranged in a heatmap to show the highest score per row. This highlighted the ICN with the strongest correspondence with each of the BrainMap networks, as well as the diagonal showing a one-to-one or one-to-two correspondence for reverse inference. ‘BM’ is short for BrainMap.

# Chapter Four

Do Activity and Functional Connectivity Tell the Same Story about Psychopathology?
An Analysis of Cognitive Deficits in Schizophrenia

Summary

The fields of functional, and functional connectivity, magnetic resonance imaging (fMRI / fcMRI) have been developing separate analysis techniques to study the mechanisms such as working memory deficits that are thought to underlie psychopathology. In schizophrenia research, the working memory deficits discovered using general linear models (GLMs) and network aberrations or disorganization described using independent component analyses (ICAs) and graph theory have all been previously described, but not with regards to the same sample.

GLM and ICA analyses were performed using FSL's FEAT and MELODIC toolboxes, respectively. Pre-processing was identical for the ICA and GLM analyses and the ICA pipeline also included a PCA data reduction step, a whole-brain probabilistic group ICA and a meta-ICA permutation procedure. After back-transformation, the participant ICN timecourses were compared to the task engagement predictor to determine differential task associations of the ICNs. These participant-level ICN timecourses were also used to compute graph metrics of signal entropy, connectivity strength and diversity, and the relationships between entropy and strength and diversity.

Task activation was observed in prefrontal and posterior parietal brain regions in controls, but the prefrontal activation was absent in Sz patients. In addition, a contrast of activation in the two groups showed group differences in the medial prefrontal cortex and anterior temporal lobe. The default mode network (DMN) was found to have an anticorrelation with the task, which was the strongest task association observed among the ICNs for both schizophrenia patients and controls, and this ICN also shared a medial prefrontal region with the contrast map showing differences between the two groups. The

analyses of the relationship between activity and connectivity showed that, in general, as the networks were recruited by the task, their coherence timecourses diverged from the timecourse of BOLD activity. Importantly, this relationship was more pronounced for persons with schizophrenia that for controls, which implies that this ICN recruitment deficit is worth investigation as a novel endophenotype of schizophrenia. The relationships between the strength and diversity of interconnectivity and the entropy of ICN dynamics also showed group differences, while the strength and diversity of interconnectivity did not by themselves. This further suggests a possible compensatory mechanism in states of dysfunction like schizophrenia.

## Introduction

In recent years, there has been considerable interest in decomposing complex behavioral traits and states of dysfunction along cognitive, affective and personality dimensions that span from the normative range of functioning to psychopathology. There are several initiatives directed at grounding these observed behaviors in neuroscientific evidence and, through these approaches, discovering the neurobiological underpinnings of endophenotypes and how they relate to the etiology of diseases like schizophrenia become more tractable problems (Barch et al., 2013). The fields of functional, and functional connectivity, magnetic resonance imaging (fMRI / fcMRI) have both been developing analysis techniques germane to this research directive (Calhoun & Adali, 2001; Smith et al., 2004), but there is still a need for more convergence between the these types of analyses. For instance, by using both approaches, it is possible to characterize in the vivo brain in task-specific, as well as task-independent states, but it is not well understood how well these types of information complement each other (Xu et al., 2013).

In schizophrenia research, the working memory deficits discovered using general linear models (GLMs) and network aberrations or disorganization described using independent component analyses (ICAs) and graph theory have all been previously described, but not with regards to the same sample (Kim et al., 2009). Hence, little is known about the underlying relationship between the information derived from these metrics, and how they can be combined to provide a more complete picture of the cognitive deficit endophenotype of psychopathology (Çetin et al., 2014). Consequently, data from a sample of persons with schizophrenia and controls who performed the

Sternberg Item Recognition Task (SIRT) were analyzed using a combined GLM, graph theory and ICA pipeline. This data was taken from the Minnesota site of the Functional Imaging Biomedical Informatics Network (fBIRN) study (Potkin et al., 2009), and the subsequent analyses were performed with three goals. The first aim was to use the GLMs to reveal disease-related differences in the activation of brain regions related working memory. Second, an ICA was used to describe the brain networks observed across all participants and to determine the extent to which each of these networks responded to working memory demands in a disease-relevant fashion. Third, graph theory was used to describe global connectivity differences between persons with schizophrenia and controls, and whether these differences were comparable in the set of task-relevant networks. This pipeline was designed to reveal distinct, but convergent, sets of information regarding disease-related differences in how the brain is engaged by a working memory task, as well as the manner in which the task influences the dynamics between brain networks. Hence, this proof-of-principle study should serve to determine whether a combined methodological approach is amenable to answering questions about the dimensions of psychopathology.

## Methods

### *Participants*

25 individuals (12 persons with schizophrenia, 13 controls) were included in this analysis and were enrolled at the University of Minnesota site of the Functional Imaging Biomedical Informatics Research Network (FBIRN) study. The FBIRN study is a multi-site functional magnetic resonance imaging (fMRI) study that was conducted with the goal of examining the clinical and cognitive phenotypes associated with schizophrenia (Steven G Potkin & Ford, 2009)All individuals included in this sample had received written, informed consent in advance of participation in the FBIRN study, and the Institutional Review Board of the University of Minnesota approved all relevant experiments.

All participants were assessed using the SCID (Structured Clinical Interview for DSM-IV-TR) as a part of the inclusion criteria (First, Spitzer, Miriam, & Williams, 2002). All control participants were found to be free of any Axis I disorder, and trained personnel gave all patients diagnoses of schizophrenia using the SCID DSM-IV-TR after the clinical assessments. The persons with schizophrenia were pre-screened for compliance with prescribed antipsychotic medication regimens before continuing in the study.

### *Experimental Design*

All participants completed runs of the Sternberg Item Recognition Paradigm (SIRP/SIRT) in the scanner as a part of a larger task battery. The SIRP is a block-design working memory task that was designed to assess the working memory constructs of serial search, maintenance and retrieval (Sternberg, 1966). During the SIRP, the participant is given a list of items to memorize during the encode phase. In this case, the encoded items were sets of either one, three or five digits, which the participant then had to correctly recognize and then record the appropriate response during the probe phase of the task. If the encoded digit was included in the probe set then the participant pressed one button to indicate "yes" and another button to indicate "no" if it was not.

***MR Acquisition and Imaging Parameters***

For all individuals, 6 minute scans (TR = 2 s; 177 volumes) were collected during the completion of the SIRP. All scans were acquired on a 3T Siemens Trio MRI scanner using a 6 channel transmit, 12-channel receive head coil. A whole-brain functional scan each was collected during the completion of the task (EPI; TR= 2000ms, TE = 30ms; FA = 90°; voxel size = 3.4375 x 3.4375 x 4 $mm^3$; number of slices = 27, slice thickness = 4mm, spacing between slices = 1 mm, interleaved slice acquisition, AC-PC line orientation). A high-resolution structural T1-weighted image (MPRAGE) was also acquired for each participant.

***Image Data Preprocessing***

The imaging data were preprocessed and analyzed using the FMRIB FSL 4.1.9 software package (http://www.fmrib.ox.ac.uk/fsl). Pre-statistical processing steps included high-pass temporal filtering, motion correction via the MCFLIRT linear registration program (Jenkinson et al., 2002), brain extraction using the BET tool, interleaved slice-timing correction, and spatial smoothing using a 5-mm full-width half-maximum Gaussian kernel. For each participant, the functional scans were registered to the corresponding high-resolution T1 images and then to the 2mm MNI standard brain using the nonlinear FNIRT algorithm with a 2mm resampling resolution and 10mm warp kernel (Andersson, Jenkinson, & Smith, 2007).

### *fMRI Image Data Analysis*

#### *Intrinsic Connectivity Network (ICN) Generation*

The functional scans collected were submitted to FSL's temporal concatenation group independent component analysis program (MELODIC) and this was used to produce a set of data-driven networks that were representative of the underlying cortical and sub-cortical brain areas (Beckmann & Smith, 2004). A dimensionality constraint of thirty (30) components was employed since about one third of components tended to be artifactual and this dimensionality has previously been shown to produce a reasonable set of non-artifactual networks after the removal of noise components (Moodie, Wisner & MacDonald III, 2014). Consequently, any components that were identified as noise or

artifacts due to masking voxels outside the brain, in the ventricles, or white matter, were not included in the analyses. The remaining non-artifactual components are henceforth referred to as ICNs (Beckmann, 2012; Calhoun et al., 2009; Zuo et al., 2010). To address potential scan sub-group order and initial random value effects, a meta-ICA permutation procedure was employed. As a result, multiple MELODICs were run and used to derive a set of meta-level ICNs which had reliable estimates of the central tendencies of the networks (for more details, see Wisner et al., 2013). Once the set of meta-level ICNs was generated, FSL's spatio-temporal regression (dualreg) algorithm was used for the back-transformation of participant-level network spatial maps and timecourses from the canonical ICN data (http://www.fmrib.ox.ac.uk/analysis/dualreg).

*General Linear Models (GLMs)*

All GLM analyses were performed using FSL's FEAT toolbox. The pre-processing steps were identical for the ICA and GLM analyses in order to allow for an accurate comparison of the results from the two methods. In the GLM, one main omnibus regressor for task engagement was included as an explanatory variable (EV) in the regression model (GLM). This boxcar EV was convolved with a double gamma hemodynamic response function (HRF) and used to determine the main effects of task engagement for both groups (controls and persons with schizophrenia). Additionally, two GLM Contrasts of BOLD activation between the groups (control > Sz and Sz > control) were also included.

*Network Timecourse Analyses*

After back-transformation into participant-level space, the ICN timecourses were then aggregated and averaged within group to create canonical group timecourses. In order to assess a disease related effect on ICN dynamics, these group timecourse vectors were then contrasted between controls and persons with schizophrenia. This was done by applying serial t-tests and then adjusting the significance level for multiple comparisons across ICNs ($p < 0.05/17$).

To determine the task-relevance of the ICNs, Pearson correlations were performed between the participant-level ICN time courses and corresponding design matrix vectors, which contained the values for the GLM predictor convolved with the HRF. After correlating the task engagement predictor with the ICN timecourses, the correlation scores were averaged within group (control vs. Sz) per ICN and these mean correlations were plotted per group. To test whether each ICN had a significant relationship to the task predictor, serial t-tests were performed for all ICNs within each group. Since several tests were performed for each group, the significance level for all tests was adjusted for multiple comparisons across ICNs and groups ($p < 0.05/(17*2)$)

*ICA vs. GLM Analyses*

One of the main goals in this analysis was to determine if there was a relationship between the information yielded by the ICA and GLM analyses, and whether this relationship also showed disease-related differences. The major distinction between the two approaches (GLM vs. ICA) is that GLMs include a priori assumptions about the nature of the data when generating activation maps, while an ICA derives model-free, data-driven network maps (ICNs). The activation maps produced by the GLM reveal the areas that have a suprathereshold, statistically significant relationship to the given predictor, but does not reveal areas that have a subthreshold association, or that are task-irrelevant (Calhoun, Adali, Stevens, Kiehl, & Pekar, 2005). On the other hand, the ICA can be said to be agnostic to the task design and, hence, networks that are unrelated to the task have as much representation as the networks that are task-relevant in the ICA results.

In the network timecourse analysis (above), the ICA time courses are compared to the model time course predictor (EV) to determine the task-relevance of ICNs. Subsequently, two techniques were used to provide a direct comparison of the two techniques.

The comparison of BOLD activity and ICN task-relevance:

[1] Mean voxel-derived BOLD activity timeseries were also extracted from the preprocessed functional data for each participant. The voxels were masked by the binary cluster map resulting from the control > Sz contrast (which was the only contrast that yielded significant clusters). These timeseries were then aggregated and averaged within group (control vs. Sz) to produce group-average activity timeseries. These canonical

BOLD timecourses were then tested for group differences using a t-test. The ICN timeseries were then correlated with the voxel-derived activity timeseries within group to establish the relationship between ICN connectivity and BOLD activity in the voxels of interest. In order to determine the relationship between ICN task relevance and ICN similarity to the underlying activity, these correlations were plotted against ICN task-relevance scores in scatterplots per group. The scores from each metric were then correlated within group in order to see if the correspondence of scores from the ICN task-relevance and the ICN-activity relationship was significant. An ANOVA was then performed to test group differences in this relationship.

[2] To aid visualization of these relationships the average group BOLD activity vectors (control vs. Sz) were scaled and centered around the zero point on the x-axis, while preserving the proportional relationship between the magnitude scores in the two timecourses. As the DMN was the ICN with the strongest task association, average DMN timecourses were created for each group (control vs. Sz) and scaled in the same manner as the activity timeseries. The timecourse of the predictor for task engagement was also plotted so the fluctuations in BOLD activity and ICN coherence could be contrasted with the task.

*Signal Entropy, Connectivity Strength and Diversity*

The ICN timeseries were all correlated with each other within participant. These participant-level correlation matrices were then used to compute graph metrics for univariate entropy, as well as bivariate strength and diversity. The scores for these metrics were averaged and plotted within group (control vs. Sz). Pearson correlations were also computed between entropy and strength and diversity, respectively.

The individual-level, back-transformed ICN timeseries were used as the basis of the analysis of ICN time course entropy as well as all subsequent analyses. Univariate entropy here is defined as the Shannon entropy (Shannon, 1948), and is measured for each signal, i.e. within each ICN and then averaged across ICNs and participants within each group. For the bivariate metrics, the mean score for the $i^{th}$ column of the connectivity matrix represents how well each node (ICN) is connected to all other nodes in the graph and, hence, the strength of the graph in this analysis is defined as the average strength across all ICNs. Similarly, the variance of the $i^{th}$ column of the connectivity matrix represents the variability in the strength of connectivity for each ICN and, hence, the diversity is the average variability within group (Lynall et al., 2010).

### *3D Brain Figure Generation*

The Mango (the Multi-image Analysis GUI) viewer from the Research Imaging Institute of University of Texas Health Science Center (http://ric.uthscsa.edu/mango/index.html) was used to generate three-dimensional glass brain representations of the ICNs. The canonical ICN spatial maps from the ICA were used as overlays in renderings on a 3D

surface build of the MNI 152 T1 1-mm brain template. These 3D renderings were then made translucent so that the subsurface structures contained in each ICN were also visible. This was useful for several networks that contained sub-cortical structures such as the thalamus / basal ganglia network.

## Results

### *Generation of Intrinsic Connectivity Networks*

17 non-artifactual, physiologically relevant ICA components were identified as Intrinsic Connectivity Networks (ICNs) and the spatial maps and time courses of these ICNs were used for all subsequent analyses in this paper (Figure 2). The canonical ICNs were then used as templates for back-transformation into individual-level space, which yielded a set of ICNs for each participant that included individual-level variance. After back-transformation, the ICNs were then aggregated into two groups of networks for control participants and schizophrenia patients, respectively, so that group comparisons could be made in order to detect disease-related differences.

### *General Linear Model of Task Engagement*

The task-engagement predictor, which included both the encoding and probe phases of the task, was used to derive a main effect of being on-task for both controls and

persons with schizophrenia. Task activation was observed in inferior and dorsolateral prefrontal regions in controls (Figue 3a), but the prefrontal activation seen in controls was absent in persons with Sz (Figure 3b). A contrast of the activation between the two groups revealed higher activity in controls than patients in the medial prefrontal cortex and anterior temporal lobe (Figure 3c). There were no brain regions that showed higher activity in patients than healthy controls. It was noted that the contrast reveal a group difference in the medial prefrontal cortex, which is one of the brain regions that constitutes the DMN (Figure 3d), and this observation will be explored further in later analyses.

*Contrasts of Canonical Group Timecourses and Task-Relevance of ICN Timecourses*

Importantly, there were significant group differences in the magnitude of coherence over time within all networks (i.e. the magnitude of ICN timecourses), for instance in the default mode network ($t = 1907.998$, $df = 287.121$, p-value $< 2.2e\text{-}16$) (Table 1). However, when the average ICN task relevance scores were contrasted between controls and schizophrenia patients, none of the networks exhibited group differences in the overall magnitude of task-engagement after corrections for multiple comparisons.

After back-transformation, the participant-level ICN timecourses were correlated with each person's corresponding design matrix vector for the task engagement predictor. These scores were then averaged within group and plotted (Figure 3). Both control participants and persons with Sz showed significant negative task associations in the

default mode network, precuneus network, and the temporal lobe network, with the default mode network anticorrelation being the strongest observed task-ICN association in both groups (Tables 2 & 3).

*Relationship between ICN Timecourses and the BOLD Activity within the Contrast Map*

After averaging the BOLD timeseries within the medial prefrontal and inferior temporal regions generated in the control > Sz contrast, this average BOLD activity timecourse was found to overlap most with the medial-prefrontal / temporal component in controls ($r = 0.54$, $p < 0.001$) (Table 4). On the other hand, this activity connectivity relationship was highest with the default mode network in patients ($r = 0.60$, $p < 0.001$) (Table 5). After aggregating the participant-level BOLD activity timecourses within group, significant group differences were detected in activity levels within the contrast map, with lower activity observed in schizophrenia patients ($t = 8.52$, $df = 2379.48$, p-value < 2.2e-16). However, as in the case of the task-relevance scores, the relationship between the ICN timecourses and the average time course of BOLD activity within the contrast map also exhibited no sensitivity to group differences after Bonferroni correction.

*Correspondence of ICN Task Relevance Scores and ICN Correlations with BOLD Activity Timeseries*

The ICN task relevance scores (correlation between the ICN timecourses and the GLM predictor) and the connectivity-activity correlations (between the ICN timecourses

and BOLD activity timecourses) were plotted against each other to determine if ICN task engagement influenced the how well the ICN dynamics matched the underlying activity (Figures 6 & 7). In addition, a contrast of this relationship between groups was performed to examine any meaningful disease-related differences in how the ICN dynamics diverged from the underlying activity as a function of task engagement. It was observed that for both groups, there was a negative correspondence of ICN task relevance and the similarity of connectivity to activity. This correspondence in controls (Figure 6) showed a significant negative trend ($r = -0.60$, $p = 0.01$, $R^2 = 0.36$) and this negative correspondence (Figure 7) was even more pronounced in persons with Sz ($r = -0.88$, $p = 2.81e\text{-}06$, $R^2 = 0.78$). An ANOVA of group differences in the relationship between these two variables further showed that intranetwork connectivity diverges from the underlying activity when the ICNs are task relevant in a manner that is significantly more negative in patients ($F = 14.05$, $p = 7.07e\text{-}4$). These findings were corroborated by the observable differences in the canonical DMN timecourses and group activity timecourses (Figure 8).

*Graph Theory Metrics*

The analysis of Shannon entropy did not show any significant group differences between persons with schizophrenia and controls using a t-test and correction for multiple comparisons (Figure 9). There was also no group difference observed for the strength of interconnectivity (Figure 10). Similarly the analysis of group differences in the diversity of interconnectivity also showed slight, non-significant difference, with the diversity interconnectivity being higher in persons with schizophrenia than controls (Figure 11).

The Pearson correlation between signal entropy and connectivity strength revealed that there was a significant group difference in this metric. The relationship between entropy and strength was higher for patients than controls, indicating that as signal entropy increased, so did the strength of interconnectivity (Figure 12). This was also the case for the relationship between signal entropy and the diversity of interconnectivity, where a significant group difference was also observed, with the connectivity diversity increasing as signal entropy increased (Figure 13).

## Discussion

The analyses in this study were undertaken for the purpose of examining both hypothesis-driven activity metrics and exploratory functional connectivity measures in the same data set. This combined approach was designed to provide a more comprehensive perspective on the functioning of brain systems and associated cognitive phenomena, as well as how the integration of findings from these domains better informs phenotypes relevant to disease states like schizophrenia. In this study, working memory was assessed in persons with schizophrenia and matched controls using the Sternberg item recognition paradigm (SIRP) in fMRI scans. GLMs, ICA and graph theory metrics were applied to the data from all functional scans, including both patients and controls, to

identify similarities in the results yielded by these techniques and what they reveal about schizophrenia.

*General Linear Model of Task Engagement*

The GLM revealed that, in controls, activation was localized in dorsolateral prefrontal and inferior frontal regions that had previously been associated with the rearrangement and manipulation of information in working memory tasks (Baldo & Dronkers, 2006; Koenigs, Barbey, Postle, & Grafman, 2009; Marshuetz, Smith, Jonides, DeGutis, & Chenevert, 2000; Minzenberg & Laird, 2009). On the other hand, the frontal activation associated with this phenomenon was not observed in persons with schizophrenia. Hence, brain activity was observed in regions that have been classically been association with working memory function in controls, but there appears to be a working memory deficit in schizophrenia (Brown et al., 2009; Silver, Feldman, Bilker, & Gur, 2003). A contrast of activation in controls and patients revealed disease-related differences in the medial prefrontal cortex as well as the anterior temporal lobe. The medial prefrontal cortex has been previously been implicated as an area that has shown functional deficits in schizophrenia (Pomarol-Clotet et al., 2010) and is one of the nodes of the default mode network (Raichle et al., 2001), the role of which will be discussed further. The anterior temporal lobe structures detected in the contrast have also been previously associated with functional deficits in schizophrenia (Calhoun et al., 2006; Calhoun, Kiehl, Liddle, & Pearlson, 2004), and specifically with activation deficits in working memory paradigms like the SIRP (Henseler, Falkai, & Gruber, 2009; Kim et al.,

2010). Hence, the activation results in this study are supported by the existing literature and this aids the interpretability of the subsequent functional connectivity analyses.

*ICN Timecourse Profiles and Task-Relevance*

The functional scan data from both participants and controls was decomposed into a set of 17 global ICNs. However, after back-transformation into participant-level space and averaging within group, it was found that all of the ICNs exhibited significantly lower coherence in schizophrenia patients. The timecourse dynamics of an ICN reflects changes in the coherence between activity in voxels within the network over time. Hence, this result reveals a magnitude effect seen across all ICNs, in which persons with schizophrenia have an overall lower level of coherence within their networks. This assertion is supported by the dysconnectivity phenotype that has been previously described in schizophrenia (Fornito, Zalesky, Pantelis, & Bullmore, 2012; Lynall et al., 2010; Meda, Stevens, Folley, Calhoun, & Pearlson, 2009; Meyer-lindenberg, 2010; Repovš & Barch, 2012; Woodward et al., 2009)

In both patients and controls, these ICNs were found to have varying degrees of engagement by the task. Several ICNs were found to have significant positive associations with the task timeline in both groups and these included ICNs with relevant functions, such as a sequence learning and recall network, the basal ganglia, insula and cerebellum. In particular, the strongest positive association was seen in the left-executive/posterior parietal network, which contained the same regions seen in the activation main effect analyses. Similarly, significant negative task associations were

seen in both groups in networks that contained default mode regions, and these regions also overlapped with regions revealed in the group contrast. Specifically, the spatial location of the network with the highest task association (the default mode network) overlapped with the region more activated in controls when compared to persons with schizophrenia. This indicates that the DMN is potentially one of the most relevant, disease-sensitive ICNs. Overall, several ICA-derived networks (ICNs) exhibited strong positive or negative associations with the task, which is evidence of specific but differential task engagement even in regions not captured by the GLM. Moreover, the information about network task relevance provides context and greater interpretability for the results seen in the GLM activation analyses.

The ICNs did not reveal any group differences in their levels of engagement by the task. This could be explained by the global ICNs being derived from data from both controls and persons with schizophrenia, instead of being derived, for instance, from the healthy controls. This was done in order to not bias the network-related analyses towards characteristics of one group or another. Hence, the pooling of data could have driven the overall profile fluctuations in coherence in ICN timecourses to a central tendency between the two groups. This means that while there was a magnitude effect of ICN timecourse coherence, if the profiles of task engagement were similar between groups irrespective of magnitude, this could explain the lack of group differences observed in the correlations between the ICN timecourses and the task predictor. However, as noted above, the magnitudes of coherence dynamics over time in the ICNs were significantly higher in controls than patients in *all* ICNs. Hence, even though patients' ICNs were able

to be engaged by the task in a comparable fashion, there was still an underlying deficit in network intraconnectivity in schizophrenia.

*Relationship between ICN Timecourses and the BOLD Activity within the Contrast Map*

The voxel-level BOLD activity was averaged from the medial prefrontal and temporal regions in order to determine the relationship between the ICNs and the underlying brain activity in the areas most sensitive to group differences. As was observed in the GLM contrast of activation in the two groups, there was a significant difference in the level of BOLD activity in the voxels within the contrast mask. Hence, the voxel-level activity also reflects the disease-related difference discovered in the GLM. For the correlation between ICN dynamics and BOLD activity, it is notable that the highest correspondence for controls was seen in the ICN that had both medial prefrontal and temporal aspects, which are the two regions the activity was derived from. Hence, this shows a convergence of the connectivity and activity metrics. This network also had a strong, but lower correlation with activity in patients, which resulted in the default mode network showing the strongest correspondence between activity and intranetwork connectivity in patients. The differing results from the two groups are likely due to aberrations resulting from schizophrenia and, particularly, the lower correspondence of the medial prefrontal / temporal network and activity in patients supports the notion of dysfunction in those regions.

Contrary to the group contrast of the BOLD activity, group differences in the relationship between the ICN timecourses and this raw activity did not survive p-value

adjustments. This is similar to the lack of significant group differences in task relevance and could also be due to the ICNs being derived from data from both groups. Another consideration was that the omnibus predictor for task engagement was used in this analysis to facilitate a proof-of-principle comparison of GLM activation and ICN connectivity, but it is perhaps too general to detect more subtle disease-related perturbations in the networks caused by specific task events.

*Correspondence of ICN Task Relevance Scores and ICN Correlations with BOLD Timeseries*

In the task relevance vs. ICN correspondence with activity metric, there were varying associations of the connectivity profiles of the ICNs and activity within the control vs. schizophrenia contrast region. For some ICNs, their coherence timecourses matched the BOLD activity, while in some ICNs there was no relationship, and in other ICNs there was an anticorrelation between the ICN timecourses and the activity timecourse. Overall, there was a significantly negative relationship between ICN task relevance and ICN associations with activity. This implies that ICN coherence might be driven down as a function of task demands on the networks in this paradigm, at least with respect to activity in the regions that displayed GLM differences between groups. This does not necessarily have to hold for activity in all other regions, but research in other domains has demonstrated similar findings in which increasing task performance lead to proportional decreases in interneuronal connectivity (Cohen & Maunsell, 2009). In addition, the proportional anticorrelation between ICN task relevance and how well ICN

dynamics matched activity was significantly more pronounced for schizophrenia patients. This could mean that there was an advantageous divergence of ICN dynamics and activity when those ICNs are being recruited by a task, but that too much divergence from activity could be maladaptive for optimal ICN functionality, and is indicative of a disease state of network deregulation.

*Graph Theory Metrics*

Previously observed differences in the relationship between signal entropy and connectivity strength and diversity in schizophrenia were recapitulated in this study (Bassett, Nelson, Mueller, Camchong, & Lim, 2012). However, the significant decreases in strength and increases in diversity that had previously observed in schizophrenia were not present in this sample (Lynall et al., 2010). This could be due to sample size, and there not being enough power to detect this difference. However, previous differences were identified in data from resting state scans, whereas the participants in this study had performed a working memory task. Hence, these difference could also be state dependent and future studies will need to test this hypothesis. Nevertheless, there were clear differences in the interconnectivity profiles of the networks of persons with schizophrenia. While there was no relationship between entropy and the strength or diversity of interconnectivity in controls, there was a significantly more positive relationship between signal entropy and connectivity strength and diversity in schizophrenia. Here, entropy describes the level of uncertainty inherent to the ICN signal, which in this case is their timecourse dynamics. Since, there were not significant differences in the strength and diversity of interconnectivity, it is possible that when engaged by tasks, such as tests of

working memory, the networks in the brains of schizophrenia patients are compensating for increased entropy, by introducing a state of relative hyperconnectivity, which then gets expressed as a normalization of connectivity strength and diversity (Camchong et al., 2011; Liu et al., 2012; Whitfield-Gabrieli et al., 2009).

*Limitations*

While this study serves a proof of concept, all task events were modeled simultaneously in order to assess general task engagement across the domains of activation and functional connectivity. Consequently, differences that may arise from the encoding versus the recall of items cannot be assessed, neither can differences arising from increases in working memory load. Another limitation is that this is a relatively small sample, which means that these findings should be corroborated in a larger data set.

*Conclusion*

Overall, there appears to be a strong relationship between the intrinsic connectivity and activity of the brain and this relationship is relevant to the disease state of schizophrenia. The results from the ICA-derived and GLM metrics revealed both task relevance and group differences in congruent regions. Additionally, ICN task-relevance had a negative correspondence to the ICN relationship to activity in both groups, but this effect was more pronounced in persons with schizophrenia. Hence, this implies that as ICNs were being engaged by the task they resembled the underlying activity less, at least

in the areas showing group differences in the GLM. The observation that this correspondence is even more negative in persons with schizophrenia indicates that GLM differences in activation in the task could be driven by, and is at least related to perturbations in ICN coherence.

It is interesting that the DMN showed the strongest task relevance in this paradigm using an omnibus predictor. This is likely due to the fact that other ICN contributions, such as task-positive networks recruited by specific task features are not being captured as well by the predictor. On the other hand, the DMN has a consistent anticorrelation with the task engagement predictor, which indicates that it is reliably being disengaged by the task, in its characteristic fashion (Lin, Hasson, Jovicich, & Robinson, 2011; Raichle et al., 2001; Snyder & Raichle, 2012). This is supported by the observation that in the plot of the task timeline, BOLD activity and DMN group timecourses, network coherence in the DMN increases in the "off" periods of the task. It is also interesting that the magnitude of changes in DMN coherence is higher in controls that patients, which supports previous work showing that the DMN does not appropriately disengage during a task in persons with schizophrenia (Jang et al., 2011; Kim et al., 2009; Krajcovicova, Mikl, Marecek, & Rektorova, 2012; Meda et al., 2009).

Not only are there disease-relevant findings related to BOLD activity, GLM activation and the intranetwork characteristics of ICNs, but the interconnectivity of ICNs is also different in schizophrenia and analyses of this interconnectivity have revealed a potential compensatory mechanism. In conclusion, the combination of activation and functional connectivity methodologies was able to yield information about cognitive deficits in schizophrenia that had been previously undiscovered. Hence, when used in

conjunction, these analyses can provide greater insight into the brain mechanisms that underlie the dimensions of psychopathology (Barch et al., 2013).

Tables

**Table 1. Summary of T-Tests of Group Differences in the Raw ICN Timecourses**

| ICN | Control Mean | Sz Mean | p | CI LB (95%) | CI UB (95%) |
|---|---|---|---|---|---|
| 1 | 590.69 | 290.43 | 0.00 | 299.97 | 300.56 |
| 2 | 375.49 | 182.63 | 0.00 | 192.67 | 193.06 |
| 3 | 276.18 | 132.89 | 0.00 | 143.15 | 143.43 |
| 4 | 357.81 | 166.57 | 0.00 | 191.07 | 191.42 |
| 5 | 275.17 | 129.74 | 0.00 | 145.02 | 145.83 |
| 6 | 230.40 | 109.54 | 0.00 | 120.71 | 121.02 |
| 7 | 399.76 | 196.40 | 0.00 | 203.18 | 203.54 |
| 8 | -53.83 | -18.75 | 0.00 | -35.35 | -34.81 |
| 9 | 356.26 | 174.10 | 0.00 | 181.99 | 182.34 |
| 10 | 420.74 | 199.71 | 0.00 | 220.80 | 221.26 |
| 11 | 404.84 | 197.40 | 0.00 | 207.24 | 207.65 |
| 12 | 436.61 | 211.79 | 0.00 | 224.66 | 224.98 |
| 13 | 445.90 | 215.73 | 0.00 | 229.92 | 230.40 |
| 14 | 465.71 | 229.02 | 0.00 | 236.48 | 236.89 |
| 15 | 470.26 | 205.17 | 0.00 | 264.93 | 265.24 |
| 16 | 542.40 | 229.25 | 0.00 | 312.91 | 313.38 |
| 17 | -69.04 | -45.42 | 0.00 | -23.91 | -23.32 |

**Note.** This table provides the group means, p-values and confidence intervals associated with tests of the significance of group differences in the raw ICN timecourses between controls and persons with schizophrenia. All participant-level scores were averaged within group per ICN to create canonical group ICN timecourse vectors. The canonical timecourses for the two groups (controls vs. Sz) were submitted to a Welch Two Sample t-test per ICN. The ICNs are ordered in the same fashion as the three-dimensional representations in Figure 2. The 'Control Mean' and 'Sz mean' columns contain the estimates of the mean timecourse coherence over time for ICNs in controls and schizophrenia patients, respectively. All ICNs passed the corrected significance threshold ($p < 0.0015$) and, hence, no rows needed to be bolded. 'Sz' is short for schizophrenia; 'CI' refers to the confidence interval; 'LB' is the lower bound of the confidence interval; 'UB' is the upper bound of the confidence interval.

**Table 2. Summary of Correspondence between ICN Timeseries and the Sternberg Working Memory Task Design in Controls**

| ICN # | r | p | CI LB (95 %) | CI UB (95 %) |
|---|---|---|---|---|
| 1 | 0.00 | 0.755 | -0.18 | 0.19 |
| 2 | 0.26 | 0.004 | 0.10 | 0.42 |
| 3 | -0.09 | 0.113 | -0.21 | 0.03 |
| 4 | 0.09 | 0.220 | -0.06 | 0.24 |
| 5 | -0.07 | 0.245 | -0.20 | 0.06 |
| 6 | -0.15 | 0.007 | -0.25 | -0.05 |
| 7 | 0.20 | 0.007 | 0.07 | 0.34 |
| 8 | -0.05 | 0.465 | -0.20 | 0.10 |
| 9 | **-0.29** | **0.001** | **-0.42** | **-0.14** |
| 10 | **-0.48** | **0.000** | **-0.51** | **-0.40** |
| 11 | **0.19** | **0.000** | **0.12** | **0.26** |
| 12 | -0.01 | 0.632 | -0.11 | 0.08 |
| 13 | **-0.19** | **0.000** | **-0.26** | **-0.10** |
| 14 | -0.07 | 0.183 | -0.17 | 0.04 |
| 15 | 0.15 | 0.009 | 0.04 | 0.26 |
| 16 | 0.16 | 0.018 | 0.03 | 0.29 |
| 17 | 0.04 | 0.309 | -0.04 | 0.13 |

**Note.** This table provides the p-values and confidence intervals associated with the task-relevance scores in controls depicted in Figure 4. All scores for ICN task relevance in controls were submitted to a t-test again zero per ICN. The ICNs are ordered in the same fashion as the three-dimensional representations in Figure 2. The 'r' column contains the average ICN task relevance correlation scores per ICN for controls. The rows representing ICNs that passed the corrected significance threshold ($p < 0.0015$) were bolded. 'CI' refers to the confidence interval; 'LB' is the lower bound of the confidence interval; 'UB' is the upper bound of the confidence interval.

**Table 3. Summary of Correspondence between ICN Timeseries and the Sternberg Working Memory Task Design in Persons with Schizophrenia**

| ICN # | r | p | CI LB (95 %) | CI UB (95 %) |
|---|---|---|---|---|
| 1 | 0.03 | 0.527 | -0.09 | 0.15 |
| 2 | **0.30** | **0.001** | **0.16** | **0.44** |
| 3 | -0.21 | 0.005 | -0.32 | -0.08 |
| 4 | 0.10 | 0.072 | -0.01 | 0.21 |
| 5 | -0.16 | 0.003 | -0.24 | -0.07 |
| 6 | **-0.19** | **0.001** | **-0.27** | **-0.10** |
| 7 | **0.27** | **0.000** | **0.18** | **0.37** |
| 8 | -0.12 | 0.027 | -0.22 | -0.02 |
| 9 | **-0.23** | **0.000** | **-0.29** | **-0.15** |
| 10 | **-0.44** | **0.000** | **-0.52** | **-0.32** |
| 11 | 0.09 | 0.026 | 0.01 | 0.16 |
| 12 | -0.07 | 0.273 | -0.20 | 0.07 |
| 13 | **-0.22** | **0.000** | **-0.30** | **-0.13** |
| 14 | -0.06 | 0.261 | -0.18 | 0.05 |
| 15 | 0.04 | 0.420 | -0.08 | 0.16 |
| 16 | 0.15 | 0.007 | 0.05 | 0.26 |
| 17 | 0.00 | 0.750 | -0.11 | 0.11 |

**Note.** This table provides the p-values and confidence intervals associated with the task-relevance scores in schizophrenia patients depicted in Figure 4. All scores for ICN task relevance in patients were submitted to a t-test again zero per ICN. The ICNs are ordered in the same fashion as the three-dimensional representations in Figure 2. The 'r' column contains the average ICN task relevance correlation scores per ICN for patients. The rows representing ICNs that passed the corrected significance threshold ($p < 0.0015$) were bolded. 'CI' refers to the confidence interval; 'LB' is the lower bound of the confidence interval; 'UB' is the upper bound of the confidence interval.

**Table 4. Summary of the Relationships between ICN Relationship of ICN Timeseries and the Average Voxel BOLD Timeseries within the Controls > Schizophrenia Contrast Mask in Controls**

| ICN # | r | p | CI LB (95 %) | CI UB (95 %) |
|---|---|---|---|---|
| 1 | 0.13 | 0.238 | -0.10 | 0.37 |
| 2 | 0.01 | 0.734 | -0.20 | 0.21 |
| 3 | **0.54** | **0.000** | **0.44** | **0.62** |
| 4 | 0.05 | 0.442 | -0.10 | 0.20 |
| 5 | **0.41** | **0.000** | **0.22** | **0.60** |
| 6 | 0.16 | 0.046 | 0.00 | 0.33 |
| 7 | **-0.38** | **0.001** | **-0.50** | **-0.20** |
| 8 | -0.17 | 0.096 | -0.36 | 0.04 |
| 9 | 0.23 | 0.017 | 0.05 | 0.41 |
| 10 | **0.36** | **0.001** | **0.19** | **0.53** |
| 11 | 0.14 | 0.008 | 0.04 | 0.23 |
| 12 | **0.25** | **0.001** | **0.12** | **0.38** |
| 13 | **0.38** | **0.001** | **0.20** | **0.56** |
| 14 | 0.26 | 0.038 | 0.02 | 0.50 |
| 15 | 0.15 | 0.044 | 0.00 | 0.29 |
| 16 | -0.12 | 0.354 | -0.37 | 0.15 |
| 17 | 0.03 | 0.539 | -0.10 | 0.16 |

**Note.** This table provides the p-values and confidence intervals associated with the tests of significance for the relationship between ICN dynamics and the BOLD activity in the contrast map in controls depicted in Figure 5. All scores for this connectivity-activity in controls were submitted to a t-test again zero per ICN. The ICNs are ordered in the same fashion as the three-dimensional representations in Figure 2. The 'r' column contains the average correlation scores per ICN for controls. The rows representing ICNs that passed the corrected significance threshold ($p < 0.0015$) were bolded. 'CI' refers to the confidence interval; 'LB' is the lower bound of the confidence interval; 'UB' is the upper bound of the confidence interval.

**Table 5. Summary of the Relationships between ICN Timeseries and the Average Voxel BOLD Timeseries within the Controls > Schizophrenia Contrast Mask in Persons with Schizophrenia**

| ICN # | r | p | CI LB (95 %) | CI UB (95 %) |
|---|---|---|---|---|
| 1 | -0.01 | 0.741 | -0.23 | 0.22 |
| 2 | -0.18 | 0.081 | -0.37 | 0.03 |
| 3 | **0.48** | **0.000** | **0.29** | **0.66** |
| 4 | 0.07 | 0.349 | -0.10 | 0.25 |
| 5 | **0.50** | **0.000** | **0.33** | **0.66** |
| 6 | **0.28** | **0.001** | **0.14** | **0.42** |
| 7 | **-0.43** | **0.000** | **-0.53** | **-0.26** |
| 8 | -0.03 | 0.646 | -0.22 | 0.17 |
| 9 | **0.38** | **0.000** | **0.24** | **0.52** |
| 10 | **0.60** | **0.000** | **0.32** | **0.87** |
| 11 | 0.14 | 0.086 | -0.02 | 0.31 |
| 12 | 0.20 | 0.019 | 0.04 | 0.37 |
| 13 | **0.51** | **0.000** | **0.36** | **0.65** |
| 14 | 0.20 | 0.040 | 0.01 | 0.39 |
| 15 | 0.10 | 0.054 | 0.00 | 0.21 |
| 16 | -0.32 | 0.022 | -0.53 | -0.06 |
| 17 | 0.12 | 0.137 | -0.04 | 0.28 |

**Note.** This table provides the p-values and confidence intervals associated with the tests of significance for the relationship between ICN dynamics and the BOLD activity in the contrast map in persons with schizophrenia depicted in Figure 5. All scores for this connectivity-activity in patients were submitted to a t-test again zero per ICN. The ICNs are ordered in the same fashion as the three-dimensional representations in Figure 2. The 'r' column contains the average correlation scores per ICN for patients. The rows representing ICNs that passed the corrected significance threshold ($p < 0.0015$) were bolded. 'CI' refers to the confidence interval; 'LB' is the lower bound of the confidence interval; 'UB' is the upper bound of the confidence interval.

Figures

**Figure 1. The Task Design of the Sternberg Item Recognition Paradigm**

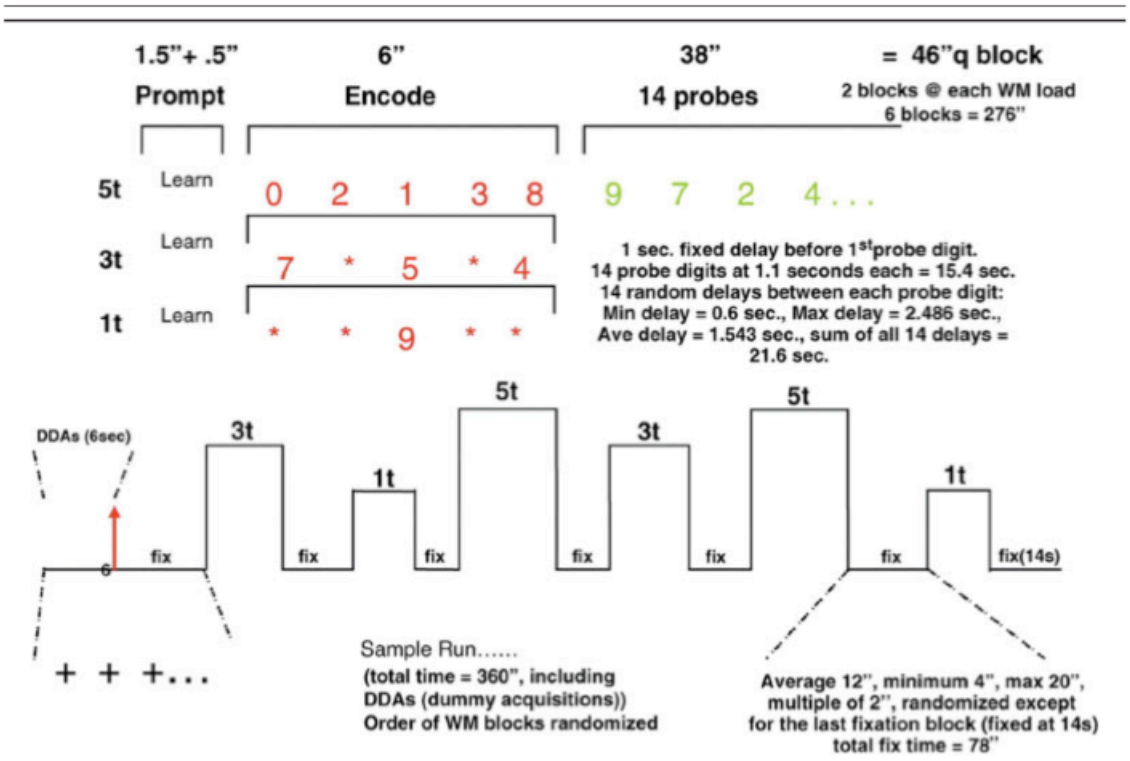


**Figure 1.**

Kim et al. (2009). Dysregulation of Working Memory and Default- Mode Networks in Schizophrenia Using Independent Component Analysis, an fBIRN and MCIC Study. *Human Brain Mapping* 30:3795–3811

**Note.** This figure is a depiction of the task structure of the Sternberg Item Recognition task (SIRT). For this analysis, an omnibus regressor was employed to look at general effects of task engagement in a proof-of-principle ICA-GLM pipeline. Hence, the predictor models all three levels of digit encoding and all probes.

**Figure 2.**

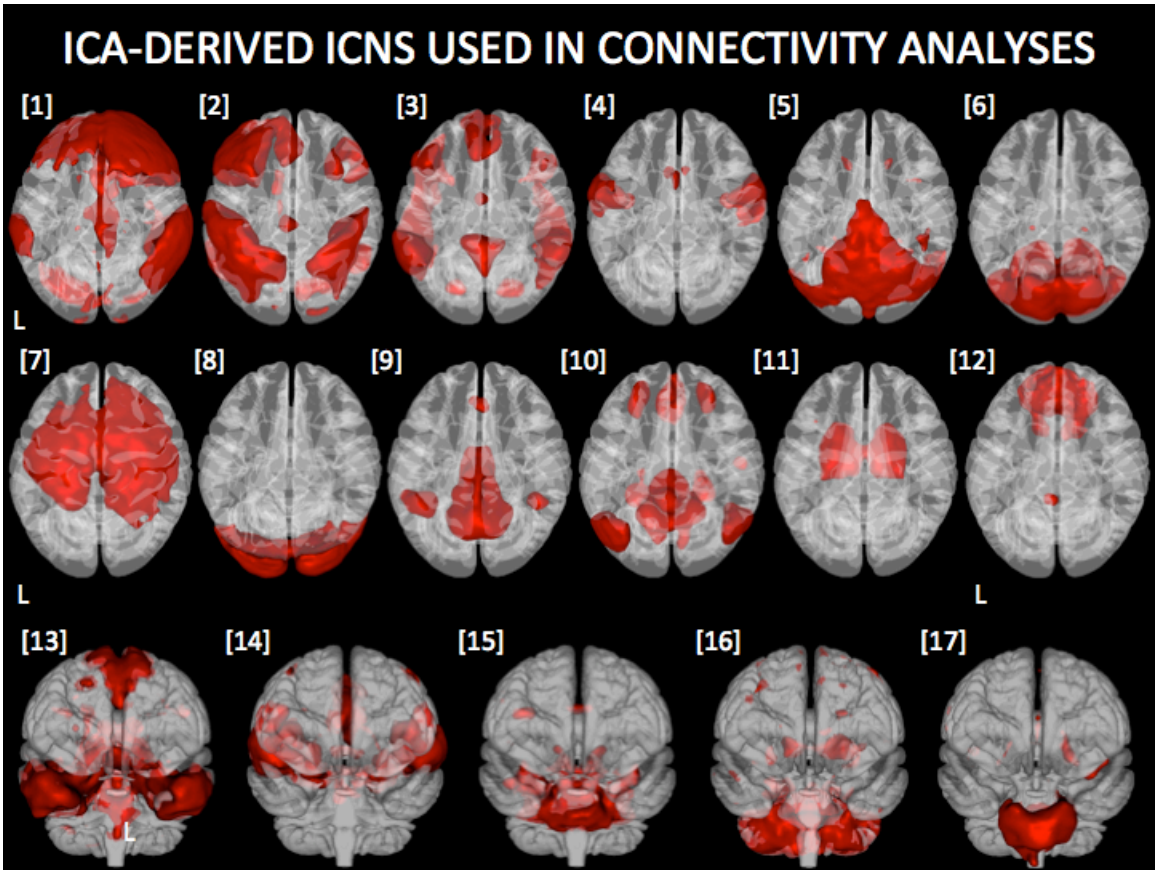


**Note.** The FSL MELODIC probabilistic ICA algorithm was used to generate canonical Intrinsic Connectivity Networks (ICNs) from the SIRT data. The set of canonical ICA components were visually inspected and all artifacts such as motion artifacts, or components with significant amounts of voxels masking areas outside the brain, in white matter, or in ventricles were excluded. The resulting set of non-artifactual components were the set of ICNs and have been overlaid on glass brains at a threshold of $z = 6$.

**Figure 3. GLM Results and ICN with subcomponents overlapping with regions in the Control > Sz Contrast**

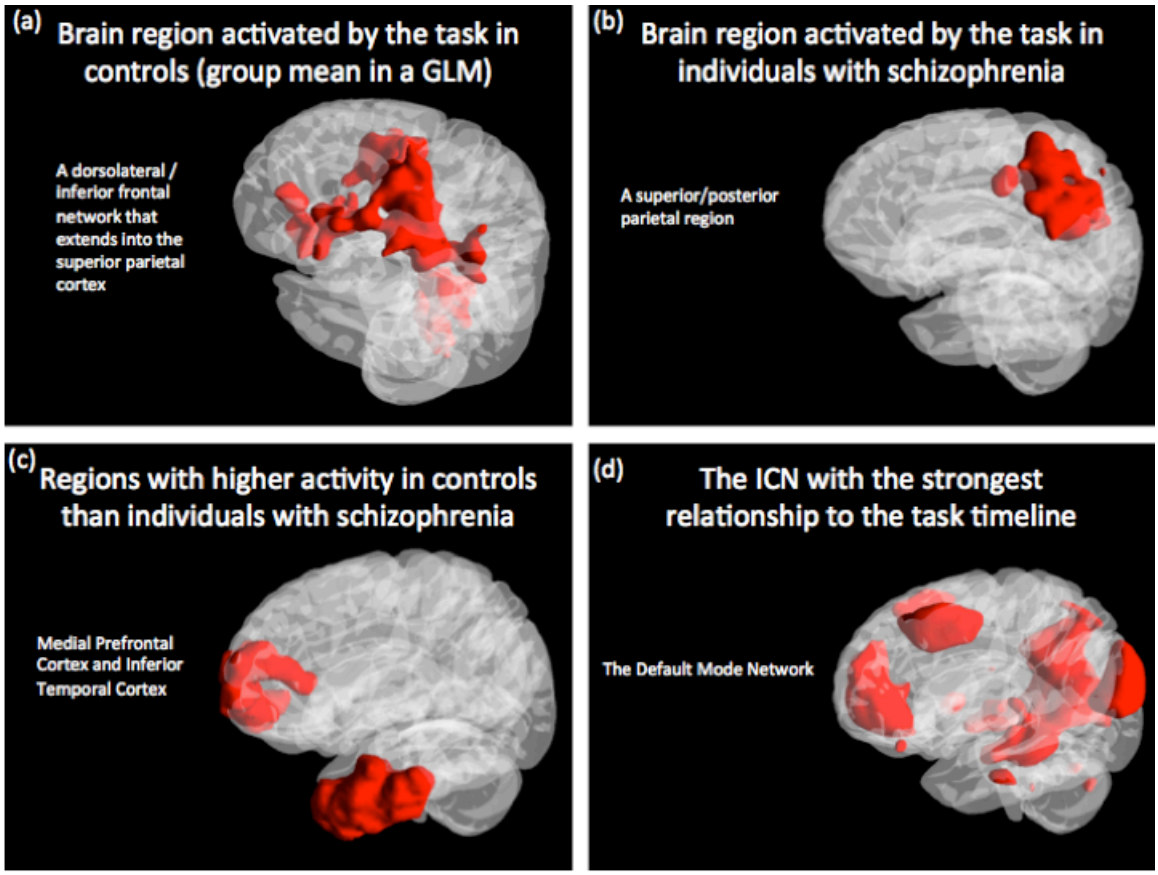


**Note.** (a) The activation map resulting from the analysis of the main effect of task engagement for the control group has been overlaid on a translucent glass brain (b) This is a map of the main effect of task engagement in persons with schizophrenia. (c) This map shows the areas resulting from a contrast of activation that was significantly higher in controls than persons with schizophrenia. (d) This is a sagittal rendering of the default mode network (ICN 10), which is the ICN that had the strongest association with the task-engagement predictor used in the GLM (depicted in Figure 7).

**Figure 4.**

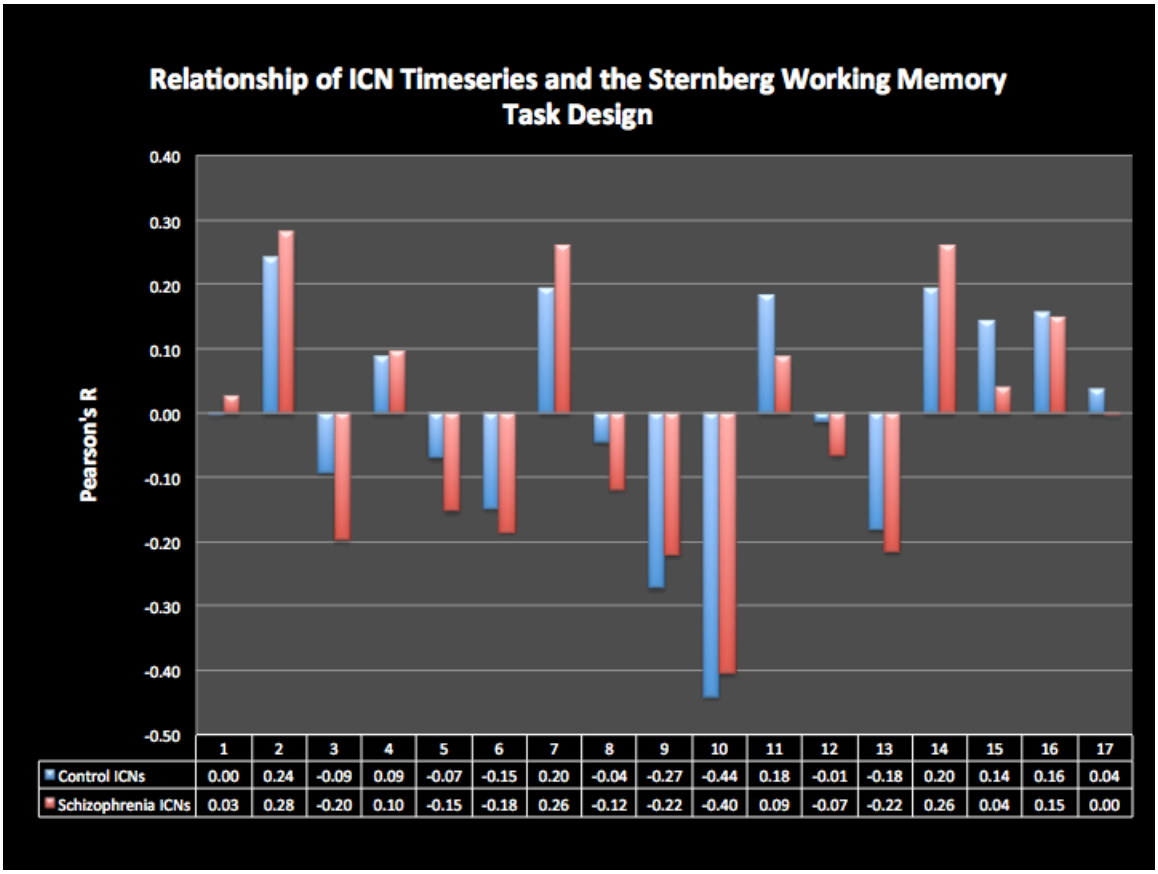


**Note.** The participant-level timeseries for each ICN was correlated with the predictor used for the activation analyses in order to determine the extent of task engagement for each of the ICNs. These task-relevance scores were average within group (control vs. schizophrenia) and plotted. The ICN numbers are the same as the ICNs plotted on glass brains overlays in Figure 1 (above).

**Figure 5.**

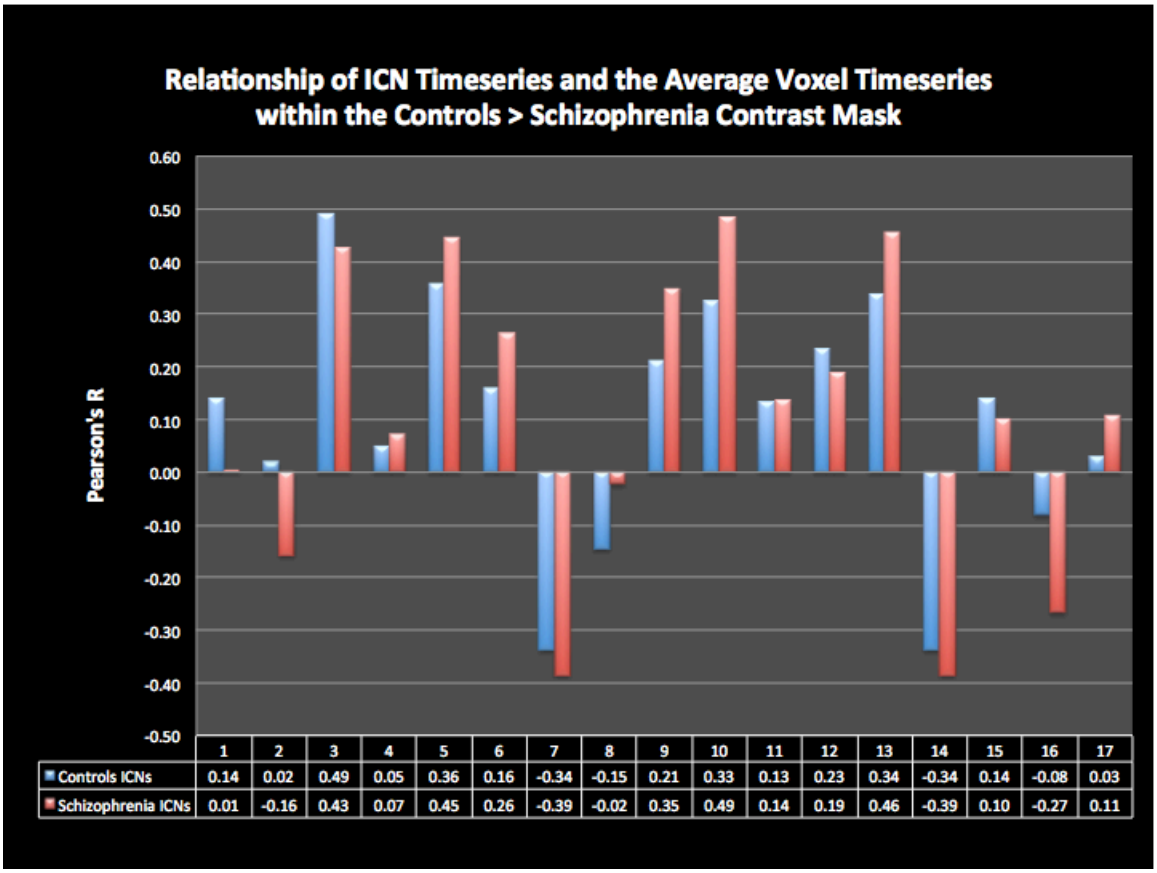


**Note.** The contrast map depicted in Figure 2(c) above was binarized and used as a mask within which raw voxel values were extracted from the participant-level, pre-processed functional data. These voxel values were average within group to create average voxel-derived BOLD activity timeseries for both groups (controls and persons with schizophrenia). These activity timeseries were correlated with all participant timeseries within each group and these activity-connectivity correlation scores were aggregated and averaged within each group (control vs. Sz) and plotted here. ICN numbers correspond to those in Fig. 1.

**Figure 6.**

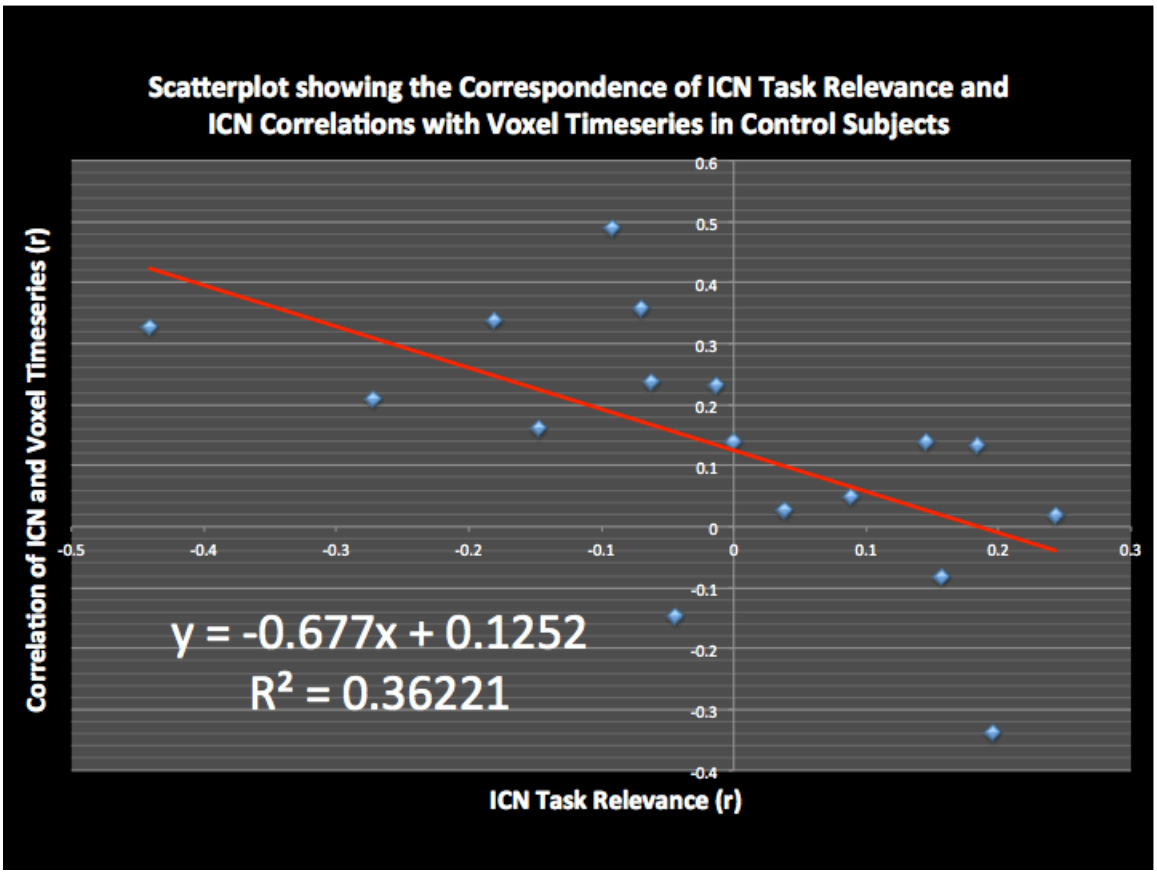


Note. The ICN task-relevance scores (Figure 3) and the connectivity-activity correlation scores (Figure 4) were plotted here in a scatterplot in order to visualize the correspondence between the network relationships to the task and raw activity. The ICN relationship to the task is on the x-axis and the ICN timeseries relationship to the voxel-derived BOLD activity is on the y-axis. A trendline has been added and the amount of variance explained ($R^2$) is included below.

**Figure 7.**

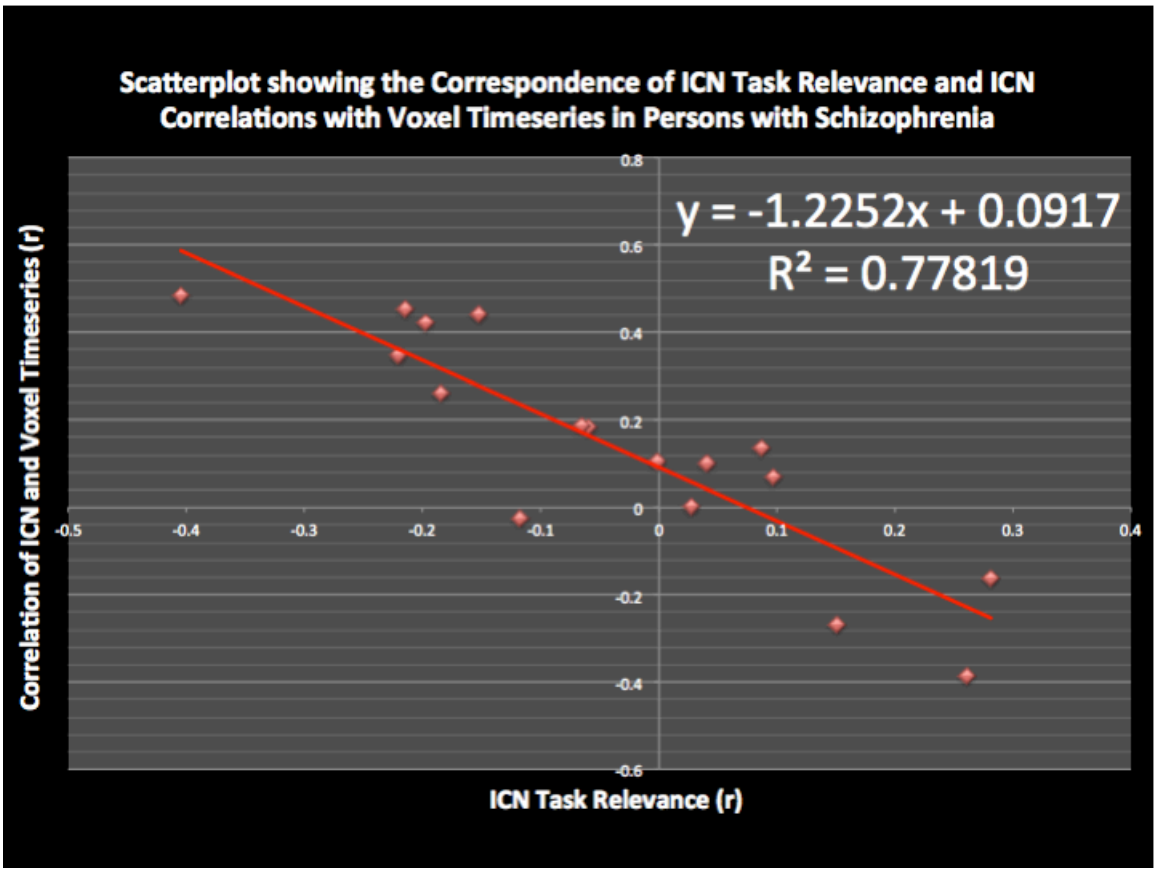


**Note.** The ICN task-relevance scores (Figure 3) and the connectivity-activity correlation scores (Figure 4) were plotted here in a scatterplot in order to visualize the correspondence between the network relationships to the task and raw activity. The ICN relationship to the task is on the x-axis and the ICN timeseries relationship to the voxel-derived BOLD activity is on the y-axis. A trendline has been added and the amount of variance explained ($R^2$) is included below.

**Figure 8.**

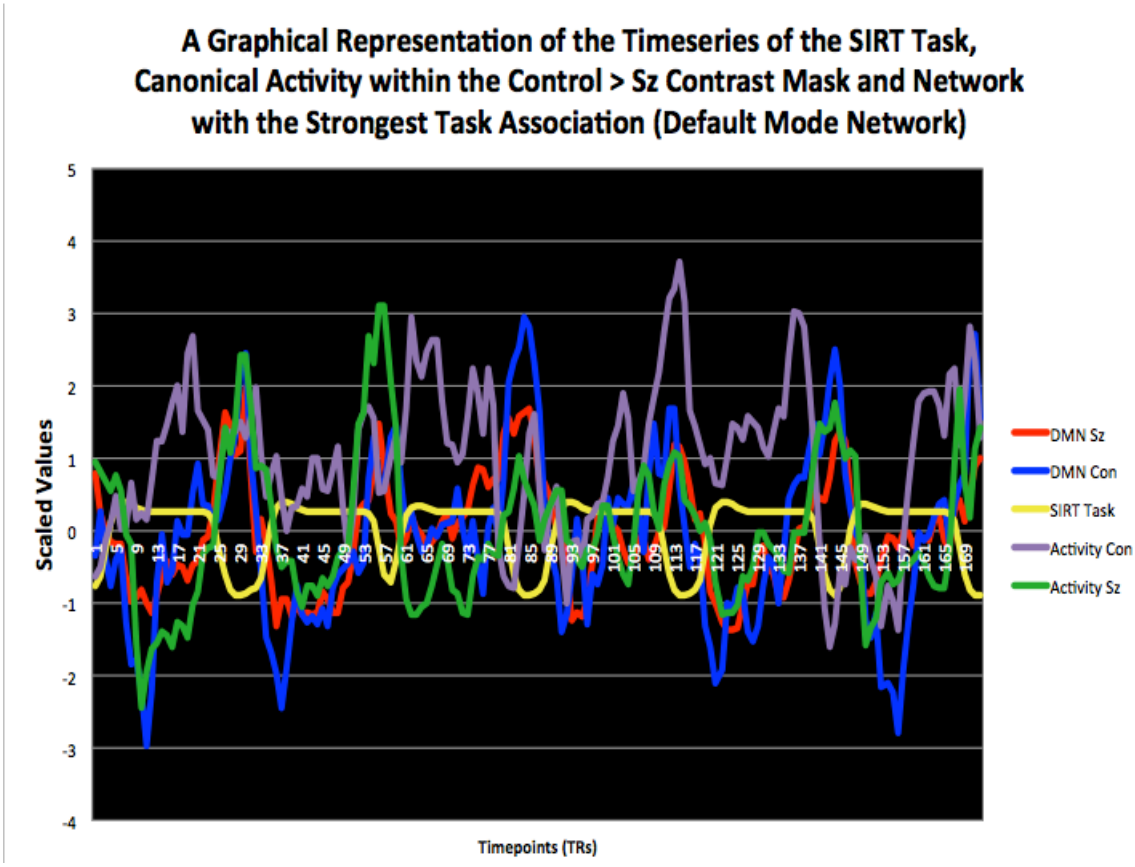


**Note.** This figure is meant to be a graphical representation of the various timeseries for qualitative comparison. The relationships between the timeseries in each domain has been preserved and they have been scaled and centered around the zero point on the y-axis. "DMN Sz" refers to the time course of the Default Mode Network for the schizophrenia group. "DMN Con" is the average timecourse of the DMN for controls. "SIRT Task" is the time course of the predictor for task engagement used in the GLM. "Activity Con" refers to the BOLD activity in the voxels contained within the Controls > Sz mask for the control group. "Activity Sz" is the BOLD activity within the Controls > Sz mask for the schizophrenia group.

**Figure 9.**

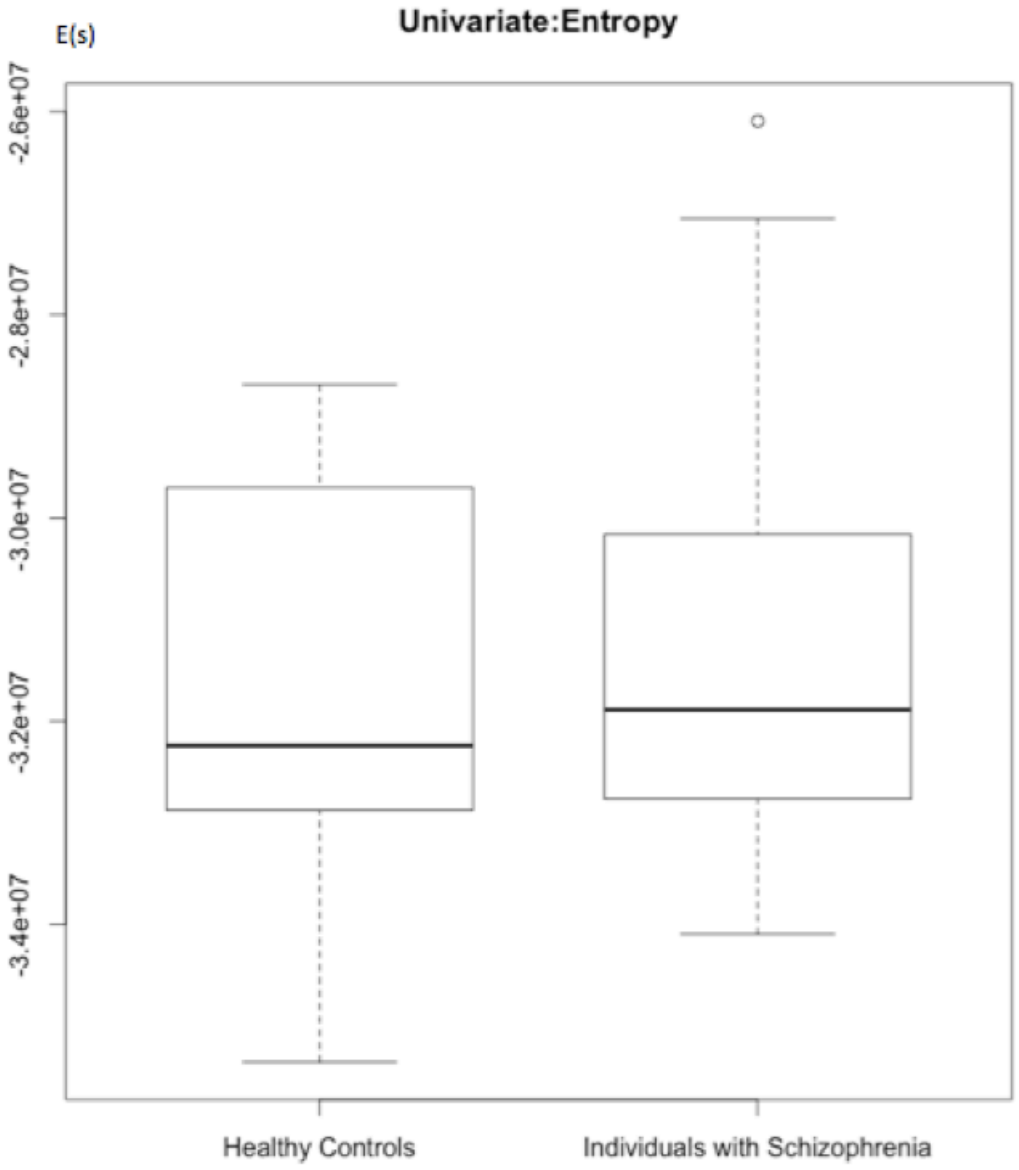


**Note.** Box plot showing group differences in the intrinsic connectivity networks' (ICN) timeseries entropy between the three groups. Entropy here is defined as the Shannon entropy (see methods).

**Figure 10.**

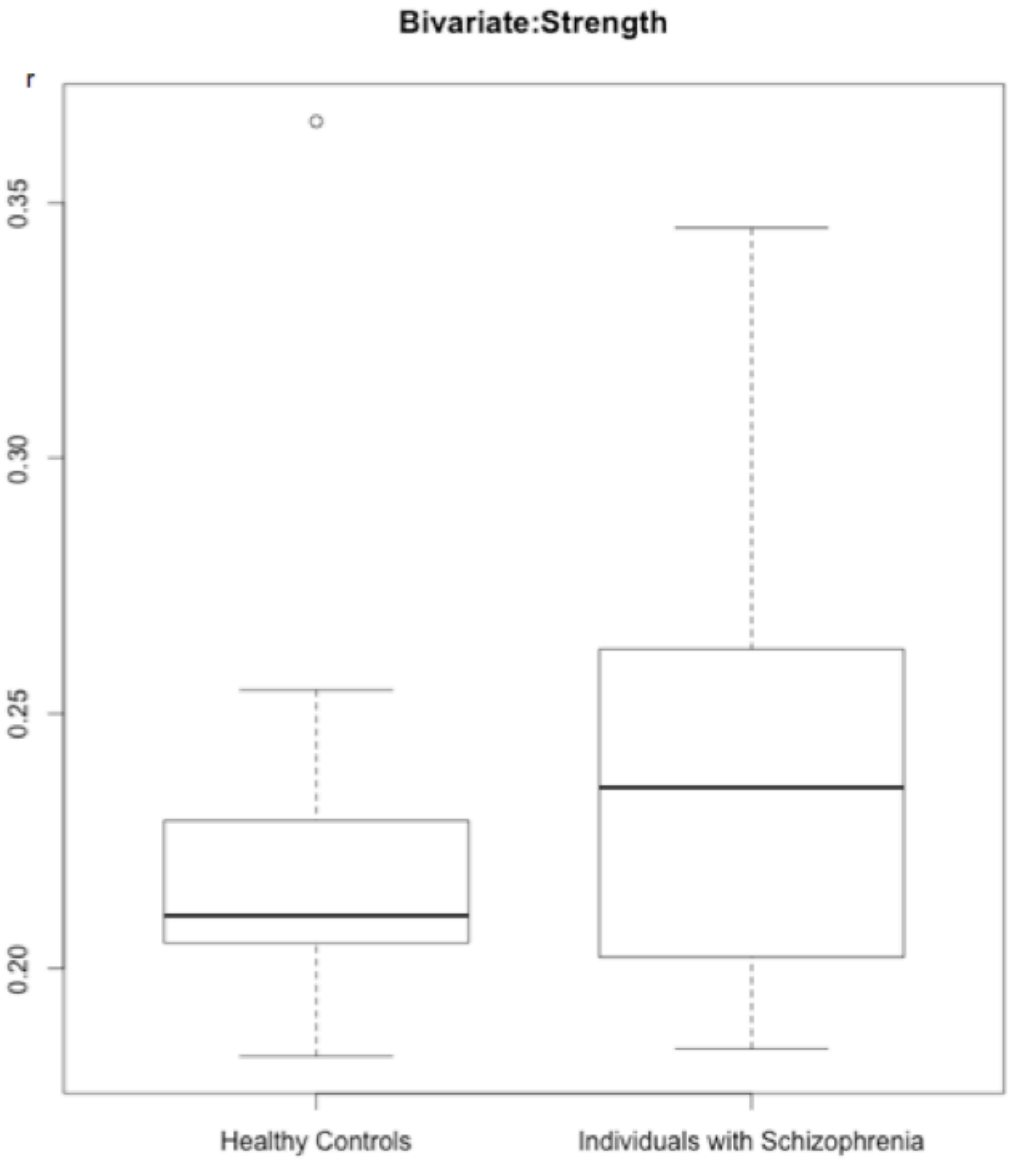


**Note.** Box plot showing group differences in connectivity strength between the three groups. Significance thresholds were established using one-tailed t-tests and corrected for multiple comparisons ($p < 0.017$).

**Figure 11.**

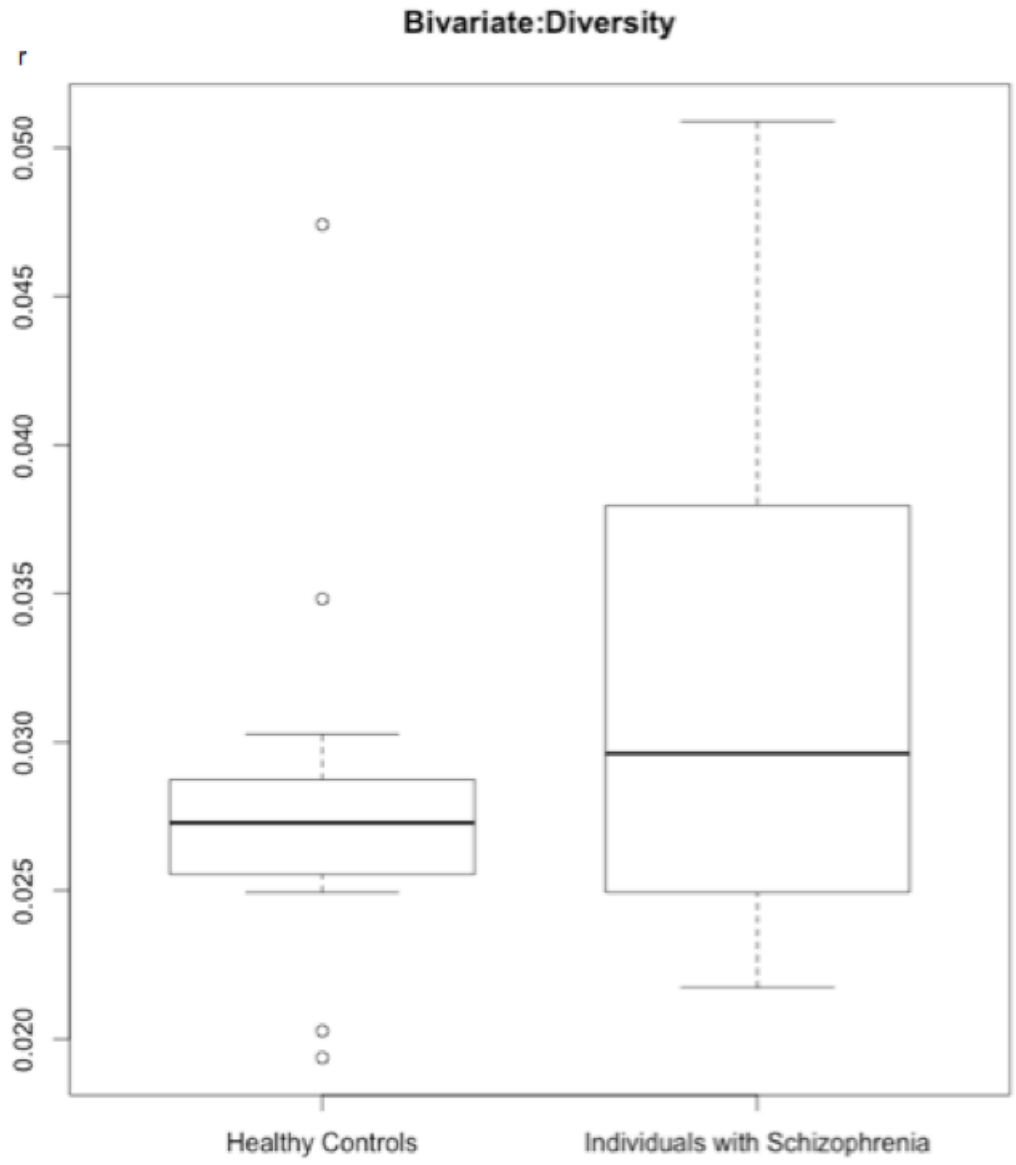


**Note.** Box plot showing group differences in connectivity diversity between the three groups. Significance thresholds were established using one-tailed t-tests and corrected for multiple comparisons ($p < 0.017$).

**Figure 12.**

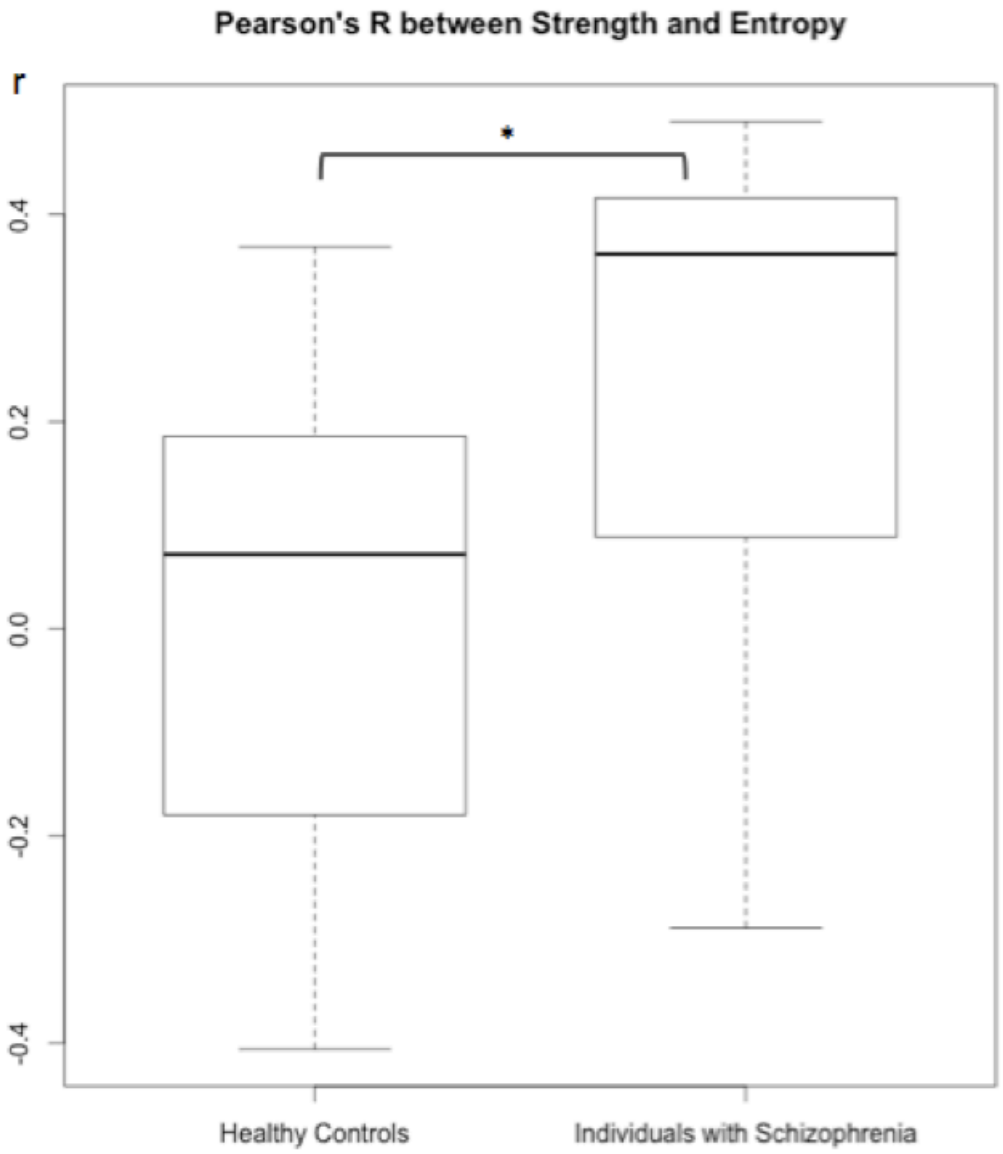


**Note.** After generating the canonical components in the ICA, the resulting set of Intrinsic Connectivity Networks (ICNs) was back-transformed into participant-level space. The participant-level ICN timecourses were then used in graph theory analyses in a novel technique analogous to using pre-defined regions of interest (ROIs) such as those in the AAL or Freesufer atlases. In this case, the ICN themselves are the nodes, which is advantageous since they are derived from the data, instead of arbitrarily pre-defined. The ICN timecourses were all correlated with each other within the set of ICNs for each participant. The ICN signal entropy was calculated, as well as the connectivity strength and diversity. In this figure, the Pearson correlation between signal entropy and the strength of interconnectivity is plotted for both groups.

**Figure 13.**

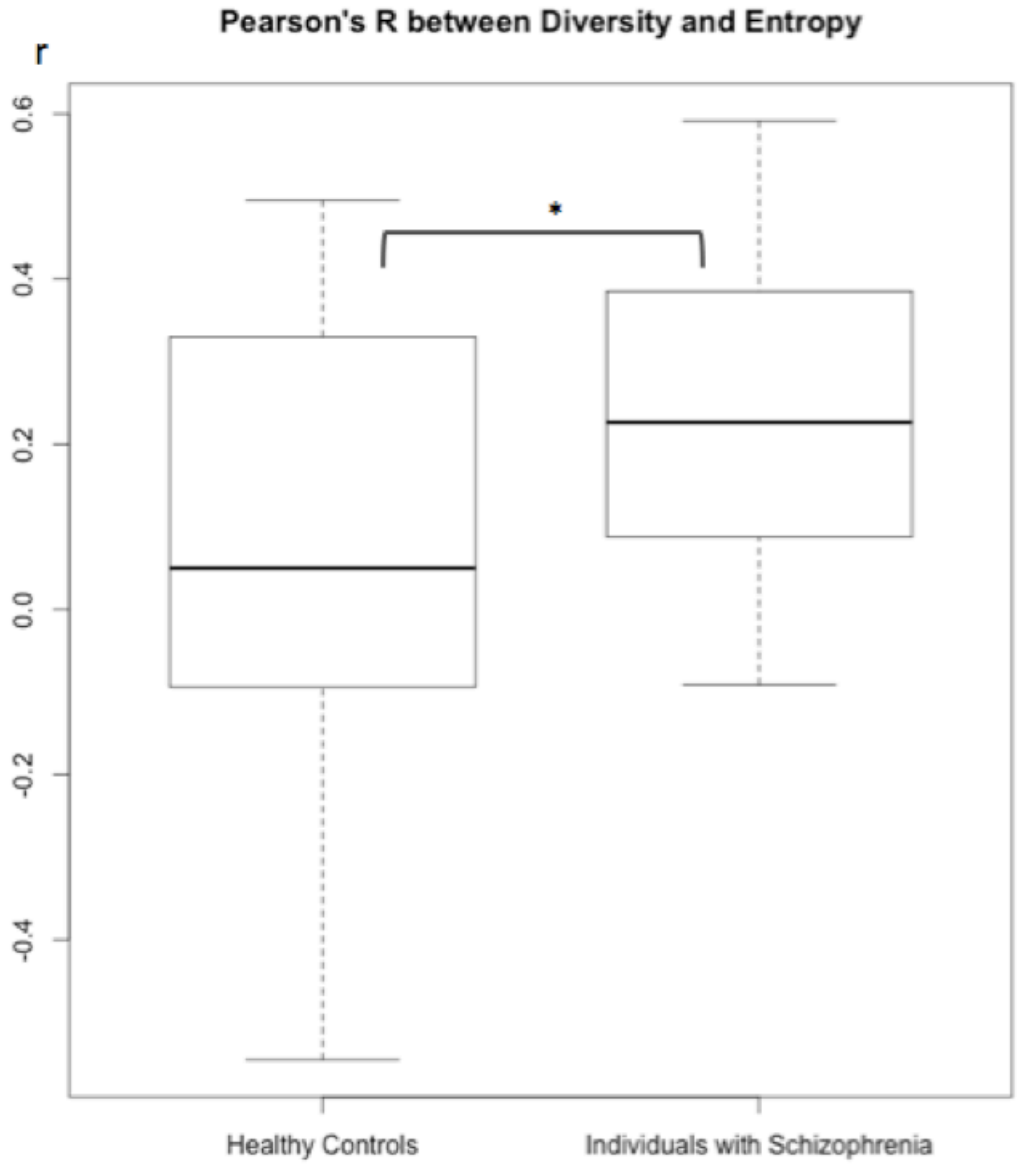


**Note.** In this figure the ICN timecourses were also used to make a correlation matrix from which the diversity of connectivity was calculated. As in Figure 8., the entropy is defined as the Shannon entropy and the entropy signal is the ICN timecourses themselves. Here the correlation between signal entropy and connectivity diversity is plotted for both groups. Metrics for entropy, strength and diversity were calculated and plotted individually as well, but in this analysis, those metrics did not yield significant results. This could be due to the relatively small sample included in this analysis, but this could also be due to the fact that this study employs a task design, whereas previous studies that have used these metrics tend to use resting state scans.

# Chapter Five

Common Connectivity Phenotypes in Rapid Eye Movement Sleep Behavior Disorder and Parkinson's Disease: The Search for an Intermediate Phenotype

Summary

Rapid eye movement sleep behavior disorder (RBD) is a prodromal syndrome of Parkinson's disease and an early manifestation of the underlying alpha-synuclein neuropathology. This implies that there should be functional signatures shared between the two clinical states that are detectable in vivo that also aid in the classification of disease state. To assess common in-vivo phenotypes, resting state data was collected on a 3T clinical MRI platform and a novel functional connectivity magnetic resonance imaging (fcMRI) approach, which combined independent component analysis (ICA) and graph theory, was used to evaluate deficits in interconnectivity among 15 PD, 14 RBD and 13 control participants.

Whole brain and network-level analyses revealed the largest deficits in network connectivity in PD compared with controls, with less severe group differences between RBD and controls. Importantly, the network-level analysis demonstrated a nested decrease in network interconnectivity, with the greatest number of aberrant networks detected in the PD group, and a subset in the RBD group. In addition, a disease classification algorithm was able to predict PD cases by being trained on RBD cases with 0.87 sensitivity and 0.68 specificity. The functional alterations in cortical networks in RBD suggest that pathophysiological changes already extend beyond the brainstem. Additionally, these findings demonstrate progressive reductions in connectivity between brain networks, with less severe deficits in RBD than PD. Moreover, the phenotypes observed in RBD can be used to predict PD status in a cross-sectional sample, which suggests that RBD is likely a pre-clinical intermediate phenotype.

## Introduction

Parkinson's disease (PD) is a neurodegenerative disorder characterized by progressive deposition of abnormal alpha-synuclein aggregates (i.e., synucleinopathy) and affects 1% of the population over the age of 60 years (Samii, Nutt, & Ransom, 2004). Several lines of evidence suggest that PD initially affects structures that relate to non-motor features such as the olfactory bulb: hyposmia, enteric plexus: constipation, and pons: rapid eye movement behavioral disorder (RBD). Subsequently, the substantia nigra is affected which leads to the classic motor features, followed by cortical pathology resulting in cognitive decline (Borek, Amick, & Friedman, 2006; Braak, Ghebremedhin, Rub, Bratzke, & Del Tredici, 2004; Luk et al., 2013). RBD, a disorder of dream enactment, is often the heralding clinical feature of PD. Under non-pathological conditions, REM sleep is characterized by active mentation combined with skeletal muscle paralysis. In RBD, REM atonia is lost and patients will act out their dreams, often violently with thrashing, punching, and kicking. Previous studies have demonstrated that approximately 50% of individuals with RBD convert to PD or another synucleinopathy within a decade of diagnosis (Iranzo, Santamaria, & Tolosa, 2009; Postuma, Aarsland, et al., 2012; Schenck, Boeve, & Mahowald, 2013). Further, RBD combined with other non-motor features, such as anosmia and/or constipation, increase the risk of early conversion (Bezard & Fernagut, 2014).

Structural magnetic resonance techniques such as diffusion tensor imaging (DTI) have identified abnormalities in PD (Cho et al., 2010; Vaillancourt et al., 2009) as well as in RBD (Hanyu et al., 2012; Unger et al., 2010). While, resting state functional MRI has also demonstrated functional connectivity abnormalities in PD, for instance in the default

mode network (van Eimeren, Monchi, Ballanger, & Strafella, 2009), fcMRI techniques are just now being applied to RBD (Ellmore et al., 2013) and have not been applied to comparisons of the two disorders. Dopamine-dependent differences in functional connectivity between the basal ganglia and cortex have also been found in PD (Williams et al., 2002; Yu, Liu, Wang, Chen, & Liu, 2013), and similar differences have also been reported for associations between several other brain regions, particularly cortical regions related to motor functioning (Sharman et al., 2012; Wu et al., 2011). It has been shown that these imaging phenotypes can predate the onset of impairments such as recognition memory deficits and, hence, imaging methods are being developed for in vivo classification of PD (Ibarretxe-bilbao et al., 2011; Long et al., 2012; Morales et al., 2012; Prodoehl et al., 2013).

As RBD is a prodromal syndrome of PD, we sought to evaluate alterations in connectivity among participants with RBD compared to PD as well as controls. Additionally, we sought to utilize ICA and graph theory as the means of capturing the functional networks and assessing their interconnectivity. ICA has been utilized as a powerful data-driven tool for deriving intrinsic connectivity networks (ICNs) from functional data, and graph theory has been recently been used to describe the complex interactions between brain regions (Stephen M Smith, 2012). Hence, the combination of these methodologies allows for the examination of the morphology and connectivity of the ICNs underlying the common phenotypes in PD and RBD, and could help establish RBD as an intermediate phenotype of PD. Finally, we were interested if whether the connectivity profile present in RBD could be used as an in vivo clinical classifier of

disease state, as this provides an potential means for developing a tool for the early identification of PD in pre-motor or presymptomatic individuals.

## Methods and Materials

### *Participants*

Fifteen individuals with PD, 14 individuals with idiopathic RBD and 13 controls (16 females, 26 males, mean age 60.0 ± 11.5) were included in this analysis from a larger sample recruited for a $^{123}$I-Ioflupane (DaTSCAN) study to evaluate individuals with PD and those at risk for developing PD. The Institutional Review Board of the University of Minnesota approved all protocols and all participants gave informed consent before participating in the study. All participant information was de-identified at the beginning of the study and all participants were pre-screened using exclusionary criteria for both PD and idiopathic RBD.

All participants were initially assessed using the Unified PD Rating Scale (UPDRS)-based criteria (Poewe, Rascol, Sampaio, Stebbins, & Goetz, 2003). In addition, the enrolled PD patients all met the research diagnostic criteria established by the Queen Square Brain Bank (Brooks, 2012; Massano & Bhatia, 2012). All PD patients were medicated at the time of the study and did not have notable sleep disturbances. All RBD patients were diagnosed with a clinical history of dream enactment along with an in laboratory polysomnogram confirming REM sleep without atonia (AASM, 2001). RBD patients were excluded if the onset of dream enactment coincided with use of serotonergic antidepressant medication. Additionally, participants were excluded if they presented with a clinically significant acute or unstable physical or psychological disease

on screening or in their history. In addition, exposure to investigational or radiological drugs within the 4 weeks prior to the scan was included as another exclusionary criteria. Control subjects who were enrolled did not have a first degree relative with PD and were without a significant central nervous system neurological condition.

***MR Acquisition and Imaging Parameters***

A resting-state functional scan, a field map and a high resolution T1 weighted anatomical images were acquired on a 3T Siemens TIM Trio MRI scanner using the system standard 12-channel receive-only head coil. For the resting state BOLD fMRI acquisition (EPI; TR=2000ms, TE=30ms, voxel size=3.4x3.4x4mm, matrix size=64x64, 34 AC-PC aligned single oblique axial slices with interleaved slice acquisition, 260 volumes, 9 min) the participants were instructed to close their eyes, remain awake, and not think about anything in particular. A field map acquisition (TR=300ms, TE=1.94/4.40ms, voxel and orientation matching fMRI scan, 1 min) was acquired just after the resting state scan. A structural T1-weighted image (MPRAGE, TR=2530ms, TE=3.65ms, TI=1100ms, flip angle=7 degrees, voxel size=1x1x1mm, 11 min) was collected and used for the anatomical registration of the functional scans.

***Image Data Preprocessing***

All data were preprocessed and analyzed with the FMRIB FSL 4.1.9 software (http://www.fmrib.ox.ac.uk/fsl). Preprocessing included the exclusion of the first 3 volumes to allow for magnetization stabilization, motion correction with the MCFLIRT linear registration algorithm (Jenkinson et al., 2002), B0 unwarping, interleaved slice-timing correction, brain extraction using the BET algorithm, spatial smoothing with a 5-

mm full-width half-maximum Gaussian kernel, and high-pass temporal filtering. The images were registered to high-resolution T1 anatomical images and the MNI 2mm brain image using FLIRT.

### *FMRI Image Data Analysis*

#### *Intrinsic Connectivity Network (ICN) Generation*

Data-driven ICA components were derived from the EPI functional scans using the using FSL's temporal concatenation independent component analysis (TICA) software in the MELODIC ICA toolkit (Beckmann & Smith, 2004). This probabilistic TICA algorithm was used to generate global spatial maps and timeseries from the full matrix of voxel signals from scans from all participants. The MELODIC algorithm was constrained to thirty (30) components, which allowed for the standardization of the total number of components generated at the group and participant levels. The resulting components were subjected to a permutation procedure, which diminished any initial random value and participant-order effects (K. Wisner et al., 2013).

The global ICA-derived components were then visually inspected and components that did not include neuronal signal, such as component with voxels outside the brain in the ventricles, were removed (Beckmann, 2012). The remaining components were identified as ICNs and were included in subsequent analyses. These global ICNs were then used as templates for back-transformation of individual-level spatial maps and timeseries with FSL's dual spatio-temporal regression software.

#### *Signal Entropy, Connectivity Strength and Diversity*

The individual-level, back-transformed ICN timeseries were used as the basis of the analysis of ICN time course entropy as well as all subsequent analyses. Univariate entropy here is defined as the Shannon entropy (Shannon, 1948) and is measured for each signal, i.e. within each ICN and then averaged across ICNs and participants within each group. For the bivariate metrics, the mean score for the $i^{th}$ column of the connectivity matrix represents how well each node (ICN) is connected to all other nodes in the graph and, hence, the strength of the graph in this analysis is defined as the average strength across all ICNs. Similarly, the variance of the $i^{th}$ column of the connectivity matrix represents the variability in the strength of connectivity for each ICN and, hence, the diversity is the average variability within group (Lynall et al., 2010).

*Interconnectivity Analyses*

To examine how well each individual network is connected with all other networks, we computed a *individual-level cross-correlation*. The individual-level ICN timeseries underwent an exhaustive cross-correlation procedure in which each ICN was correlated with every other ICN in order to produce correlation matrices. The cross-correlation scores were averaged across all participants per ICN within each group and a statistical threshold based on the z-transformed overall ICN correlation values and sample size was used to determine which of the ICNs exhibited significant interconnectivity.

To determine mean interconnectivity differences across groups, ICN timeseries were concatenated across participants within each group in order to generate a group vector. In this *group-level cross-correlation* metric, these concatenated timeseries vectors

were then all correlated with each other within group and these scores were contrasted using a t-test. All group comparisons were done using a one-tailed alpha ($p < 0.05$), which was then corrected for the comparison of the three groups using a Bonferroni correction that yielded an adjusted "multivariate significance" alpha ($p < 0.017$).

*Random Forests Prediction of Disease State*

A random forest machine learning algorithm was employed to determine the accuracy of classification of group status between control, RBD and PD and, hence, disease severity. The forests were populated by decision trees which were trained to distinguish persons with RBD from controls using their scores for connectivity strength and diversity. This forest was then used to predict PD status based on the classes from the training data. Hence, the algorithm returned vectors of assignments for both the PD and control connectivity profiles, in which control was "0" and PD was "1". After group status was predicted using the classification algorithm, the two vector of predicted and real scores were correlated. In addition sensitivity and specificity were calculated using the following formulas:

Sensitivity = true positives / true positives + false negatives

Specificity = true positives / true positives + false positives

In order to provide an unbiased classification, the matrix of scores for controls was split into two test and train subgroups for the purposes of training and testing the

classification algorithm. However, since the control subgroups were smaller than the training (RBD) and testing (PD), these subgroups were intermixed with another group of age matched controls, on which data had also been collected at the University of Minnesota. Hence, there were 10 subjects in the control training group, 14 subjects in the RBD training group, 10 subjects in the control testing group and 15 subjects in the PD testing group. There were no significant differences between the separate groups of controls in either demographics or connectivity scores.

### *3D Brain Figure Generation*

All brain images were generated using Mango (the Multi-image Analysis GUI) viewer from the Research Imaging Institute of University of Texas Health Science Center (http://ric.uthscsa.edu/mango/index.html). All ICN overlays from the global ICA output were rendered on a 3D surface build off the MNI 152 T1 1-mm brain template. This 3D rendering was then made translucent to reveal the subsurface structures contained in each ICN. This was particularly important for sub-cortical structures such as the basal ganglia network or subgenual OFC & ACC network.

## Results

The UPDRS scores for the three groups were as follows: PD = 24.20 ± 9.24, RBD = 8.53 ± 5.82, control = 2.92 ± 2.53. The multi-group ICA, which was performed with data from all three groups, produced 22 common non-artifactual ICNs (Fig. 1). Of these 22 ICNs, 7 contained areas related to motor functioning, including the midbrain, cerebellum, primary motor cortex (M1) and corresponding somatosensory areas, pre-

motor and supplementary regions, as well as the posterior parietal cortex. After all global maps were generated, these networks were also back-transformed into individual-level space in order to capture possible disease-relevant variance, which would be reflected as patient and control group differences.

In the univariate whole brain analysis, no significant differences were found in the entropy of the ICN timeseries when comparing the control and PD groups ($t = 1.09$, $df = 25.78$, $p = 0.14$, $d= 0.41$), the control and RBD groups ($t = 0.45$, $df = 15.59$, $p = 0.67$, $d = 0.17$), or RBD and PD groups ($t = 0.94$, $df = 16.65$, $p = 0.18$, $d = 0.36$) (Fig. 2). In the bivariate analyses, a significant difference was observed in connectivity strength between the control and PD groups ($t = 3.23$, $df = 22.73$, $p = 0.002$, $d = 1.24$), the difference between the control and RBD groups ($t = 2.05$, $df = 21.059$, $p = 0.027$, $d = 0.80$) was near significance after Bonferroni correction, and a weaker trend level difference was observed between the RBD and PD groups ($t = 1.57$, $df = 26.88$, $p = 0.06$, $d = 0.58$) (Fig. 3). For the diversity of connectivity, a significant difference was again found between the control and PD group ($t = 3.42$, $df = 25.49$, $p = 0.001$, $d = 1.29$). However, the comparisons of the control and RBD groups ($t = 1.91$, $df = 23.73$, $p = 0.03$, $d = 0.74$) and the RBD and PD groups ($t = 1.77$, $df = 26.77$, $p = 0.04$, $d = 0.65$) were only at trend level after Bonferroni correction (Fig. 4).

Given that previous relationships have been established between signal entropy and the strength and diversity of connectivity (Bassett, Nelson, Mueller, Camchong, & Lim, 2012), these relationships were assessed and it was observed that there were indeed group differences for the scores for the Pearson correlation between strength and entropy (Fig. 5) and the Pearson correlation between diversity and entropy (Fig. 6). Significant

group differences were observed for group comparisons between controls and PD ($t = 3.03$, $df = 25.2$, $p = 0.003$), controls and RBD ($t = 2.33$, $df = 20.5$, $p = 0.015$), but not PD vs RBD ($t = 0.12$, $df = 24.37$, $p = 0.45$) for the correlation between strength and entropy within group. For the t-tests of the scores from the Pearson's correlation of diversity and entropy per group, the comparison of the scores for the control and PD groups ($t = 3.1$, $df = 23.28$, $p = 0.002$) showed a significant group difference, but the scores of the control and RBD groups ($t = 1.65$, $df = 18.55$, $p = 0.06$) were not significantly different, neither were those for PD vs RBD groups ($t = 0.73$, $df = 24.44$, p-value = 0.24).

For the individual-level ICN cross-correlation, in the control group, 17 ICNs passed the threshold. For RBD, 14 ICNs passed threshold and were a subset of the 17 ICNs found in the controls. Similarly, for the PD group, only 10 ICNs passed threshold, which were again a subset of the 14 found in RBD group, and the larger set in controls (Figure 7).

For the group-level cross-correlation, the t-test of interconnectivity scores showed that the control group had higher mean interconnectivity scores than both the PD group ($t = 4.16$, $df = 390.87$, $p = 0.00002$) and RBD group ($t = 2.00$, $df = 489.98$, $p = 0.023$), but the comparison of the control and RBD groups only had marginal multivariate significance ($p < .017$). In addition, it was observed that the RBD group had a higher group-level cross-correlation score when compared to the PD group ($t = 2.80$, $df = 547.09$, $p = 0.003$), even after Bonferroni correction.

The random forest classifier that was trained on a subgroup of controls versus RBD patients was tested on how well it could distinguish a separate group of controls from PD patients. It returned a vector of group assignments for controls (0) versus

persons with Parkinson's disease (Figure 1). It was found that there was a correlation of r = 0.69 between the predicted and real scores and the Parkinson's classification algorithm had a sensitivity of 0.87 and a specificity of 0.68.

## Discussion

The combined ICA - graph theory analyses of the connectivity profiles of the PD, RBD and control groups is a novel analysis strategy that is unlike seed-based approaches or typical ICA or graph theory analyses, in that it combines the data-driven network depiction of ICA and the descriptive power of graph theory to examine both global and network-level phenomena. Using this methodology, several metrics showed that there were significant differences between the three groups. Moreover all the metrics revealed connectivity phenotypes in which the RBD group was intermediate between the PD and control groups, with a nested decrease in network interconnectivity going from controls to RBD to PD being the most striking finding.

In the univariate analysis of network entropy, there were no significant differences between the groups. However, this is not inconsistent with our previous findings of no significant differences in entropy related to disease state between persons with schizophrenia and controls (Bassett, Nelson, Mueller, Camchong, & Lim, 2011). Bivariate connectivity strength was strongest for controls, and less so for both the RBD and PD groups. Interestingly, while there was a significant connectivity strength difference between the control and PD groups, the differences between the control and PD group as well as PD and RBD groups were not significant after multiple comparison

correction. Of note, the RBD group strength was in between that of the control and PD groups, thus suggesting an intermediate phenotype. These findings are consistent with other investigations that have demonstrated numerous subclinical abnormalities in cognitive functioning in persons who have not yet manifested PD (Fantini, Postuma, Montplaisir, & Ferini-strambi, 2006; Postuma, Gagnon, & Montplaisir, 2012b; Postuma, Aarsland, et al., 2012).

For the bivariate analysis of diversity of connectivity, it was again found that diversity was highest for controls and lower for persons with both RBD and PD. Again there was a trend showing that RBD was intermediate between controls and PD, but the differences between the control and RBD as well as RBD and PD groups showed a strong trend, but did not reach significance after multiple comparison correction. In our previous analysis of connectivity diversity between controls and persons with schizophrenia, it was found that the schizophrenia group had significantly higher diversity than controls (Bassett et al., 2011), which contrasts with our findings in PD. This suggests that the diversity of connectivity is sensitive to different types of disease-related aberrations and, in schizophrenia, neuronal disorganization results in cognitive and behavioral deficits, as well as aberrant sensory and limbic processing, which is also reflected in an increase in connectivity diversity. In the case of PD, it is known that synuclein pathology often extends throughout the brain, which is then reflected in a decrease in connectivity diversity. In addition, the decrease in diversity demonstrated in RBD cases as compared to controls is consistent with the progressive deposition of alpha-synuclein pathology in brainstem and cortical regions.

While there were no significant group differences for signal entropy, the correlations between connectivity strength and signal entropy showed significant differences when comparing the control group to both the PD and RBD groups. Similarly, there was a significant difference between the control and PD groups for the correlation of entropy and diversity and this inverse association was again strongest for controls and weakest for the PD cases. This means that higher connectivity strength and diversity leads to lower signal entropy in a non-pathological state and this relationship is diminished with increasing pathology. Based upon this trend and our other connectivity findings we would suggest that the lack of significant group differences in entropy is simply due to a lack of power.

In the interconnectivity analysis, it was observed that, of all the 22 functional networks, 17 ICNs exhibited significant interconnectivity in the control group. Of these 17 networks, a subset of 14 exhibited significant interconnectivity for the RBD group, and an even smaller subset of 10 for the PD group. Hence, there was a nested decrease in interconnectivity between the PD, RBD and control groups, respectively. This observation was corroborated by the analysis of the canonical ICN timeseries per group, in which it was found that the mean interconnectivity was highest for the control group, significantly lower for the RBD group and, significantly lower still for the PD group. This group nesting implies that there is a common set of ICNs that generally have high interregional connectivity in healthy controls, but that some of these ICNs have decreased connectivity when individuals present with RBD, and that these same ICNs have deficient interconnectivity in the case of PD, in combination with an additional set of

ICNs. Hence, this suggests that there is a common network-level deficit in both RBD and PD cases, but that this deficit is more severe for PD.

To test this assertion, a random forests classifier was trained on a sample of RBD cases and controls and tested on its ability to identify PD cases. The high level of sensitivity and specificity that was obtained by this machine learning algorithm supports our findings that there is a sub-clinical state that is detectable in RBD and that is also informative of PD. While the accuracy was not perfect, we believe that as more information is gained about the in vivo states of both PD and it's pre-clinical syndromes such as RBD, we will have greater predictive power to use phenotypes from the pre-clinical states to predict the onset of PD. However, the ultimate test will be to predict disease onset in pre-clinical patients in a longitudinal design in order to see how well these in vivo phenotypes can inform early detection models.

In conclusion, these findings demonstrate that there is a nested decrease in interconnectivity across RBD and PD, with increasing network dysfunction evident in a more advanced disease state (Ibarretxe-bilbao et al., 2011). Furthermore, we used these fcMRI metrics to detect increasing dysfunction in brain networks, as we used machine learning of the RBD connectivity profile to classify the PD connectivity profile. This finding is supported by a study in which regional fluctuation and synchronization differences between PD and controls allowed for blind separation of the two groups with good accuracy, specificity and sensitivity (Long et al., 2012). Hence, the interconnectivity phenotypes can serve as a possible biophysiological marker of disease progression even prior to the onset of relevant clinical symptoms, which make these metrics potentially useful in clinical trials.

Figures

**Figure 1.**

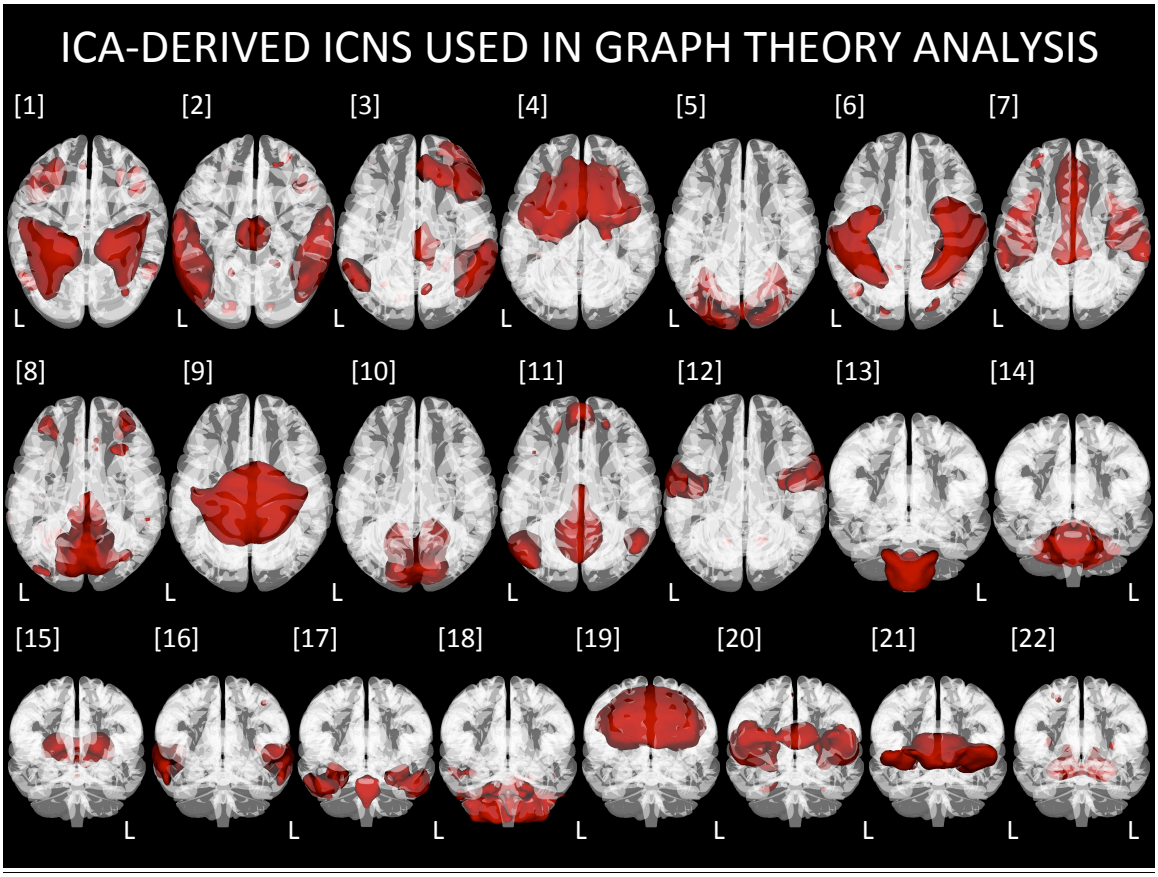


**Note.** 3D overlays of spatial maps from intrinsic connectivity networks (ICNs) generated from the independent component analysis of fMRI data from the Parkinson's disease (PD), rapid eye movement sleep behavior disorder (RBD) and control groups. Global spatial maps were derived and thresholded (z = 6) and rendered in either axial or coronal orientations.

**Figure 2.**

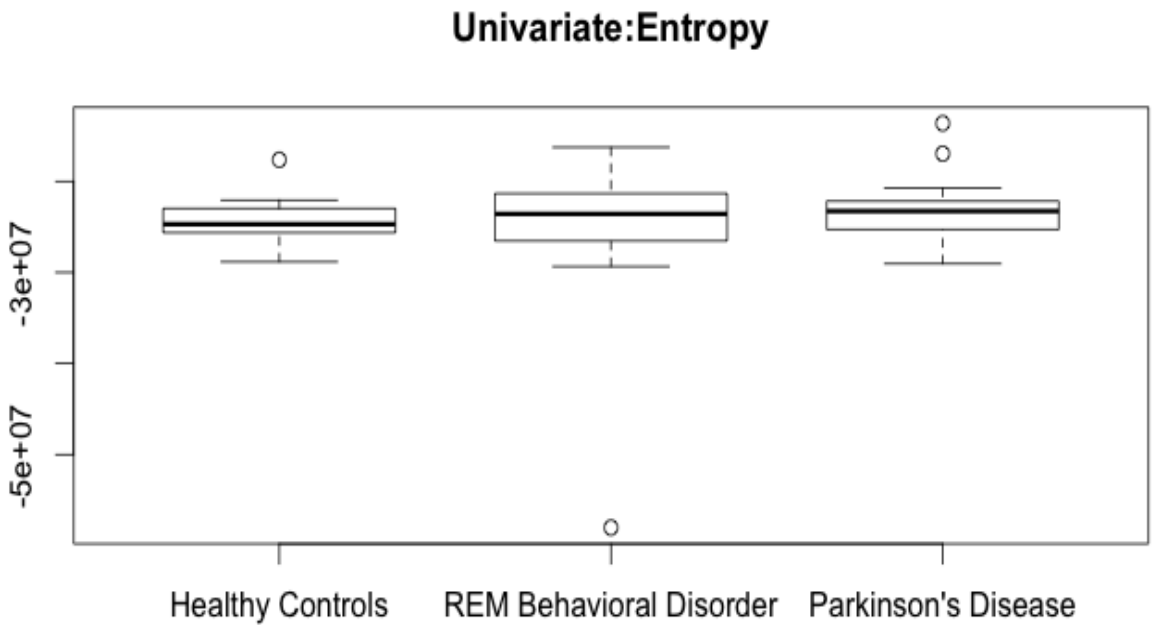


**Note.** Box plot showing group differences in the intrinsic connectivity networks' (ICN) timeseries entropy between the three groups. Entropy here is defined as the Shannon entropy (see methods).

**Figure 3.**

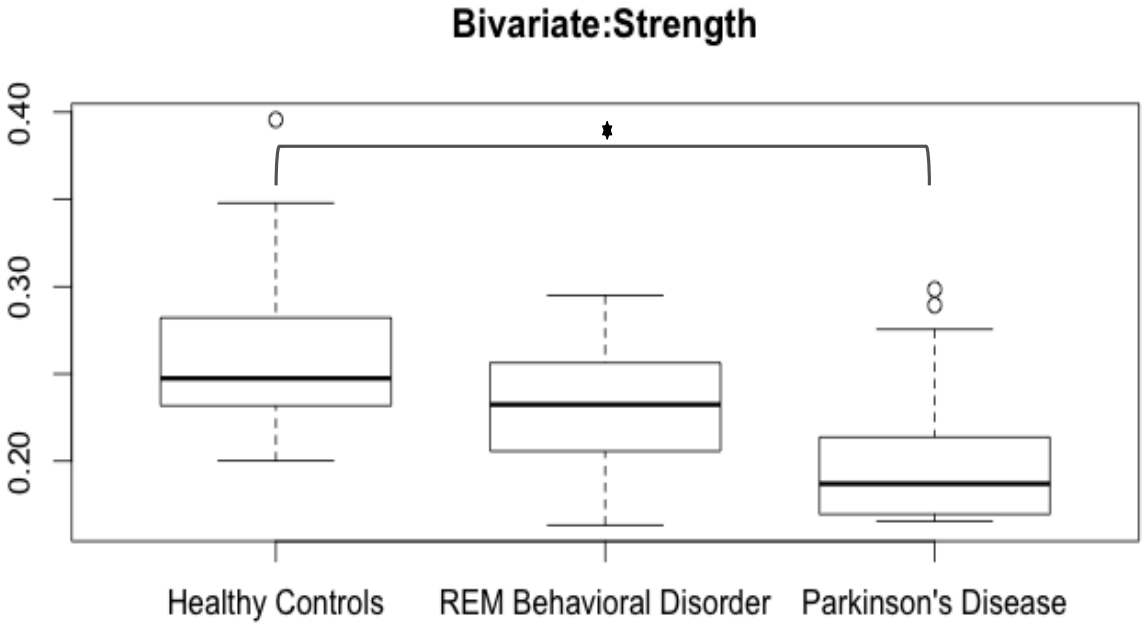


**Note.** Box plot showing group differences in connectivity strength between the three groups. Significance thresholds were established using one-tailed t-tests and corrected for multiple comparisons ($p < 0.017$).

**Figure 4.**

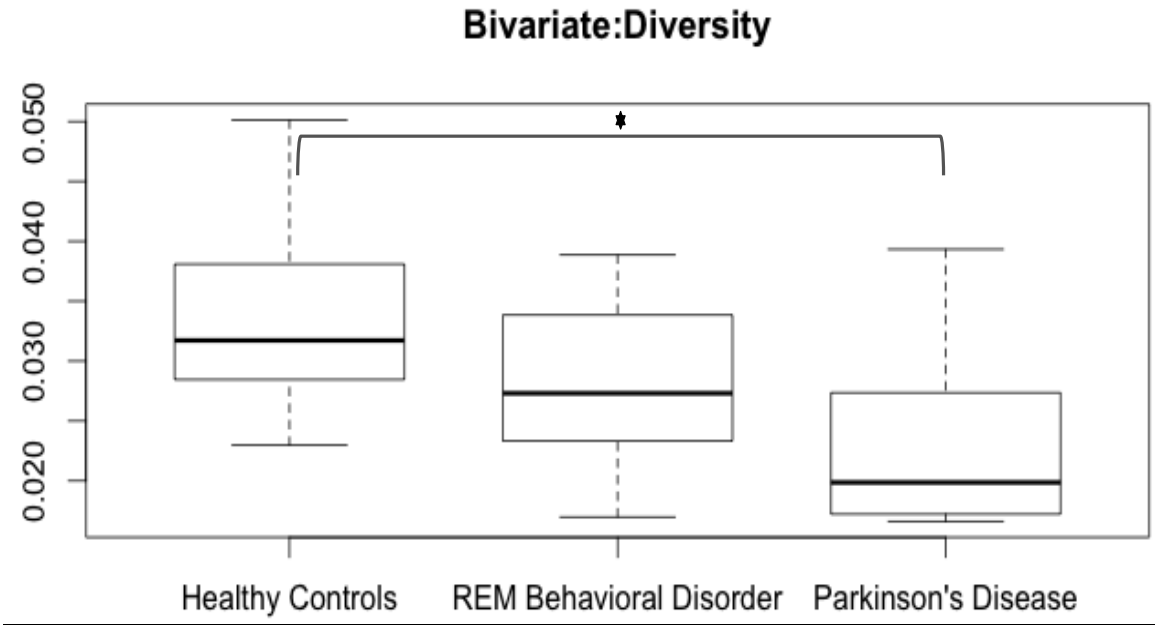


**Note.** Box plot showing group differences in connectivity diversity between the three groups. Significance thresholds were established using one-tailed t-tests and corrected for multiple comparisons ($p < 0.017$).

**Figure 5.**

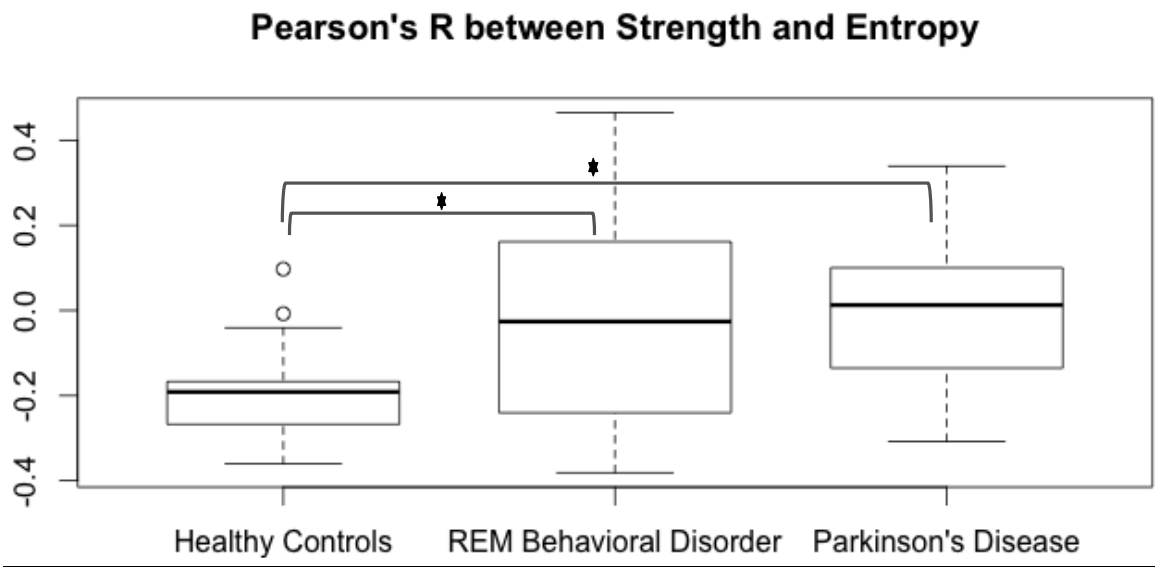


**Note.** Box plot showing group differences in the Pearson correlations of connectivity strength and intrinsic connectivity network (ICN) timeseries entropy between the three groups. Significance thresholds were established using one-tailed t-tests and corrected for multiple comparisons ($p < 0.017$).

**Figure 6.**

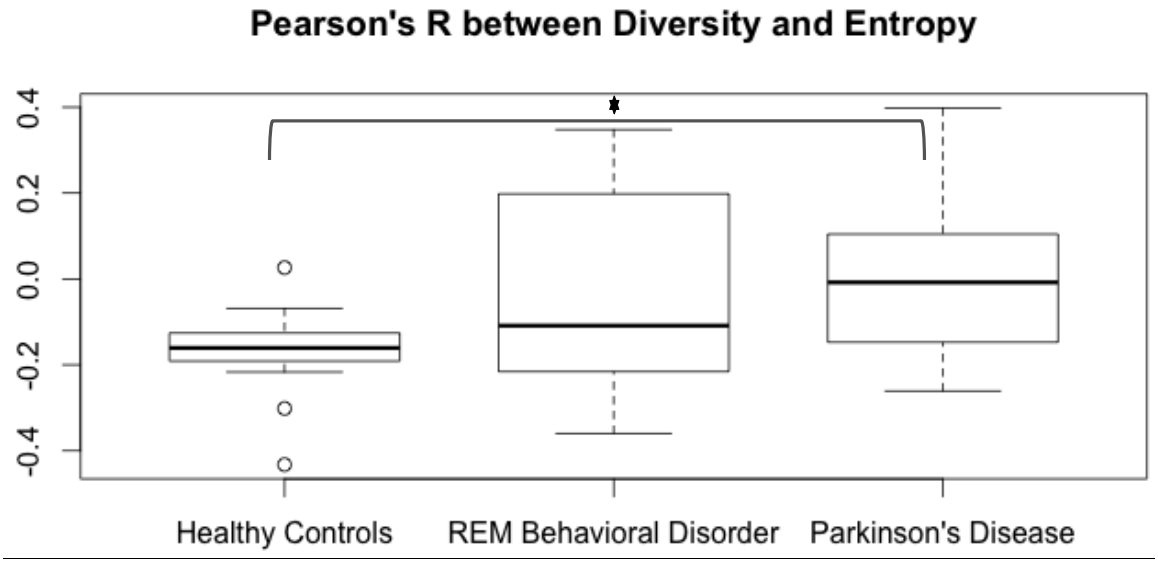


**Note.** Box plot showing group differences in the Pearson correlations of connectivity diversity and intrinsic connectivity network (ICN) timeseries entropy between the three groups. Significance thresholds were established using one-tailed t-tests and corrected for multiple comparisons ($p < 0.017$).

**Figure 7.**

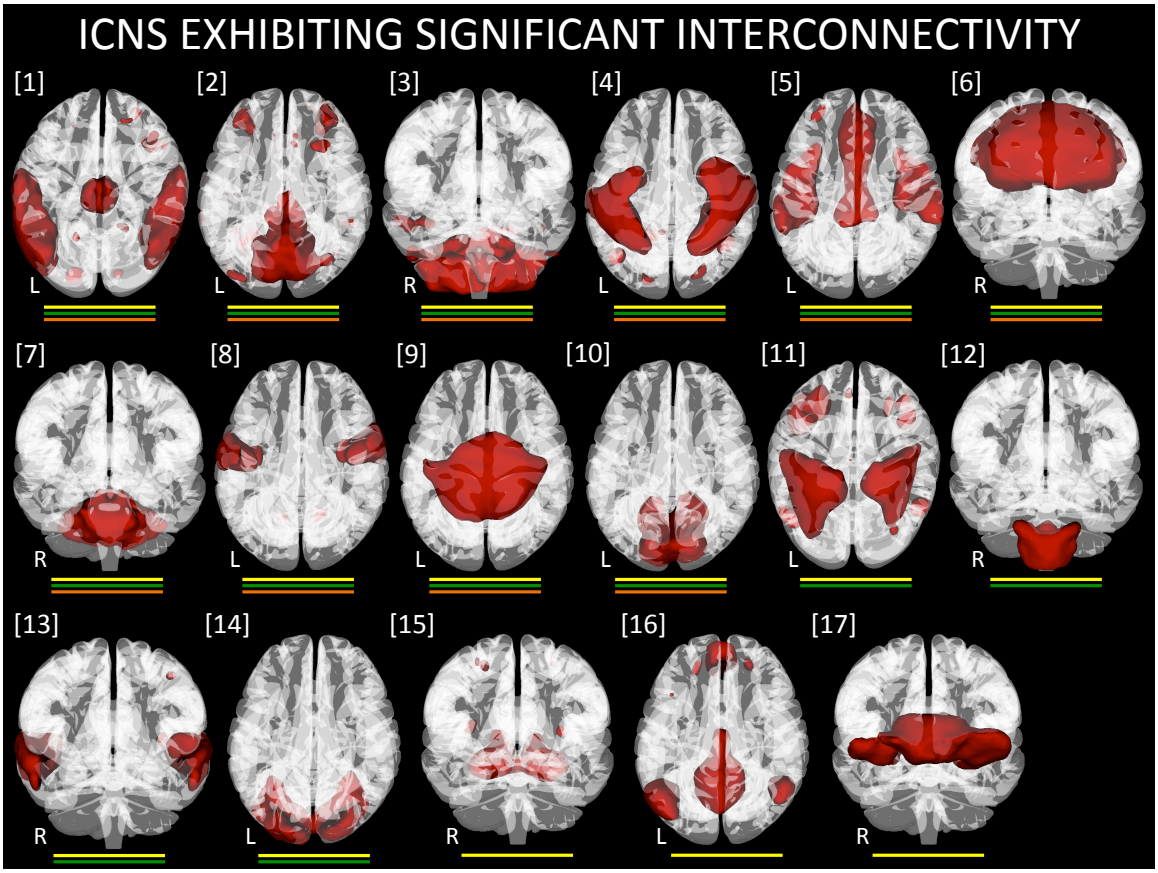


**Note.** 3D rendering of intrinsic connectivity networks (ICNs) exhibiting significant interconnectivity within the three groups. The set of 17 ICNs shown in the figure all showed significant interconnectivity in the control group, as depicted by the yellow bars. A subset, comprised of 14 of these ICNs, had significant interconnectivity in the RBD group and is labeled using the green bars. A smaller subset (10 ICNs) also exhibited significant interconnectivity in the PD group, as shown by the orange bars.

**Figure 8.**

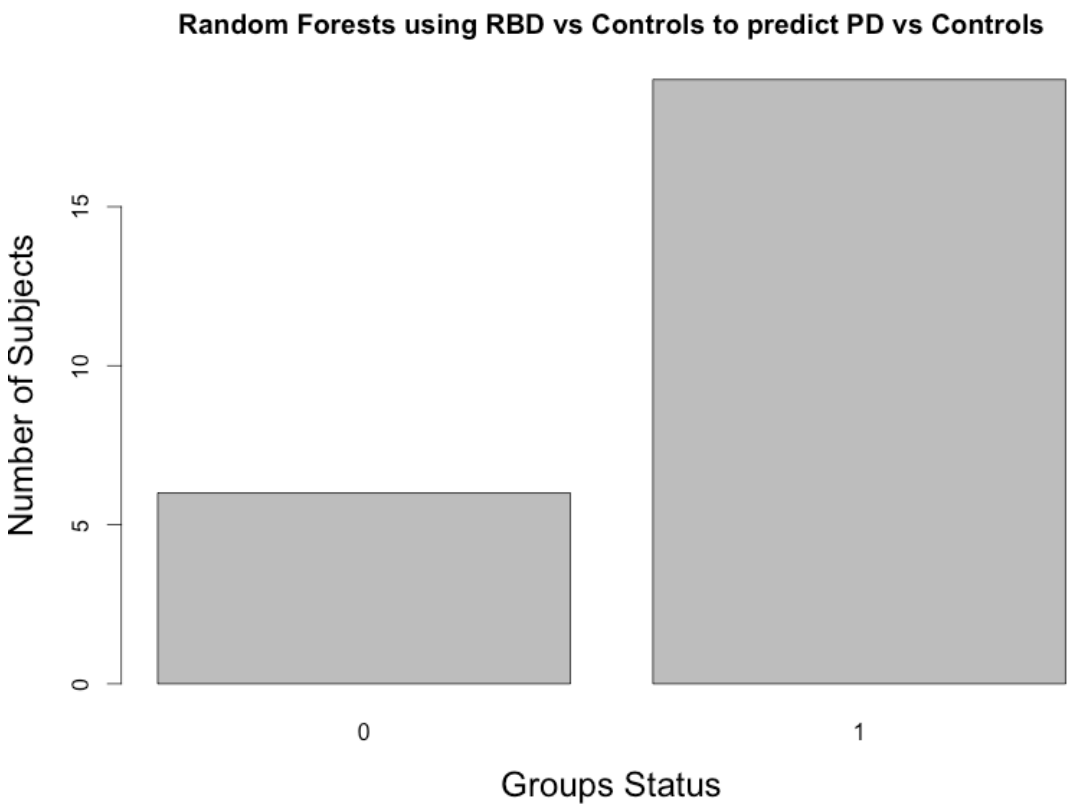


**Note.** Bar graph depiction of the results from a random forests prediction of Parkinson's disease cases based on connectivity phenotypes from RBD. Decision trees were trained to identify RBD and control cases using their respective connectivity strength and diversity profiles and then tested for their ability to distinguish a separate set of controls from PD patients. The number of predicted cases is plotted on the y-axis and the groups (control = "0", PD = "1") are on the x-axis.

# General Discussion

This research into the neurometric properties of the brain was conducted through the lens of multivariate analyses of functional activity and connectivity, and was undertaken with the objective of providing a novel, comprehensive picture of the involvement of brain networks in a variety of distinct brain states. This investigation of these intrinsic networks encompassed their characteristics at rest and as well as during cognitive engagement and ranged across states of normalcy and disease.

As a whole, this research addressed three main aims:

- First, by quantifying the consistency of the characteristics of intrinsic connectivity networks in individuals across distinct cognitive domains as well as between monozygotic twins, these analyses tested the hypothesis that there are *genetic factors* that influence brain development and functionality that confer a trait-like quality to these networks. For these networks to be *traits*, they had to be robust and stable within and across individuals over time and irrespective of circumstances. Furthermore, if these networks were trait-like for an individual, then the genetic contribution to these traits had to also manifest as familiality in twins.

- Second, it was hypothesized the dynamics of the networks should be differentially and specifically sensitive to changes in stimuli and cognitive demands depending

on their functional associations. Hence, determining the varying levels of task engagement of these networks in different task states enabled an understanding of their contributions to *cognitive states*. In addition, determining the extent to which brain networks were related to task events and task-driven activation in canonical activation paradigms tested the hypotheses that [1] the network dynamics revealed using independent component analyses of scans involving a task reflected ICN task engagement co-localized in regions overlapping with activity from general linear models; [2] the amount of covariance in the network fluctuations and the task timeline is both non-arbitrary and dependent on the physiological relevance of the network to the particular paradigm; and [3] that the manner in which tasks modulate these networks was familial.

- Third, the characteristics of networks, both during at task and at rest, provided information that was relevant to changes underlying disease states and, as a result, these network profiles also informed *endophenotypes*. The ICA-derived ICNs were examined in task states and in graph theory analyses in order to test the hypotheses that [1] that the interconnectivity of ICA-derived networks was sensitive to perturbations that arise in disease states such as schizophrenia and Parkinson's disease; [2] the degree of connectivity between these networks and network organization revealed physiologically relevant patterns; and [3] these patterns could be used to classify disease and, hence, network characteristics were useful for prediction models.

The analysis of the ICNs of twins that had performed functional localizers of hand imitation and verb generation was used to address the first aim of assessing network traits. The tasks themselves were very different and had previously been shown to evoke activity specifically in hand motor areas and language areas, respectively (Grafton and Hamilton, 2007; Iacoboni, 2005; Crivello et al., 1995; Edwards et al., 2010; Indefrey, 2011). However, the results showed that the morphology and coherence of two sets of networks derived from the functional data from the two paradigms showed a high degree of congruence. These results support the notion that there is a canonical set of networks present in the brain that is detectable irrespective of state (Deco et al., 2011; Laird et al., 2011; Smith, 2012). Additionally, the morphology and connectivity and timecourse dynamics of these ICNs were all stable over time within individuals, but the dynamics of the networks exhibited task-specific modulations that consequently drove down their congruence across tasks. This indicates that the networks are simultaneously trait-like and sensitive to transient environmental perturbation (Korgaonkar et al., 2014). This is a seminal finding, as it indicates that the ICNs are not state-dependent and unreliable, but instead are engaged in a manner that is stereotyped based on their relative contribution to cognitive functioning and relationships to the environmental stimuli. In fact, subsequent analyses not described in that study revealed that task presentation could be predicted by assessing the dynamics of task-relevant ICNs. This means that not only are ICNs trait-like, but these traits can also inform our assumptions about how the brain operates in various circumstances.

As aforementioned, if ICNs are phenotypic traits then their trait profiles should include some level of genetic contribution. Indeed, the morphology, coherence

(intranetwork connectivity) and dynamics all exhibited familiality in this monozygotic twin sample. The familiality of the ICNs was not identical across the three domains, which indicates that there are differential genetic contributions to each domain and/or the domains are differentially sensitive to developmental and environmental influences (Brun et al., 2009; Glahn et al., 2010; Lenroot & Giedd, 2008; Mueller et al., 2013; Peper, Brouwer, Boomsma, Kahn, & Hulshoff Pol, 2007). As the network timecourse dynamics were the domain that showed the highest degree of environmental perturbation across the two tasks, it would be expected that familiality models in this domain would reflect this environment influence. The average familiality across ICNs was indeed lower for the timecourse dynamics than for either the morphology (spatial overlap) or coherence of the networks. Hence, this supports the assertion that trait familiality is observable in these networks and that the trait expression is a result of both genetic and environmental influences.

The second set of twin analyses took the exploration of familiality a step further by investigating not only the genetic contribution to network profiles in a task state, but by doing so in a developmental sample. This study further explored the extent to which the network profiles complemented traditional activation analyses in order to provide a more complete depiction of a cognitive state. As in the previous study, the ICNs exhibited both task relevance and familiality, which in this study were observed with respect to reward responsivity in adolescents. Adolescence is a critical period of development and understanding the mechanisms subsuming reward responsivity is of particular importance during this period, as adolescents show a hypersensitivity to rewarding stimuli (Gullo & Dawe, 2008; Spear, 2000). Having observed that ICNs are

trait-like and show sensitivity to cognitive demands, it stands to reason that ICNs can be used answer questions about cognitive control and reward processing in the developing brain.

It was found that in a monetary decision making task, there were ICNs that were differentially engaged by the anticipation and receipt of reward. These ICNs also exhibited familiality in their morphology, coherence and timecourse dynamics. However, while the task-relevance of the timecourses showed some familiality, it was to a much lower extent compared to the familiality of the raw timecourses. There are several explanations for this, and it was originally thought that this could be due to the lack of a parametric effect of reward magnitude. This in turn was thought to be due to the reward elements of the task not engaging the adolescents enough, and these are both relevant caveats for the interpretation of the network task association analyses. However, subsequent analyses have zeroed in on the reward event epochs in an ICN event related potential (ERP) design and it was found that the magnitudes of correlations increased in task relevant networks, and this corresponded to an increase in the familiality of task-relevance. Hence, one important observation was that when going from stereotyped block-designs (used in the first study) to event-related designs such as the one used in this study, it might be important to use analyses that are tailored for these types of designs to avoid the task-relevant signal and associated familiality not being swamped by error variance unassociated with the events of interest.

A key observation is that when comparing ICN task relevance and task activation, it was found that there was a general correspondence of ICN task engagement and activation in the omnibus predictor, which was related specifically to the anticipation of

reward, but was not present in the receipt of reward. This implies that the ICNs do not have a ubiquitous correspondence to the underlying activity, but that the nature of this relationship is selective. Moreover, the lack of positive correspondence for the receipt of reward might be a marker of network dysfunction that is specific to adolescence but more work needs to be done to confirm this assertion. The timecourse dynamics of particular ICNs, with functional associations previously shown to be important in reward processing, showed task relevance in this study, and this task relevance was selectively related to reward components and the underlying activity. Hence, taken together, these results suggest that there is much more information that can be derived about cognitive states and the relative contributions of brain networks to these states when ICN-based analyses are added to traditional fMRI analyses.

The third study continued in the theme of exploring the relationship between functional connectivity and activity, but not only sought to inform cognitive states but also differences related to disease presentation (Calhoun, Eichele, & Pearlson, 2009). In this case, working memory deficits in schizophrenia were explored using a combined ICA, GLM and graph theory pipeline. The GLM revealed a hypofrontality phenotype that has come to be characteristic of schizophrenia (Silver et al., 2003), and it was observed that the medial prefrontal cortex had a deficit of deactivation and the inferior temporal cortex had lower activation in persons with schizophrenia in contrast to controls. The medial prefrontal cortex was also a region detected within the default mode network, which is the ICN that had the strongest task association of all ICNs. Moreover, it was found that the ICN timecourses diverged from the timecourse of activity when the ICNs were brought online by the task in both groups. However, this effect was more

pronounced in schizophrenia patients than in controls, which indicates a disease-related dysfunction in the networks. Hence, these results suggest that this ICN dysfunction could be explored as a novel endophenotype of schizophrenia. While there were no differences in the strength and diversity of interconnectivity, significant group differences were detected in the relationships between signal entropy and connectivity strength and diversity. This is important as it points to a possible disease-related compensatory mechanism. Summed together, these graph theory findings further corroborate the existence of an ICN dysfunction endophenotype of schizophrenia.

When contrasting the results for relationship of ICN task relevance to the underlying brain activity across the studies in chapters three and four (Pirate task in adolescents compared to SIRT in schizophrenia patients vs. controls), it is evident that the dynamics of an ICN can indeed be differentially related to the underlying activity. In the adolescent twins performing the Pirate task, ICN coherence positively matched the underlying activity, but in both patients and controls performing the SIRT task, ICN dynamics diverged from activity as they were engaged by the task. Hence, in some cases a task causes ICN dynamics to correspond positively with activity and, in other, cases, this relationship is reversed. This is likely due to how a task engages a particular network. If a complex task engages a multimodal network it could drive down coherence as separate subsystems within the network are engaged. On the other hand, a simpler, less engaging, or more stereotypical task could engage the network as a whole and cause ICN coherence to mirror the underlying activity.

The fourth study took the principle of studying ICN interconnectivity into the realm of resting state fMRI. In this case, the interconnectivity profiles of the ICNs were

used to reveal step-wise global and network-level difference between controls, a preclinical state of Parkinson's disease –REM sleep behavior disorder, and Parkinson's disease (Postuma, Gagnon, & Montplaisir, 2012a; Postuma, Aarsland, et al., 2012). In this study it was observed that RBD phenotypes were intermediate between those observed in PD and controls. This was the case for the strength and diversity of connectivity, as well as the relationships between signal entropy and connectivity strength and diversity, a group difference that was previously observed in schizophrenia (study 3). Moreover, there was a nested decrease in interconnectivity, where the set of networks with significant interconnectivity in controls decreased in RBD, and decreased even further in PD. Hence, this study was a proof-of-principle that ICNs can be employed as a more principled, non-arbitrary means of deriving the connectivity metrics used in graph theory analyses. Furthermore, these metrics provided evidence that RBD is an in vivo, intermediate phenotype of PD, as well as a possible endophenotype and biomarker of disease. This assertion was supported by showing that RBD connectivity profiles can be used to blindly identify PD cases, based on the similarity of their connectivity deficits. Hence, this technique has clear potential for being developed as a diagnostic and potential prognostic tool.

Overall, these studies have shown strong evidence of the utility of intrinsic connectivity networks as tools for studying the in vivo brain in both cognitive and clinical neuroscience approaches. By simultaneously assessing all networks across different states, these ICNs were used to establish traits in the brain in a manner which not previously possible using traditional approaches. The ICNs were shown to not only be stable across cognitive states, but sensitive to those states in a manner that is congruent with the

traditional approaches. In addition, the network characteristics, for example their state-dependent modulation, were shown to be influenced by genetic factors. Finally, both the task-related characteristics and resting state profiles of ICNs were useful for establishing novel endophenotypes of the disease states of schizophrenia and Parkinson's disease. In conclusion, this research furthers the understanding of the brain networks that constitute all aspects of brain functioning in both states of normalcy and disease by showing that ICN profiles can be assessed along a spectrum of functioning. This makes the exploration of ICNs an essential tool for investigating both constructs in cognitive neuroscience and also the dimensions of dysfunction.

# Bibliography


AASM. (2001). *THE INTERNATIONAL CLASSIFICATION OF SLEEP DISORDERS, REVISED: Diagnostic and Coding Manual*. Westchester, IL: American Academy of Sleep Medicine.

Agresti, A. (2013). *Categorical Data Analysis* (3rd ed.). Hoboken, New Jersey: Wiley Series on Probability and Statistics.

Ambrosius, U., Lietzenmaier, S., Wehrle, R., Wichniak, A., Kalus, S., Winkelmann, J., … Friess, E. (2008). Heritability of sleep electroencephalogram. *Biological Psychiatry*, *64*(4), 344–8. doi:10.1016/j.biopsych.2008.03.002

Anderson, J., Ferguson, M. A., Lopez-Larson, M., & Yurgelun-Todd, D. (2011). Reproducibility of single-subject functional connectivity measurements. *American Journal of Neuroradiology*, *32*(3), 548–555. doi:10.3174/ajnr.A2330.Reproducibility

Andersson, J.L.R., Jenkinson, M., Smith, S. (2007). Non-linear registration, aka spatial normalisation. *Oxford Centre for Functional MRI of the Brain Tech. Rep. TR07JA2*.

Arbabshirani, M. R., Havlicek, M., Kiehl, K. a, Pearlson, G. D., & Calhoun, V. D. (2012). Functional network connectivity during rest and task conditions: A comparative study. *Human Brain Mapping*, *000*. doi:10.1002/hbm.22118

Arfanakis, K., Cordes, D., Haughton, V. M., Moritz, C. H., Quigley, M. a, & Meyerand, M. E. (2000). Combining independent component analysis and correlation analysis to probe interregional connectivity in fMRI task activation datasets. *Magnetic Resonance Imaging*, *18*(8), 921–30. Retrieved from http://www.ncbi.nlm.nih.gov/pubmed/11121694

Baldo, J. V, & Dronkers, N. F. (2006). The role of inferior parietal and inferior frontal cortex in working memory. *Neuropsychology*, *20*(5), 529–38. doi:10.1037/0894-4105.20.5.529

Banerjee, M., Capozzoli, M., Mcsweeney, L., & Sinha, D. (2012). Beyond Kappa: A Review of Interrater Agreement Measures. *The Canadian Journal of Statistics*, *27*(1), 3–23.

Barch, D. M., Bustillo, J., Gaebel, W., Gur, R., Heckers, S., Malaspina, D., … Carpenter, W. (2013). Logic and justi fi cation for dimensional assessment of symptoms and related clinical phenomena in psychosis : Relevance to DSM-5. *Schizophrenia Research*, *150*(1), 15–20. doi:10.1016/j.schres.2013.04.027

Bassett, D. S., Nelson, B. G., Mueller, B. a, Camchong, J., & Lim, K. O. (2012). Altered resting state complexity in schizophrenia. *NeuroImage*, *59*(3), 2196–207. doi:10.1016/j.neuroimage.2011.10.002

Bassett, D. S., Nelson, B. G., Mueller, B. A., Camchong, J., & Lim, K. O. (2011). Altered resting state complexity in schizophrenia. *Neuroimage*. Retrieved from http://www.hubmed.org/display.cgi?uids=22008374

Beckmann, C. F. (2012). Modelling with independent components. *NeuroImage*, *62*(2), 891–901. doi:10.1016/j.neuroimage.2012.02.020

Beckmann, C. F., Jenkinson, M., & Smith, S. M. (2003). General multilevel linear modeling for group analysis in FMRI. *NeuroImage*, *20*(2), 1052–63. doi:10.1016/S1053-8119(03)00435-X

Beckmann, C., & Smith, S. (2004). Probabilistic independent component analysis for functional magnetic resonance imaging. *Institute of Electrical and Electronics Engineers Transactions on Medical Imaging*, *23*(2), 137–52. Retrieved from http://ieeexplore.ieee.org/xpls/abs_all.jsp?arnumber=1263605

Behrens, T. E. J., & Sporns, O. (2011). Human connectomics. *Current Opinion in Neurobiology*, *22*, 1–10. doi:10.1016/j.conb.2011.08.005

Belmonte, M. K., & Carper, R. a. (2006). Monozygotic twins with Asperger syndrome: differences in behaviour reflect variations in brain structure and function. *Brain and Cognition*, *61*(1), 110–21. doi:10.1016/j.bandc.2005.12.010

Bezard, E., & Fernagut, P.-O. (2014). Premotor parkinsonism models. *Parkinsonism & Related Disorders*, *20S1*, S17–S19. doi:10.1016/S1353-8020(13)70007-5

Bhaganagarapu, K., Jackson, G. D., & Abbott, D. F. (2013). An automated method for identifying artifact in independent component analysis of resting-state fMRI. *Frontiers in Human Neuroscience Methods*, *7*(343), 1–17. doi:10.3389/fnhum.2013.00343

Biggs, N., Lloyd, E., & Wilson, R. (1986). *Graph Theory, 1736-1936,*. Oxford University Press, Inc.

Biswal, B., Eldreth, D., Motes, M., & Rypma, B. (2010). Task-dependent individual differences in prefrontal connectivity. *Cerebral Cortex*, *4*(1992), 1–10. doi:10.1093/cercor/bhp284

Biswal, B., Mennes, M., & et, al. (2010). Toward discovery science of human brain function. *Proceedings of the ...*, *107*(10), 4734–4739. doi:10.1073/pnas.0911855107

Blokland, G. a M., McMahon, K. L., Hoffman, J., Zhu, G., Meredith, M., Martin, N. G., … Wright, M. J. (2008). Quantifying the heritability of task-related brain activation and performance during the N-back working memory task: a twin fMRI study. *Biological Psychology*, *79*(1), 70–9. doi:10.1016/j.biopsycho.2008.03.006

Blokland, G. a M., McMahon, K. L., Thompson, P. M., Martin, N. G., de Zubicaray, G. I., & Wright, M. J. (2011). Heritability of working memory brain activation. *The Journal of Neuroscience : The Official Journal of the Society for Neuroscience*, *31*(30), 10882–90. doi:10.1523/JNEUROSCI.5334-10.2011

Borek, L., Amick, M., & Friedman, J. (2006). Non-motor aspects of Parkinson's disease. *CNS Spectrums*, *7*(July). Retrieved from http://mbldownloads.com/0706CNS_Borek_CME.pdf

Borgwardt, S. J., Picchioni, M. M., Ettinger, U., Toulopoulou, T., Murray, R., & McGuire, P. K. (2010). Regional gray matter volume in monozygotic twins concordant and discordant for schizophrenia. *Biological Psychiatry*, *67*(10), 956–64. doi:10.1016/j.biopsych.2009.10.026

Braak, H., Ghebremedhin, E., Rub, U., Bratzke, H., & Del Tredici, K. (2004). Stages in the development of Parkinson's disease-related pathology. *Cell Tissue Res*, *318*, 121–134.

Brooks, D. J. (2012). Parkinson's disease: Diagnosis. *Parkinsonism and Realted Disorders*, *18*, S31–S33. doi:10.1016/S1353-8020(11)70012-8

Brown, G. G., McCarthy, G., Bischoff-Grethe, A., Ozyurt, B., Greve, D., Potkin, S. G., … Lim, K. O. (2009). Brain-performance correlates of working memory retrieval in schizophrenia: a cognitive modeling approach. *Schizophrenia Bulletin*, *35*(1), 32–46. doi:10.1093/schbul/sbn149

Brun, C., Leporé, N., Pennec, X., Lee, A., Barysheva, M., Madsen, S. K., … Paul M. Thompson. (2009). Mapping the Regional Influence of Genetics on Brain Structure Variability - A Tensor-Based Morphometry Study. *Neuroimage*, *48*(1), 37–49. doi:10.1016/j.neuroimage.2009.05.022.Mapping

Bullmore, E., & Sporns, O. (2009). Complex brain networks: graph theoretical analysis of structural and functional systems. *Nature Reviews. Neuroscience*, *10*(3), 186–98. doi:10.1038/nrn2575

Calhoun, V., & Adali, T. (2001). A method for making group inferences from functional MRI data using independent component analysis. *Human Brain …*, *151*, 140–151. doi:10.1002/hbm.

Calhoun, V. D., Adali, T., Kiehl, K. a, Astur, R., Pekar, J. J., & Pearlson, G. D. (2006). A method for multitask fMRI data fusion applied to schizophrenia. *Human Brain Mapping*, *27*(7), 598–610. doi:10.1002/hbm.20204

Calhoun, V. D., Adali, T., Mcginty, V. B., Pekar, J. J., Watson, T. D., & Pearlson, G. D. (2001). fMRI Activation in a Visual-Perception Task: Network of Areas Detected Using the General Linear Model and Independent Components Analysis. *NeuroImage*, *14*, 1080–1088. doi:10.1006/nimg.2001.0921

Calhoun, V. D., Adali, T., Stevens, M. C., Kiehl, K. a, & Pekar, J. J. (2005). Semi-blind ICA of fMRI: A method for utilizing hypothesis-derived time courses in a spatial ICA analysis. *NeuroImage*, *25*(2), 527–38. doi:10.1016/j.neuroimage.2004.12.012

Calhoun, V. D., Kiehl, K. a, Liddle, P. F., & Pearlson, G. D. (2004). Aberrant localization of synchronous hemodynamic activity in auditory cortex reliably characterizes schizophrenia. *Biological Psychiatry*, *55*(8), 842–9. doi:10.1016/j.biopsych.2004.01.011

Calhoun, V. D., Liu, J., & Adali, T. (2009). A review of group ICA for fMRI data and ICA for joint inference of imaging, genetic, and ERP data. *NeuroImage*, *45*(1 Suppl), S163–72. doi:10.1016/j.neuroimage.2008.10.057

Calhoun, V., Eichele, T., & Pearlson, G. (2009). Functional brain networks in schizophrenia: a review. *Frontiers in Human Neuroscience*, *3*(August), 1–12. doi:10.3389/neuro.09.017

Calhoun, V., Kiehl, K., & Pearlson, G. (2008). Modulation of temporally coherent brain networks estimated using ICA at rest and during cognitive tasks. *Human Brain Mapping*, *29*(7), 828–838. doi:10.1002/hbm.20581.Modulation

Camchong, J., MacDonald, A. W., Nelson, B., Bell, C., Mueller, B. A., Specker, S., & Lim, K. O. (2011). Frontal hyperconnectivity related to discounting and reversal learning in cocaine subjects. *Biol Psychiatry*, *69*(11), 1117–1123. Retrieved from http://www.hubmed.org/display.cgi?uids=21371689

Casey, B., Giedd, J., & Thomas, K. (2000). Structural and functional brain development and its relation to cognitive development. *Biological Psychology*, *54*(1-3), 241–57. Retrieved from http://www.ncbi.nlm.nih.gov/pubmed/11035225

Casey, B. J., Jones, R. M., Levita, L., Libby, V., Pattwell, S. S., Ruberry, E. J., … Somerville, L. H. (2010). The storm and stress of adolescence: insights from human imaging and mouse genetics. *Developmental Psychobiology*, *52*(3), 225–35. doi:10.1002/dev.20447

Çetin, M. S., Christensen, F., Abbott, C. C., Stephen, J. M., Mayer, A. R., Cañive, J. M., … Calhoun, V. D. (2014). Thalamus and posterior temporal lobe show greater inter-network connectivity at rest and across sensory paradigms in schizophrenia. *NeuroImage*. doi:10.1016/j.neuroimage.2014.04.009

Chen, C.-H., Gutierrez, E. D., Thompson, W., Panizzon, M. S., Jernigan, T. L., Eyler, L. T., … Dale, A. M. (2012). Hierarchical genetic organization of human cortical surface area. *Science (New York, N.Y.)*, *335*(6076), 1634–6. doi:10.1126/science.1215330

Chiang, M.-C., McMahon, K. L., de Zubicaray, G. I., Martin, N. G., Hickie, I., Toga, A. W., … Thompson, P. M. (2011). Genetics of white matter development: a DTI study of 705 twins and their siblings aged 12 to 29. *NeuroImage*, *54*(3), 2308–17. doi:10.1016/j.neuroimage.2010.10.015

Cho, Z., Oh, S., Kim, J., Park, S.-Y., Kwon, D.-H., Jeong, H.-J., … Jeon, B. S. (2010). Direct Visualization of Parkinson ' s Disease by In Vivo Human Brain Imaging Using 7 . 0T Magnetic Resonance Imaging. *Movement Disorders*, *xx*(xxx), 1–6. doi:10.1002/23465

Chou, Y., Panych, L., Dickey, C. C., Petrella, J. R., & Chen, N. (2012). Investigation of long-term reproducibility of intrinsic connectivity network mapping: a resting-state fMRI study. *American Journal of Neuroradiology*, *33*(5), 833–838. doi:10.3174/ajnr.A2894.Investigation

Cohen, M. R., & Maunsell, J. H. R. (2009). Attention improves performance primarily by reducing interneuronal correlations, *12*(12). doi:10.1038/nn.2439

Crews, F., He, J., & Hodge, C. (2007). Adolescent cortical development: a critical period of vulnerability for addiction. *Pharmacology, Biochemistry, and Behavior*, *86*(2), 189–99. doi:10.1016/j.pbb.2006.12.001

Crivello, F., Tzourio, N., Poline, J., Woods, R. P., Mazziotta, J. C., & Mazoyer, B. (1995). Intersubject Variability in Functional Neuroanatomy of Silent Verb Generation: Assessment by a New Activation Detection Algorithm Based on Amplitude and Size Information.pdf. *NeuroImage*, *2*(253-263).

Deco, G., & Corbetta, M. (2012). The Dynamical Balance of the Brain at Rest. *The Neuroscientist*, (December 2010). doi:10.1177/1073858409354384

Deco, G., Jirsa, V. K., & McIntosh, A. R. (2011). Emerging concepts for the dynamical organization of resting-state activity in the brain. *Nature Reviews. Neuroscience*, *12*(1), 43–56. doi:10.1038/nrn2961

Deco, G., Jirsa, V., Mcintosh, A. R., Sporns, O., & Ko, R. (2009). Key role of coupling, delay, and noise in resting brain fluctuations. *Proceedings of the National Academy of Sciences of the United States of America*, *106*(25), 10302–10307.

Duarte-Carvajalino, J. M., Jahanshad, N., Lenglet, C., McMahon, K. L., de Zubicaray, G. I., Martin, N. G., … Sapiro, G. (2012). Hierarchical topological network analysis of anatomical human brain connectivity and differences related to sex and kinship. *NeuroImage*, *59*(4), 3784–804. doi:10.1016/j.neuroimage.2011.10.096

Edwards, E., Nagarajan, S., & Dalal, S. (2010). Spatiotemporal imaging of cortical activation during verb generation and picture naming. *Neuroimage*, *50*(1), 291–301. doi:10.1016/j.neuroimage.2009.12.035.Spatiotemporal

Ellmore, T. M., Castriotta, R. J., Hendley, K. L., Aalbers, B. M., Furr-stimming, E., Hood, A. J., … Schiess, M. C. (2013). Altered Nigrostriatal and Nigrocortical Functional Connectivity in Rapid Eye Movement Sleep Behavior Disorder. *Sleep*, *36*(12), 1885–1892.

Ernst, M., & Mueller, S. C. (2008). The adolescent brain: insights from functional neuroimaging research. *Developmental Neurobiology*, *68*(6), 729–43. doi:10.1002/dneu.20615

Fantini, M. L., Postuma, R. B., Montplaisir, J., & Ferini-strambi, L. (2006). Olfactory deficit in idiopathic rapid eye movements sleep behavior disorder. *Brain Research Bulletin*, *70*, 386–390. doi:10.1016/j.brainresbull.2006.07.008

First, M. B., Spitzer, R. L., Miriam, G., & Williams, J. B. W. (2002). *Structured Clinical Interview for DSM-IV-TR Axis I Disorders, Research Version, Patient Edition. (SCID-I/P)*. New York, New York: Biometrics Research, New York State Psychiatric Institute.

Fornito, A., & Bullmore, E. (2012). Connectomic intermediate phenotypes for psychiatric disorders. *Frontiers in Psychiatry*, *3*(April), 1–15. doi:10.3389/fpsyt.2012.00032

Fornito, A., Zalesky, A., Pantelis, C., & Bullmore, E. T. (2012). Schizophrenia, neuroimaging and connectomics. *NeuroImage*, *62*(4), 2296–2314. doi:10.1016/j.neuroimage.2011.12.090

Fox, M. D., & Raichle, M. E. (2007). Spontaneous fluctuations in brain activity observed with functional magnetic resonance imaging. *Nature Reviews. Neuroscience*, *8*(9), 700–11. doi:10.1038/nrn2201

Galvan, A., Hare, T. a, Parra, C. E., Penn, J., Voss, H., Glover, G., & Casey, B. J. (2006). Earlier development of the accumbens relative to orbitofrontal cortex might underlie risk-taking behavior in adolescents. *The Journal of Neuroscience : The Official*

*Journal of the Society for Neuroscience*, *26*(25), 6885–92. doi:10.1523/JNEUROSCI.1062-06.2006

Galvan, A., Hare, T., Voss, H., Glover, G., & Casey, B. J. (2007). Risk-taking and the adolescent brain: who is at risk? *Developmental Science*, *10*(2), F8–F14. doi:10.1111/j.1467-7687.2006.00579.x

Glahn, D. C., Winkler, a M., Kochunov, P., Almasy, L., Duggirala, R., Carless, M. a, … Blangero, J. (2010). Genetic control over the resting brain. *Proceedings of the National Academy of Sciences of the United States of America*, *107*(3), 1223–8. doi:10.1073/pnas.0909969107

Gottesman, I., & Gould, T. (2003). The Endophenotype Concept in Psychiatry: Etymology and Strategic Intentions. *American Journal of Psychiatry*, *160*(4), 636–645. Retrieved from http://ajp.psychiatryonline.org/article.aspx?volume=160&page=636

Grafton, S. T., & Hamilton, A. F. de C. (2007). Evidence for a distributed hierarchy of action representation in the brain. *Human Movement Science*, *26*(4), 590–616.

Greicius, M., Kiviniemi, V., Tervonen, O., Vainionpää, V., Alahuhta4, S., Reiss, A. L., & Menon, V. (2008). Persistent Default-Mode Network Connectivity During Light Sedation. *Human Brain Mapping*, *29*(7), 839–847. doi:10.1002/hbm.20537.Persistent

Greicius, M., & Krasnow, B. (2003). Functional connectivity in the resting brain: a network analysis of the default mode hypothesis. *Proceedings of the …*, *100*(1), 253–8. doi:10.1073/pnas.0135058100

Gullo, M. J., & Dawe, S. (2008). Impulsivity and adolescent substance use: rashly dismissed as "all-bad"? *Neuroscience and Biobehavioral Reviews*, *32*(8), 1507–18. doi:10.1016/j.neubiorev.2008.06.003

Guo, C. C., Kurth, F., Zhou, J., Mayer, E. A., Eickhoff, S. B., Kramer, J. H., & Seeley, W. W. (2012). NeuroImage One-year test – retest reliability of intrinsic connectivity network fMRI in older adults. *NeuroImage*, *61*(4), 1471–1483. doi:10.1016/j.neuroimage.2012.03.027

Guo, Y., & Pagnoni, G. (2008). A unified framework for group independent component analysis for multi-subject fMRI data. *NeuroImage*, *42*(3), 1078–93. doi:10.1016/j.neuroimage.2008.05.008

Hagmann, P., Cammoun, L., Gigandet, X., Gerhard, S., Grant, P. E., Wedeen, V., … Sporns, O. (2010). MR connectomics: principles and challenges. *Journal of Neuroscience Methods*, *194*, 34–45. doi:10.1016/j.jneumeth.2010.01.014

Hallmayer, J., Cleveland, S., Torres, A., Phillips, J., Cohen, B., Torigoe, T., … Risch, N. (2011). Genetic heritability and shared environmental factors among twin pairs with autism. *Archives of General Psychiatry*, *68*(11), 1095–102. doi:10.1001/archgenpsychiatry.2011.76

Hampson, M., & Driesen, N. (2006). Brain connectivity related to working memory performance. *The Journal of Neuroscience*, *26*(51), 13338–13343. doi:10.1523/JNEUROSCI.3408-06.2006.Brain

Hanyu, H., Inoue, Y., Sakurai, H., Kanetaka, H., Nakamura, M., Miyamoto, T., … Iwamoto, T. (2012). Parkinsonism and Related Disorders Voxel-based magnetic resonance imaging study of structural brain changes in patients with idiopathic REM sleep behavior disorder. *Parkinsonism and Related Disorders*, *18*(2), 136–139. doi:10.1016/j.parkreldis.2011.08.023

Henseler, I., Falkai, P., & Gruber, O. (2009). A systematic fMRI investigation of the brain systems subserving different working memory components in schizophrenia. *The European Journal of Neuroscience*, *30*(4), 693–702. doi:10.1111/j.1460-9568.2009.06850.x

Hermundstad, A. M., Bassett, D. S., Brown, K. S., Aminoff, E. M., Clewett, D., Freeman, S., … Carlson, J. M. (2013). Structural foundations of resting-state and task-based functional connectivity in the human brain. *Proceedings of the National Academy of Sciences of the United States of America*, *110*(15), 6169–74. doi:10.1073/pnas.1219562110

Honey, C. J., Thivierge, J.-P., & Sporns, O. (2010). Can structure predict function in the human brain? *NeuroImage*, *52*(3), 766–76. doi:10.1016/j.neuroimage.2010.01.071

Hothorn, T., & Hornik, K. (2011). exactRankTests: Exact Distributions for Rank and Permutation Tests. *R package version 0.8-22.* Retrieved from http://cran.r-project.org/package=exactRankTests

Iacoboni, M. (2005). Neural mechanisms of imitation. *Current Opinion in Neurobiology*, *15*(6), 632–7. doi:10.1016/j.conb.2005.10.010

Ibarretxe-bilbao, N., Zarei, M., Junque, C., Jose, M., Segura, B., Vendrell, P., … Tolosa, E. (2011). NeuroImage Dysfunctions of cerebral networks precede recognition memory deficits in early Parkinson ' s disease. *NeuroImage*, *57*(2), 589–597. doi:10.1016/j.neuroimage.2011.04.049

Indefrey, P. (2011). The spatial and temporal signatures of word production components: a critical update. *Frontiers in Psychology*, *2*(255), 1–16. doi:10.3389/fpsyg.2011.00255

Indefrey, P., & Levelt, W. J. M. (2004). The spatial and temporal signatures of word production components. *Cognition*, *92*, 101–144. doi:10.1016/j.cognition.2002.06.001

Iranzo, A., Santamaria, J., & Tolosa, E. (2009). The clinical and pathophysiological relevance of REM sleep behavior disorder in neurodegenerative diseases. *Sleep Medicine Reviews*, *13*(6), 385–401. doi:10.1016/j.smrv.2008.11.003

Jackson, P. L., Meltzoff, A. N., & Decety, J. (2006). Neural circuits involved in imitation and perspective-taking. *NeuroImage*, *31*(1), 429–439.

Jahanshad, N., Lee, A. D., Barysheva, M., McMahon, K. L., de Zubicaray, G. I., Martin, N. G., … Thompson, P. M. (2010). Genetic influences on brain asymmetry: a DTI study of 374 twins and siblings. *NeuroImage*, *52*(2), 455–69. doi:10.1016/j.neuroimage.2010.04.236

Jang, J. H., Jung, W. H., Choi, J.-S., Choi, C.-H., Kang, D.-H., Shin, N. Y., … Kwon, J. S. (2011). Reduced prefrontal functional connectivity in the default mode network is related to greater psychopathology in subjects with high genetic loading for schizophrenia. *Schizophrenia Research*, *127*(1-3), 58–65. doi:10.1016/j.schres.2010.12.022

Jenkinson, M., Bannister, P., Brady, M., & Smith, S. (2002). Improved Optimization for the Robust and Accurate Linear Registration and Motion Correction of Brain Images. *NeuroImage*, *17*, 825–841. doi:10.1006/nimg.2002.1132

Kim, D. Il, Manoach, D. S., Mathalon, D. H., Turner, J. A., Mannell, M., Brown, G. G., … Calhoun, V. D. (2009). Dysregulation of Working Memory and Default- Mode Networks in Schizophrenia Using Independent Component Analysis , an fBIRN and MCIC Study. *Human Brain Mapping*, *3811*(30), 3795–3811. doi:10.1002/hbm.20807

Kim, M. a, Tura, E., Potkin, S. G., Fallon, J. H., Manoach, D. S., Calhoun, V. D., & Turner, J. a. (2010). Working memory circuitry in schizophrenia shows widespread cortical inefficiency and compensation. *Schizophrenia Research*, *117*(1), 42–51. doi:10.1016/j.schres.2009.12.014

Koenigs, M., Barbey, A. K., Postle, B. R., & Grafman, J. (2009). Superior parietal cortex is critical for the manipulation of information in working memory. *The Journal of Neuroscience : The Official Journal of the Society for Neuroscience*, *29*(47), 14980–6. doi:10.1523/JNEUROSCI.3706-09.2009

Korgaonkar, M. S., Ram, K., Williams, L. M., Gatt, J. M., & Grieve, S. M. (2014). Establishing the resting state default mode network derived from functional

magnetic resonance imaging tasks as an endophenotype: A twins study. *Human Brain Mapping*, *35*(8), 3893–902. doi:10.1002/hbm.22446

Koski, L., Iacoboni, M., Dubeau, M., Woods, R. P., & John, C. (2003). Modulation of Cortical Activity During Different Imitative Behaviors Modulation of Cortical Activity During Different Imitative Behaviors. *Journal of Neurophysiology*, *89*, 460–471. doi:10.1152/jn.00248.2002

Krajcovicova, L., Mikl, M., Marecek, R., & Rektorova, I. (2012). The default mode network integrity in patients with Parkinson's disease is levodopa equivalent dose-dependent. *Journal of Neural Transmission*, *119*, 443–454. doi:10.1007/s00702-011-0723-5

Kristo, G., Rutten, G.-J., Raemaekers, M., de Gelder, B., Rombouts, S., & Ramsey, N. (2012). Task and task-free FMRI reproducibility comparison for motor network identification. *Human Brain Mapping*, *000*(July). doi:10.1002/hbm.22180

Krueger, R. F., Hopwood, C. J., Wright, A. G. C., & Markon, K. E. (2014). Challenges and Strategies in Helping the DSM Become More Dimensional and Empirically Based. *Current Psychiatry Reports*, *16*(12), 515. doi:10.1007/s11920-014-0515-3

Lahaye, P., Poline, J., & Flandin, G. (2003). Functional connectivity: studying nonlinear, delayed interactions between BOLD signals. …, *20*(2003), 962–974. doi:10.1016/S1053-8119(03)00340-9

Laird, A. R., Fox, P. M., Eickhoff, S. B., Turner, J. A., Ray, K. L., McKay, D. R., … Fox, P. T. (2011). Behavioral Interpretations of Intrinsic Connectivity Networks. *J Cogn Neurosci*. Retrieved from http://www.hubmed.org/display.cgi?uids=21671731

Lenroot, R. K., & Giedd, J. N. (2008). The changing impact of genes and environment on brain development during childhood and adolescence: initial findings from a neuroimaging study of pediatric twins. *Development and Psychopathology*, *20*(4), 1161–75. doi:10.1017/S0954579408000552

Lessov-Schlaggar, C., Hardin, J., DeCarli, C., Krasnow, R. E., Reed, T., Wolf, P. A., … Carmelli, D. (2012). Longitudinal genetic analysis of brain volumes in normal elderly male twins. *Neurobiology of Aging*, *33*(4), 636–644. doi:10.1016/j.neurobiolaging.2010.06.002.Longitudinal

Li, B., Wang, X., Yao, S., Hu, D., & Friston, K. (2012). Task-dependent modulation of effective connectivity within the default mode network. *Frontiers in Psychology*, *3*(June), 1–11. doi:10.3389/fpsyg.2012.00206

Li, K., Guo, L., Nie, J., Li, G., & Liu, T. (2009). Review of methods for functional brain connectivity detection using fMRI. *Computerized Medical Imaging and Graphics :*

*The Official Journal of the Computerized Medical Imaging Society*, *33*(2), 131–9. doi:10.1016/j.compmedimag.2008.10.011

Li, N., Ma, N., Liu, Y., He, X.-S., Sun, D.-L., Fu, X.-M., … Zhang, D.-R. (2013). Resting-state functional connectivity predicts impulsivity in economic decision-making. *The Journal of Neuroscience : The Official Journal of the Society for Neuroscience*, *33*(11), 4886–95. doi:10.1523/JNEUROSCI.1342-12.2013

Lin, P., Hasson, U., Jovicich, J., & Robinson, S. (2011). A Neuronal Basis for Task-Negative Responses in the Human Brain, (April). doi:10.1093/cercor/bhq151

Liu, H., Kaneko, Y., Ouyang, X., Li, L., Hao, Y., Chen, E. Y. H., … Liu, Z. (2012). Schizophrenic patients and their unaffected siblings share increased resting-state connectivity in the task-negative network but not its anticorrelated task-positive network. *Schizophrenia Bulletin*, *38*(2), 285–94. doi:10.1093/schbul/sbq074

Long, D., Wang, J., Xuan, M., Gu, Q., Xu, X., Kong, D., & Zhang, M. (2012). Automatic Classification of Early Parkinson's Disease with Multi-Modal MR Imaging. *PloS One*, *7*(11), 1–9. doi:10.1371/journal.pone.0047714

Luk, K. C., Kehm, V., Carroll, J., Zhang, B., Brien, P. O., Trojanowski, J. Q., & Lee, V. M.-Y. (2013). Pathological α-Synuclein Transmission Initiates Parkinson-like Neurodegeneration in Non-transgenic Mice. *Science*, *338*(6109), 949–953. doi:10.1126/science.1227157.Pathological

Luna, B., Padmanabhan, A., & O'Hearn, K. (2010). What has fMRI told us about the development of cognitive control through adolescence? *Brain and Cognition*, *72*(1), 101–13. doi:10.1016/j.bandc.2009.08.005

Lynall, M., Bassett, D. S., Kerwin, R., Mckenna, P. J., Kitzbichler, M., Muller, U., & Bullmore, E. (2010). Functional Connectivity and Brain Networks in Schizophrenia. *The Journal of Neuroscience*, *30*(28), 9477–9487. doi:10.1523/JNEUROSCI.0333-10.2010

Malone, S. M., Luciana, M., Wilson, S., Sparks, J. C., Hunt, R. H., Thomas, K. M., & Iacono, W. G. (2014). Adolescent drinking and motivated decision-making: a cotwin-control investigation with monozygotic twins. *Behavior Genetics*, *44*(4), 407–18. doi:10.1007/s10519-014-9651-0

Marshuetz, C., Smith, E. E., Jonides, J., DeGutis, J., & Chenevert, T. L. (2000). Order information in working memory: fMRI evidence for parietal and prefrontal mechanisms. *Journal of Cognitive Neuroscience*, *12*(Supplement 2), 130–44. doi:10.1162/08989290051137459

Massano, J., & Bhatia, K. P. (2012). Clinical approach to Parkinson's disease: features, diagnosis, and principles of management. *Cold Spring Harbor Perspectives in Medicine*, *2*(6), 1–15. doi:10.1101/cshperspect.a008870

Matthews, S. C., Simmons, A. N., Strigo, I., Jang, K., Stein, M. B., & Paulus, M. P. (2007). Heritability of anterior cingulate response to conflict: an fMRI study in female twins. *NeuroImage*, *38*(1), 223–7. doi:10.1016/j.neuroimage.2007.07.015

Mazziotta, J. C., Woods, R., Iacoboni, M., Sicotte, N., Yaden, K., Tran, M., … Toga, A. W. (2009). The myth of the normal, average human brain--the ICBM experience: (1) subject screening and eligibility. *NeuroImage*, *44*(3), 914–22. doi:10.1016/j.neuroimage.2008.07.062

Mazziotta, J., Toga, A., Evans, A., Fox, P., Lancaster, J., Zilles, K., … Mazoyer, B. (2001). A probabilistic atlas and reference system for the human brain : International Consortium for Brain Mapping ( ICBM ). *Phil.Trans. R. Soc. Lond.*, *356*, 1293–1322. doi:10.1098/rstb.2001.0915

Mckeown, M. J., Makeig, S., Brown, G. G., Jung, T., Kindermann, S. S., Bell, A. J., & Sejnowski, T. J. (1998). Analysis of fMRI Data by Blind Separation Into Independent Spatial Components. *Human Brain Mapping*, *6*, 160–188.

Meda, S. a, Stevens, M. C., Folley, B. S., Calhoun, V. D., & Pearlson, G. D. (2009). Evidence for anomalous network connectivity during working memory encoding in schizophrenia: an ICA based analysis. *PloS One*, *4*(11), e7911. doi:10.1371/journal.pone.0007911

Meier, T., Wildenberg, J., Liu, J., & Chen, J. (2012). Parallel ICA identifies sub-components of resting state networks that covary with behavioral indices. *Frontiers in Human …*, *6*(281), 1–14. doi:10.3389/fnhum.2012.00281

Meyer-Lindenberg, A. (2009). Neural connectivity as an intermediate phenotype: brain networks under genetic control. *Human Brain Mapping*, *30*(7), 1938–46. doi:10.1002/hbm.20639

Meyer-lindenberg, A. (2010). From maps to mechanisms through neuroimaging of schizophrenia. *Nature*, *468*(7321), 194–202. doi:10.1038/nature09569

Miller, G. a, & Rockstroh, B. (2013). Endophenotypes in psychopathology research: where do we stand? *Annual Review of Clinical Psychology*, *9*, 177–213. doi:10.1146/annurev-clinpsy-050212-185540

Minzenberg, M., & Laird, A. (2009). Meta-analysis of 41 functional neuroimaging studies of executive function in schizophrenia. *Archives of …*, *66*(8), 811–822. Retrieved from http://archneur.jamanetwork.com/article.aspx?articleid=483150

Molloy, E., Blumenthal, J., Giedd, J. N., Liu, H., Jeffriest, N., Zijdenboss, A., & Rapoport, J. L. (2001). The Relationship Between Brain Morphometry and Cognitive Abilities in Healthy Pediatric Monozygotic Twins, (6), 2001.

Moodie, C. A., Wisner, K. M., & MacDonald, A. W. (2014). Characteristics of canonical intrinsic connectivity networks across tasks and monozygotic twin pairs. *Human Brain Mapping*, *00*(October 2013). doi:10.1002/hbm.22568

Morales, D. A., Vives-Gilabert, Y., Gomez-Ansond, B., Bengoetxea, E., Larranaga, P., Bielza, C., … Delfino, M. (2012). Predicting dementia development in Parkinson's disease using Bayesian network classifiers. *Psychiatry Research: Neuroimaging*, 1–7. doi:10.1016/j.pscychresns.2012.06.001

Mueller, S., Wang, D., Fox, M. D., Yeo, B. T. T., Sepulcre, J., Sabuncu, M. R., … Liu, H. (2013). Individual Variability in Functional Connectivity Architecture of the Human Brain. *Neuron*, *77*, 585–595.

Munn, M. a, Alexopoulos, J., Nishino, T., Babb, C. M., Flake, L. a, Singer, T., … Botteron, K. N. (2007). Amygdala volume analysis in female twins with major depression. *Biological Psychiatry*, *62*(5), 415–22. doi:10.1016/j.biopsych.2006.11.031

Naselaris, T., Kay, K., Nishimoto, S., & Gallant, J. (2011). Encoding and decoding in fMRI. *Neuroimage*, *56*(2), 400–410. doi:10.1016/j.neuroimage.2010.07.073.Encoding

Park, J., Shedden, K., & Polk, T. a. (2012). Correlation and heritability in neuroimaging datasets: a spatial decomposition approach with application to an fMRI study of twins. *NeuroImage*, *59*(2), 1132–42. doi:10.1016/j.neuroimage.2011.06.066

Pasquale, F. de, Penna, S. Della, Snyder, A. Z., Laura Marzetti, Pizzella, V., Romani, G. L., & Corbetta, M. (2012). A cortical core for dynamic integration of functional networks in the resting human brain. *Neuron*, *74*(4), 753–764. doi:10.1016/j.neuron.2012.03.031.A

Pedlow, S., Wang, Y., & Muircheartaigh, C. O. (2005). The Impact of Cluster ( Segment ) Size on Effective Sample Size. In *Paper presented at the sixtieth annual meeting of the American Association For Public Opinion Association, Fontainebleau Resort, Miami Beach, FL*. Retrieved from http://www.allacademic.com/meta/p17146_index.html

Peper, J. S., Brouwer, R. M., Boomsma, D. I., Kahn, R. S., & Hulshoff Pol, H. E. (2007). Genetic influences on human brain structure: a review of brain imaging studies in twins. *Human Brain Mapping*, *28*(6), 464–73. doi:10.1002/hbm.20398

Poewe, W., Rascol, O., Sampaio, C., Stebbins, G. T., & Goetz, C. G. (2003). The Unified Parkinson's Disease Rating Scale (UPDRS): Status and Recommendations. *Movement Disorders*, *18*(7), 738–750. Retrieved from http://www.ncbi.nlm.nih.gov/books/NBK27754/

Pomarol-Clotet, E., Canales-Rodríguez, E. J., Salvador, R., Sarró, S., Gomar, J. J., Vila, F., … McKenna, P. J. (2010). Medial prefrontal cortex pathology in schizophrenia as revealed by convergent findings from multimodal imaging. *Molecular Psychiatry*, *15*(8), 823–30. doi:10.1038/mp.2009.146

Poppe, A. B., Wisner, K., Atluri, G., Lim, K. O., Kumar, V., & Macdonald, A. W. (2013). Toward a neurometric foundation for probabilistic independent component analysis of fMRI data. *Cognitive, Affective & Behavioral Neuroscience*. doi:10.3758/s13415-013-0180-8

Postuma, R. B., Aarsland, D., Barone, P., Burn, D., Hawkes, C., Oertel, W., & Ziemssen, T. (2012). Identifying Prodromal Parkinson's Disease: Pre-Motor Disorders in Parkinson's Disease. *Movement Disorders*, *27*(5), 617–626. doi:10.1002/mds.24996

Postuma, R. B., Gagnon, J., & Montplaisir, J. Y. (2012a). Neurobiology of Disease REM sleep behavior disorder : From dreams to neurodegeneration. *Neurobiology of Disease*, *46*, 553–558. doi:10.1016/j.nbd.2011.10.003

Postuma, R. B., Gagnon, J., & Montplaisir, J. Y. (2012b). REM sleep behavior disorder: From dreams to neurodegeneration. *Neurobiology of Disease*, *46*(3), 553–558. doi:10.1016/j.nbd.2011.10.003

Potkin, S. G., & Ford, J. M. (2009). Widespread cortical dysfunction in schizophrenia: the FBIRN imaging consortium. *Schizophrenia Bulletin*, *35*(1), 15–8. doi:10.1093/schbul/sbn159

Potkin, S. G., Turner, J. a, Brown, G. G., McCarthy, G., Greve, D. N., Glover, G. H., … Lim, K. O. (2009). Working memory and DLPFC inefficiency in schizophrenia: the FBIRN study. *Schizophrenia Bulletin*, *35*(1), 19–31. doi:10.1093/schbul/sbn162

Prodoehl, J., Li, H., Planetta, P. J., Goetz, C. G., Shannon, K. M., Tangonan, R., … Vaillancourt, D. E. (2013). Diffusion Tensor Imaging of Parkinson's Disease, Atypical Parkinsonism, and Essential Tremor. *Movement Disorders*, *28*(13), 1816–1822. doi:10.1002/mds.25491

Raichle, M. E., MacLeod, a M., Snyder, a Z., Powers, W. J., Gusnard, D. a, & Shulman, G. L. (2001). A default mode of brain function. *Proceedings of the National Academy of Sciences of the United States of America*, *98*(2), 676–82. doi:10.1073/pnas.98.2.676

Ray, K. L., Mckay, D. R., Fox, P. M., Riedel, M. C., Uecker, A. M., Beckmann, C. F., … Laird, A. R. (2013). ICA model order selection of task co-activation networks. *Frontiers in Neuroscience*, *7*(237), 1–12. doi:10.3389/fnins.2013.00237

Repovš, G., & Barch, D. (2012). Working memory related brain network connectivity in individuals with schizophrenia and their siblings. *Frontiers in Human Neuroscience*, *6*(137), 1–15. doi:10.3389/fnhum.2012.00137

Revelle, W. (2011). psych: Procedures for Personality and Psychological Research Northwestern University, Evanston. *R package version 1.01.9*.

Rimol, L. M., Panizzon, M. S., Fennema-Notestine, C., Eyler, L. T., Fischl, B., Franz, C. E., … Dale, A. M. (2010). Cortical thickness is influenced by regionally specific genetic factors. *Biological Psychiatry*, *67*(5), 493–9. doi:10.1016/j.biopsych.2009.09.032

Sämann, P. G., Wehrle, R., Hoehn, D., Spoormaker, V. I., Peters, H., Tully, C., … Czisch, M. (2011). Development of the brain's default mode network from wakefulness to slow wave sleep. *Cerebral Cortex (New York, N.Y. : 1991)*, *21*(9), 2082–93. doi:10.1093/cercor/bhq295

Samii, A., Nutt, J. G., & Ransom, B. R. (2004). Parkinson's disease. *The Lancet*, *363*, 1783–1793.

Schenck, C. H., Boeve, B. F., & Mahowald, M. W. (2013). Delayed emergence of a parkinsonian disorder or dementia in 81 % of older males initially diagnosed with idiopathic REM sleep behavior disorder (RBD): 16 year update on a previously reported series. *SLEEP MEDICINE*, 1–5. doi:10.1016/j.sleep.2012.10.009

Shannon, C. E. (1948). A Mathematical Theory of Communication. *Bell System Technical Journal*, *27*(3), 379–423.

Sharman, M., Valabregue, R., Perlbarg, V., Marrakchi-Kacem, L., Vidailhet, M., Benali, H., … Lehericy, S. (2012). Parkinson's Disease Patients Show Reduced Cortical-Subcortical Sensorimotor Connectivity. *Movement Disorders*, *28*(4), 447–454. doi:10.1002/mds.25255

Shehzad, Z., Kelly, a M. C., Reiss, P. T., Gee, D. G., Gotimer, K., Uddin, L. Q., … Milham, M. P. (2009). The resting brain: unconstrained yet reliable. *Cerebral Cortex (New York, N.Y. : 1991)*, *19*(10), 2209–29. doi:10.1093/cercor/bhn256

Silver, H., Feldman, P., Bilker, W., & Gur, R. C. (2003). Working memory deficit as a core neuropsychological dysfunction in schizophrenia. *American Journal of Psychiatry*, *160*(20), 1809–1816. Retrieved from http://journals.psychiatryonline.org/article.aspx?articleid=176458

Smit, D. J. a, Boersma, M., van Beijsterveldt, C. E. M., Posthuma, D., Boomsma, D. I., Stam, C. J., & de Geus, E. J. C. (2010). Endophenotypes in a dynamically connected brain. *Behavior Genetics*, *40*(2), 167–77. doi:10.1007/s10519-009-9330-8

Smith, S., Fox, P., Millera, K. L., Glahn, D. C., Fox, P. M., Mackay, C. E., … Beckmann, C. F. (2009). Correspondence of the brain's functional architecture during activation and rest. *Proceedings of the National Academy of Sciences of the United States of America*, *106*(31), 13040–13045. Retrieved from http://www.pnas.org/content/106/31/13040.short

Smith, S. M. (2004). Overview of fMRI analysis. *The British Journal of Radiology*, *77*(suppl_2), S167–S175. doi:10.1259/bjr/33553595

Smith, S. M. (2012). The future of FMRI connectivity. *NeuroImage*, *62*(2), 1257–66. doi:10.1016/j.neuroimage.2012.01.022

Smith, S. M., Jenkinson, M., Woolrich, M. W., Beckmann, C. F., Behrens, T. E. J., Johansen-Berg, H., … Matthews, P. M. (2004). Advances in functional and structural MR image analysis and implementation as FSL. *NeuroImage*, *23 Suppl 1*, S208–19. doi:10.1016/j.neuroimage.2004.07.051

Snyder, A. Z., & Raichle, M. E. (2012). NeuroImage A brief history of the resting state : The Washington University perspective. *NeuroImage*, *62*(2), 902–910. doi:10.1016/j.neuroimage.2012.01.044

Spear, L. P. (2000). *The adolescent brain and age-related behavioral manifestations. Neuroscience and biobehavioral reviews* (Vol. 24, pp. 417–63). Retrieved from http://www.ncbi.nlm.nih.gov/pubmed/10817843

Steinberg, L. (2005). Cognitive and affective development in adolescence. *Trends in Cognitive Sciences*, *9*(2), 69–74. doi:10.1016/j.tics.2004.12.005

Sternberg, S. (1966). High-speed scanning in human memory. *Science*, *153*, 652–654.

Tarokh, L., Carskadon, M. a, & Achermann, P. (2011). Trait-like characteristics of the sleep EEG across adolescent development. *The Journal of Neuroscience : The Official Journal of the Society for Neuroscience*, *31*(17), 6371–8. doi:10.1523/JNEUROSCI.5533-10.2011

Thomason, M., Dennis, E., & Joshi, A. (2011). Resting-state fMRI can reliably map neural networks in children. *Neuroimage*, *55*(1), 650–670. doi:10.1016/j.neuroimage.2010.11.080.Resting-state

Tong, F., & Pratte, M. S. (2012). Decoding patterns of human brain activity. *Annual Review of Psychology*, *63*, 483–509. doi:10.1146/annurev-psych-120710-100412

Tost, H., Bilek, E., & Meyer-Lindenberg, A. (2011). Brain connectivity in psychiatric imaging genetics. *NeuroImage*. doi:10.1016/j.neuroimage.2011.11.007

Unger, M. M., Belke, M., Menzler, K., Heverhagen, J. T., Keil, B., Stiasny-kolster, K., & Rosenow, F. (2010). Diffusion Tensor Imaging in Idiopathic REM Sleep Behavior Disorder Reveals Microstructural Changes in the Brainstem , Substantia Nigra , Olfactory Region , and Other Brain Regions. *Sleep*, *33*(6), 767–773.

Vaillancourt, D. E., Spraker, M. B., Prodoehl, J., Abraham, I., Corcos, D. M., Zhou, X. J., & Al., E. (2009). High-resolution diffusion tensor imaging in the substantia nigra of de novo Parkinson disease. *Neurology.*, *72*((16)), 1378–84.

Van Dijk, K. R. a, Hedden, T., Venkataraman, A., Evans, K. C., Lazar, S. W., & Buckner, R. L. (2010). Intrinsic functional connectivity as a tool for human connectomics: theory, properties, and optimization. *Journal of Neurophysiology*, *103*(1), 297–321. doi:10.1152/jn.00783.2009

Van Eimeren, T., Monchi, O., Ballanger, B., & Strafella, A. P. (2009). Dysfunction of the Default Mode Network in Parkinson Disease : *Archives of Neurology*, *66*(7), 877–883. doi:10.1001/archneurol.2009.97.Dysfunction

Wallace, G. L., Eric Schmitt, J., Lenroot, R., Viding, E., Ordaz, S., Rosenthal, M. a, … Giedd, J. N. (2006). A pediatric twin study of brain morphometry. *Journal of Child Psychology and Psychiatry, and Allied Disciplines*, *47*(10), 987–93. doi:10.1111/j.1469-7610.2006.01676.x

White, T., & Gottesman, I. (2012). Brain Connectivity and Gyrification as Endophenotypes for Schizophrenia: Weight of the Evidence. *Current Topics in Medicinal Chemistry*, *12*(21), 2393–403. Retrieved from http://www.ingentaconnect.com/content/ben/ctmc/2012/00000012/00000021/art00010

Whitfield-Gabrieli, S., Thermenos, H. W., Milanovic, S., Tsuang, M. T., Faraone, S. V., McCarley, R. W., … Seidman, L. J. (2009). Hyperactivity and hyperconnectivity of the default network in schizophrenia and in first-degree relatives of persons with schizophrenia. *Proceedings of the …*, *106*(4), 1279–1284. Retrieved from http://www.pnas.org/content/106/4/1279.short

Williams, D., Tijssen, M., Bruggen, G. Van, Bosch, A., Insola, A., Lazzaro, V. Di, … Brown, P. (2002). Dopamine-dependent changes in the functional connectivity between basal ganglia and cerebral cortex in humans. *Brain*, *125*, 1558–1569. Retrieved from http://brain.oxfordjournals.org/content/125/7/1558.short

Wisner, K., Atluri, G., Lim, K., & MacDonald III, A. (2013). Neurometrics of intrinsic connectivity networks at rest using fMRI: Retest reliability and cross-validation

using a meta-level method. *NeuroImage*, *76*, 236–51. Retrieved from http://www.sciencedirect.com/science/article/pii/S1053811913002218

Woodward, N. D., Waldie, B., Rogers, B., Tibbo, P., Seres, P., & Purdon, S. E. (2009). Abnormal prefrontal cortical activity and connectivity during response selection in first episode psychosis, chronic schizophrenia, and unaffected siblings of individuals with schizophrenia. *Schizophr Res*, *109*(1-3), 182–190. Retrieved from http://www.hubmed.org/display.cgi?uids=19179050

Wu, T., Long, X., Wang, L., Hallett, M., Zang, Y., Li, K., & Chan, P. (2011). Functional Connectivity of Cortical Motor Areas in the Resting State in Parkinson's Disease. *Human Brain Mapping*, *32*, 1443–1457. doi:10.1002/hbm.21118

Xu, J., Potenza, M. N., & Calhoun, V. D. (2013). Spatial ICA reveals functional activity hidden from traditional fMRI GLM-based analyses. *Frontiers in Neuroscience*, *7*(August), 1–4. doi:10.3389/fnins.2013.00154

Yang, Y., Joshi, A., Joshi, S., Baker, L., Narr, K. L., Raine, A., … Damasio, H. (2012). Genetic and environmental influences on cortical thickness among 14-year-old twins. *Neuroreport*, *23*(12), 702–706. doi:10.1097/WNR.0b013e328355a62a.Genetic

Yang, Y., Remmers, E. F., Ogunwole, C. B., Kastner, D. L., Gregersen, P. K., & Li, W. (2011). Effective sample size: Quick estimation of the effect of related samples in genetic case-control association analyses. *Computational Biology and Chemistry*, *35*(1), 40–9. doi:10.1016/j.compbiolchem.2010.12.006

Yu, R., Liu, B., Wang, L., Chen, J., & Liu, X. (2013). Enhanced Functional Connectivity between Putamen and Supplementary Motor Area in Parkinson's Disease Patients. *PloS One*, *8*(3), e59717. doi:10.1371/journal.pone.0059717

Zagha, E., & McCormick, D. a. (2014). Neural control of brain state. *Current Opinion in Neurobiology*, *29*, 178–186. doi:10.1016/j.conb.2014.09.010

Zuo, X., Kelly, C., Adelstein, J. S., Klein, D. F., Castellanos, F. X., & Milham, M. P. (2010). Reliable intrinsic connectivity networks : Test – retest evaluation using ICA and dual regression approach. *NeuroImage*, *49*(3), 2163–2177. doi:10.1016/j.neuroimage.2009.10.080